EVALUATION OF GARDINER DAM'S ONGOING MOVEMENT

A Thesis Submitted to the College of

Graduate Studies and Research

In Partial Fulfillment of the Requirements

for the Degree of Masters of Science

In the Department of Civil and Geological Engineering

University of Saskatchewan

Saskatoon

By

Jody William Scammell

PERMISSION TO USE

In presenting this thesis in partial fulfilment of the requirements for a Postgraduate degree from the University of Saskatchewan, I agree that the Libraries of this University may make it freely available for inspection. I further agree that permission for copying of this thesis in any manner, in whole or in part, for scholarly purposes may be granted by the professor or professors who supervised my thesis work or, in their absence, by the Head of the Department or the Dean of the College in which my thesis work was done. It is understood that any copying or publication or use of this thesis or parts thereof for financial gain shall not be allowed without my written permission. It is also understood that due recognition shall be given to me and to the University of Saskatchewan in any scholarly use which may be made of any material in my thesis.

Requests for permission to copy or to make other use of material in this thesis in whole or part should be addressed to:

Head of the Department of Civil and Geological Engineering

University of Saskatchewan

Engineering Building

57 Campus Drive

Saskatoon, Saskatchewan, S7N 5A9

ABSTRACT

Gardiner Dam is located on the South Saskatchewan River approximately 100 km south of Saskatoon, SK. After the start of construction, the River Embankment experienced downstream movement in the shale portion of the foundation. Observed movements are occurring on a well-defined shear plane within the shale layer. This continuing foundation deformation raises concerns regarding the long-term stability of the structure and the effect of continuing deformation on the integrity of the embankment and ancillary works. The mechanism(s) responsible for the ongoing movements are not fully understood. As such, prediction of on-going deformation has had only a limited success.

In the work presented in this dissertation, historic geotechnical instrumentation data was used to identify a potential mechanism of movement within the shale foundation. The potential mechanism thus identified can be briefly described as a combination of elastic deformation and consolidation within the shale. As the reservoir level rises, part of the increase in horizontal thrust is transferred to the shale. Since the shale is relatively stiff and has a low hydraulic conductivity, the increase in loading is; therefore, transferred to the porewater, resulting in generation of excess porewater pressures in shale. When the reservoir is high a portion of the excess porewater pressure dissipates. The observed horizontal movement along the shear zone is then developed from elastic deformation and horizontal consolidation of the shale from dissipation of excess porewater pressure.

An analytical model was developed from the proposed conceptual model and had general success predicting the horizontal displacement based on the reservoir level and time period. However, the model was sensitive to the reservoir level and several variables within the shale including the hydraulic conductivity and porewater parameter B. Overall, the material variables such as hydraulic conductivity and B can be refined; however, without having an accurate reservoir prediction into the future, the ability for this model to predict the displacement in the foundation will be limited.

ACKNOWLEDGMENTS

I would like to acknowledge the people and organizations that provided me assistance throughout the last few years leading to the successful completion of this work.

I would like to recognize and thank Professor Jitendra Sharma, my supervisor for his guidance, time, expertise and encouragement. In addition, I would like to recognize the exceptional guidance provide by the members of my advisor committee, Doctor Rashid Bashir, Doctor Curtis Kelln and Professor Leon Wegner, the Chair of the committee. I would finally like to thank Doctor Ramakrishna Gokaraju, my external examiner for his constructive criticism.

I am grateful to my colleagues at the Water Security Agency of Saskatchewan for their support and assistance throughout this work. I am appreciative of Russ Johnson, Bill Duncan and Doug Kilgour for the discussions, guidance and encouragement, from the start of this work. I am thankful to the current Gardiner Dam Technical Monitoring site staff; Cam Leslie, Danny Marzolf and Warren Fraser, along with all the past monitoring staff, who diligently collected vast amounts of instrumentation data.

I would like to greatly thank the Water Security Agency of Saskatchewan for providing the time from work and the financial support to see this work to the successful completion.

I am most greatly thankful to my wife, Alexis, children Josephine and Braxton, and parents Dale and Karen for their overwhelming support and encouragement through the past several years.

DEDICATION

This dissertation is dedicated to my loving wife, Alexis Helene and to the two lights of my life, Josephine Mae Jane and Braxton William Dale, for all their support and encouragement.

TABLE OF CONTENTS

LIST OF FIGURES

LIST OF TABLES

CHAPTER 1 INTRODUCTION

1.1 Background

Gardiner Dam is located on the South Saskatchewan River approximately 100 km south of Saskatoon, SK (Figure 1.1). The structure was constructed for the Saskatchewan Provincial Government in the 1960's by the Prairie Farm Rehabilitation Administration (PFRA) and is currently owned by the Water Security Agency (WSA), previously known as the Saskatchewan Watershed Authority. Please note the majority of this work was completed prior to the company name change from Saskatchewan Watershed Authority to Water Security Agency; therefore, several figures throughout the document still retain the previous name and logo.

The facility consists of three-zoned earth filled embankments: the Main (River) Embankment; the Plateau Embankment; and, the Coteau Embankment (Figure 1.2). This dissertation focuses on the evaluation of on-going movements of the River Embankment. The total crest length of the dam is 4960 m at an elevation of 562.3 m. The River Embankment has a crest length of 2500 m and has a maximum height of 64 m. The River Embankment was constructed as a zoned earth embankment. The zones include a central impervious core, upstream and downstream granular section, lower berms with flatter slopes, upstream seepage blanket, and a pervious filter blanket extending from the downstream toe to a set of pressure relief wells.

The foundation conditions beneath the River Embankment consist of alluvial sand underlain by the pre-glacial Bearpaw Formation, comprised of the clay shale Snakebite member and the poorly consolidated sandstone of the Ardkenneth member (Cladwell 1968). Figure 1.3 illustrates the general stratigraphy below the River Embankment.

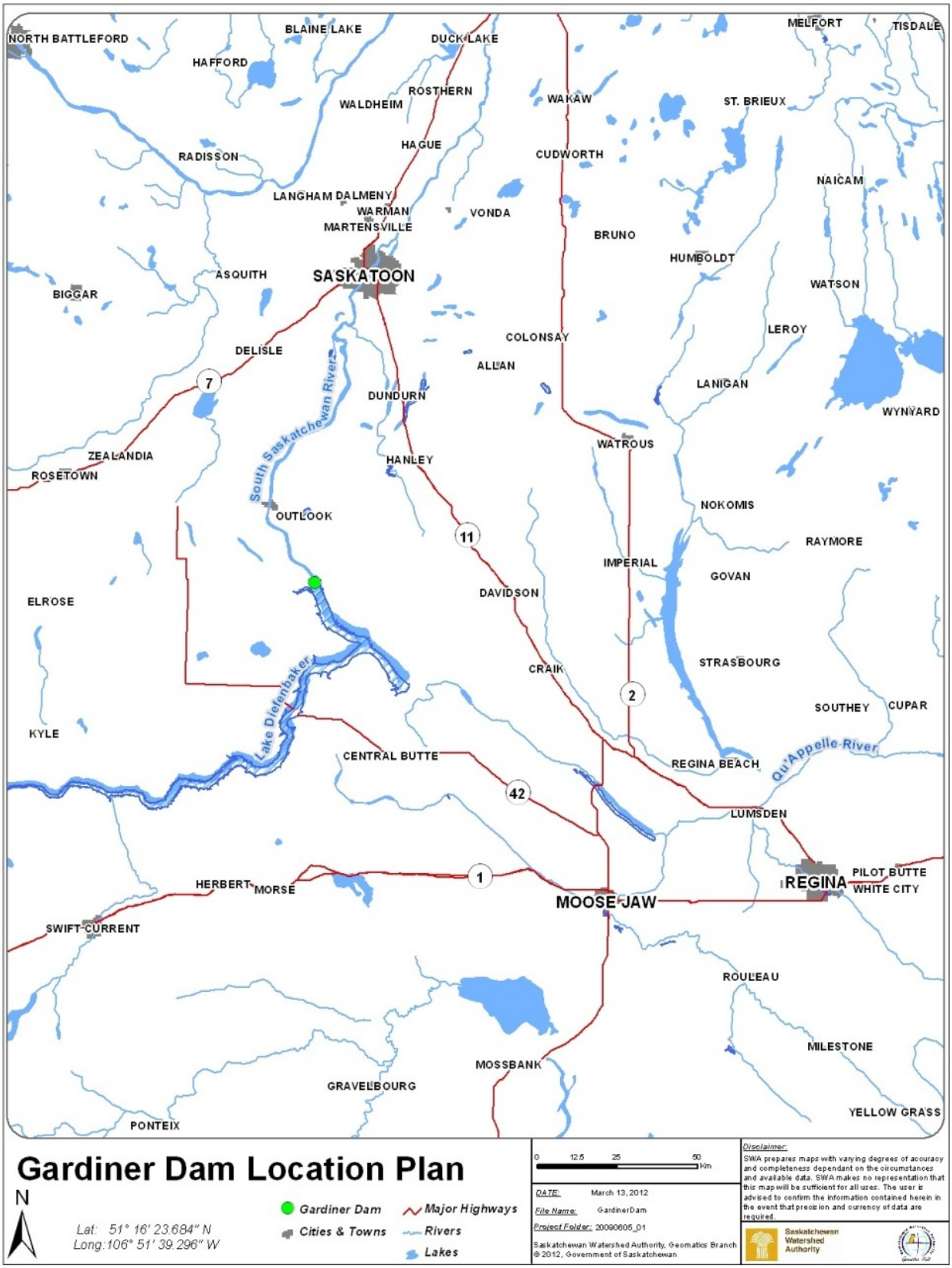

Figure 1.1 Location plan of the Gardiner Dam

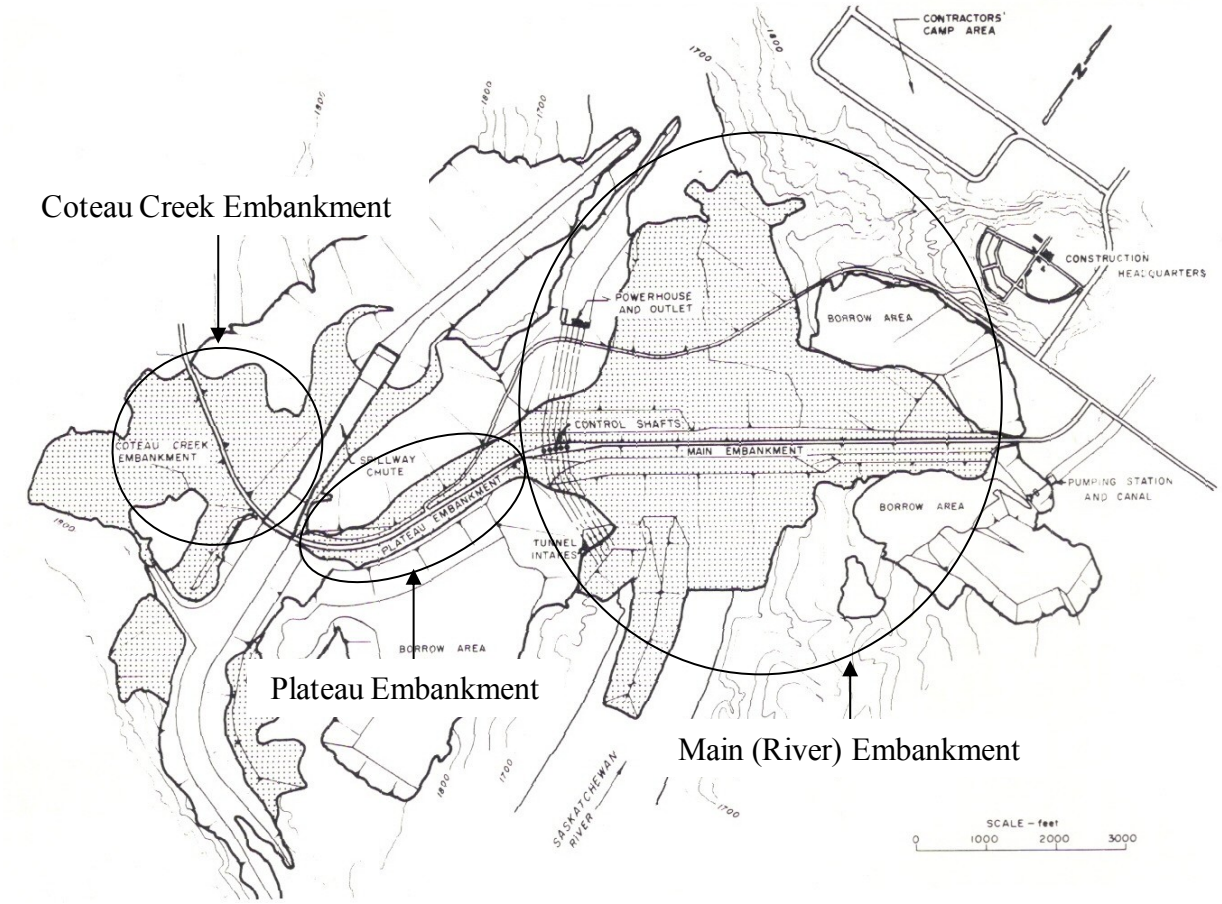

Figure 1.2 Gardiner Dam plan view layout showing the three main embankments (PFRA 1980)

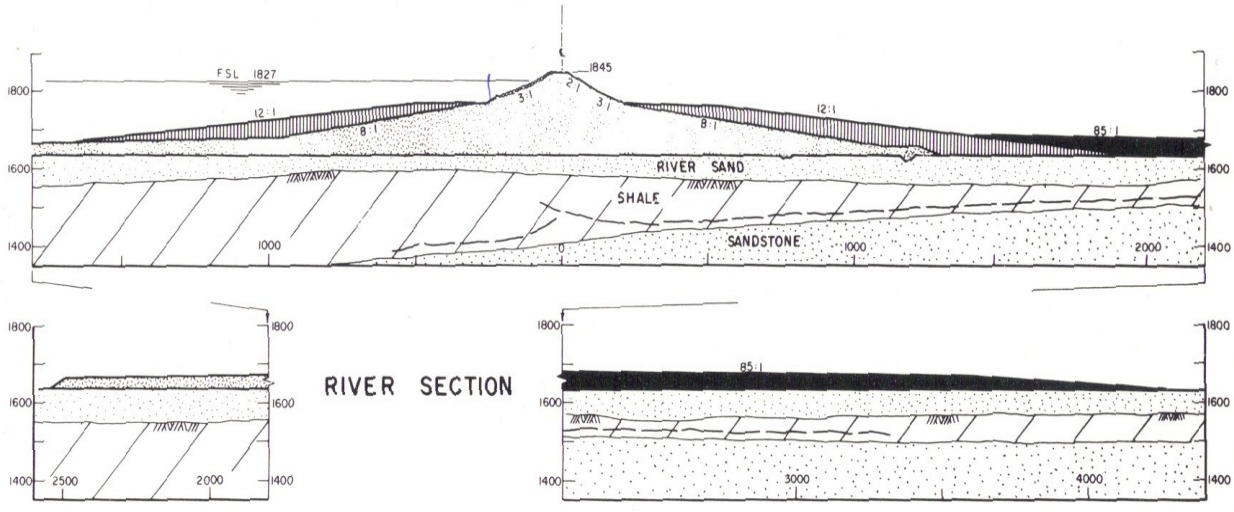

Figure 1.3 General stratigraphy of River Embankment (PFRA 1980)

Following the start of construction, the River Embankment experienced downstream movement in the shale portion of the foundation. The movement has been monitored continuously using inclinometer casings and surface monitoring line pins since it was first identified during construction. The inclinometer casings have indicated the existence of a well-defined shear plane within the shale layer. The continuing foundation deformation raises concerns regarding the long-term stability of the structure. A second concern is the effect of continuing deformation on the integrity of the embankment and ancillary works and the potential maintenance measures required to retain the works in operating condition.

During the design, construction and post-construction phases, the stability of the dam was evaluated using limit equilibrium techniques (PFRA 1955a, PFRA 1960a, PFRA 1962, Jaspar and Peters 1979). In addition to these stability models, several other stress-deformation models have attempted to replicate the continued foundation deformations with limited success (Morgenstern and Simmons 1980, Morgenstern and Simmons 1982, PFRA 1992). From the outcome of these modelling attempts, it is fairly evident that the key mechanisms responsible for inducing the downstream movement in the foundation were not fully understood. As such, prediction of foundation movement in relation to an increase in reservoir level was not been successful.

1.2 Objectives

The primary objective of this work was to address the gap in the knowledge, with regards to the understanding of the mechanisms of movement occurring in the foundation of the River Embankment. The knowledge gap was addressed through the development of a conceptual level model. The historic geotechnical monitoring data and modelling results were used to development this model. A secondary objective of this work was to verify the theoretical conceptual model with a simple analytical model.

1.3 Scope

A conceptual model was used to represent the historic monitoring data. The conceptual model consisted of one representative cross-section through the River Embankment. This cross-section included the embankment and the foundation materials above the Ardkenneth Sandstone member.

Movements in the entire dam structure are critical to the integrity of the project; however, only movements within the shale were evaluated as these movements are considered to be the most critical for the long-term integrity of the structure. Key factors, such as shale shear strength, compressibility and hydraulic conductivity, as well as piezometric heads, loading conditions, and reservoir rate effects, potentially affect the downstream movement within the foundation and were reviewed as part of the development of the conceptual model.

Before and during construction, a large number of samples and lab tests were completed on the foundation and embankment materials. Additionally, in 2009, a sampling and testing program was undertaken in the vicinity of the shear zone within the shale layer. These historical records were reviewed in order to assist in the interpretation of recorded movements; however, the laboratory testing was not evaluated in detail as there are many uncertainties in the data that warrant further careful scrutiny. Also, since the objective of this project is to create a conceptual model, no further field investigations or material testing was conducted as part of this work.

The River Embankment has been monitored continuously from before construction to the date of this work. The monitoring includes a large number of geotechnical instrumentation including, slope inclinometer casings, piezometers, settlement gauges, surface monitoring survey pins and seepage monitoring. The slope inclinometer casings generally have been constructed through the embankment and beyond the identified shear zone within the shale. The piezometer tips are located in various zones of the embankment fill and foundation materials. Large portions of the monitoring data were reviewed; however, only a limited number of instruments were used for detailed interpretation and analysis.

To achieve the secondary objective of this work, a simple analytical model was developed using a spreadsheet to complete the calculations. This simple analytical model allowed for various computations to be completed in an efficient manner and assisted in verifying the developed conceptual model. In addition, numerical stress-strain and seepage simulations were used to explore and verify the physical process for the development of the conceptual model. The stress-strain and seepage model were not used in the prediction of the deformation.

1.4 Thesis Structure

This thesis is structured to provide a logical map to follow the development and verification of a conceptual model representing the annual movements of Gardiner Dam.

CHAPTER 2 provides a summary of the relevant literature reviewed throughout this work. The literature review provides a background on the concepts presented. This chapter also discusses the background of the Gardiner Dam site. This includes a description of the structures, brief history on the construction, design and analysis, and finally a description of the geotechnical instrumentation. In addition to the description of project site, the theoretical concepts used for the development of the conceptual model are also discussed.

CHAPTER 3 presents a review of the historical geotechnical instrumentation data. CHAPTER 4 discusses the instrumentation data interpretation and the observed correlations. The instrumentation review and interpretation provide the basis for the development of the conceptual model.

CHAPTER 5 describes the development of an analytical model to represent and verify the proposed conceptual model. The analytical model developed a link between the observed correlations in the historic instrumentation data through theoretical concepts presented in the literature review.

CHAPTER 6 describes the application of a simple analytical model. This discussion includes the model boundary conditions, material properties, simplifying assumptions, geometry and transfer of the theoretical calculations to the model.

CHAPTER 7 describes the calibration and sensitivity of the analytical model. In addition, the modelled results of two additional time periods and their comparison to the observed data are presented.

CHAPTER 8 provides a discussion of the comparison of the analytical model results and the observed data. This chapter also describes the limitation of the conceptual model and recommendations for further work.

CHAPTER 2 LITERATURE REVIEW

2.1 Overview

The deformation of a water retaining embankment is generally influenced by two major factors: 1) the material properties (stiffness, shear strength and hydraulic conductivity) of the foundation and the embankment and 2) the loading caused by the construction of the embankment and the filling of the reservoir. The literature review presented in this chapter focused on the material properties in the movement zone within the shale to develop an understanding of the resistive and deformation properties.

Since this work involved a specific site, a brief overview of the geology will be provided. The field instrumentation details will also be discussed as the interpretation of their measurements is a critical aspect of this work. Finally, the previous modelling attempts will be reviewed to understand what has been completed and where gaps in the knowledge may exist.

2.2 Porewater Response to Loading

The porewater response of a geomaterial during undrained loading is an important aspect of embankment engineering. When an embankment is under construction, the predicted response of the porewater due to material placement affects the effective stress within the foundation and the expected deformation due to consolidation.

Skempton (1954) described the elastic porewater pressure response to an increase in the deviatoric loading in terms of two pore-pressure coefficients "A" and "B". Skempton related the changes in the pore-pressure, which occur as a result of the changes in principal stresses, using the following:

$$\Delta u = B\left[\Delta\sigma_3 + A(\Delta\sigma_1 - \Delta\sigma_3)\right] \quad (2\text{-}1)$$

where Δu is the change in pore-pressure, A and B are pore-pressure coefficients, $\Delta\sigma_3$ is the change in all around stress, and $\Delta\sigma_1$ is the change in the normal stress.

The B pore-pressure coefficient relates the change in the pore-pressure to all around stress and is dependent on the ratio between the compressibility of the soil matrix and the compressibility of porewater. This relationship is shown with the following (Skempton 1954):

$$\frac{\Delta u}{\Delta \sigma_3} = B = \frac{1}{1+\frac{n\beta}{m_v}} \tag{2-2}$$

where n is the porosity of the soil matrix, β is the compressibility of water and m_v is the coefficient of volume change in the soil. Skempton found that if a material is considered very compressible compared to water and the soil is undrained, the value of B approaches 1. Further to this, Skempton (1954), Bishop (1973) and Bishop (1976) found that as the soil compressibility becomes closer to or greater that water, the porewater response deviates from this classical approach and only a portion of the total stress is applied to the porewater and the remainder is applied to the soil skeleton; therefore, reducing B. This indicates that as the compressibility of the soil approaches the compressibility of water, B becomes less than 1 and as the compressibility of the soil becomes much stiffer than water, B will approach 0.

To add to the usefulness of the pore-pressure coefficients for embankment construction, Skempton (1954) introduced $\overline{B}$ as a porewater coefficient. $\overline{B}$ relates the change in porewater pressure to changes in major principal stress as follows:

$$\bar{B} = \frac{\Delta u}{\Delta \sigma_1} = B\left[1 - (1 - A)\left(1 - \frac{\Delta \sigma_3}{\Delta \sigma_1}\right)\right] \tag{2-3}$$

During construction of the River Embankment, $\overline{B}$ was inferred to range between 0.73 and 0.75 for embankment heights greater than 27 m (Ringheim 1964, Jaspar and Peters 1979). The inferred $\overline{B}$ values were assumed to occur immediately following loading of the embankment where the shale would be acting in an undrained manner. As a result, $\Delta\sigma_3/\Delta\sigma_1 = 1$; therefore, Equation (2-3) indicates that $B=\overline{B}$.

The typical values of B for shale at Gardiner Dam during laboratory testing ranged between 0.3 and 0.7 (PFRA 1965a). However, it was indicated by PFRA that the samples tested may not have been fully saturated or had unsaturated characteristics, as a result lowering the B value greatly (Skempton 1954). Therefore, the results presented by PFRA must be considered

cautiously. In addition, the samples tested were also not located directly beneath the River Embankment or at a similar depth as the observed movement zone considered in this work. The samples tested were collected closer to the surface, with two samples collected from relatively shallow rotary drilled holes and the other two samples were collected from the access portal to the tunnels within several meters of the surface (PFRA 1965a). Given the locations where the samples were collected, there is likelihood that the samples would be disturbed as compared to a sample collected at greater depth in the shale.

The inferred B value was then used to back calculate the Young's Modulus of the foundation shale to allow for the comparison to the Young's Modulus of similar heavily overconsolidated shales in the literature. The following steps describe how the Young's Modulus was back calculated. First, the coefficient of volume compressibility was calculated from B as follows:

$$m_v = \frac{n\beta}{\frac{1}{B}-1} \tag{2-4}$$

Next, the constrained modulus, D' was determined from the coefficient of volume compressibility m_v using the following (Lamb and Whitman 1969):

$$D' = \frac{1}{m_v} \tag{2-5}$$

Finally, the Young's Modulus was calculated from constrained modulus using the following (Lamb and Whitman 1969):

$$E' = \frac{D'(1+\nu')(1-2\nu')}{(1-\nu')} \tag{2-6}$$

assuming ν'=0.2, (Mayne and Poulos 1999), B=0.75, compressibility of water 4.6e-7 1/kPa and n=0.36, the Young's modulus was back calculated to be 1809 MPa.

From the literature, the shale of the Upper Colorado Group near Cold Lake, AB which has similar characteristics to the shale at Gardiner Dam, ranged between E'= 400 - 1250 MPa (Gautam and Wong 2006). Additionally, when the shale from outside the local Western Canadian area was looked at, the E' was found to range up to 32000 MPa (Jizba 1991 and Sarout et al. 2006). It can be seen that the back calculated Young's Modulus from the inferred

measurements is slightly above the range of the shale in Western Canada. However, given the sensitivity of determining the Young's Modulus in the laboratory, this is considered a reasonable match.

2.3 Consolidation of Material

The theory of consolidation can be described as deformation of soil caused by the application of total stress and the flow of water from void spaces until equilibrium is reached (Terzaghi et al. 1996). Terzaghi's initial derivation of the Theory of Consolidation assumed a one dimensional model. Terzaghi's model assumed a constant load is applied to a column filled with a saturated elastic porous medium, lateral expansion of the column is prevented and drainage only occurs at the top and bottom of the model. Biot (1941) expanded this theory to a three dimensional condition where the loading variable is allowed to fluctuate with time, variability in the hydraulic conductivity and compressibility was also considered as the sample compresses, lateral deformation was allowed and porewater flow was allowed in all directions.

The basic assumed soil properties for both the one dimensional and three dimensional models are similar and include: material isotropy, linear and reversible elastic stress-strain relationship, small strain conditions, incompressible porewater, and the flow of porewater is dependent on Darcy's law (Biot 1941).

For this work, consolidation was considered as one dimensional. This assumption was reasonable because the shale was considered to be constrained laterally due to the laterally uniform loading of embankment, creating an effectively constrained condition. In addition, due to the large lateral extents of the shale, the dominating hydraulic condition was the shortest drainage path, which is towards the upper and lower limits of the shale; therefore, reducing the likelihood of lateral drainage.

As stress is applied to a saturated soil, excess pore-pressure develops according to the porewater response of the material. The excess pressure then drains, according to the hydraulic conductivity and stiffness of the material. As the excess pressure dissipates, deformation occurs with the reorganization of soil partials within the soil matrix through the process of consolidation (Terzaghi et al. 1996).

Terzaghi et al. (1996) defined two states of consolidation, primary consolidation and secondary compression. Primary consolidation was described as the deformation which occurred with the transfer of the total stress from the excess porewater pressure to the soil skeleton as the excess pressure dissipates. Secondary compression was described by Bjerrum (1967) as the movement or creep following the change in the stress condition applied to a soil. Secondary compression is ongoing following a change in the stress condition applied to the soil; however, it is relatively small in comparison to the deformations observed during primary consolidation. Therefore, secondary compression is difficult to observe while primary consolidation is occurring and is effectively subdued. Given that primary consolidation dominates the deformation following an applied load and secondary compression requires a relative significant time period to be measured, only primary consolidation will be considered throughout this work. This implies that time dependent deformation are assumed negligible.

2.4 Residual Shear Strength

Skempton (1964) described the concept of residual shear strength as the drop in shearing resistance when a sample is strained past the peak strength. This drop in peak is initially thought to be due to an increase in water content followed by a reduction in strength with the realignment of the clay particles in the direction of shear. The strength of a mass of clay may not be dependent on the peak strength of the intact portion of the sample, but may be dominated by the residual strength of the disturbed material.

The amount of deformation required in the field to develop residual shear strength depends on the existence of pre-formed fissures or joints. James (1971) identified that a field displacement of a few feet is required to reduce internal angle of friction by a few of degrees for intact material. Skempton (1985) found that if a soil has not yet mobilized its peak shear strength, the shear strains required to reach residual shear strength will be between 20% and 50% greater than the shear strains required to reach peak shear strength.

Two different types of laboratory testing procedures have been used to determine the residual strength of cohesive soils. The test procedures include a ring shear testing (Bishop et al. 1971, Bromhead 1986, Stark and Eid 1993, and Meehan et al. 2007) and a multiple reversal direct

shear testing (Skempton 1964). Both these methods of measuring residual shear strength give comparable results (Bromhead 1986).

Stark and Eid (1994) and Dewoolkar and Huzjak (2005) found that the effective normal stress and residual shear strength have a non-linear relationship. As the effective normal stress increases, the residual shear strength decreases. This illustrates the importance of using the appropriate effective normal stress during laboratory testing for the determination of residual strength for design values.

2.5 Shear Strength of Saskatchewan Shale

Several investigations have been completed on shales in Saskatchewan in relation to the shear strength. Sauer (1978) and Sauer et al. (1990) found that glaciated heavily over consolidated clay shales of Saskatchewan have a high likelihood of having experienced glacial ice thrusting. As a result, these shales are likely to have experienced shear strains that are large enough for the mobilization of residual shear strength on ice-thrusting-induced fissures and joints.

Clifton et al. (1986) investigated a landslide in an eroded glacial melt water spillway channel with movements occurring in the Bearpaw formation shale. Using multiple reversal direct shear method, they measured the residual shear strength parameters for this shale to range between ϕ_r'=8-15° and c_r'=0-50kPa, where ϕ_r' is the residual friction angle and c_r' is the residual cohesion. For the same shale, they obtained residual shear strength parameters of between ϕ_r'=5-7° and c_r'=0 kPa by conducting a back analysis of the landslide using limit equilibrium slope techniques (Clifton et al. 1986).

The residual shear strength of the Lea Park shale, which has had a depositional environment similar to the shale at Gardiner Dam site (Sauer 1984), was investigated with a combination of limit equilibrium slope stability back analysis and laboratory testing (Insley et al. 1977, Krahn et al. 1979, Sauer 1983, Sauer 1984, Christiansen and Sauer 1984, Sauer and Christiansen 1987, Eckel et al. 1987, Wilson et al. 1989, Misfeldt et al. 1991, and Kelly et al. 1995). The residual shear strength parameters were found to range between ϕ_r'=5-15° and c_r'=0 kPa in the laboratory using multiple reverse direct shear and between ϕ_r'=3.9-10.4° and c_r'=0 kPa using limit equilibrium slope stability back analysis.

2.6 Shear Strength of Shale at Gardiner Dam Site

Shear strength parameters of shale at the Gardiner Dam site underwent an evolution from the values measured initially from lab testing to back-calculated values after construction. Because the measurement of porewater pressure during laboratory shear testing was not the norm, the initial lab testing relied on a fast shearing rate to ensure undrained conditions. The results were then analyzed in a total stresses environment. As laboratory equipment became more sophisticated and as the understanding of the site improved, drained and undrained tests with porewater pressure measurement were completed and their results were analyzed using effective stresses.

Results of lab testing completed up to 1955 are summarized in PFRA (1955a). These lab tests included quick direct shear tests, quick triaxial tests and unconfined compression tests, which relied on sufficiently fast rate of shearing to preserve undrained conditions during shearing. Total stress analysis was then used to obtain shear strength parameters from the results of these tests (PFRA 1955a). In spite of a large number of samples tested, it was difficult to establish well-defined shear strength parameters for the three consistencies (i.e. soft, medium and hard) of shale. The shear strength parameters for shale, determined from these lab tests and subsequently used in the stability modelling analyses, were $\phi = 10°$ and c = 103 kPa for the soft shale and $\phi = 25°$ and c = 206 kPa for the medium to hard shale.

Results of lab testing completed up to 1966 are summarized in PFRA, 1966a. The multiple reversal direct shear technique was used with a few variations on undisturbed samples in this testing program. Undisturbed samples containing the field shear planes were used to measure the residual angle of friction, which was found to be between $\phi_r' = 3.5\text{-}8°$. Tests conducted on precut, and prepolished samples found the residual angle of friction to be $\phi_r' = 6°$.

PFRA (1981) describe the results of the continued laboratory testing program from 1969 to 1978; these results were used for further refining of the residual shear strength parameters of the shale. Shear tests were completed on four types of samples including: intact undisturbed; intact with a precut shear plane; remolded with a precut shear plane; and intact containing the field shear plane. The peak and residual shear strength parameters were obtained from the results of multiple reversal direct shear tests. It was found that the soft and hard shale had similar residual

angle of friction that ranged from ϕ_r'=2.5 to 7.2° with an average of 4.4°. The residual effective cohesion ranged from c_r'=0 to13 kPa with an average of 2 kPa. The residual shear strength parameters measured using samples containing the field shear plane ranged from ϕ_r'=2.5 to 4.5° with an average 3.2° and c_r'=0 to 5 kPa with an average 1 kPa.

Stark and Eid (1994) conducted multi-stage ring shear tests on samples of 32 different clays and shales including Lea Park shale and Bearpaw shale. They found the residual shear strength envelope to be non-linear. That is, the residual shear strength parameters were different for different values of effective normal stress. They explained this non-linearity of residual shear strength envelope on the basis of better alignment of the plate-like clay particles along the shear plane at higher normal effective stresses, which results in mobilization of lower residual shear strength. This finding was later confirmed by Dewoolkar and Huzjak (2005). For the Bearpaw shale from the Gardiner Dam site, Stark and Eid (1994) found the residual friction angle value of ϕ_r'=9.8° and 8.8° for effective normal stress values of 200 kPa and 400 kPa, respectively.

2.7 Dams on Shale and Clay

Few dams have been built on shale foundation on the Western Prairies of Canada with foundation conditions similar to those at Gardiner Dam. The published literature on these dams focused mainly on the initial design issues, selection of design parameters and short-term monitoring; very little information was available on long-term monitoring of these dams.

Matheson et al. (1987) described the design, construction and performance of the 54-m-high Nipawin Dam. The Nipawin Dam is founded on the late Cretaceous Ashville formation shale underlain by the highly artesian Swan River formation. Laboratory testing during design of the shale showed the residual effective friction angle of ϕ_r'=9°. The Ashville shale was found to have a $\overline{B}$ = 0.7 in response to the embankment construction which compares well to the $\overline{B}$ = 0.73-0.75 that was inferred from the shale at Gardiner Dam (Ringheim 1964, Jaspar and Peters 1979).

2.8 Gardiner Dam Site Geology

The bedrock sequence in the vicinity of Gardiner Dam consists of the Upper Cretaceous formations (Cladwell 1968). The bedrock geology of site and surrounding area consists of the Bearpaw formation. The Lea Park and Bearpaw formations were formed within the same marine

conditions and consist of the same material, separated only by the regression of the Lea Park Pakowki Sea (Cladwell 1968 and Sauer 1984).

The Bearpaw formation is comprised of ten alternating layers of silty sand material and sandy clay material with a total thickness of 350 m. The sand layers within the Bearpaw formation are generally thinner than the clay layers.

Gardiner Dam is founded on Snakebite shale that is underlain by the Ardkenneth sandstone. The Snakebite shale has a maximum thickness of 82 m; however, beneath the River Embankment its thickness is between 25 and 30 m. The Snakebite shale is a massive, medium to dark grey silty clay that exhibits brownish grey weathering patterns and limited laminations. It also contains two prominent 25-mm-thick bentonitic seams, fossiliferous septaria, and yellow to buff fibrous calcite. Some bentonitic seams are present with ragged contacts and others are only present as streaks, indicating disruptions in the deposition of volcanic ash. Several bedding planes exist in the Snakebite shale and are thought to be caused by glacial loading, unloading or thrust (Sauer 1978 and PFRA 1980).

The Ardkenneth sandstone is located approximately 40 to 90 m below river level. The member was described as a grey (pale grayish brown when weathered), poorly consolidated, silty, sandstone with clay lenses and nodules of yellow iron oxide.

Glacial events significantly altered the preglacial topography of the bedrock at Gardiner Dam (PFRA 1955b). The preglacial site consisted of a highly eroded, badland topography. Successive glaciations eroded and deposited glacial drift within the site. The river valley rapidly lowered through melt water erosion. Following the melting of the ice, a lake was created over the area with several fluctuations in level, resulting in deposition of stratified materials ranging from fine sand to gravel. After the glacial lake receded, rapid erosion occurred, creating deep incisions in shale in the valley, followed by extensive slumping. The river valley has since experienced aggrading of river sand material with localized slumping (PFRA 1955b, Pollock 1962, and Christiansen 1979).

With the deep and rapid incising of the shale following the last deglaciation, slumping of the Snakebite shale was prevalent. The slumped material is highly disturbed and is found on the

lower slopes along with so called “shale tongues” interlaying in river sand of the valley (Jaspar and Peters 1979).

The Snakebite shale was subdivided into three categories, including soft, medium, and hard, based on its water content (Peterson 1958). The soft zone water content had a maximum value of approximately 38%, the medium zone water had a maximum of approximately 33% and the hard zone water content was approximately 27% (Peterson 1958). The less plastic shale was found to consist of 50-70% illite and 10-20% montmorillonite. The more plastic shale was found to consist of 10-20% illite and 50-70% montmorillonite (Jaspar and Peters 1979).

The undisturbed preconsolidation pressure of the late Cretaceous shale including the Bearpaw formation was found to vary between 11000 kPa and 17000 kPa (Sauer et al. 1993). In addition, Sauer et al. (1990) found that a reduction of the preconsolidation pressure of zones of the late Cretaceous shale through glacial shearing at depths greater than 30 m is possible. The preconsolidation pressure through the zones of glacial shear generally ranged between 400 and 1800 kPa. The zones of reduced preconsolidation pressure are separated by zones of intact high preconsolidation pressure shale.

2.9 Geotechnical Field Instrumentation

Monitoring the performance of geotechnical structures and foundation is important from the viewpoint of validating design, providing warning of impending failure, and future performance evaluations. The designers of Gardiner Dam intended the use of instrumentation as the best indicator of the stability of the dam during and after its construction (Jaspar and Peters 1979).

2.9.1 Instrumentation for Monitoring of Dam Movement

Instrumentation installed for monitoring of the movement of Gardiner Dam included slope inclinometer casings, surface monitoring pins, settlement and rebound gauges. Earlier installations of slope inclinometer casings used aluminum casing; whereas plastic casing was used for later installations. The inclinometer probe used until 1970 was found to be somewhat imprecise and was replaced with a probe that used servo accelerometers to measure tilt, thereby increasing its precision. It was estimated that the pre-1970 inclinometer probe had a precision of

up to ±25 mm/30 m, whereas the servo accelerometer probe had a precision of ±7.5 mm/30 m (Peters and Ellis 1972).

Where inclinometers were either not installed at all or not installed to sufficient depth, surface survey pins were used for the monitoring of both horizontal and vertical movements. The movement pins consisted of either a 3.3-m-long shear pin installed in a protective casing or a 1-m-long steel bar driven into the surface (Peters and Ellis 1972). The majority of the surface movement pins were 1-m-long steel bar type. Because of the shallow nature of their installation, surface monitoring pins are susceptible to frost displacement.

Vertical movements were measured with United States Bureau of Reclamation (USBR) telescopic pipe settlement gauges and specially-adapted rebound gauges (Peters and Ellis 1972). The precision of settlement gauge systems was expected to be ±1-5 mm (Dunnicliff 1988).

2.9.2 Piezometric Instrumentation

Piezometric levels within the foundation and the embankment were measured with either Casagrande piezometers, USBR twin tube piezometers or a select number of vibrating wire piezometers. For the most part, the initially installed piezometric instruments performed satisfactorily and with little modification (Peters and Ellis 1972).

Casagrande Piezometers

Typical Casagrande piezometer tips consist of a cylindrical porous ceramic tube connected via a rubber bushing to a 10-mm-internal-diameter saran plastic tubing. The tips are typically placed in a sand pack with a bentonite seal and the remainder of the borehole is sealed with bentonite grout. Casagrande tips are considered very reliable; however, they tend to have slower response time due to the volume of water that is required to be displaced. During freezing situations, antifreeze mixture may have to be used and the specific gravity of the fluid corrected during reading (Dunnicliff 1988).

USBR Piezometers

USBR piezometer tips consist of a porous tip connected to two gauges via two 48-mm-internal-diameter polyethylene tubes. The maximum length of the piezometer tubing was 910 m (Peters and Ellis 1972). The largest potential error is caused by a vertical section of the tubing being

filled with gas causing a discontinuous fluid column (Dunnicliff 1988). Another potential source of error is the change in density due to temperature change (Dunnicliff 1988).

Vibrating Wire Piezometers

Several Vibrating wire piezometers were installed at Gardiner Dam in the late 1980s. The data from several of the vibrating wire tips installed in the late 1980s appears to be unreliable, mainly because the vibrating wire technology was in its infancy at that time and there was a high probability of the above-mentioned errors present at the time of installation. The major sources of error with this type of instrument include corrosion of the measuring wire and creep of the wire under tension. Creep of the wire causes a zero shift in the instrument; however, several investigations have indicated that such a zero shift is typically small, and that the problem can be mitigated by heating to relieve stress from the wire and clamps prior to assembly (Dunnicliff 1988).

Literature indicated that changes in atmospheric pressure can have an influence on the measured piezometric pressure when using sealed (total pressure) piezometer tips (Anochikwa et al. 2012). Two sealed vibrating wire piezometers were used throughout this evaluation, VW179 and VW639. Both of the piezometers were not corrected for atmospheric pressure changes. Unfortunately, from the time of installation of the vibrating wire piezometers, no atmospheric data was collected locally. Due to the infrequent measurement of these two instruments and the fluctuation of the measurement, which is in the order of several meters per reservoir cycle, the effect of correcting for atmospheric conditions was considered minimal for this level of study, but is recommended to be investigated further.

2.10 Previously Completed Modelling of Gardiner Dam

The previously completed analytical models of Gardiner Dam can be split into two groups, with one group dealing with the stability aspects of the embankment and the other group dealing with the modelling deformation aspects of the embankment.

2.10.1 Stability Models

The stability models used the limit equilibrium method of evaluation and were completed before, during and immediately after the construction of the embankment. Initially, the models were

developed using total stress analysis. Later on, with improved understanding of soil behavior, stability models were developed using effective stress analysis.

The first attempt at analyzing the stability of the Gardiner Dam embankment was based on total stress analysis using the Ordinary Method of Slices. During this stage, the shear strength parameters were obtained from laboratory testing and from back analysis of the surrounding natural slope failures. The calculated factor of safety was found to be acceptable using the parameters obtained from laboratory testing and was found to be marginal using the parameters obtained from back analysis of failed slopes (PFRA 1955a).

At the start of the embankment construction, several shallow slope failures developed prompting a reevaluation of the embankment stability using effective stress analysis. The material properties used were obtained from the back analysis of surrounding slopes. Lower factor of safety values were obtained from effective stress stability analyses and subsequently, the stability of the embankment was downgraded from acceptable to marginal (PFRA 1960a).

Following the reduction in the factor of safety, the dam embankment was redesigned with flatter slopes, wider berms, modifications to the core shape, and reduction of the construction rates. The stability evaluations were then completed using Janbu's composite surface, an extension of Bishop's circular arc method. Deeper slip surfaces were also considered in this evaluation. The minimum factor of safety for the embankment was increased following the modifications described above. During this evaluation, the River Embankment's lower slopes were flattened from 1V:8H to 1V:12H, and ultimately 1V:85H at the downstream extent (PFRA 1962 and Jaspar and Peters 1979).

The previously described stability evaluations were all completed by assuming that the slip surface passed through the soft shale, close to the River Sand-Snakebite shale interface. However, the results of the instrumented monitoring program indicated that movements were occurring in the hard shale near the shale's contact with the Ardkenneth sandstone.

Following the completion of the embankment construction, its stability was further evaluated using the Morgenstern-Price method and a composite slip surface representing the observed displacement. The calculated factor of safety from this evaluation was found to be acceptable.

The analysis showed that in order to achieve a factor of safety of 1.0 using back calculation, an ϕ_r' value of 2° would have to be assumed for the shear zone (Jaspar and Peters 1979). The geometry of the embankment at various stages of construction is illustrated in Figure 2.1.

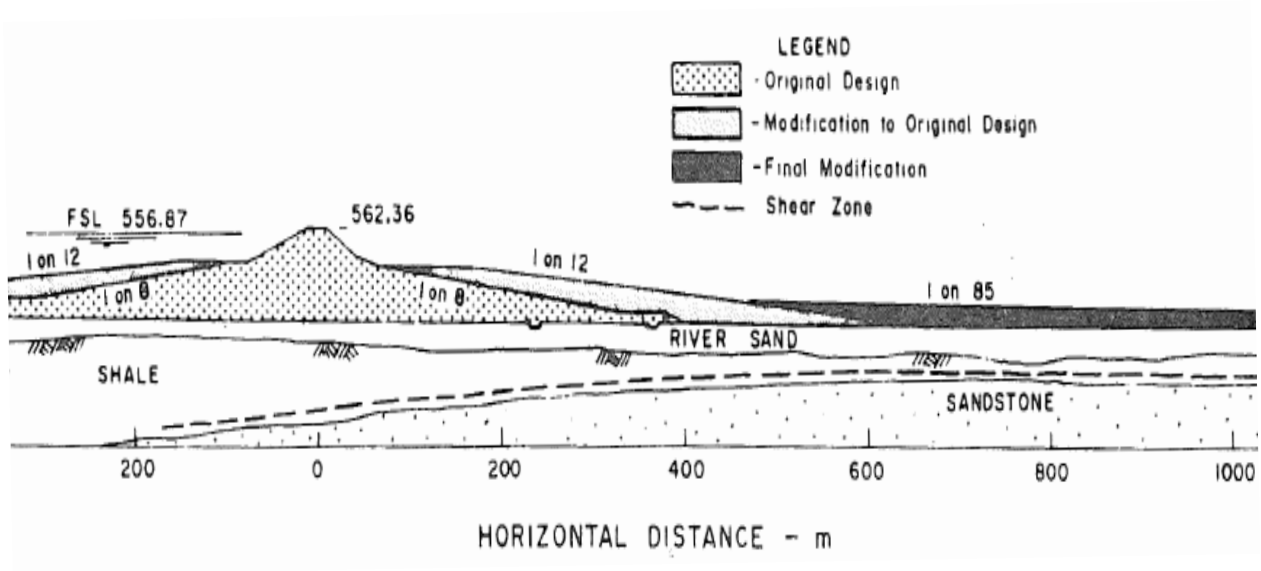

Figure 2.1 Stages of River Embankment design and construction (Jaspar and Peters 1979)

2.10.2 Deformation Models

Following construction, annual displacements were identified within the shale shear zone. In an attempt to predict the annual displacements, a finite element stress-deformation model was completed in the late 1970s. This finite element stress-deformation model was intended to represent the River Embankment; however, with the modelling capabilities at the time, this was found to be not feasible. Due to its smaller size and similar movements, the Coteau Embankment was selected for the finite element stress-deformation analysis, with the hope that the deformation mechanism revealed by the analysis would be transferrable to the River Embankment. Ultimately, a comparison to the River Embankment was not completed. The model's primary purpose was to reveal and understand the correct deformation mechanism and not to be excessively concerned about predicting the magnitude of movements. Total stress analysis was used for this evaluation because the coupling of pore-pressure and stress response for effective stress analysis was not computationally feasible at the time of the evaluation. The finite element evaluation revealed that the primary reason for movement of the embankment was the reservoir acting on materials that undergo non-linear deformation within the shear zone at

high levels of shear strength mobilization (Morgenstern and Simmons 1980, Morgenstern and Simmons 1982).

In an attempt to predict the annual deformations, a simple mechanical model was also developed to predict displacements based on historical movements and reservoir level. The model consisted of a spring representing the resisting elements, a mass representing the embankment and both were acted on by a force representing the hydrostatic pressure of the reservoir. The observed displacement and reservoir level were used to create a correlation to set the parameters on the model. It was found that to maximize the confidence in the predictions from this model, similar hydrograph patterns were needed. It was also found that if any difficulties were encountered in curve fitting the model to recently observed data perfectly, the model's predictions would be compromised (PFRA 1992).

2.11 Knowledge Gaps

The literature review identified that the mechanism causing movement within the shale was not well understood. The previous modelling attempts have not been able to accurately predict the displacements in the foundation. The previous modelling attempts included stability modelling using limit equilibrium analysis, a mechanical model, and a stress-strain model of an adjacent embankment. The stability model did not provide an indication of the deformation or of the mechanism of movement. The mechanical model only attempted to provide a "black box" correlation between the reservoir fluctuation and displacement. Finally, the finite element model was limited by the computation capabilities at the time and was unable to accurately predict the movement magnitude. Therefore, the scope of this work was developed from the lack of understanding of the mechanism of movement within the foundation of the embankment.

Through the literature review the knowledge gaps were identified and the general concepts that were used through the remainder of the thesis were developed. The following chapter will review the historical instrumentation data and will be used to develop a conceptual model to fill the identified knowledge gap.

CHAPTER 3 SUMMARY OF INSTUMENTATION DATA

3.1 Overview

This section provides an overview of the historical instrumentation data review undertaken. The historical data provided guidance in terms of the interpretation of the critical variables affecting the deformation and stability of the River Embankment. These critical variables included: the compressibility and residual shear strength of shale, the piezometric pressure, and loading conditions.

The historical data used throughout this work focused mainly on the post-construction movements from 1969 forward; however, a brief discussion of the deformations during construction is also provided for completeness.

The following general process was followed in order to complete the review of historical instrumentation data. 1) Initially, temporal plots of monitoring data were evaluated to establish the overall trends. 2) The monitored data was then compared with reservoir fluctuations over a recent10-year period to determine if reservoir fluctuations influenced the monitored data. 3) The instrumentation was then compared to the embankment geometry and foundation stratigraphy to determine their effect. 4) Following the initial evaluation of the instrumentation data, detailed investigations were undertaken to determine potential correlations that could be of assistance in developing a conceptual deformation model of the embankment.

The plots included in this chapter provide only the salient aspects of the data reviewed. Appendix A provides a more comprehensive presentation of data. Figure 3.1 illustrates the location of crucial instrumentation on the River Embankment

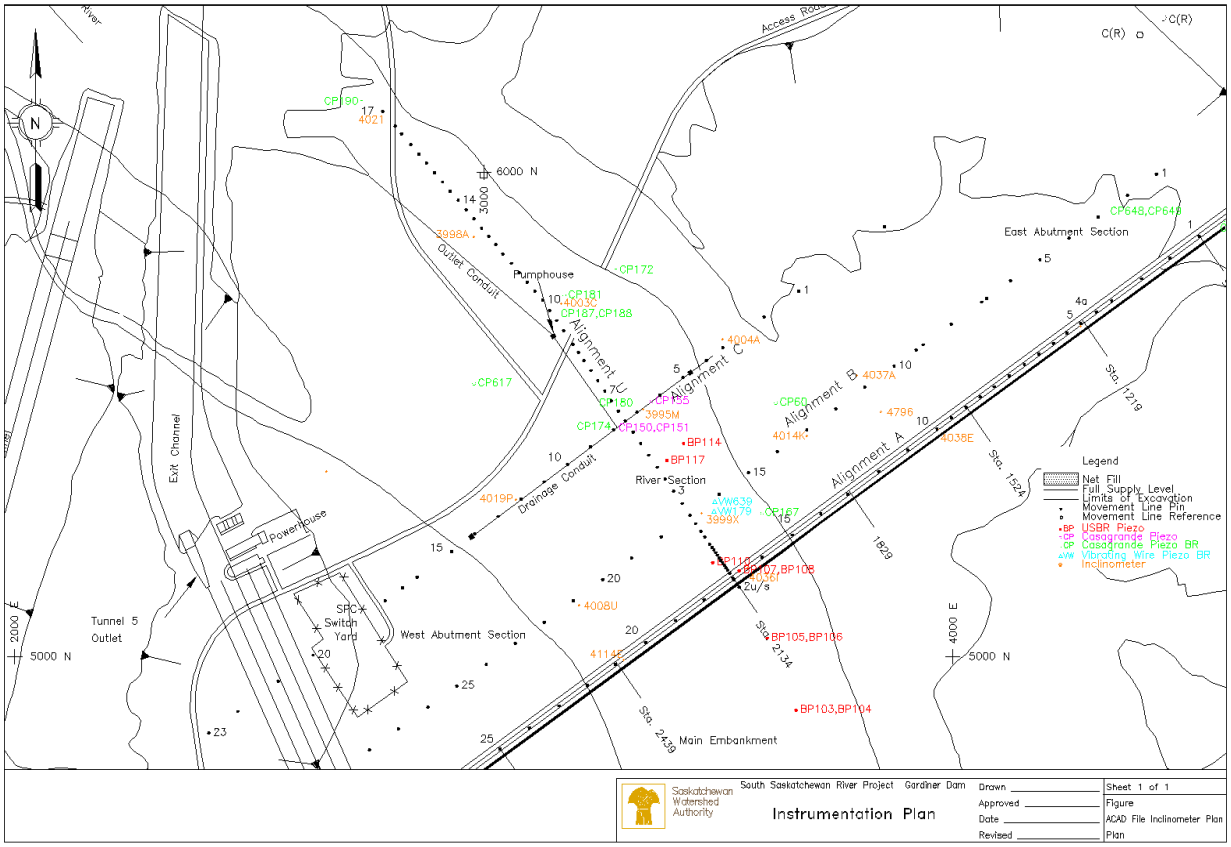

Figure 3.1 River Embankment, plan of critical instrumentation

3.2 Construction and Early Performance of the Embankment

The River Embankment was constructed in several stages. The stages prior to river diversion included building a large section of the embankment from the West Abutment to the Plateau Embankment and the East Abutment, therefore, leaving a section open for the river to pass. Following this stage, the river was diverted through the tunnels and the River Embankment was completed.

Prior the diversion of the river, the West and the East Abutments of the River Embankment experienced movement primarily in both the upstream and downstream directions with secondary movements towards the open river section. During these stages of construction, slope inclinometer casings and surface monitoring pins were quickly destroyed; therefore, a continuous record of displacement was not possible (Jaspar and Peters 1979).

In early 1964, the river was diverted through the tunnels and construction of the remainder of the River Embankment commenced. During the early stages of this phase of construction some of

the foundation shear zone displacements were not recorded as the installed slope inclinometer casings were not deep enough to intercept the later identified shear zone. The foundation displacement was detected from the surface monitoring pins installed in the Relief Well Drainage Conduit, 400 m downstream of centerline. In late 1965, deeper slope inclinometer casings such as SI3999 and SI3995 were installed and the shear zone in the hard shale near the shale contact with the Ardkenneth sandstone was discovered. Prior to the direct monitoring of the deep shale shear zone, an estimated 1 m of downstream movement occurred at SI3999 in 1964-1965. During construction of the River Embankment, approximately 2 m of settlement occurred in the foundation below the crest and 2 m of horizontal downstream movement was seen at SI3999.

The post-construction displacements were observed to typically increase during the raising of reservoir level. The displacements stopped as the reservoir level remained stable or was lowered. The major portion of the displacement occurred within 700 m downstream of the dam centerline and little to no movement occurred further downstream of this point (Jaspar and Peters 1979, Rahman and Kilgour 2000).

The piezometers installed in the shear zone showed an increase in porewater pressure during embankment construction. Since the end of construction, these piezometers show dissipation of excess porewater pressures. The piezometric levels in the sandstone were lowered by pumping since 1967 in order to increase the dissipation of excess porewater pressure in the shale; however, this strategy had limited success (Jaspar and Peters 1979, Rahman and Kilgour 2000).

3.3 Reservoir Level Fluctuations

The reservoir level was directly related to the flow patterns of the South Saskatchewan River basin, which stretches upstream of Lake Diefenbaker to the Rocky Mountains. The size of the drainage basin lead to the development of a distinct inflow pattern consisting of a relatively low winter flow, relatively small spring peak in April from local runoff, and a larger peak in May or June from snowmelt in the mountains. The inflow then receded to the winter flow in August or September (PFRA 1980).

The inflow pattern developed into a distinct reservoir level pattern. The reservoir level was typically lowest at the start of May followed by an increase to the peak at the end of June. The

reservoir level then remained stable until the end of October, before it dropped off steadily until spring. The annual reservoir level magnitude and timing varied greatly from year to year, creating great difficulty predicting it accurately beyond a few months.

The median operating range of reservoir level between 1980 and 2010 was considered the normal range for this work (Grajczyk 2012). The historic operation range between 1980 and 2010 is shown in Figure 3.2 and Figure 3.3. The median reservoir level range of Lake Diefenbaker was from elevation 550.8 m to 556.0 m (5.2 m fluctuation) as shown in Figure 3.4. The historic maximum (highest) reservoir level was near full supply level (FSL) elevation 556.9 m and the minimum (lowest) reservoir level was at elevation 547.6 m. The maximum historic fluctuation in reservoir level was 9.3 m.

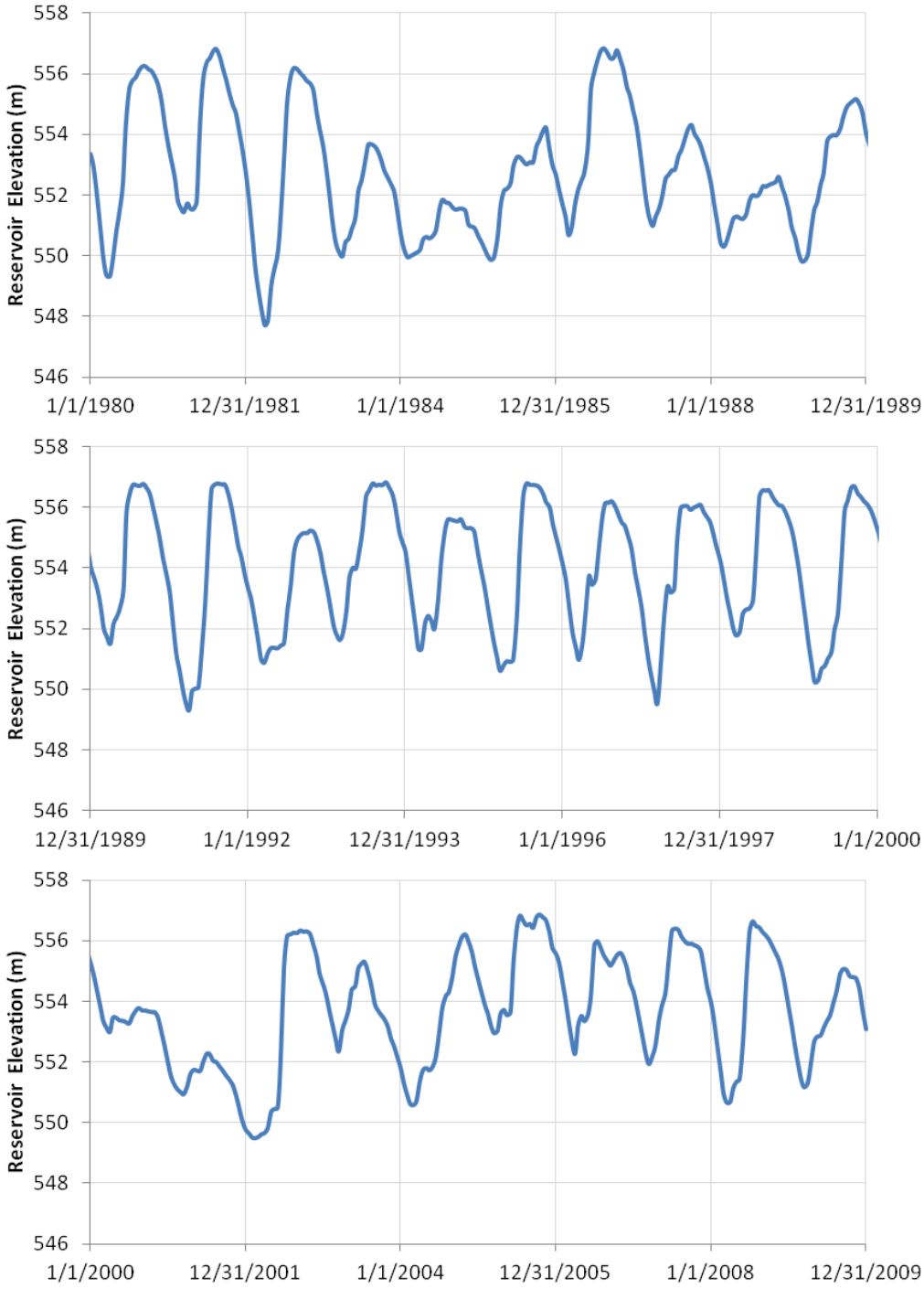

Figure 3.2 Historic record of reservoir level from 1980 to 2010

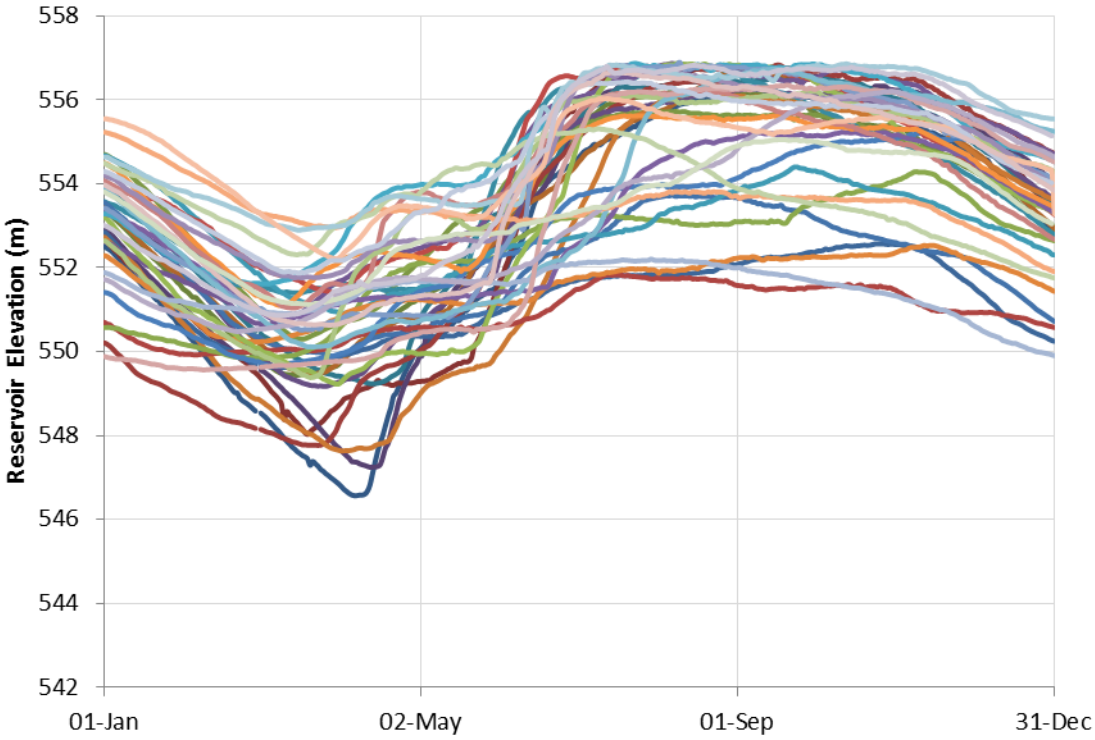

Figure 3.3 Annual reservoir level cycles from 1980 to 2010

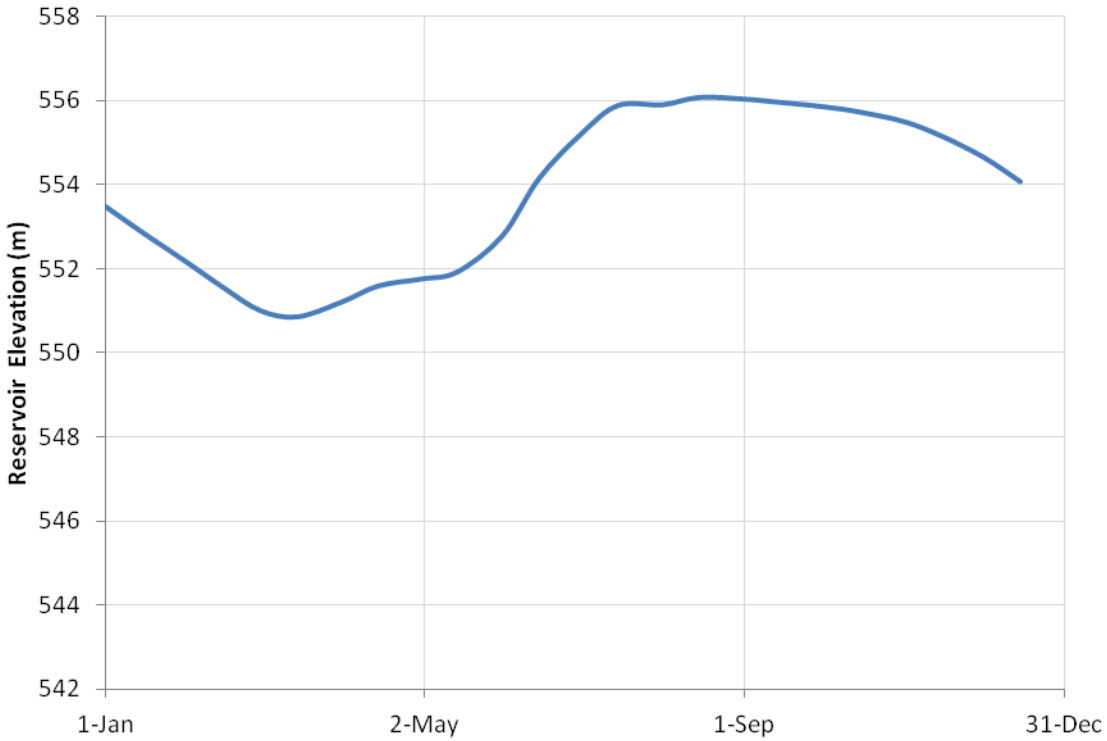

Figure 3.4 Median reservoir level for a typical operating year

3.4 Vertical Movements

Vertical displacement within the foundation and on the embankment surface has been measured since construction using surface movement line pins and USBR settlement gauges. The surface vertical displacement was monitored on three lines parallel to the dam center line, Line A (dam center line), Line B (150 m downstream) and Line C (400 m downstream), and one line perpendicular to the dam center line, Line U (Station 2134). The foundation vertical displacements were monitored on two parallel lines, at dam center line and 125 m downstream. The locations of these instruments are illustrated in Figure 3.5.

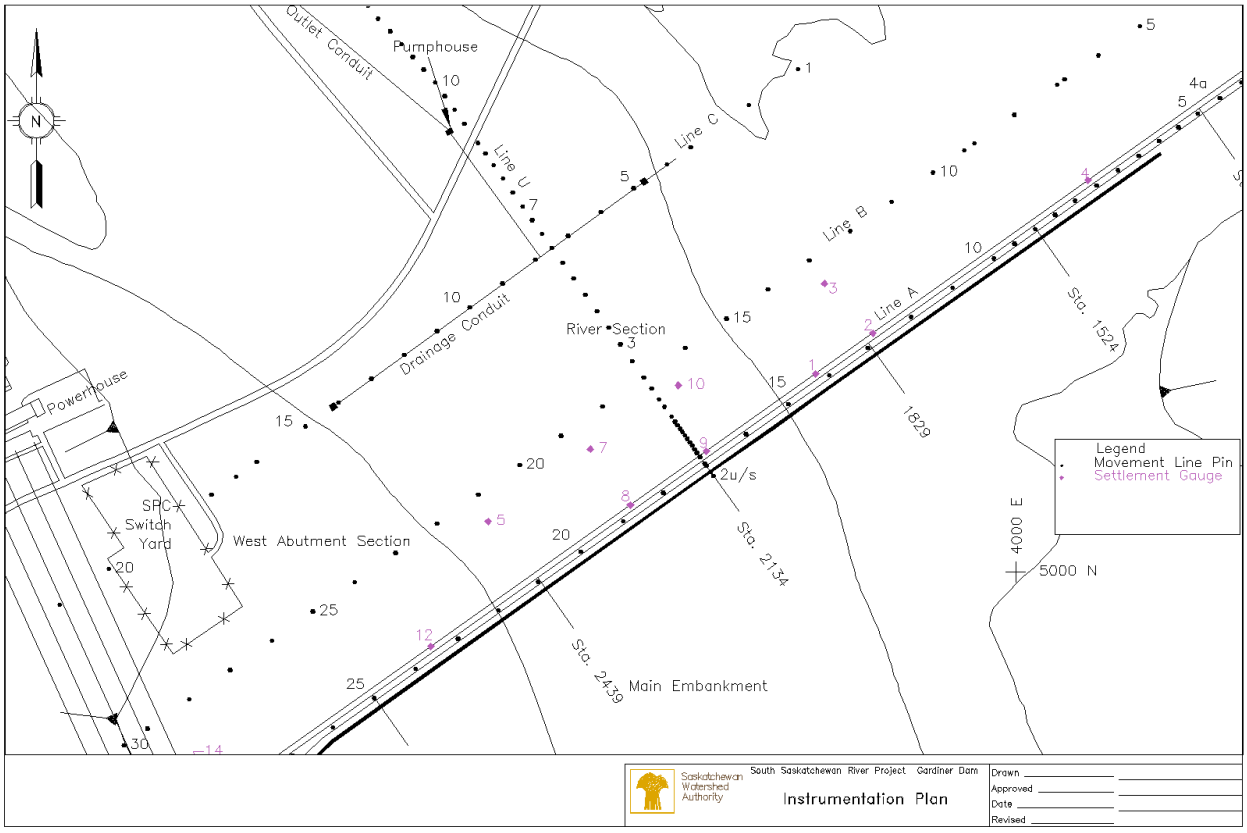

Figure 3.5 Plan view of the River Embankment showing vertical displacement instrumentation

Throughout this evaluation, the movement line pins were used for observing trends and the deeper settlement gauges were relied upon for accuracy. Due to the relatively shallow installation of the surface pins, they were frost susceptible and may not be reliable. Because of the larger number of movement line pins, they were thought to be still useful for interpretation of vertical displacement.

Temporal variation of vertical displacement was evaluated from 1970 to 2010. Figure 3.6 illustrates the post-construction vertical displacement of the foundation monitored at two instrument locations SG9 (embankment centerline), and SG10 (125m downstream). The embankment continued to settle with time; however, the rate of settlement decreased steadily. This decrease is likely the result of dissipation of excess porewater pressures developed in shale during construction and the embankment and shale approaching the end of primary consolidation. As expected, the embankment settled at a higher rate at the dam centerline than at the downstream toe of the dam because of the variation in vertical stress. The vertical stress was greater at the dam centerline compared with that at the downstream toe of the embankment.

Figure 3.7 presents a comparison between vertical displacement vs. time plots at locations SG9 and SG10 and reservoir level vs. time plot for the ten year period between 1995 and 2005. Although the vertical displacement measurements were more sporadic than the reservoir level measurements, it was possible to assume from these measurements that the rate of settlement of the embankment increased with the raising of the reservoir level and that the embankment hardly settled during the lowering of the reservoir level. It is also possible to observe that the increased movement rates occurred during a drop in the reservoir level. However, this may be a function of the sporadic nature of the measurement frequency. Since the measurement were generally taken at the reservoir peak and lowest point, it was not possible to determine the actual response of the vertical movement to changes in reservoir level.

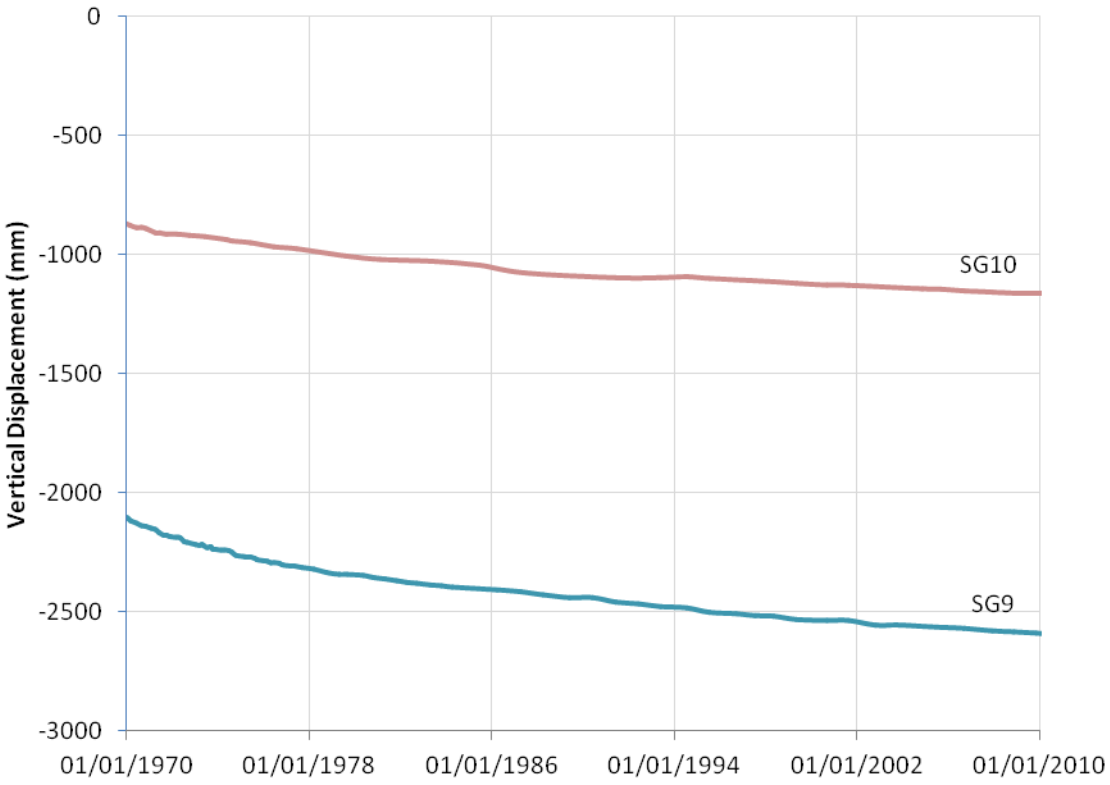

Figure 3.6 Foundation vertical displacement vs. time plot along Station 2134, 1970 to 2010: SG9 (embankment centerline), and SG10 (125 m downstream)

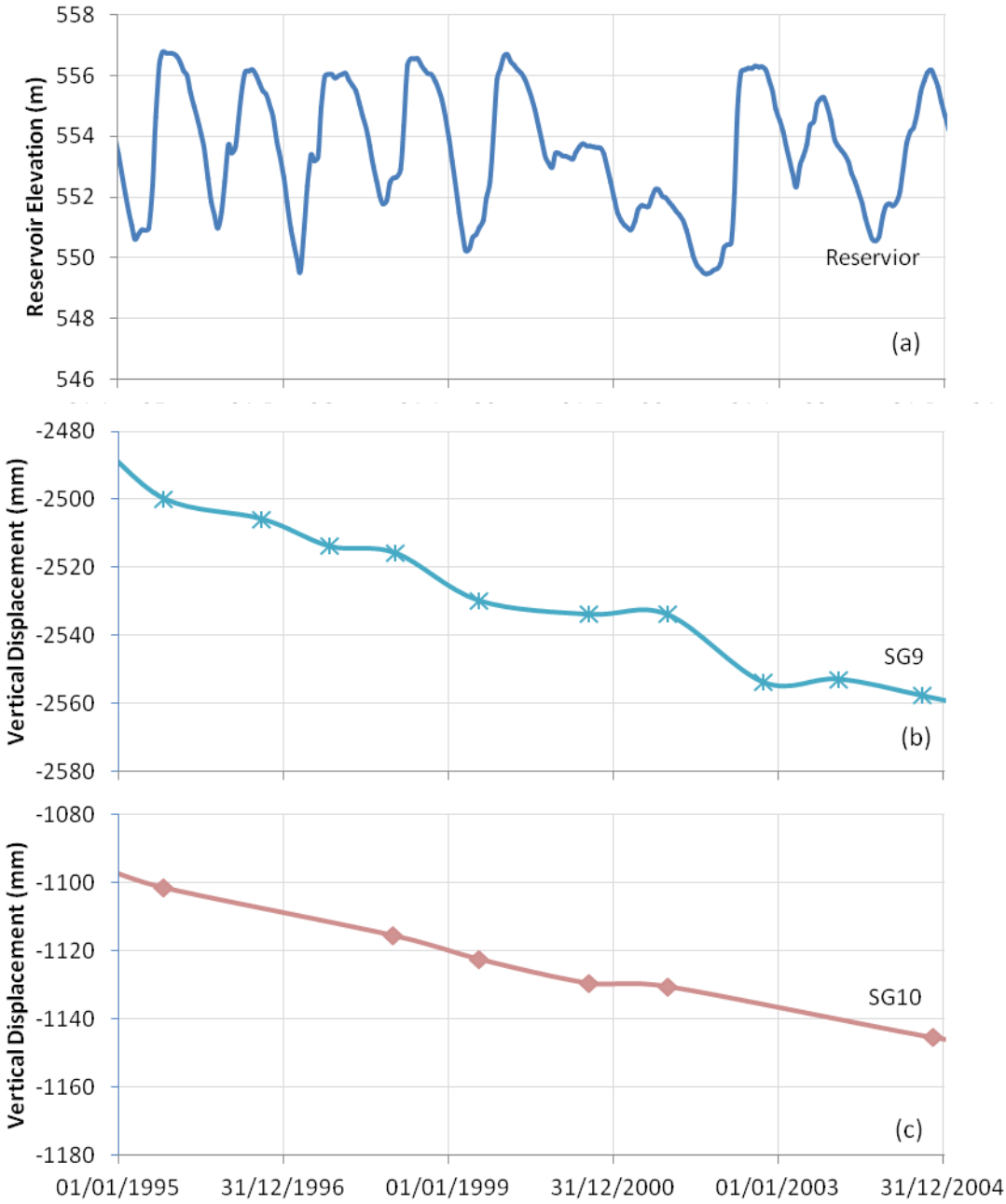

Figure 3.7 Foundation vertical displacement response to reservoir level fluctuations, 1995 to 2005: (a) Reservoir elevation, (b) SG9 vertical displacement (embankment centerline), and (c) SG10 vertical displacement (125 m downstream)

The foundation stratigraphy greatly influenced the vertical displacements within the foundation and on the surface. To illustrate the influence of the foundation stratigraphy, the measured displacements for select time periods were plotted against a scaled section as shown in Figure 3.8 to Figure 3.10 and the effects due to the foundation stratigraphy against a scaled profile are shown in Figure 3.11. The magnitude of vertical displacement on the surface and the foundation decreased downstream of the embankment centerline and to the right and left of Station 2134. As time progressed, the magnitude of the displacement lines become closer, indicating a smaller displacement rate, similar to Figure 3.6. The surface and foundation displacements also indicated a similar pattern with a more distinct pattern of movement in the foundation than in the movement line pins. Figure 3.8 to Figure 3.10 shows that the presence of the disturbed landslide debris, identified as a tongue of shale at Station 2100, within the river sand had a marked increase in the settlement measured in this area. The disturbed shale would be expected to have a lower preconsolidation pressure than the surrounding relatively intact shale; therefore, allowing for more displacement with the same embankment stress.

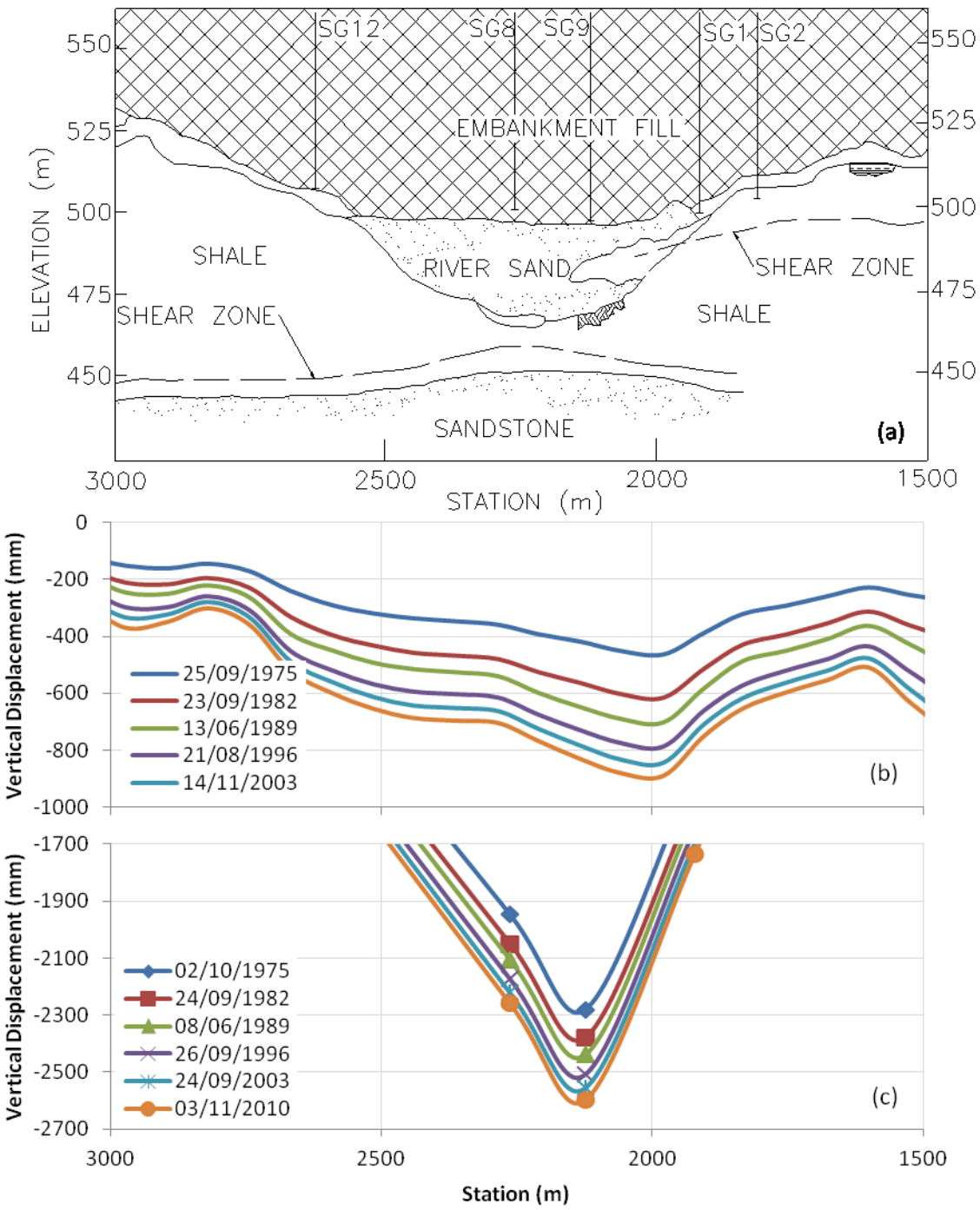

Figure 3.8 Distribution of vertical displacement, embankment centerline: (a) Foundation stratigraphy and embankment geometry, (b) Movement line pins vertical displacement, and (c) Foundation vertical displacement

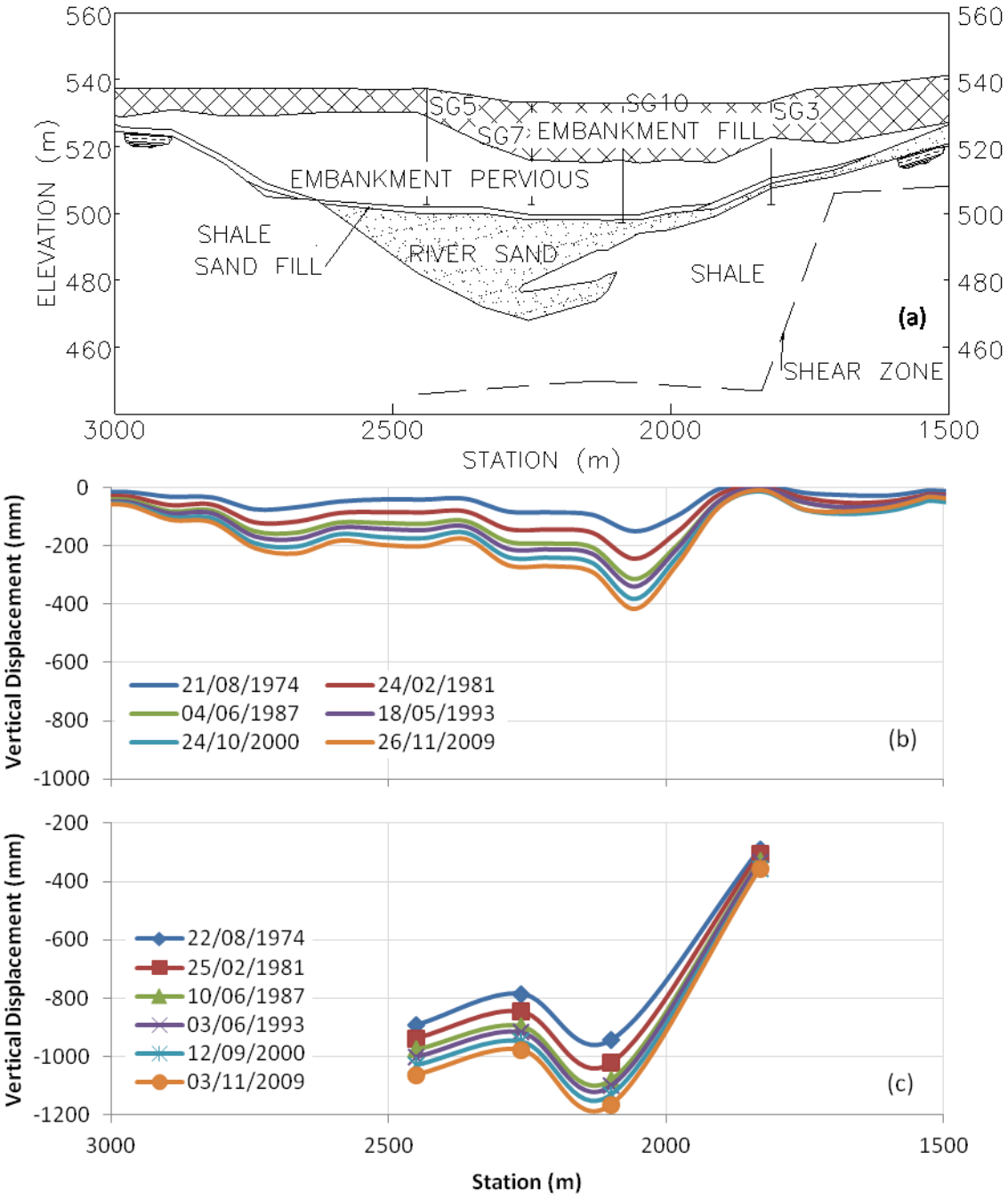

Figure 3.9 Distribution of vertical displacement, 150m downstream: (a) Foundation stratigraphy and embankment geometry, (b) Movement line pins vertical displacement, and (c) Foundation vertical displacement

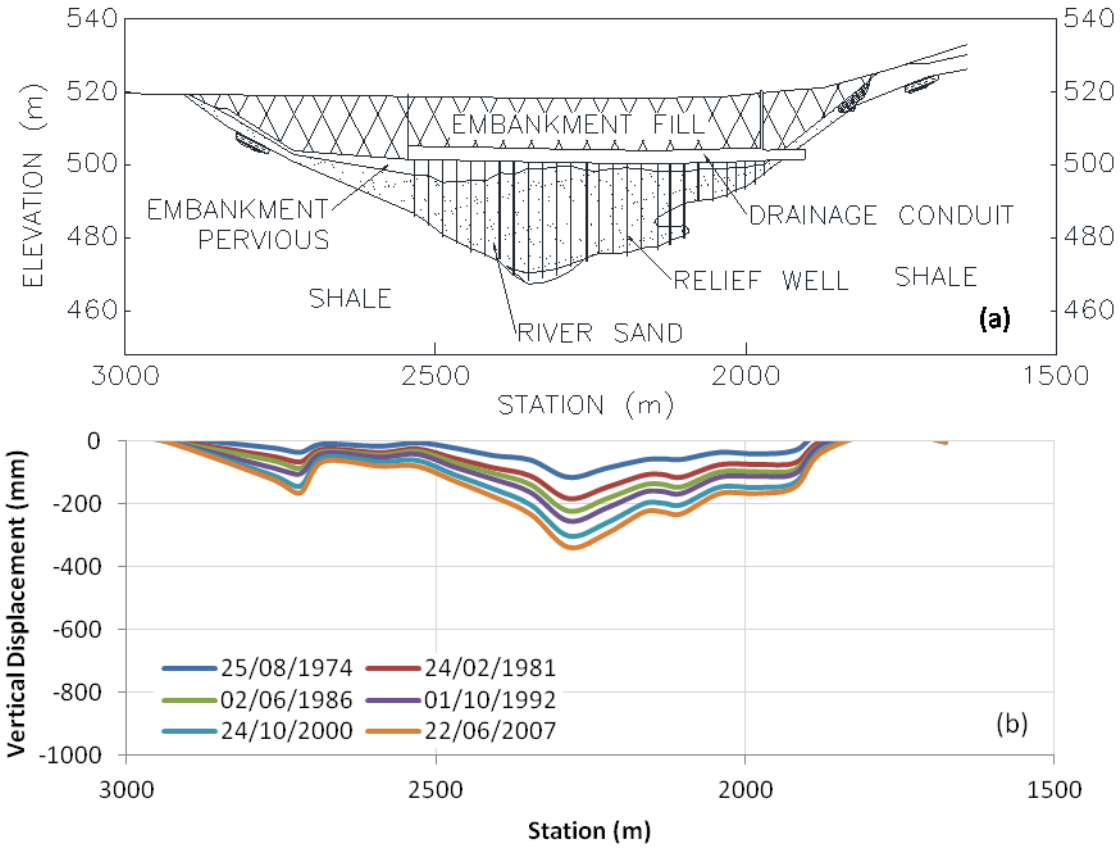

Figure 3.10 Distribution of vertical displacement, 400 m downstream: (a) Foundation stratigraphy and embankment geometry, and (b) Movement line pins vertical displacement

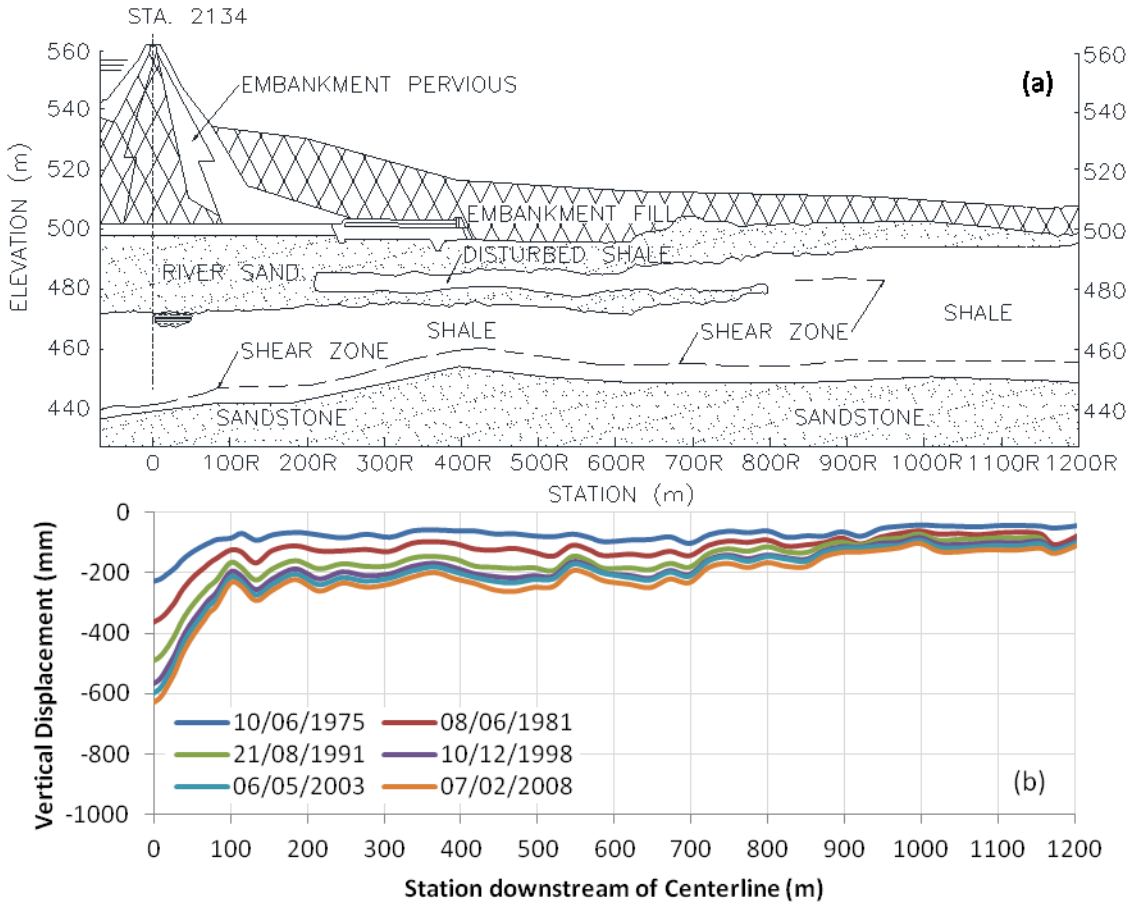

Figure 3.11 Distribution of vertical displacement, Station 2134: (a) Foundation stratigraphy and embankment geometry, and (b) Movement line pins vertical displacement

3.5 Horizontal Movements

The horizontal displacements were monitored with the use of inclinometer casing and surface movement line pins. The movement line pins were located on three lines parallel to the dam centerline and on one line perpendicular to the centerline similar to the vertical movement pins. Inclinometer casings of interest in this evaluation were installed roughly parallel to Station 2134 and at the same locations as Line A (dam center line), Line B (150 m downstream), and Line C (400 m downstream) as shown in Figure 3.12.

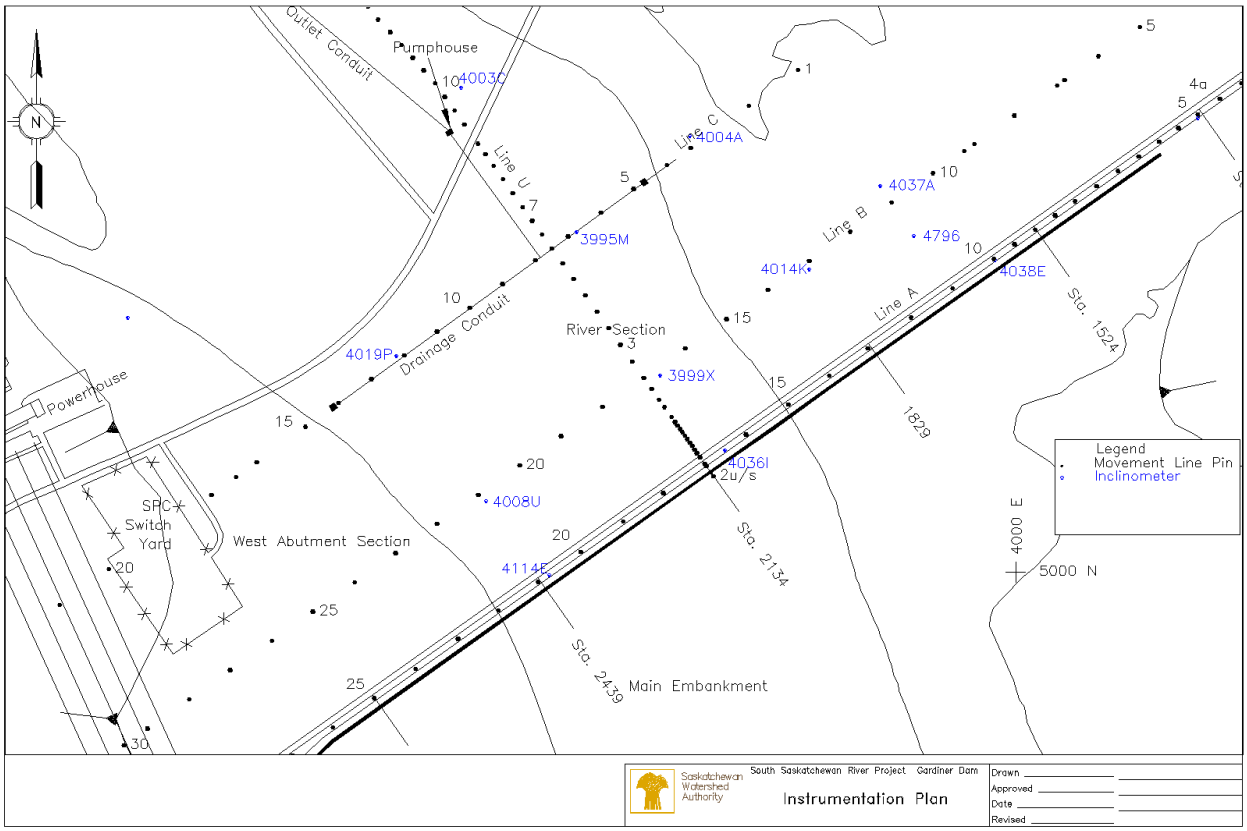

Figure 3.12 Plan view of the River Embankment showing horizontal displacement instrumentation

During this evaluation, it was found to be difficult to compare the total magnitude of the horizontal displacements measured between instrument types as they were installed at different times and at different stages of construction. The displacement for inclinometers for the dam center line (SI4114, SI4036, and SI4038) were reported from 1969 forward; whereas, the displacement from the remainder of the inclinometers were reported from 1965 forward. Therefore, this evaluation only compared the relative horizontal displacements. The discussion of the foundation moments in this section was limited to the shear zone displacement.

The horizontal displacement compared to time was evaluated using the monitoring data obtained from four inclinometer casings along Line U (Sta. 2134 m) between 1970 and 2010. These select instruments recorded the shear zone displacement from the dam centerline to approximately halfway towards the downstream limit of the embankment. The foundation horizontal displacement rates decreased since construction and became near asymptotic as shown

in Figure 3.13. The largest magnitudes as well as the largest rate of horizontal displacement occurred near the downstream toe of the main embankment.

The influence of reservoir level fluctuations on the shear zone horizontal displacements was investigated with the help of the monitoring data obtained using inclinometer SI3999 (150 m downstream). SI3999 was selected for this evaluation as it recorded the largest annual deformation within the foundation shear zone. The foundation horizontal movements indicate a relationship with the reservoir level fluctuations, as illustrated in Figure 3.14. When the reservoir level increased, the foundation displacement magnitude and rate also increased. When the reservoir decreased or remained low, there was minimal horizontal displacement.

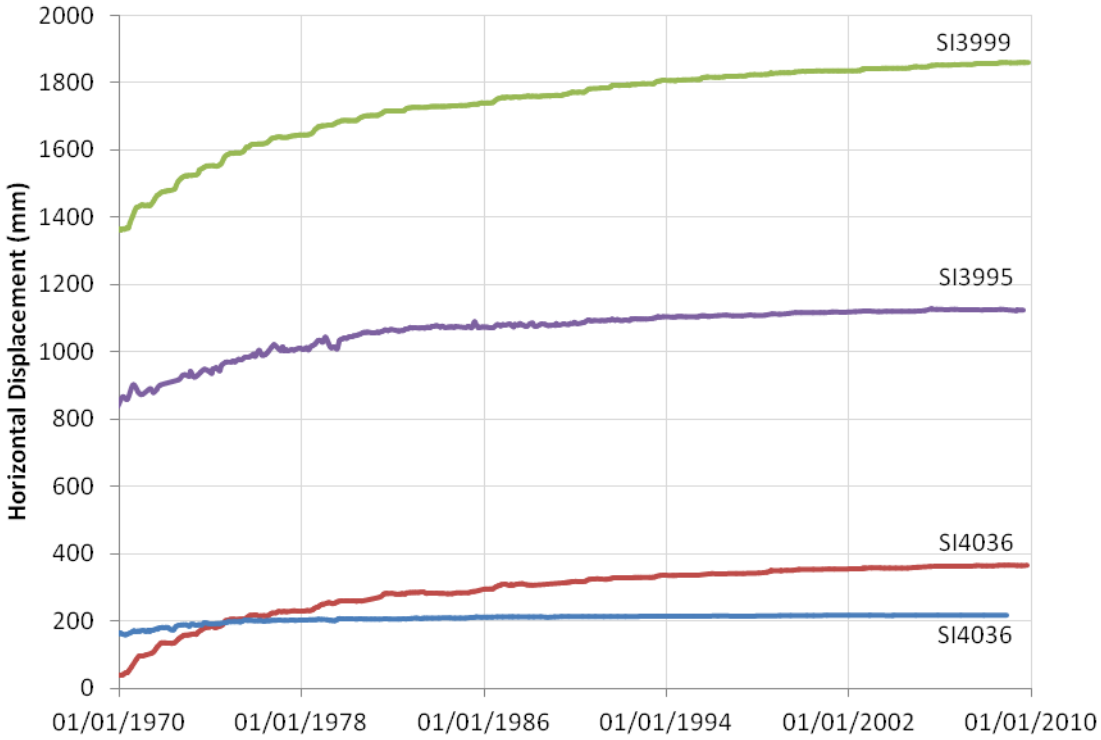

Figure 3.13 Shale shear zone horizontal displacement vs. time plot along Station 2134, 1970 to 2010: SI4036 (embankment centerline), SI3999 (150 m downstream), SI3995 (400 m downstream), and SI4003 (670 m downstream)

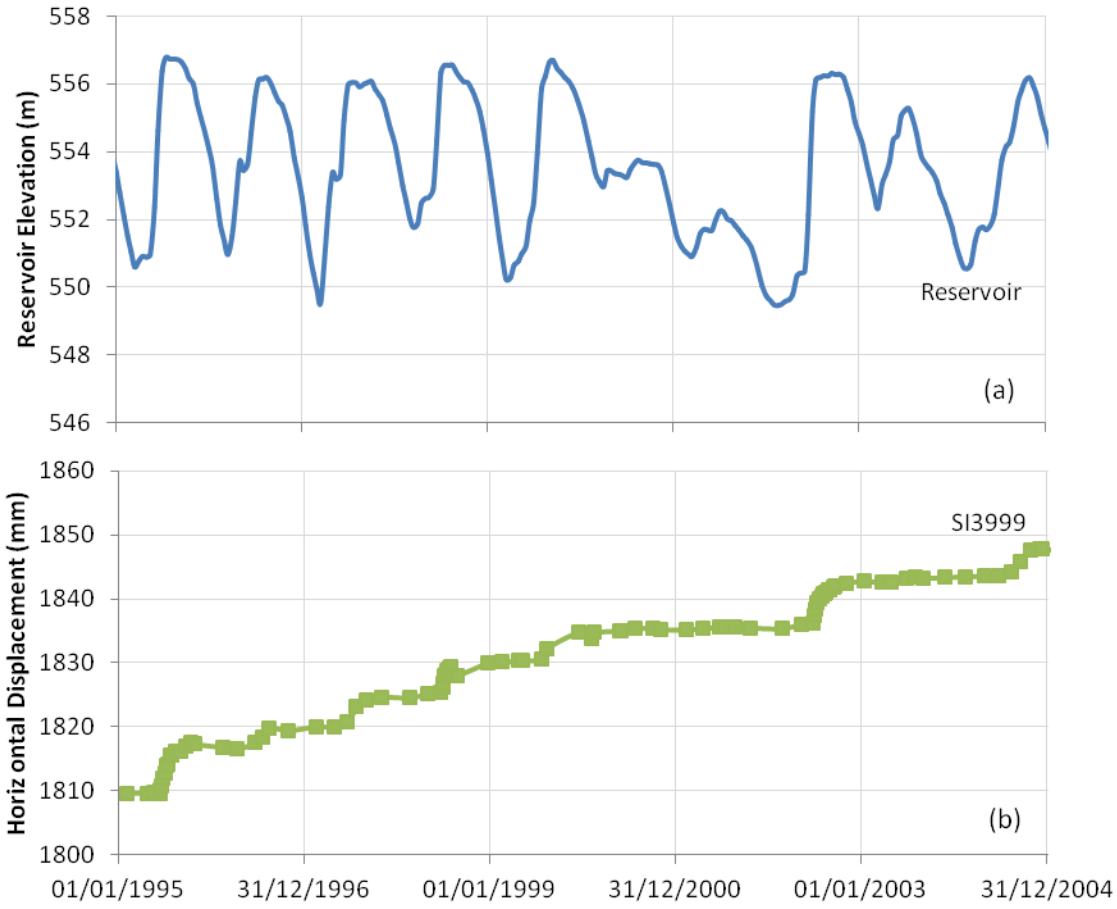

Figure 3.14 Shale shear zone horizontal displacement response to reservoir level fluctuation, 1995 to 2005: (a) Reservoir elevation, and (b) SI3999 shear zone horizontal displacement (150 m downstream)

The pattern of horizontal movement was generally consistent during each reservoir cycle; however, the measured magnitude varied from year to year. There also appears to be a correlation between the magnitude of change in the annual reservoir level and the magnitude of horizontal displacement, with larger increases in reservoir level, resulting in larger increase in displacement.

The influence of embankment geometry and foundation stratigraphy was evaluated in two steps. The first step involved evaluating the distribution of horizontal displacement profile from the foundation to the embankment surface, measured with the same four select inclinometers as discussed previously. The second step involved comparing the movement line pins and shear zone horizontal displacement profiles with the geometry of the embankment and stratigraphy of the foundation.

The first step involved comparing the embankment geometry and foundation stratigraphy against the inclinometer casing profiles. Since each inclinometer casing can only withstand a finite displacement, several inclinometer casings have been installed at the same location. Therefore, only the most recent inclinometer casings profiles are illustrated in Figure 3.15 through Figure 3.18. Each of the reviewed inclinometer casing profiles indicated a defined shear zone within the shale material near the contact with underlying sandstone. In addition, Figure 3.15 illustrates tilting has occurred at the shale/river sand contact where disturbed shale was present in the foundation. From these figures, it can be seen that the shear zone near the bottom of the shale dissipates beyond 400 m downstream as there is no shear zone present at SI4003.

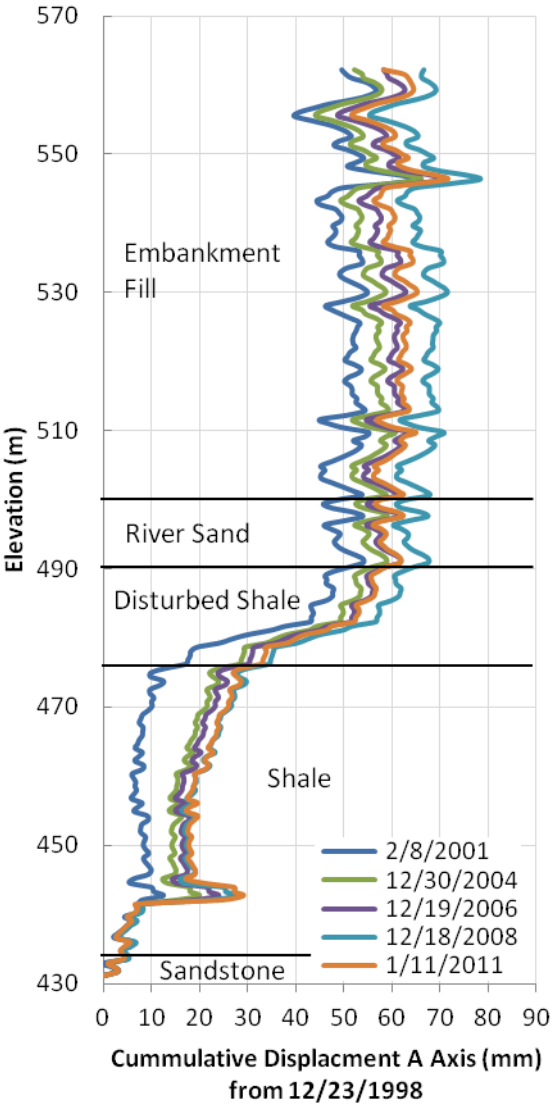

Figure 3.15 Horizontal displacement vs. depth profile at inclinometer location SI4036 (embankment centerline)

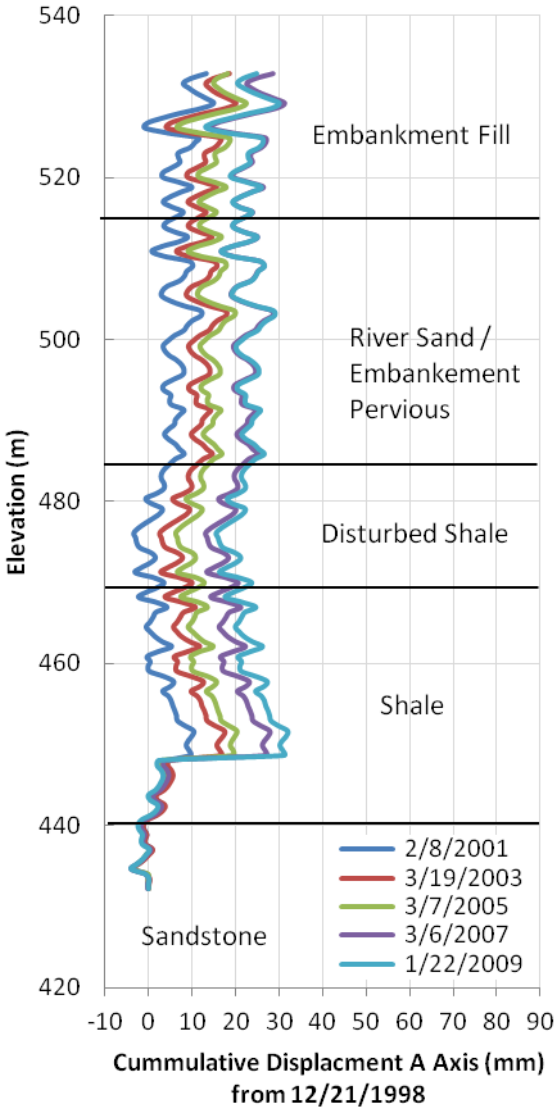

Figure 3.16 Horizontal displacement vs. depth profile at inclinometer location SI3999 (150 m downstream)

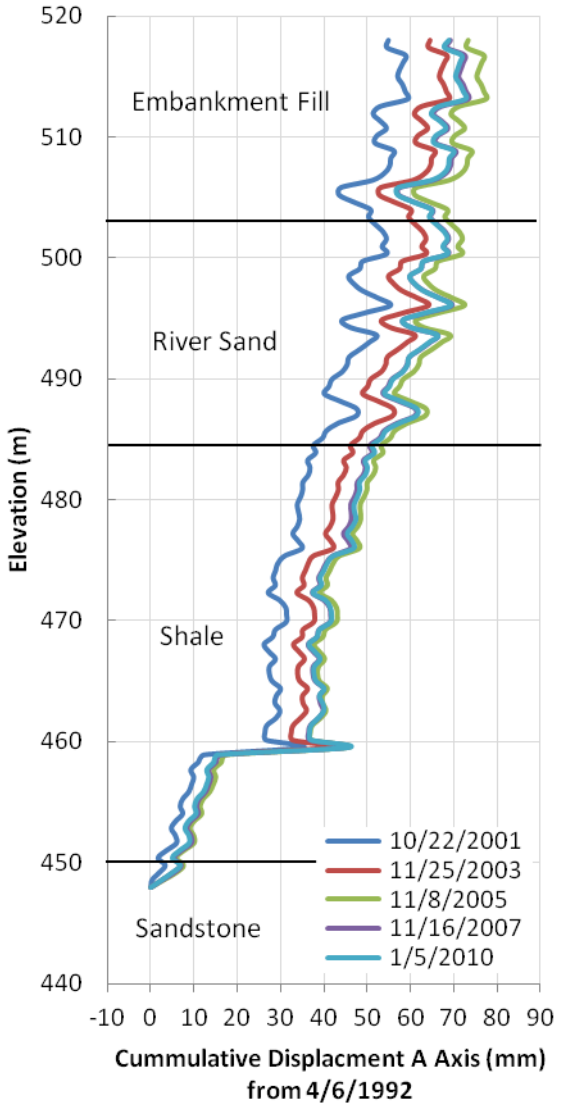

Figure 3.17 Horizontal displacement vs. depth profile at inclinometer location (400 m downstream)

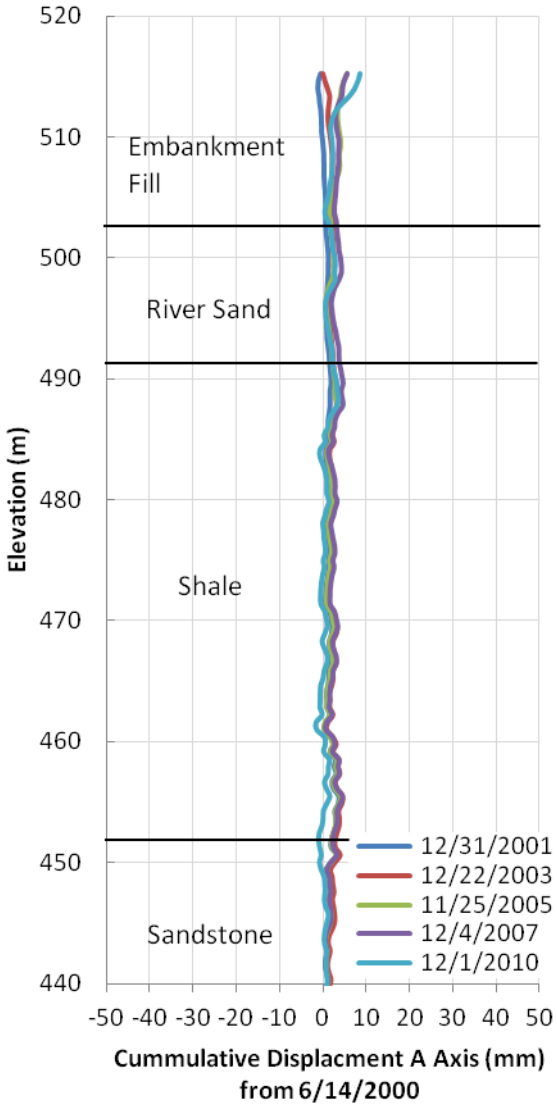

Figure 3.18 Horizontal displacement vs. depth profile at inclinometer location SI4003 (670 m downstream)

The second step evaluated the influence of the embankment geometry and foundation stratigraphy by comparing the measured horizontal displacements for select time periods to a scaled cross-section of the embankment and the foundation. The effect of the embankment geometry and foundation stratigraphy on the horizontal displacement is shown in Figure 3.19 to Figure 3.22. The horizontal displacement within the foundation shown in these figures was the measured shear zone displacement and does not represent a total deformation from the bottom to the top of the inclinometer casing.

The horizontal displacement parallel to the dam center line was greatest where the embankment height was the largest and decreased away from this position as shown Figure 3.19 to Figure 3.21. The horizontal displacement perpendicular to the dam centerline along Station 2134, was greatest at 150 m downstream of the embankment centerline and decreased in the upstream and downstream directions as shown Figure 3.22.

These figures illustrate that displacements measured at the foundation shear zone and the surface movement line pins show a similar pattern. The horizontal displacements measured using the movement line pins are slightly greater than those measured in the shear zone. There could be two reasons for this: 1) since the pins were relatively shallow they were susceptible to frost action and downward creep (Eigenbrod et al. 1987 and Williams 1966) and 2) since only the shear zone displacements are reported on these plots, a portion of the displacements experienced throughout the inclinometer profile have not been reported; i.e. movement above the shear zone.

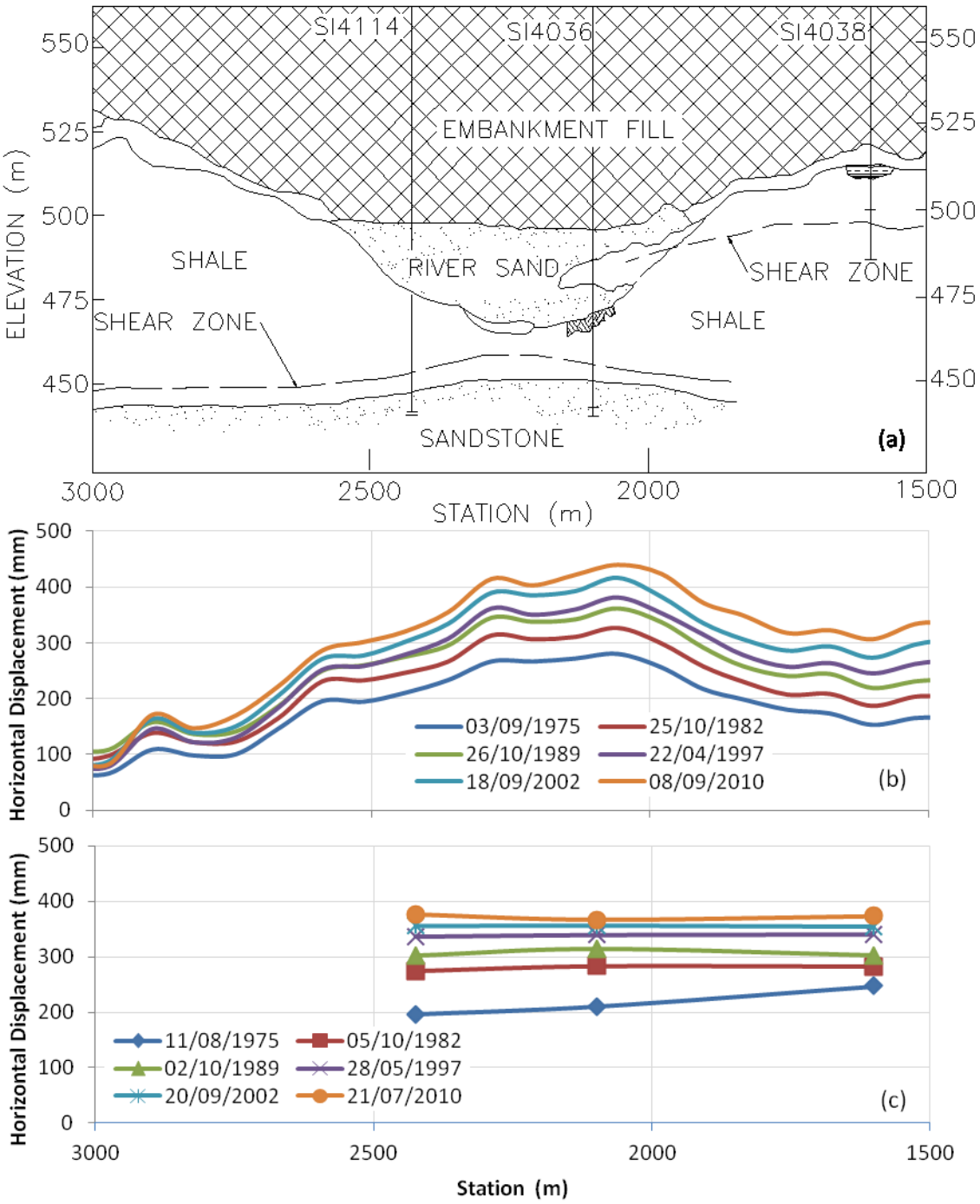

Figure 3.19 Distribution of horizontal displacement, dam centerline: (a) Foundation stratigraphy and embankment geometry, (b) Horizontal displacements measured using movement line pins, and (c) Horizontal displacement of the shear zone within the foundation

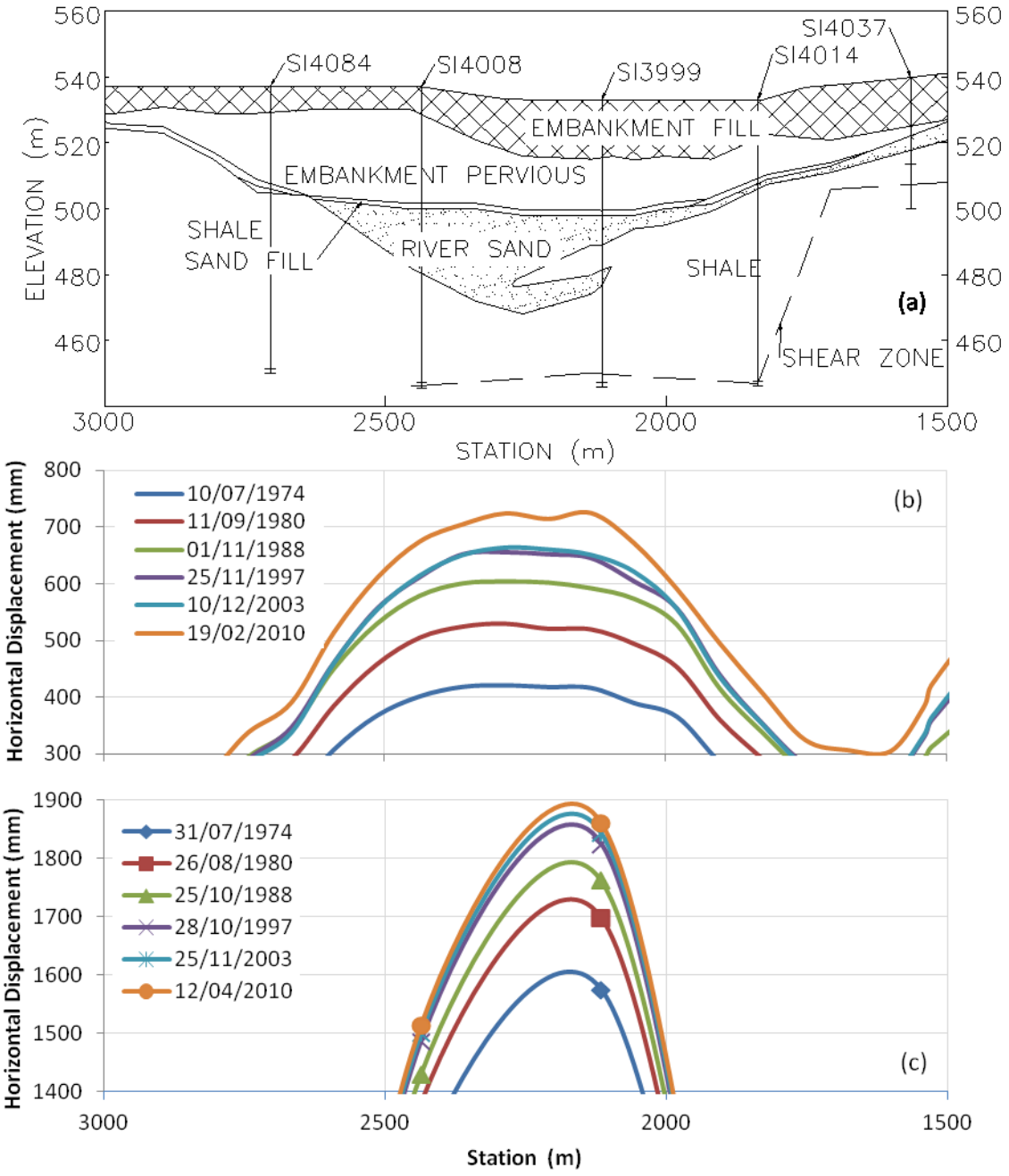

Figure 3.20 Distribution of horizontal displacement, 150m downstream: (a) Foundation stratigraphy and embankment geometry, (b) Horizontal displacements measured using movement line pins, and (c) Horizontal displacement of the shear zone within the foundation

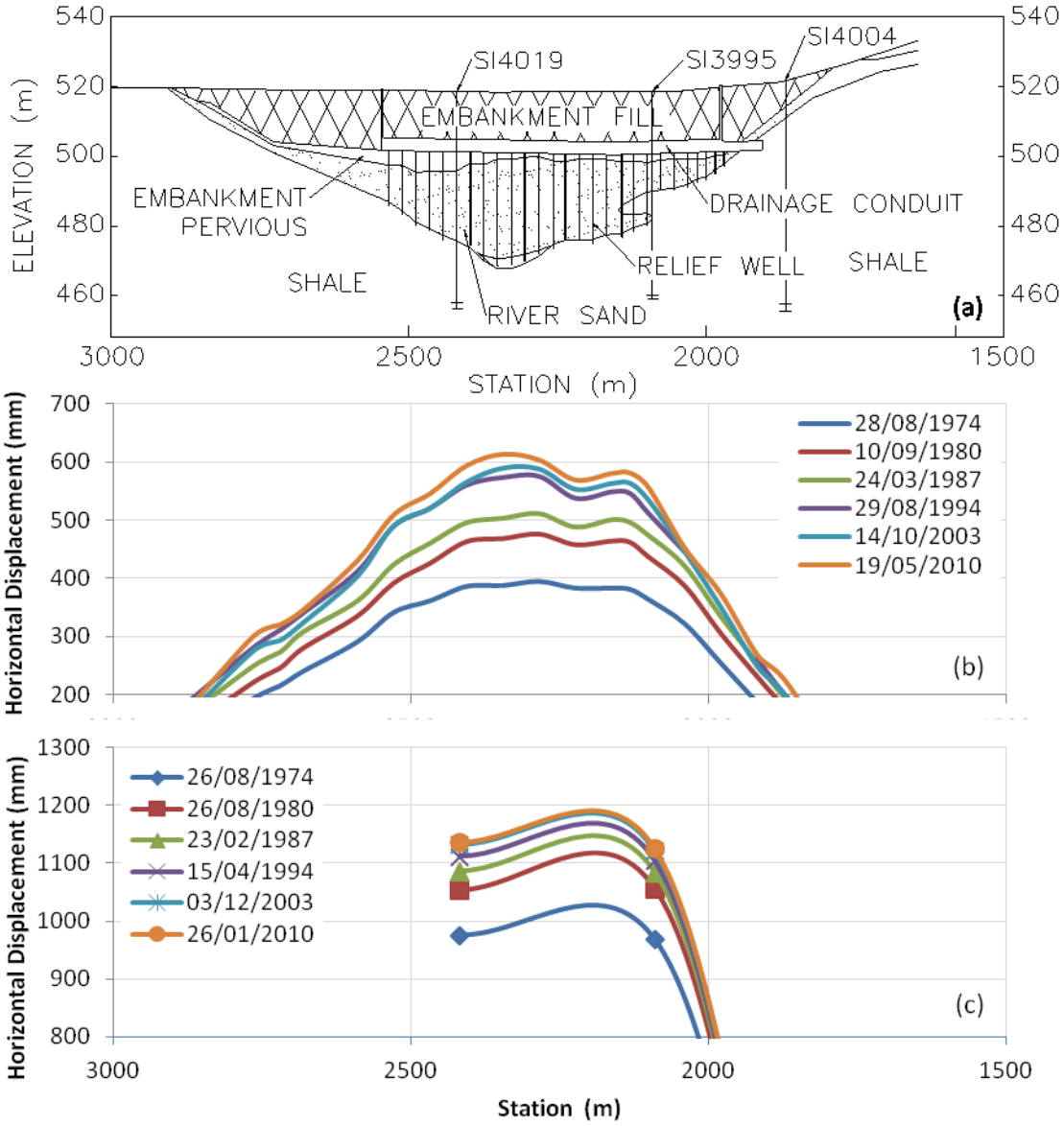

Figure 3.21 Distribution of horizontal displacement, 400 m downstream: (a) Foundation stratigraphy and embankment geometry, (b) Horizontal displacements measured using movement line pins, and (c) Horizontal displacement of the shear zone within the foundation

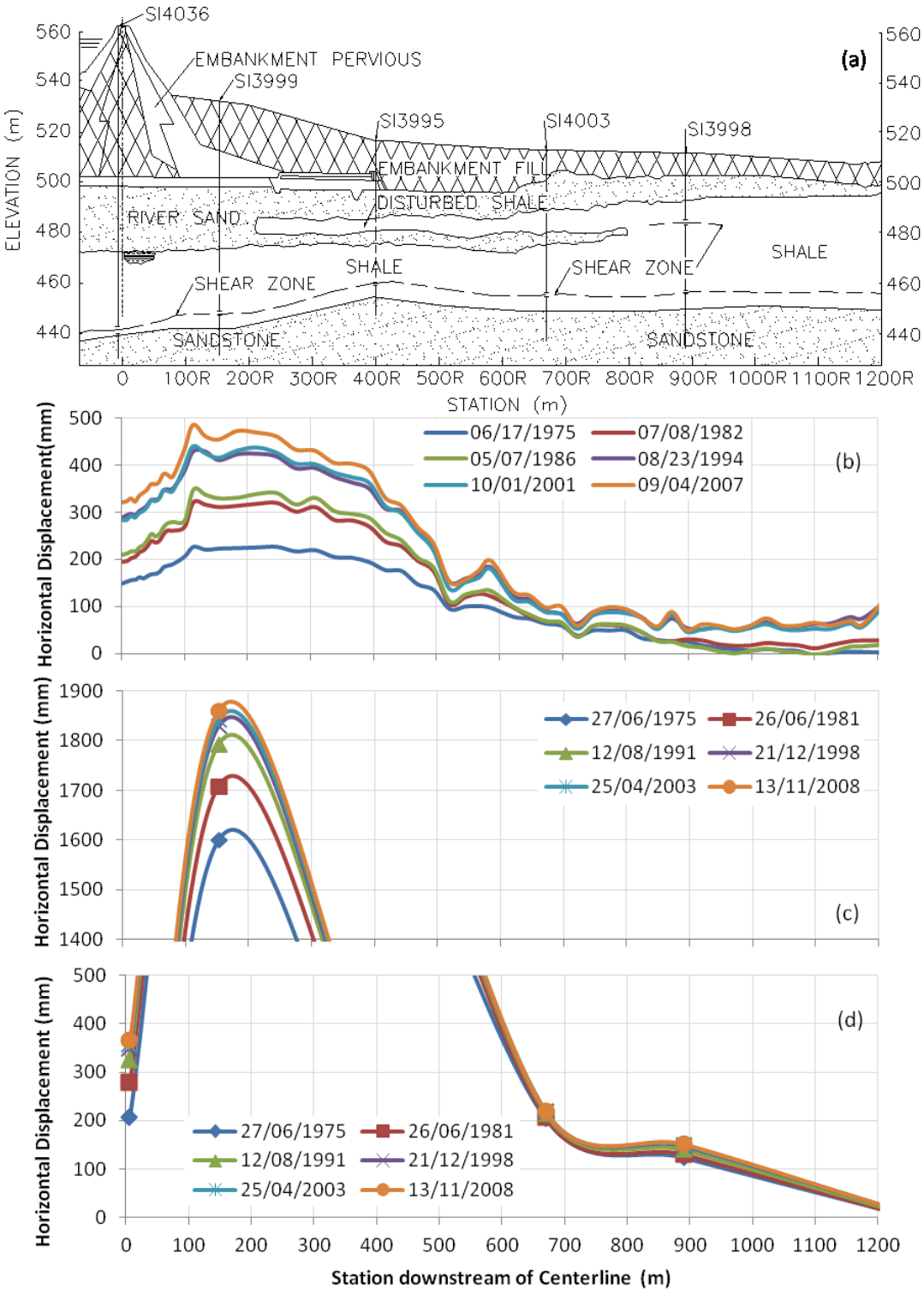

Figure 3.22 Distribution of horizontal displacement, Station 2134: (a) Foundation stratigraphy and embankment geometry, (b) Horizontal displacements measured using movement line pins, (c) and (d) Horizontal displacement of the shear zone within the foundation

3.6 Piezometric Measurements

The piezometric levels within the shale, the river sand and the sandstone zones of the foundation are discussed in this section. The piezometric levels within these zones were considered the most influential on the stability and deformation of the embankment. The piezometers used in this evaluation were generally located perpendicular to the dam centerline a long Line U (Station 2134) as illustrated in Figure 3.23.

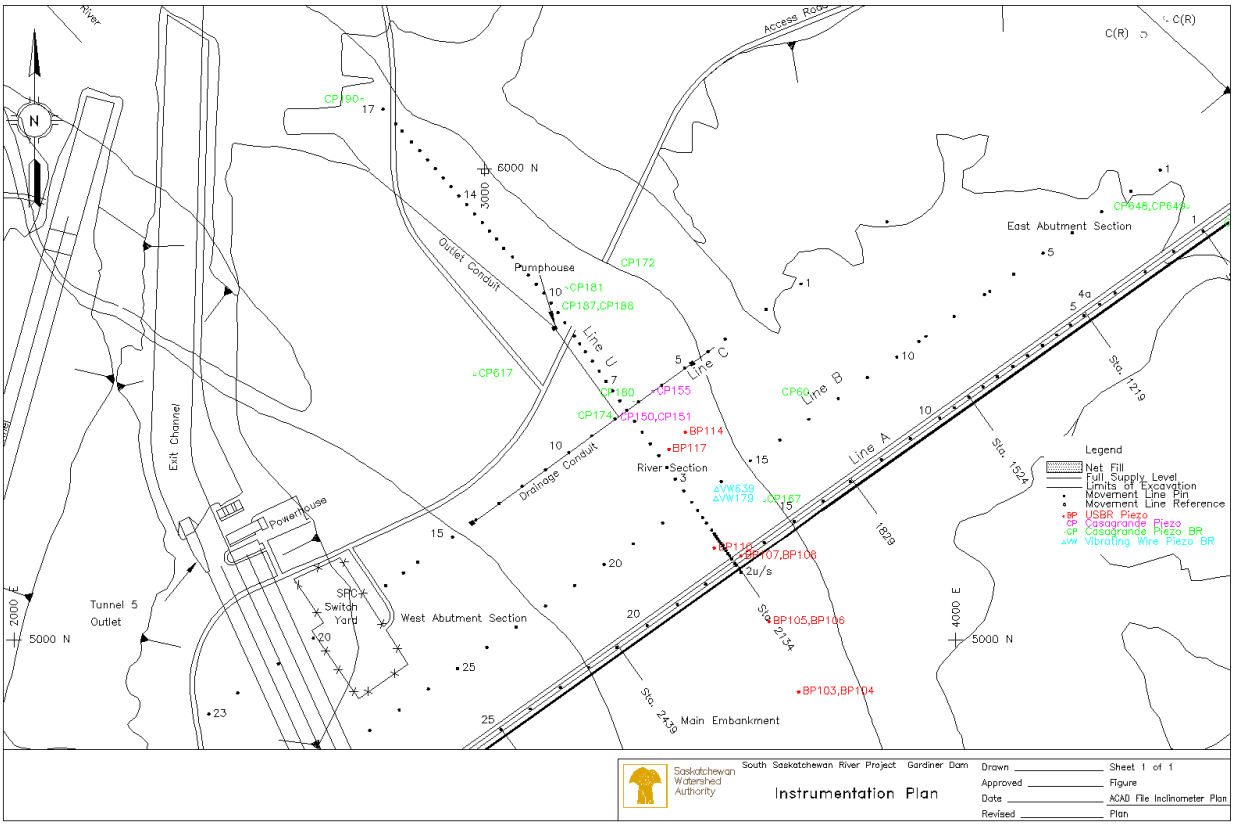

Figure 3.23 Plan view of the River Embankment showing locations of piezometers

The piezometric response of the shale was evaluated separately from the response recorded in the river sand and sandstone given the large difference in hydraulic conductivities of these materials. The piezometric response of the piezometers along Station 2134 is illustrated on Figure 3.24.

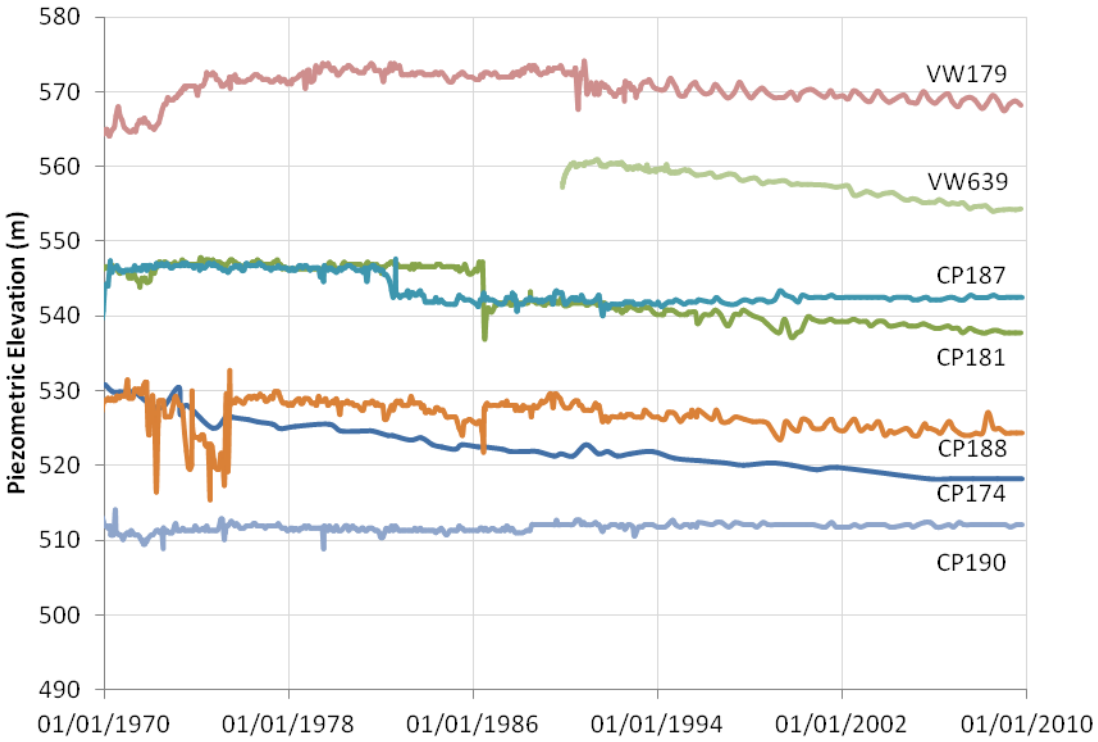

Figure 3.24 Shale piezometric level vs. time plot along Station 2134, 1970 to 2010: VW179 (150 m downstream), VW639 (150 m downstream), CP174 (400 m downstream), CP188 (678 m downstream), CP181 (678 m downstream), CP187 (678 m downstream), and CP190 (1488 m downstream)

The effect of the fluctuations in reservoir level on the piezometric response within the shale was investigated using two piezometers, VW179 (150m downstream) and CP181 (678m downstream), as illustrated in Figure 3.25. It is apparent that the piezometric levels within the shale were influenced greatly by the reservoir level fluctuations and have a well-developed correlation. From these plots, it can be seen that the piezometric level recorded by VW179 was approximately 15m greater than the reservoir level; yet, it still fluctuated at the same frequency as the reservoir level.

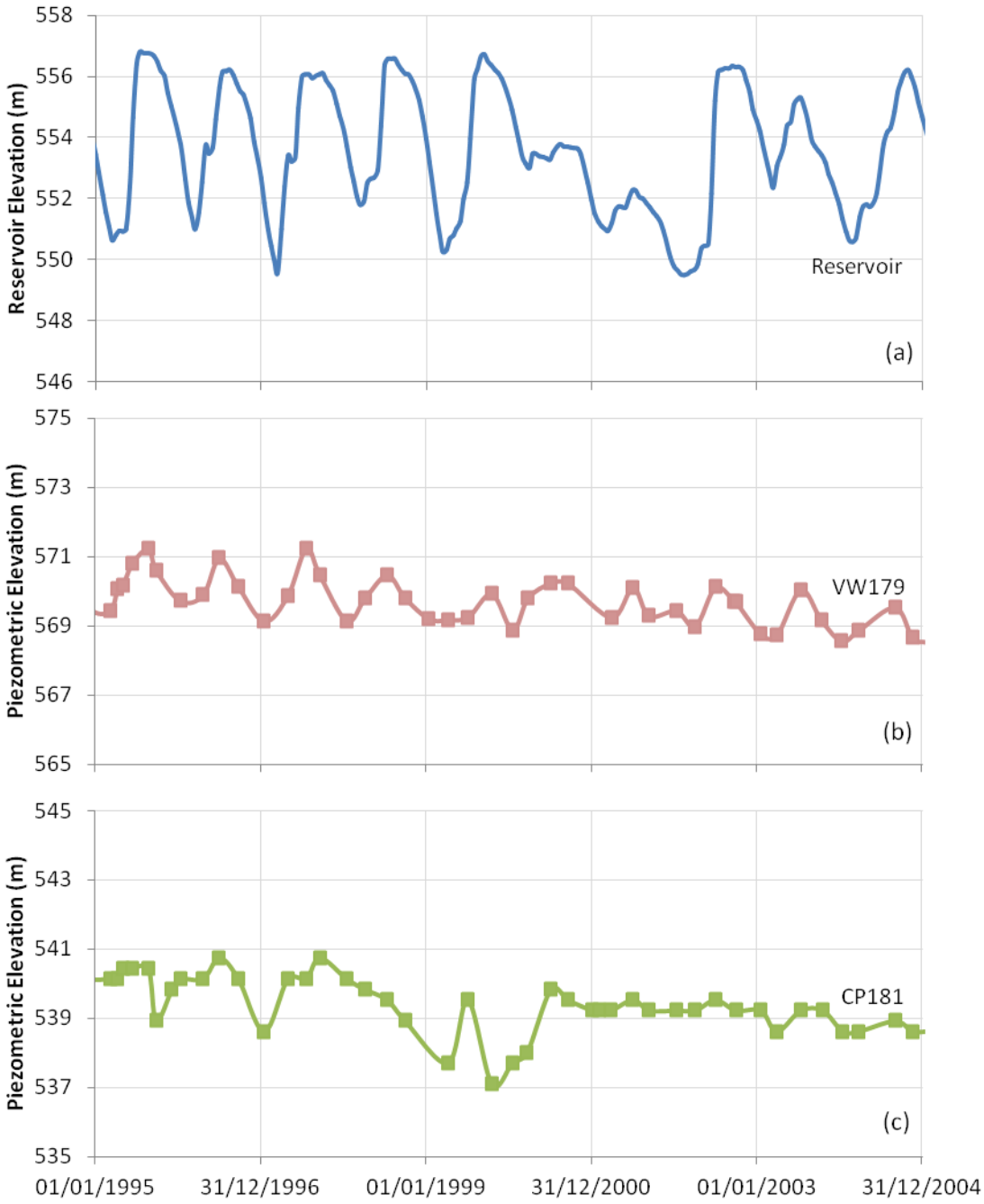

Figure 3.25 Shale piezometric response to reservoir level fluctuations, 1995 to 2004: (a) Reservoir level, (b) Piezometric elevation in shale at VW179 (150 m downstream), and (c) Piezometric elevation in shale at CP181 (678 m downstream)

As with the shale piezometers, the time dependent variation of the piezometric levels in the river sand and sandstone was evaluated using monitoring data obtained from select piezometers. The river sand piezometers represent the piezometric profile from BP101 (457 m upstream) to CP151 (395 m downstream). The sandstone piezometric profile was represented by two piezometers, CP60 (237 m downstream) and CP617 (649 m downstream).

The river sand and the sandstone indicated minimal change in the piezometric level over time as shown on Figure 3.26 and Figure 3.27. This is expected as the material is relatively free draining and would have dissipated any excess pressure from construction relatively quickly. The sandstone was also been pumped with two dewatering wells since shortly after construction to improve the drainage from the shale.

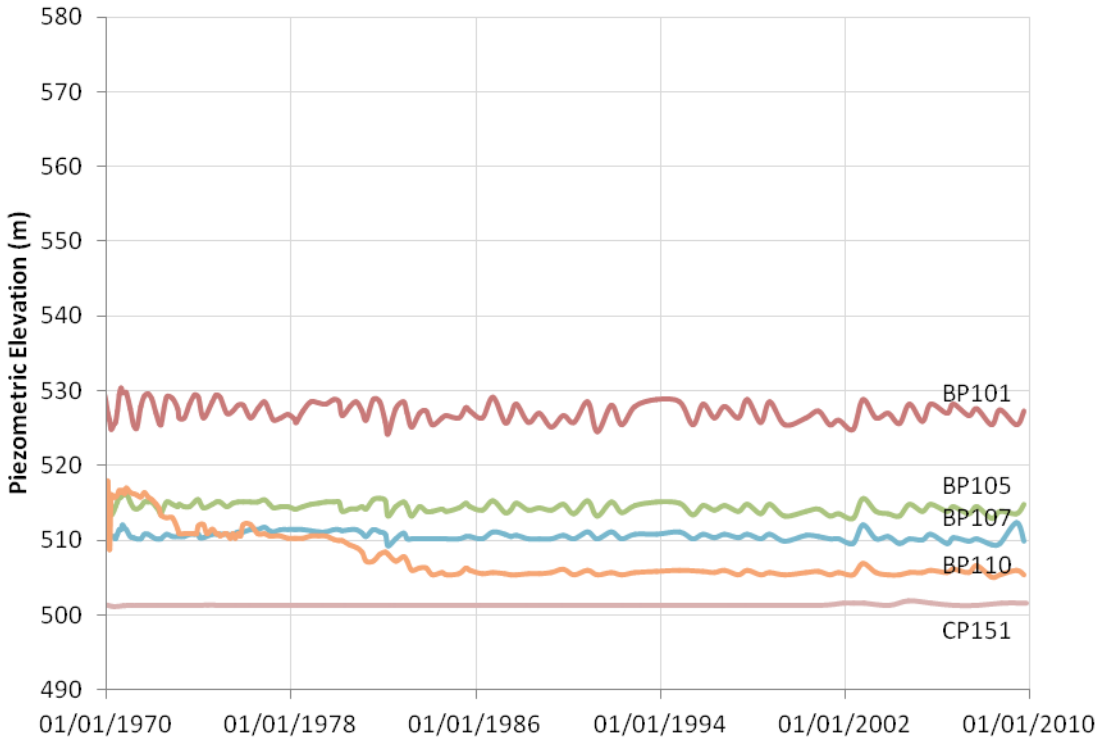

Figure 3.26 River sand piezometric level vs. time plot along Station 2134, 1970 to 2010: BP101 (457 m upstream), BP105 (147 m upstream), BP107 (centerline), BP110 (137 m downstream), and CP151 (395 m downstream)

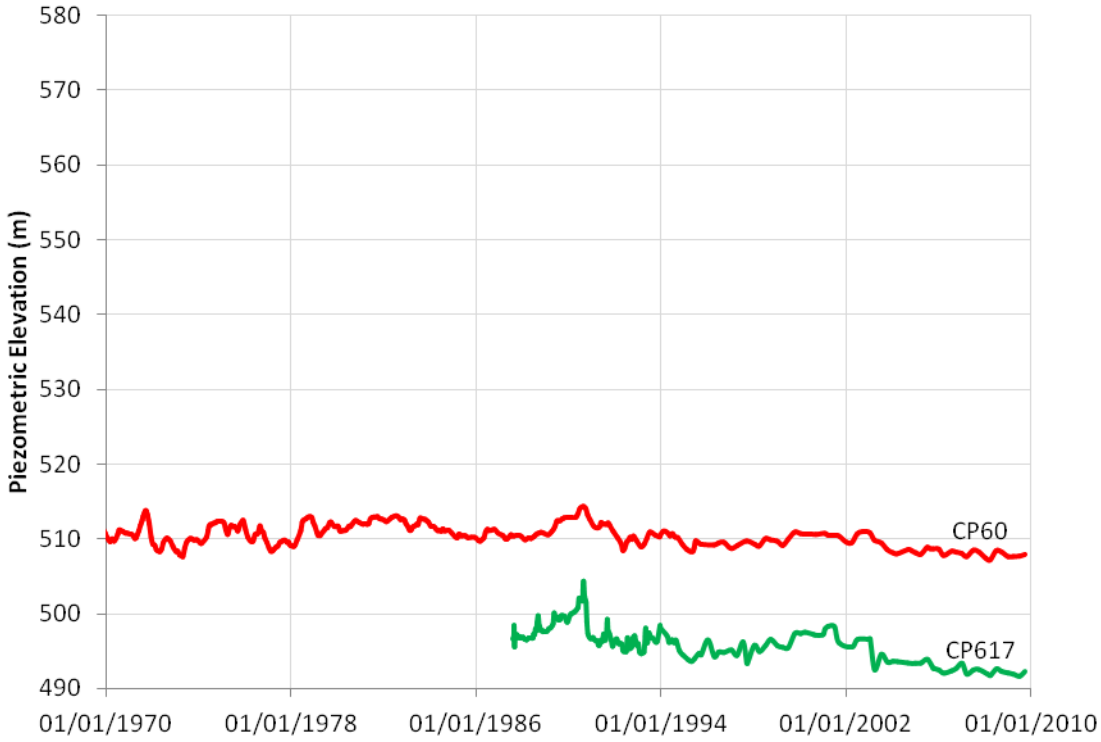

Figure 3.27 Ardkenneth sandstone piezometric level vs. time plot along Station 2134, 1970 to 2010: CP60 (237 m downstream), and CP617 (649 m downstream)

The piezometric response caused by reservoir fluctuation was evaluated using BP105 (147m upstream), BP107 (embankment centerline) and CP60 (237 m downstream) as illustrated in Figure 3.28. It is apparent that the piezometric level within the river sand and the sandstone were both influenced substantially by the reservoir level. Figure 3.28 also illustrates that the magnitude of the piezometric change was only a portion of the reservoir change, indicating a head loss between the reservoir and the piezometer location.

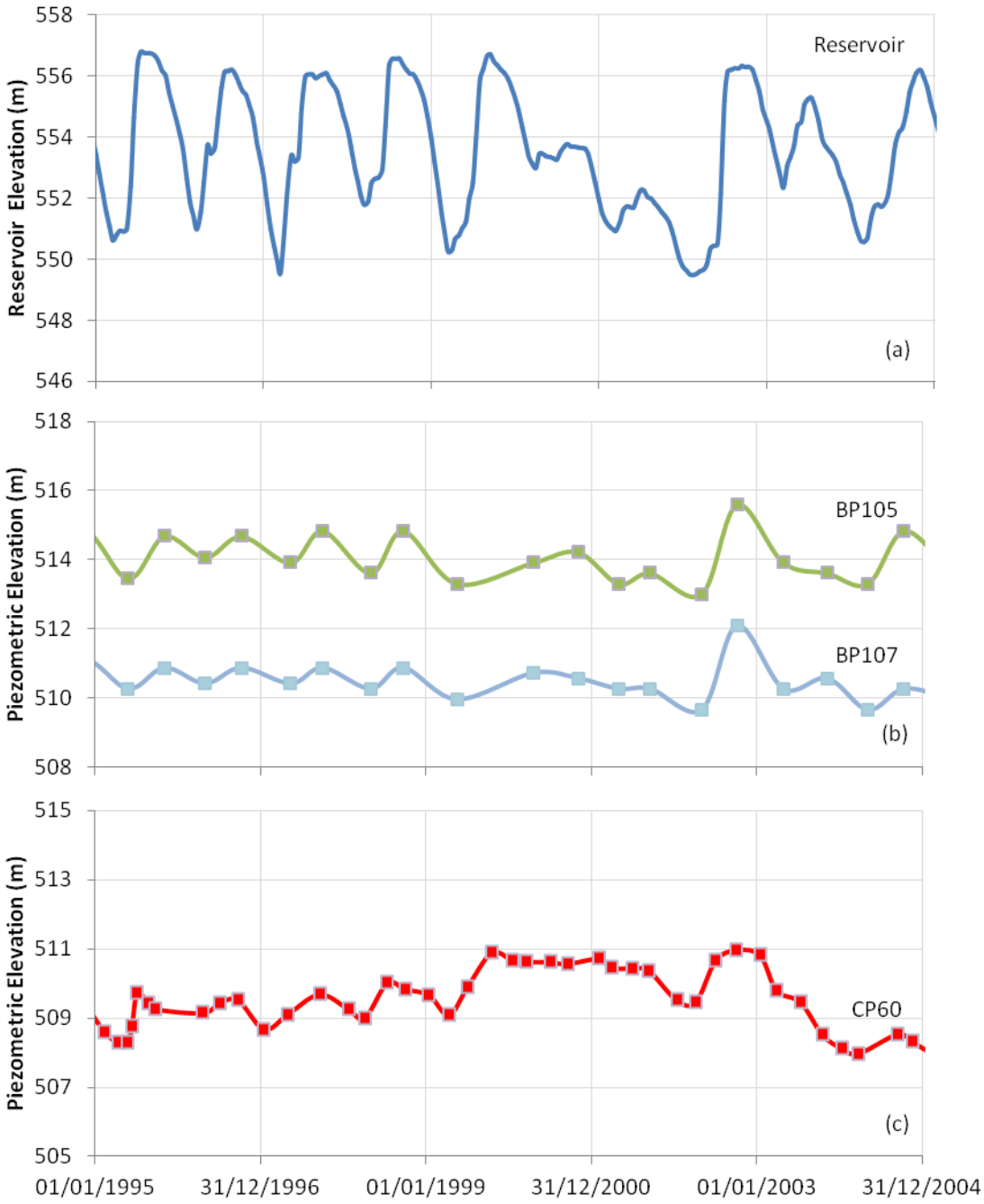

Figure 3.28 River sand and Ardkenneth sandstone piezometric response to reservoir level fluctuations, 1995 to 2004: (a) Reservoir elevation, (b) River sand piezometric level BP105 (174m upstream) and BP107 (centerline), and (c) Ardkenneth sandstone piezometric level CP60 (237 m downstream)

The influence of foundation stratigraphy on piezometric response within each of the three foundation zones was evaluated along Station 2134 during the high reservoir period of 2010. Figure 3.29 illustrates the comparison between the piezometric levels within the zones and the foundation stratigraphy.

Within all the foundation zones, the piezometric levels had a downstream gradient indicating drainage towards the tailwater. The river sand and the sandstone had similar gradients and similar piezometric levels at comparable positions. The shale illustrates a steeper gradient downstream and its piezometric levels was several meters higher than those of the river sand above and sandstone below, indicating that the drainage of porewater was taking place from the shale towards the river sand and the sandstone, i.e. double drainage.

The gradient towards the river sand and the sandstone was also indicated by a nest of piezometers located 700 m downstream of the centerline. These piezometers CP187, CP181 and CP188 were located within the shale at different elevations, as illustrated on Figure 3.29. The piezometric levels measured by these piezometers indicated a gradient towards the river sand and the sandstone away from CP181.

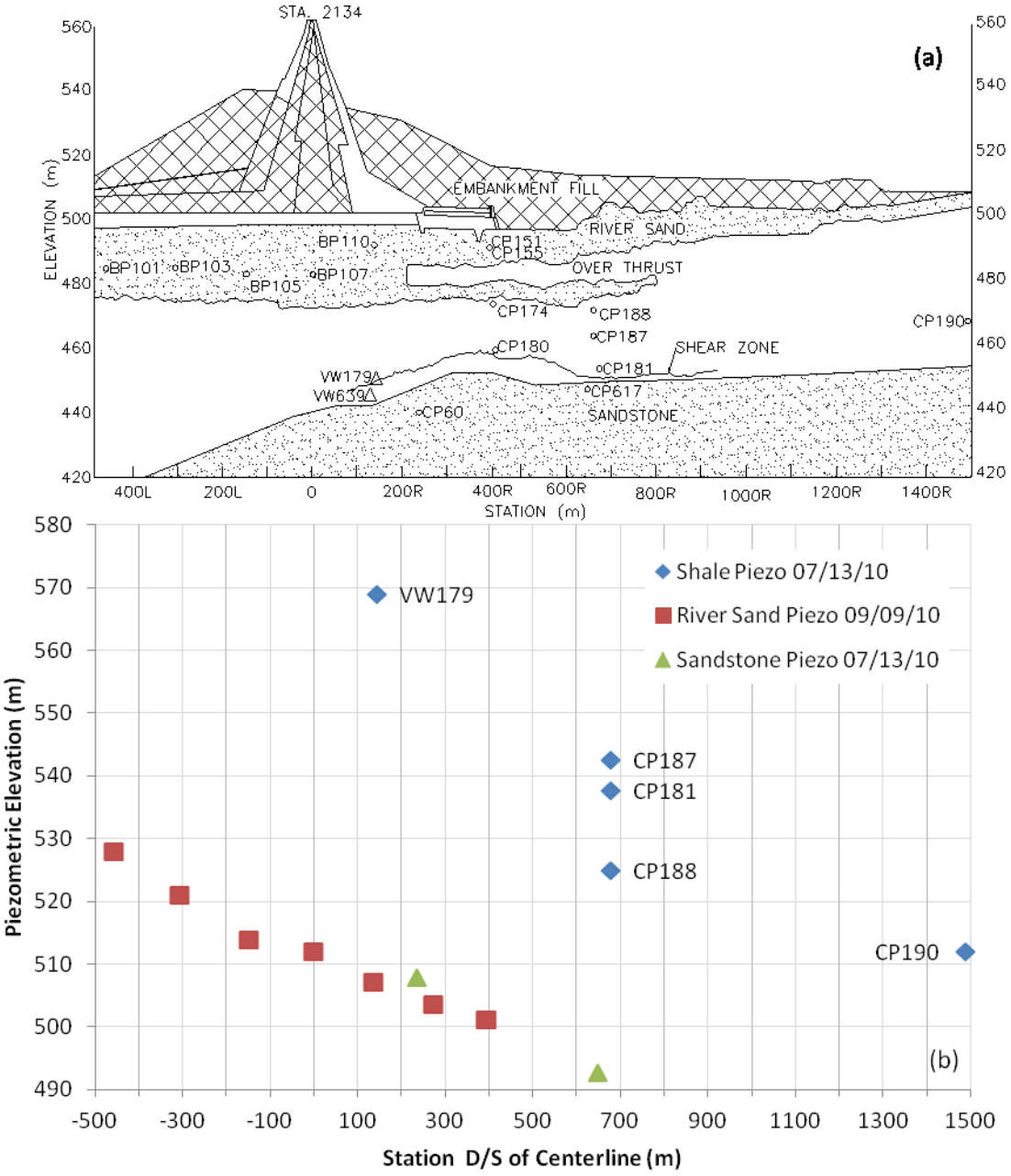

Figure 3.29 Piezometric response to foundation stratigraphy, Station 2134: (a) Foundation stratigraphy and embankment geometry, and (b) Shale, River sand and Ardkenneth sandstone piezometric elevation

3.8 Historical Instrumentation Review Conclusion

The historic monitoring data of the River Embankment was presented in this chapter. The critical monitoring data reviewed included the reservoir level, vertical displacements, horizontal displacements, and piezometric level within the embankment and foundation. The next chapter will use this monitoring data to develop correlations between the observed deformations within the foundation and other sources of influence.

CHAPTER 4 DEVELOPMENT OF CONCEPTUAL MODEL

4.1 Overview

The review of the historic instrumentation data identified several possible correlations. These possible correlations were then evaluated further to develop a conceptual model to represent the mechanism for the deformations within the foundation.

The correlations presented herein are based on the observed instrumentation monitoring data. It is worth pointing out that the piezometer readings and the inclinometer sweeps were taken relatively infrequently or sporadically. For example, the shear zone displacement at SI3999 was generally monitored on a monthly basis during the raising of reservoir level and only once or twice during the lowering of reservoir level. The vibrating wire piezometers and Casagrande piezometers were monitored every one to three months. Given the sporadic nature of the instrumentation readings, it is common to not have all the instrumentation readings on any given day or week. Clearly, this affects the accuracy of correlations that are established using the instrumentation monitoring data. It is important; therefore, to focus on trends instead of magnitudes while examining these correlations.

The instrumentation data within the shale, river sand and sandstone illustrate the effect the reservoir had on the piezometric level and horizontal deformation. As the reservoir level increased the piezometric level also increased proportionally as shown in Figure 3.25 and Figure 3.28. Similarly, when the reservoir level increased, an increase in downstream horizontal displacement at the shear zone also occurred, as illustrated in Figure 3.14. Too further discuss the correlations observed, a detailed look at two time periods from January 1, 1995 to January 1, 1997 and January 1, 2005 to January 1, 2007 were conducted.

4.2 Piezometer Review

The correlation between the shale, river sand and sandstone piezometric levels and reservoir level will be discussed in this section. To facilitate this discussion, a detailed look at two time periods from January 1, 1995 to January 1, 1997 and January 1, 2005 to January 1, 2007 for VW179 were evaluated as illustrated in Figure 4.1 and Figure 4.2 respectively.

From these figures it can be seen that as the reservoir increased, the piezometric level in each of the material zones increased proportionally to the increase in the total head of the reservoir. Minimal time lag was observed in the shale and a noticeable time lag was observed in the river sand and the sandstone.

An increase in the piezometric level within the foundation materials would be expected with an increase in reservoir level, due to a change in the upstream total head and resulting increase in total stress. As time progressed, the increase in the total head would be expected to then transfer throughout the foundation. The transfer of the total head is a function of the hydraulic conductivity and stiffness of the materials and the stratigraphy and geometry of the site. There would be an expected decrease in the total head further downstream from the reservoir assuming an adequate amount of time is provided to allow equilibrium to be reached. The time required for the transfer of the total head increase in the downstream direction would be dependent on the hydraulic conductivity of the material zone.

Because both the river sand and the shale are both relatively stiff materials, the total stress would be expected to transfer through this material relatively quickly. When the total stress was applied to the river sand, the stress would be then transferred to the porewater and dissipated almost instantaneously because of its high hydraulic conductivity. On the other hand, when the total stress is applied to the shale, the stress would be applied to the porewater pressure similarly to the river sand, but would take a significant amount of time to dissipate because of low hydraulic conductivity.

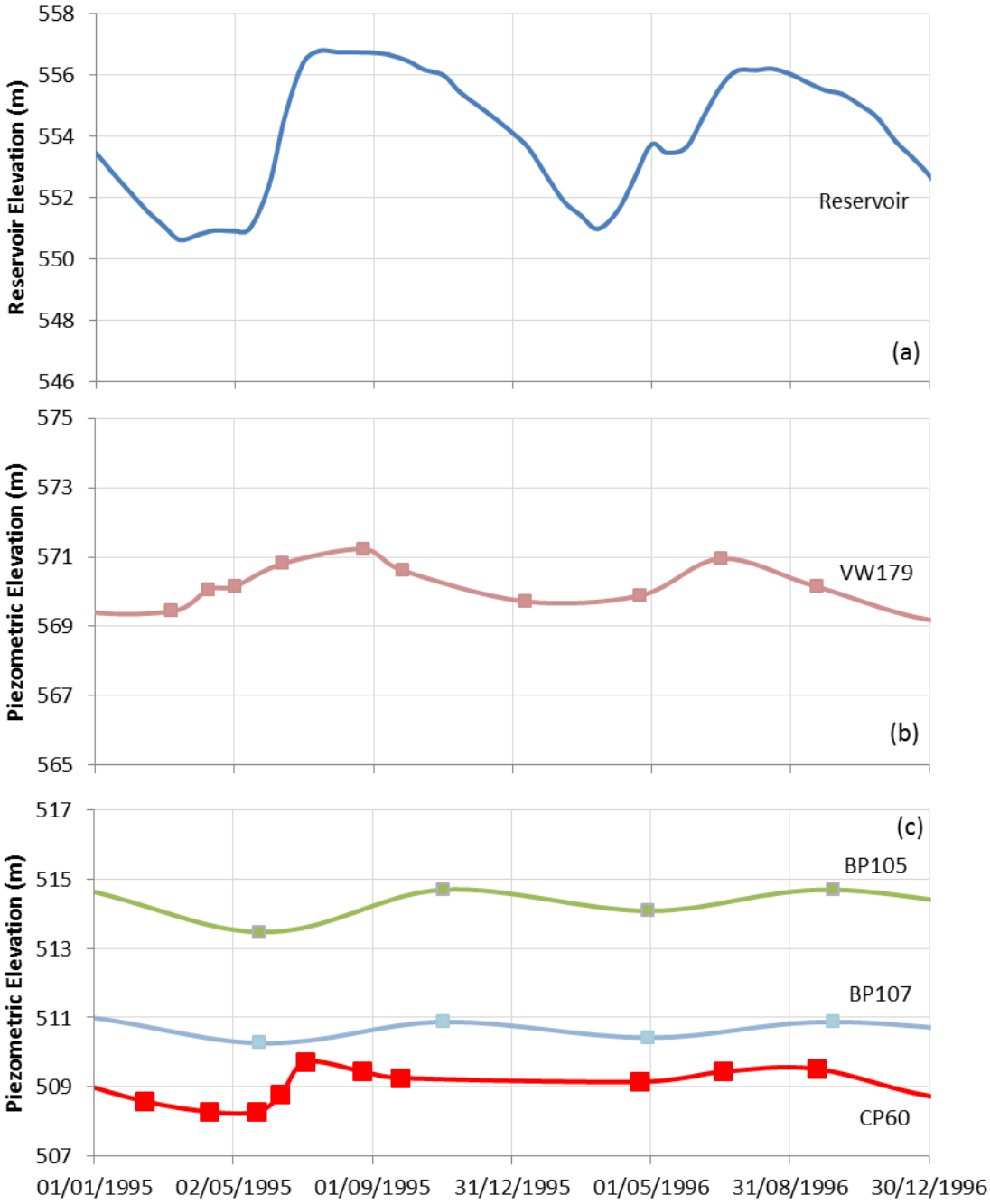

Figure 4.1 Shale piezometric response to reservoir level fluctuations, 1995 to 1997: (a) Reservoir level, (b) Piezometric elevation in shale at VW179 (146 m downstream), and (c) Piezometric elevation in river sand at BP105 (174 m upstream), BP107 (centerline), and sandstone at CP60 (237 m downstream)

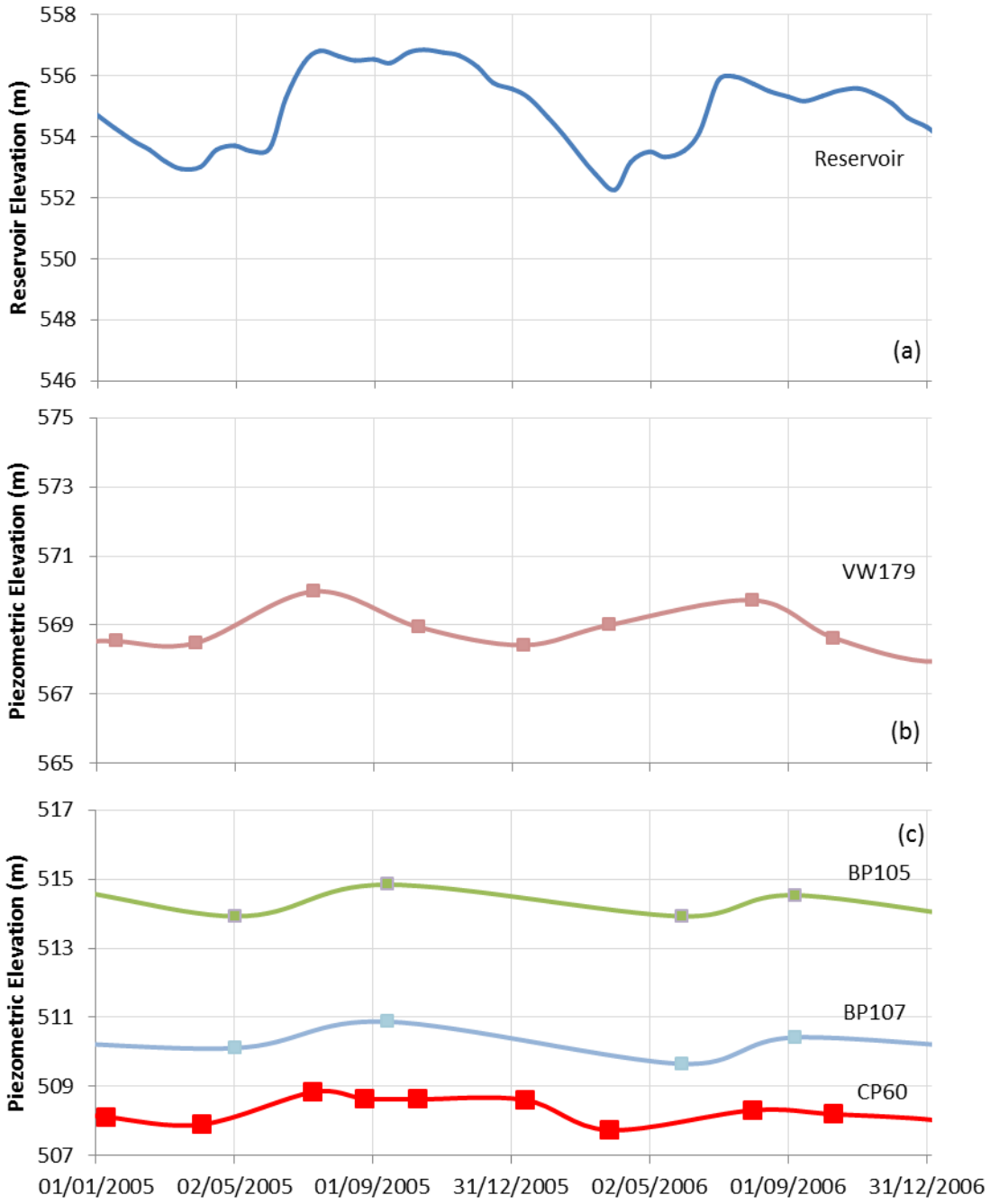

Figure 4.2 Shale piezometric response to reservoir level fluctuations, 2005 to 2007: (a) Reservoir level, (b) Piezometric elevation in shale at VW179 (146 m downstream), and (c) Piezometric elevation in river sand at BP105 (174 m upstream), BP107 (centerline), and sandstone at CP60 (237 m downstream)

The piezometric level with the shale is also greater than that of both the river sand and sandstone, indicating the gradient is predominantly out of shale. This gradient was developed due to the excess porewater pressure caused by the construction of the embankment. Therefore, the pore-pressure in the shale cannot vary without a reversal of the gradient or a total stress change applied to the shale.

Provided that it is not possible for a reversal of the gradient out of the shale given the current reservoir operating range, a change in the porewater pressure must then be a result of a total stress change applied to the shale. Given that the most significant load fluctuation to the shale locally is the reservoir, it is proposed that the total stress change is a result of the reservoir fluctuation.

4.2.1 Regional Groundwater Considerations

The surrounding regional groundwater system was evaluated as a source of influence over the piezometric level in the shale. The influence of the regional groundwater systems appeared to be improbable due to the timing of unique fluctuation of the reservoir. Generally, an increase in reservoir level began in late May and peaked in late June, similar to the foundation piezometric level. The regional groundwater system, on the other hand, would be expected to be at its highest level during the local runoff period which would normally be in late March to mid-April.

Several piezometers were located directly adjacent to the dam, within the till and the shale, CP648 to CP651, as illustrated in Figure 4.3. The piezometric response in the till and shale indicated a time lag behind the reservoir fluctuation as expected, shown in Figure 4.4. This was expected due to the fact that as the reservoir increased against the abutment, the phreatic surface required time to increase through the abutment. Therefore, there was not a clear indication of a regional ground water fluctuation within these piezometers. However, it would be reasonable to assume that because of the closeness to the reservoir, any change in the regional system would be dominated by the fluctuation in the reservoir. The evaluated piezometers were not located at a great enough distance to be considered unaffected by the fluctuation of the reservoir and confirm this. Assuming that this assumption is correct, it provides further verification that the regional groundwater regime would have minimal hydraulic impact on the piezometric level in the foundation beneath the embankment.

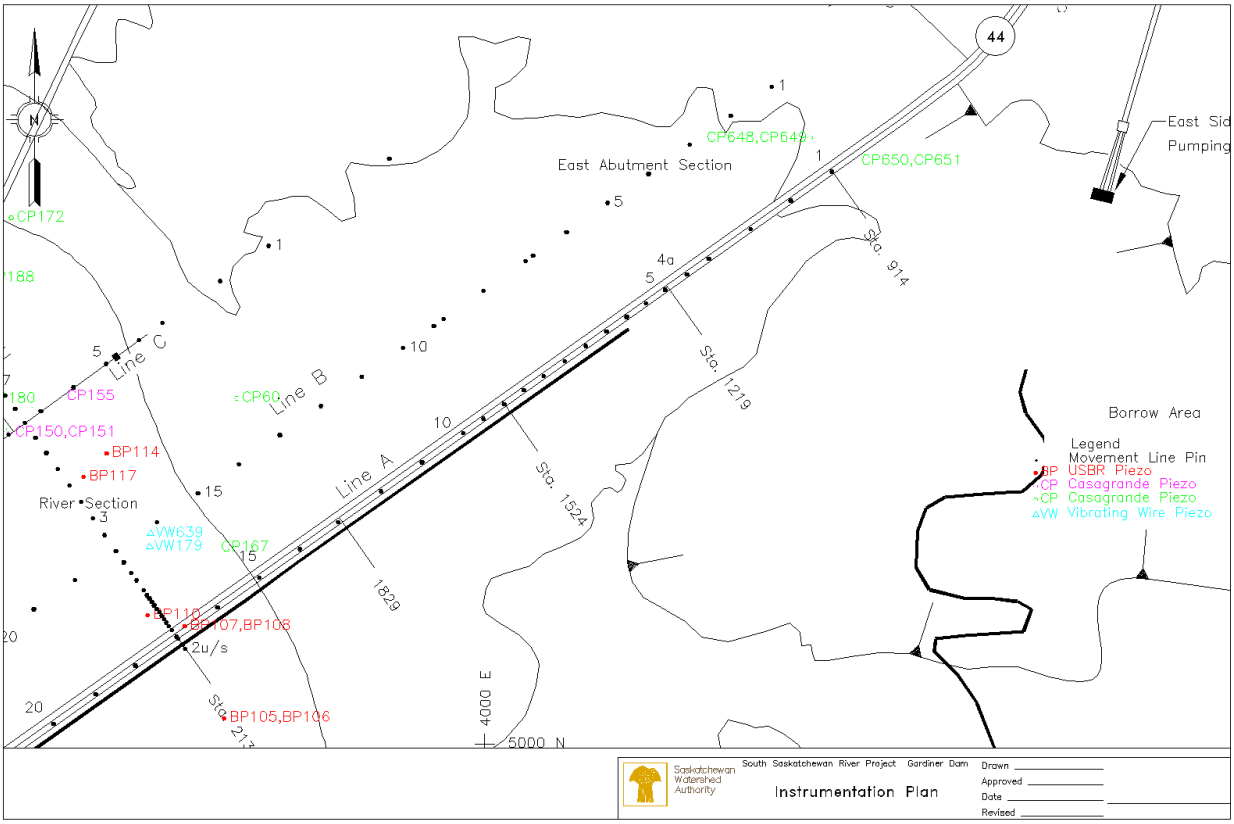

Figure 4.3 Plan view of East Abutment showing piezometers in till and shale

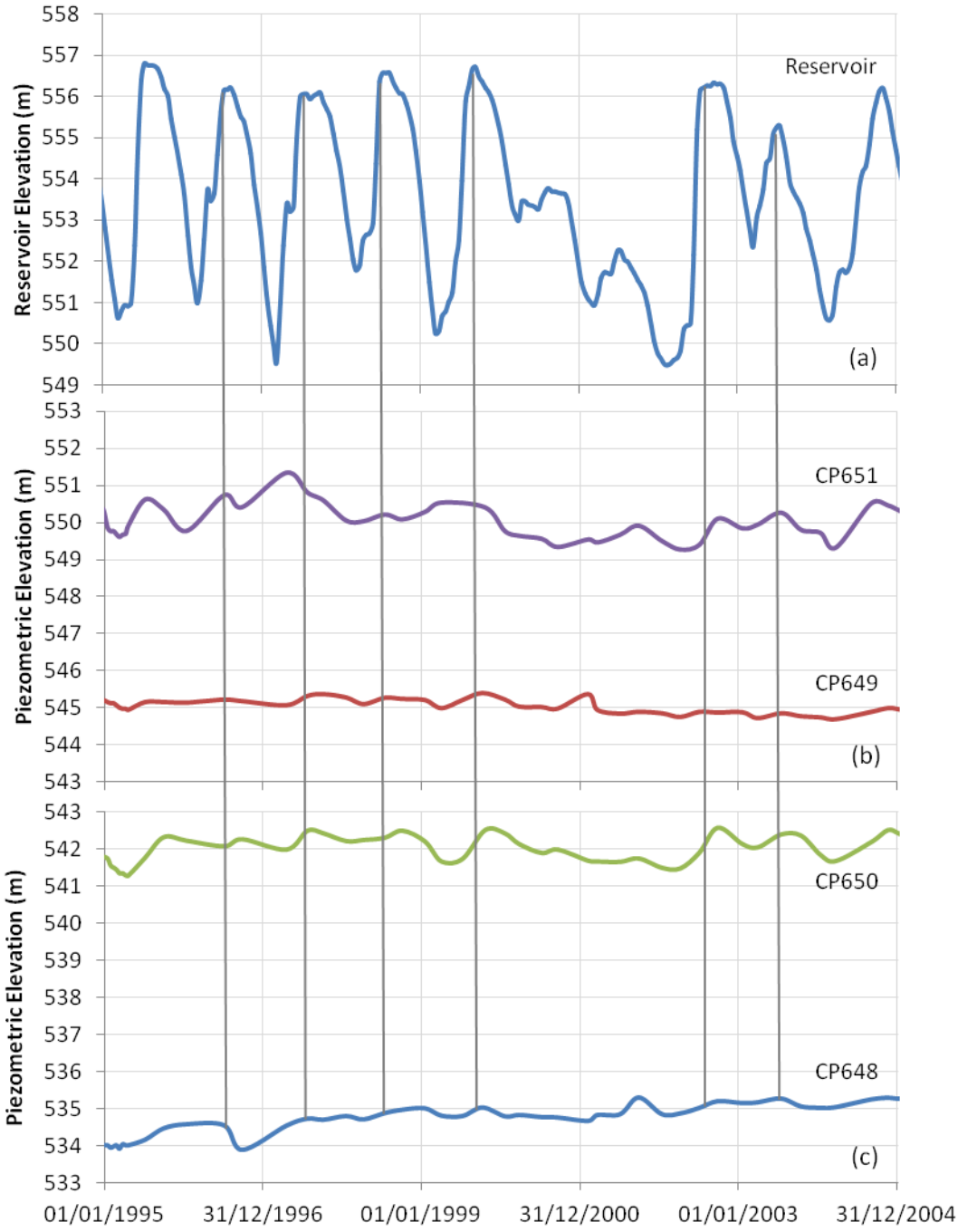

Figure 4.4 Till and shale piezometric response to reservoir level fluctuations, East Abutment 1995 to 2004: (a) Reservoir elevation, (b) Till piezometric level, and (c) Shale piezometric level

4.2.2 Confirmation of the Piezometric Response Mechanism

The purpose of this section is to confirm the proposed mechanism of the stress and piezometric response due to reservoir loading. There was no attempt to match the magnitude of stress change or pore-pressure change throughout this section. This evaluation confirmed the assumption that a piezometric response at the downstream boundary of the conceptual model domain was possible due to a stress change in the shale from an incremental reservoir increase. In addition, the models also confirmed the stress change in the shale was the largest influence on the piezometric response. This section discusses the results of the evaluations with a brief overview of the model domain, material properties and boundary conditions. More discussion of domain, material properties and boundary conditions is located in Appendix B.

A finite element stress-strain model was developed to confirm these assumptions. The secondary objective of the stress-strain model was to evaluate the pattern of the stress in the shale as a result of the increase in the reservoir level.

Modelling Scenarios

Several model scenarios were evaluated to investigate the pore pressure response in the shale to the increase in reservoir level. A standalone load load/deformation evaluation was completed followed by a standalone porewater model and finally a coupled porewater/stress response model was completed.

Model Domain

The general modeling methodology included developing a simplified representation of the insitu geometry and stratigraphy from 520 m upstream of the dam center line to 520 m downstream of the centerline. The domain also extended vertically from the embankment surface to 25 m into the sandstone. This domain included in this model is significantly larger than that considered throughout the remainder of this thesis. The preexisting pore pressures were also assumed to be zero as the objective is to find the relative change in pore pressure with a change in reservoir. Figure 4.5 illustrates a representative section of the model domain used thorough this evaluation.

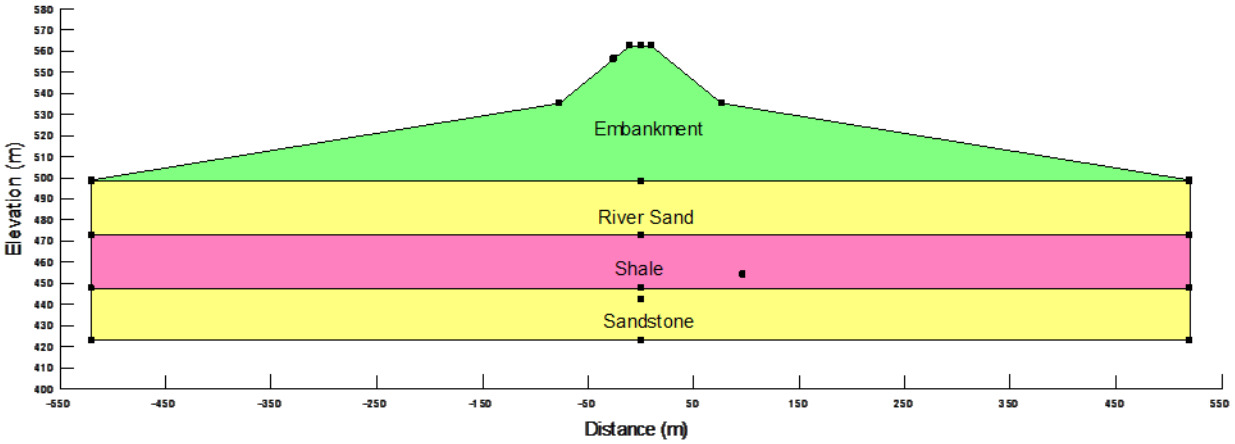

Figure 4.5 Representative model domain

Model Boundary Conditions

This section describes the hydraulic and stress-strain boundary conditions applied to the model domain. The boundary conditions described include all three modeling scenarios. The upstream and downstream boundary conditions were both considered no flow boundaries and fixed in the x direction. The bottom of the domain boundary conditions were considered to be a no flow boundary and fixed in both the x and y directions. A reservoir was applied to the upstream surface of the model domain, i.e. the embankment upstream face.

The reservoir was initially applied at 550m. The model then simulated 11 days to allow the stress to redistribute and a portion of the excess pressure to dissipate. The reservoir load was then increased to 556 m and then simulated for 11 days again to allow for the stress to redistribute and a portion of the excess pressure to dissipate.

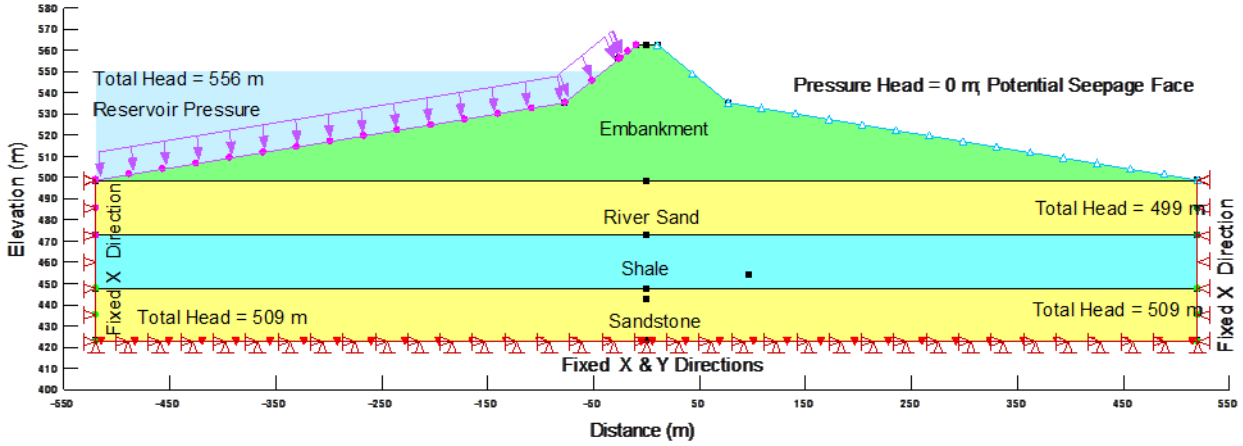

Figure 4.6 provides a representative illustration of the boundary conditions applied.

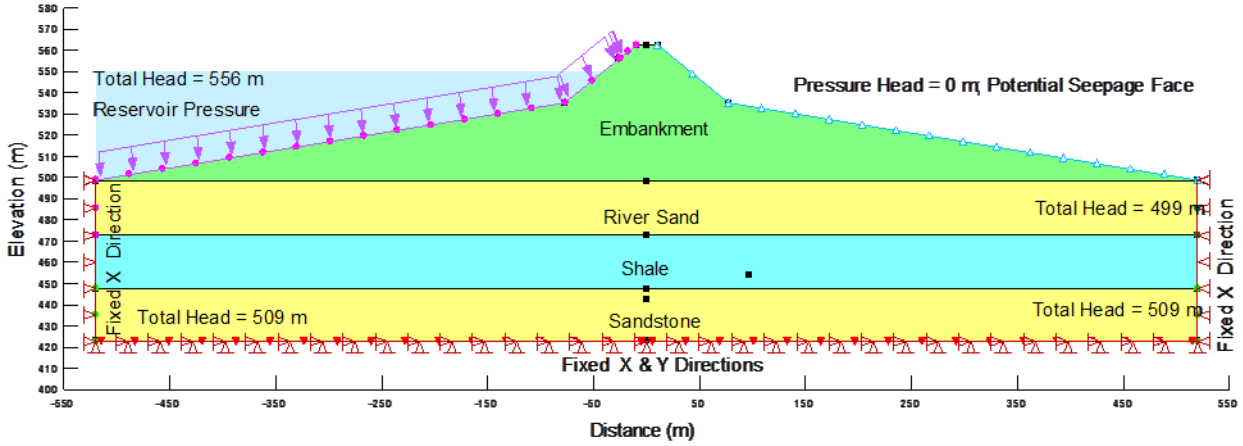

Figure 4.6 Representative model boundary conditions

Material Properties

The material properties of the embankment, river sand and the sandstone were held constant through the modeling scenarios. The Young's Modulus of the shale was varied between E'=139, the minimum laboratory tested shale at Gardiner Dam and 1250 MPa based on the range of values in the literature within Western Canadian shale (PFRA 1966b, Gautam and Wong 2006). The hydraulic conductivity of the shale was varied between k= 1e-9 to 1e-13 m/s (PFRA 1960b, PFRA 1980).

Domain Finite Element Mesh

To compute the numerical model, a finite element mesh is required. A similar mesh was developed for all three modeling scenarios with the automatic mesh generator provided in

Geostudio, (GEO-SLOPE INTERNATIONAL LTD 2012) with a global element size of 5 m. Figure 4.7 illustrates a representative finite element mesh used for this evaluation.

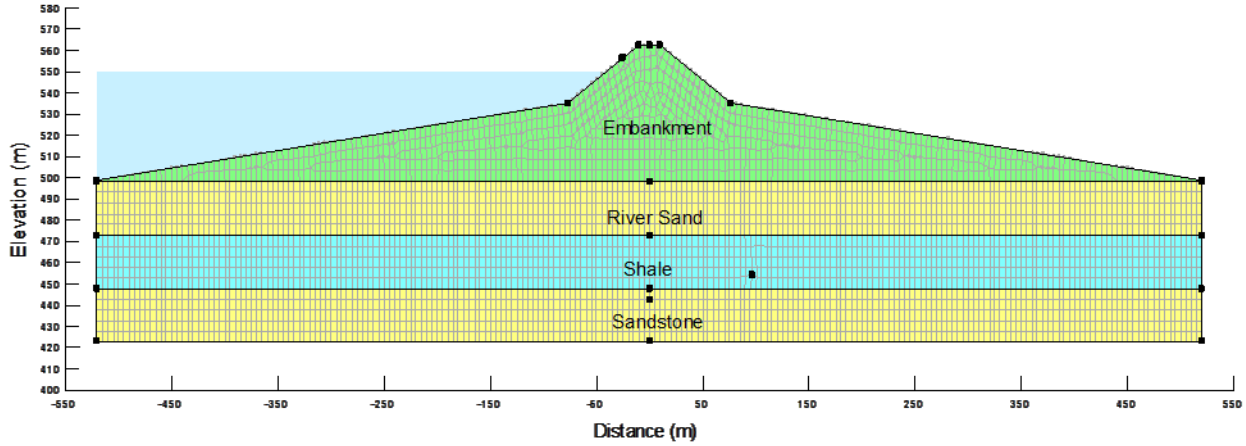

Figure 4.7 Representative model finite element mesh (5 m element size)

Simulation Results

To allow for comparison of the models and discussion, an "observation" node was created in the model at the approximate location of piezometer VW179 (146 m downstream) in the shale. The discussion in this section, Figure 4.8 and Figure 4.9 are referenced to this node. Additional figures showing the models total stress response and total head response contours have been included in Appendix B to complement this discussion.

Several simulations of the load/deformation model were completed by varying the shale stiffness and not considering coupling between the pore pressure and the stress response in the shale. This evaluation indicated that as the stiffness of the shale increased, the magnitude of the incremental stress change also increased with an increase in reservoir level. In addition, the model indicated that as the stiffness of the shale increased, so did the distance that the stress was transferred downstream of the reservoir.

The porewater response in the shale was evaluated by varying the hydraulic conductivity of the shale without considering coupling with total stress changes. The results indicated there was a minimal effect on the piezometric level in the shale by varying the hydraulic conductivity alone. Therefore, this confirms the assumption that the total head change in the reservoir does have a limited effect on the piezometric level in the shale alone.

Finally, a coupled porewater/stress response analyses was completed by varying the stiffness and the hydraulic conductivity of the shale independently of each other. The models showed that by varying the stiffness of the shale there was minimal difference in the stress response between the coupled and uncoupled models. The coupled model also showed that with a lower hydraulic conductivity, the changes in stiffness had a greater impact on the total head with the stiffer material. On the other hand, with the lower stiffness shale, the total head decreased with a reduction in the hydraulic conductivity of the shale. This model also indicated that during coupled loading there is little influence on the total stress as a result of a change in the hydraulic conductivity of the shale and is more influenced by the stiffness of the shale.

Figure 4.8 illustrates that with a lower hydraulic conductivity, the excess porewater pressure is developed during the loading followed by dissipation of the excess pressure.

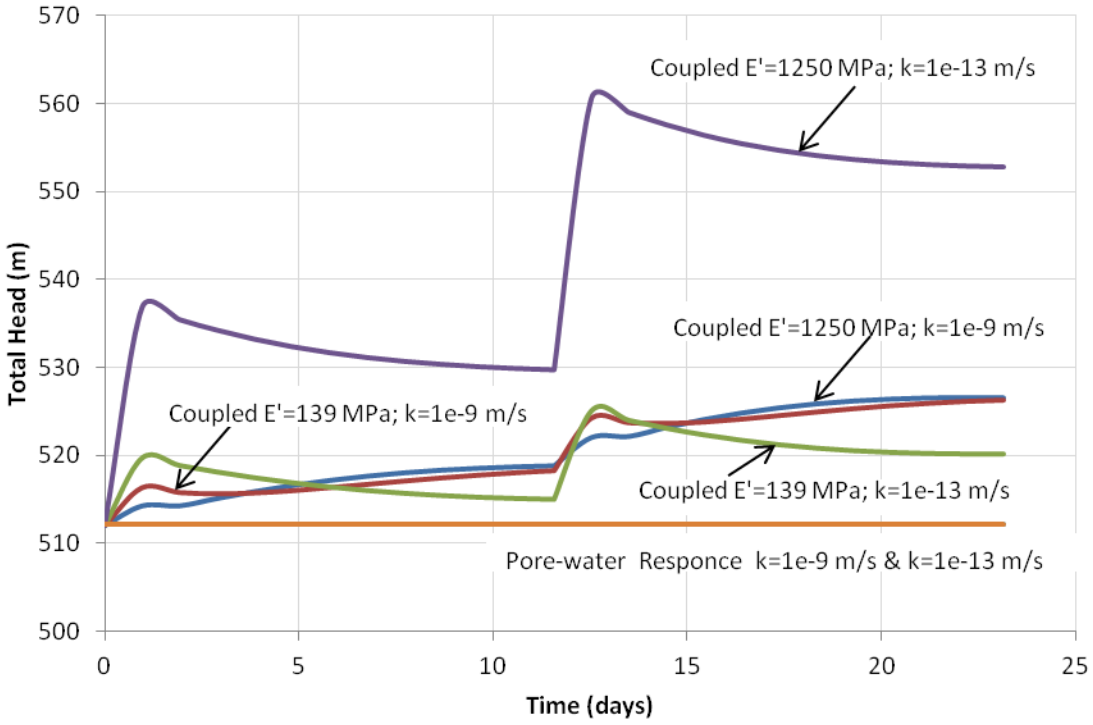

Figure 4.8 Total head response to reservoir loading in the shale at piezometer VW179 (146 m downstream)

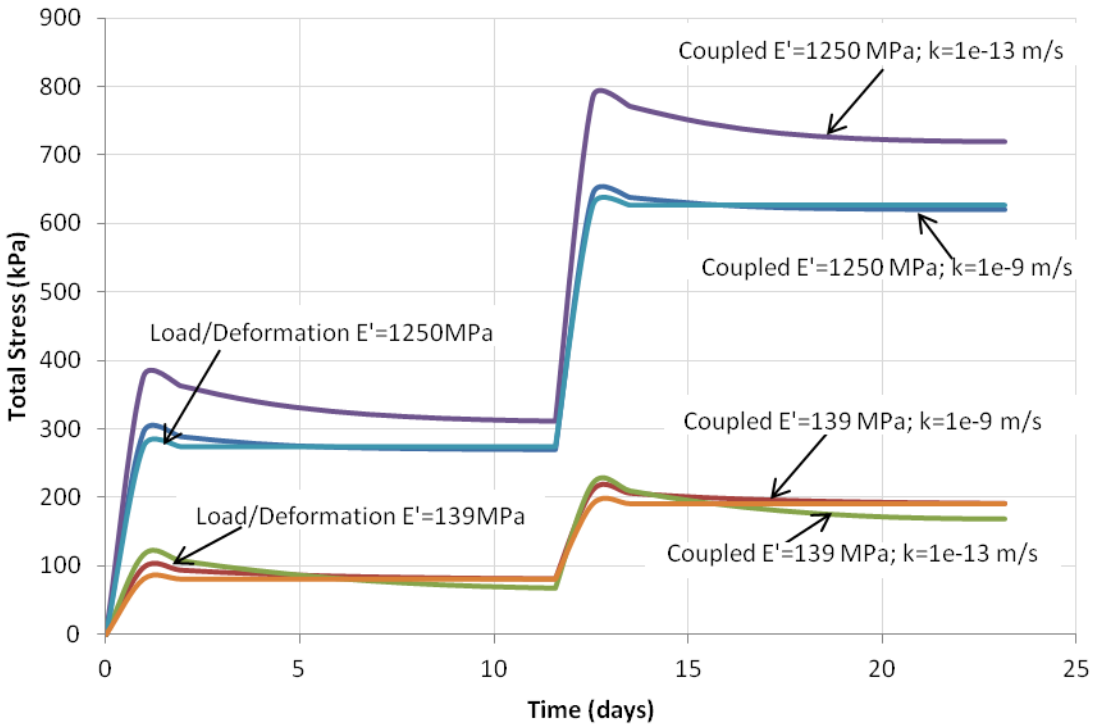

Figure 4.9 Total stress response to reservoir loading in the shale at piezometer VW179 (146 m downstream)

In conclusion, the largest total head response was due to changes in the stiffness of the shale. This confirmed the proposed piezometric response mechanism that the piezometric response in the shale is due to a stress change within the shale caused by the reservoir.

4.3 Deformation Review

The correlation between the reservoir and the shear zone displacement has previously been illustrated in Figure 3.14. For comparison, a detailed look at two time periods from January 1, 1995 to January 1, 1997 and January 1, 2005 to January 1, 2007 for VW179 was evaluated as illustrated in Figure 4.10 and Figure 4.11 respectively.

From these figures, it is evident that as the reservoir increased, a displacement occurred. However, it can also be seen that the magnitude of the displacement was not consistent with the magnitude of the reservoir level change.

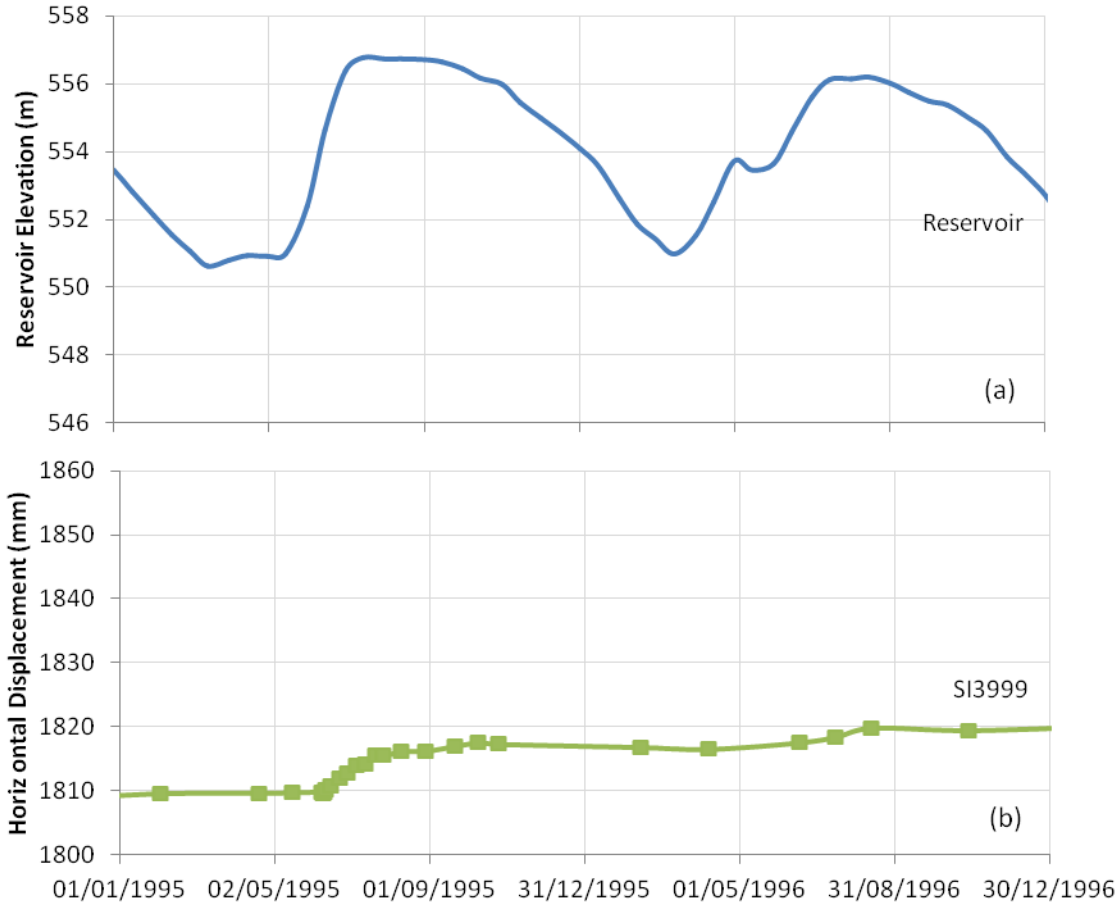

Figure 4.10 Shear zone displacement in shale at SI3999 (150 m downstream) compared to reservoir level fluctuations, 1995 to 1997

Figure 4.11 Shear zone displacement in shale at SI3999 (150 m downstream) compared to reservoir level fluctuations, 2005 to 2007

4.3.1 Deformation Correlation Mechanism

The inconsistency in the correlation of displacement magnitude with the reservoir change illustrated in the above figures indicates that stress applied to the embankment may not be solely responsible for the downstream displacement. Provided the inconsistent displacement with reservoir loading and the piezometric response to the reservoir total stress change, it appears that the displacement is effected by the development of excess porewater pressure and the time required to dissipate the excess pressures. Therefore, it is proposed that the deformation within the shale is a response to consolidation of the shale following the development of excess porewater pressure. The next section will explore the time effects caused by the fluctuation of the reservoir.

4.4 Time Considerations

By combining the effect the reservoir has on the piezometric levels and the shear zone displacement, both of these items were found to be affected by the time cycle and the magnitude of reservoir level fluctuation. These affects are shown with piezometer VW179 and inclinometer casing SI3999 during the time period January 1, 1995 to January 1, 1997 and January 1, 2005 to January 1, 2007 in Figure 4.12 and Figure 4.13 respectively.

From these figures it can be seen that as the reservoir initially increased, the shale piezometric level also went up. Following the initial increase, the reservoir remained elevated for a period of 4 to 5 months. During this time, the piezometric levels decreased slightly indicating a dissipation of a portion of the excess porewater pressure developed during the loading. When the reservoir level decreased, the piezometric level also decreased due to an unloading of the shale and porewater.

In addition, a time effect of the reservoir on the shear zone displacement was also observed. As the reservoir level increased, the displacement rate increased rapidly until the maximum reservoir level was obtained. At this point, the displacement rate decreased, with the reservoir level remaining relatively constant at an elevated level. The decreased displacement rate continued until the reservoir level was lowered, and at this point, the displacement essentially slowed to the pre-reservoir rise rate.

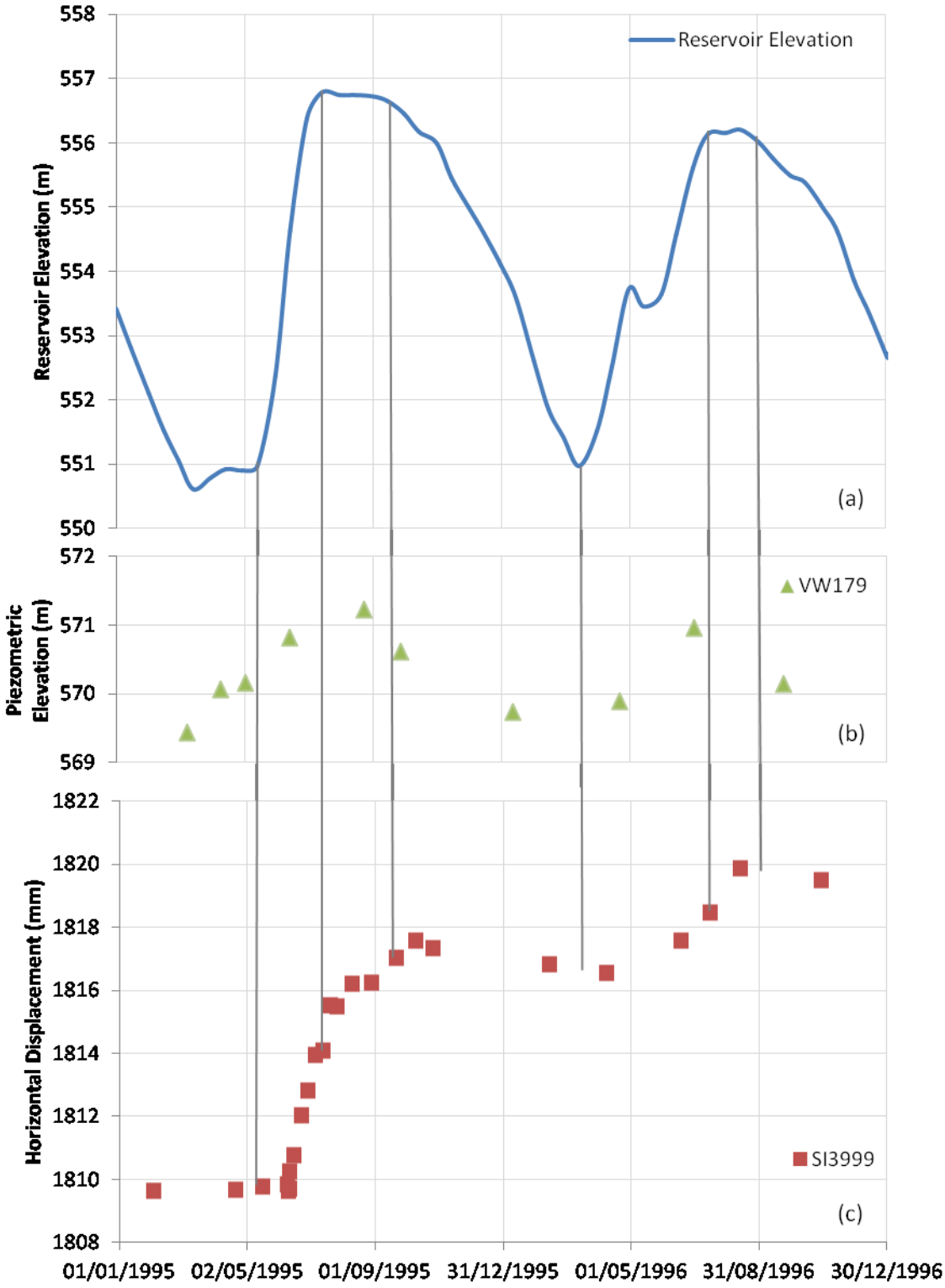

Figure 4.12 Shale piezometric and shear zone horizontal displacement response with reservoir, 1995-1997 (a) Reservoir elevation, (b) Shale piezometric elevation at VW179 (146 m downstream), and (c) Shear zone horizontal displacement SI3999 (150 m downstream)

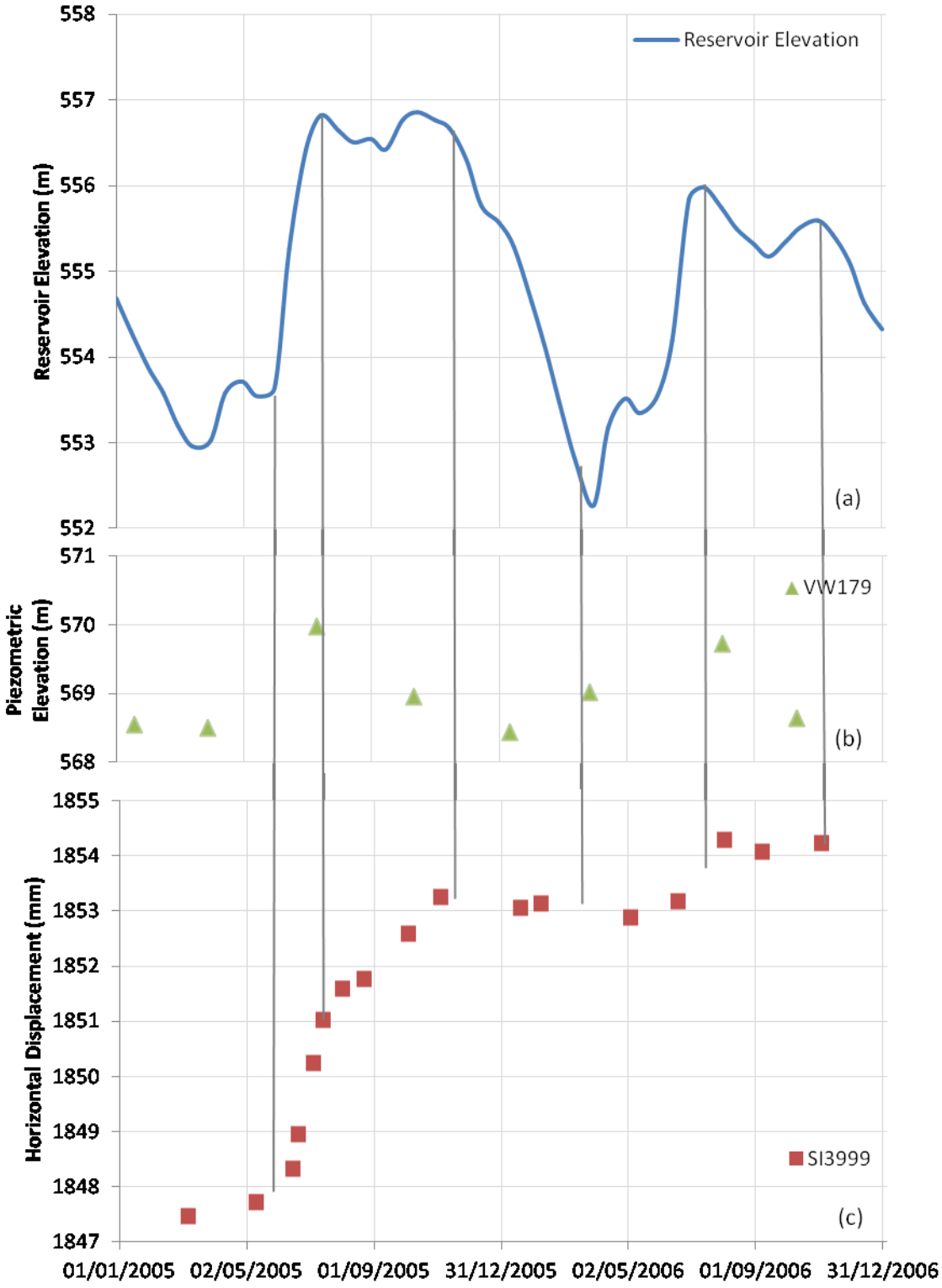

Figure 4.13 Shale piezometric and shear zone horizontal displacement response with reservoir, 2005-2007: (a) Reservoir elevation, (b) Shale piezometric elevation at VW179 (146 m downstream), and (c) Shear zone horizontal displacement SI3999 (150 m downstream)

It appears from the similar time affects observed in the shale piezometric level and shear zone displacement, a connection between the reservoir and the displacement through shale porewater pressure likely exists.

Furthermore, by comparing the reservoir, shale piezometric level and shale shear zone displacement, it is apparent that when the reservoir increased, the shale piezometric levels increased and the displacement rate also increased. As the reservoir remained elevated, the rate of dissipation of the excess porewater pressures slowed and the shear zone displacement rate also slowed. This slowing in rate of the porewater pressure dissipation indicates that the observed continued shear zone displacement was the result of consolidation of the shale. As the reservoir decreased and the load was fully removed from the porewater of the shale, the excess pore-pressured disappeared and the displacement slowed indicating that consolidation slowed to pre-reservoir increase rates.

4.5 Proposed Conceptual Model

Through the correlations in the previous sections, a proposed conceptual model was developed. The observed correlations indicated a connection between the reservoir, the piezometric response within the shale and the horizontal displacement within the shale. It is proposed that the shale has an immediate undrained response to the loading caused by the increase in reservoir level, resulting in the development of excess porewater pressure. This immediate undrained response is then followed by dissipation of a portion of the excess pressure resulting in horizontal displacements due to horizontal consolidation of the shale.

The next section will develop an analytical model to verify the proposed conceptual model.

CHAPTER 5 DEVELOPMENT OF AN ANALYTICAL MODEL

5.1 Overview

The objective of this section is to develop an analytical model to represent and verify the proposed conceptual model. The analytical model represents the mechanisms associated with the piezometric fluctuation and deformation identified with the instrumentation review. The conceptual model proposed that the mechanism causing the horizontal displacement was due to the increase in the horizontal loading created by the reservoir being partially placed on the porewater of the shale, thus creating excess piezometric pressures. Following the immediate development of the excess porewater pressure, some of the pressure dissipated causing consolidation and horizontal movement along the shear zone.

This section will discuss the geometry and extents of the analytical model, the boundary conditions, piezometric response, deformation response, and the limitation of the model.

5.2 Simplified Representative Domain

To simplify the development of the analytical model, a representative domain was developed of the embankment and foundation. The model domain consisted of a specific section of the embankment and foundation where the inclinometers and piezometers with the largest response to reservoir fluctuations were from.

The assumed limits of the domain were vertically from the surface at the dam centerline, at Station 2134 m, to the shear zone at SI3999, horizontally along the shear zone to SI3999 (150 m downstream), and vertically to the surface. The lateral extent (into the page) was assumed to be one unit width. The limits of the model domain are as shown in Figure 5.1 and Figure 5.2

The upstream vertical limit was selected as the dam centerline and SI4036, which provides an upstream boundary, through which the downstream horizontal forces will be applied. The downstream vertical limit was selected as SI3999, which is the inclinometer with the largest observed downstream displacement. The zone between these two inclinometers is expected to have the highest piezometric pressures and largest stress response to the reservoir loading increase. This was verified with the use of the simple finite element model. The bottom limit of

the model domain was selected as the horizontal plain from the shear zone at SI3999; this was selected as there was no defined shear zone above this plain. The limits of the model domain represent a block of embankment and fountain materials which was then defined as free body diagram.

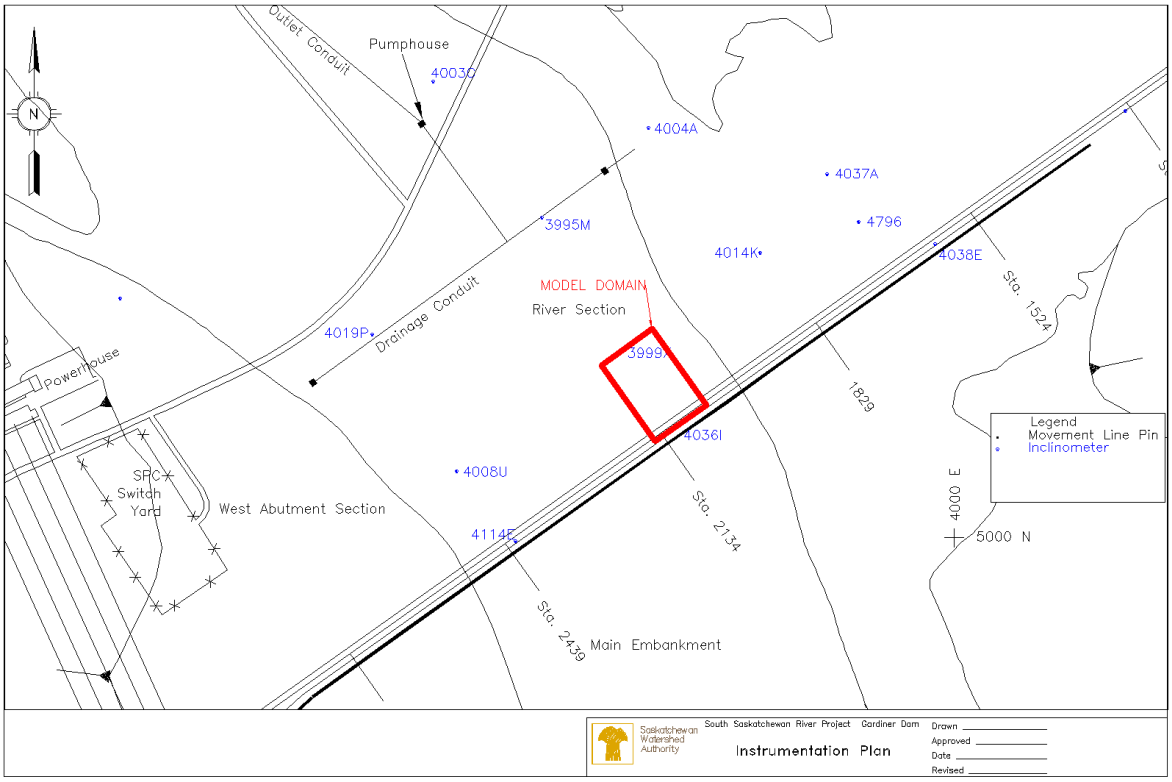

Figure 5.1 River embankment plan view, defining conceptual model domain

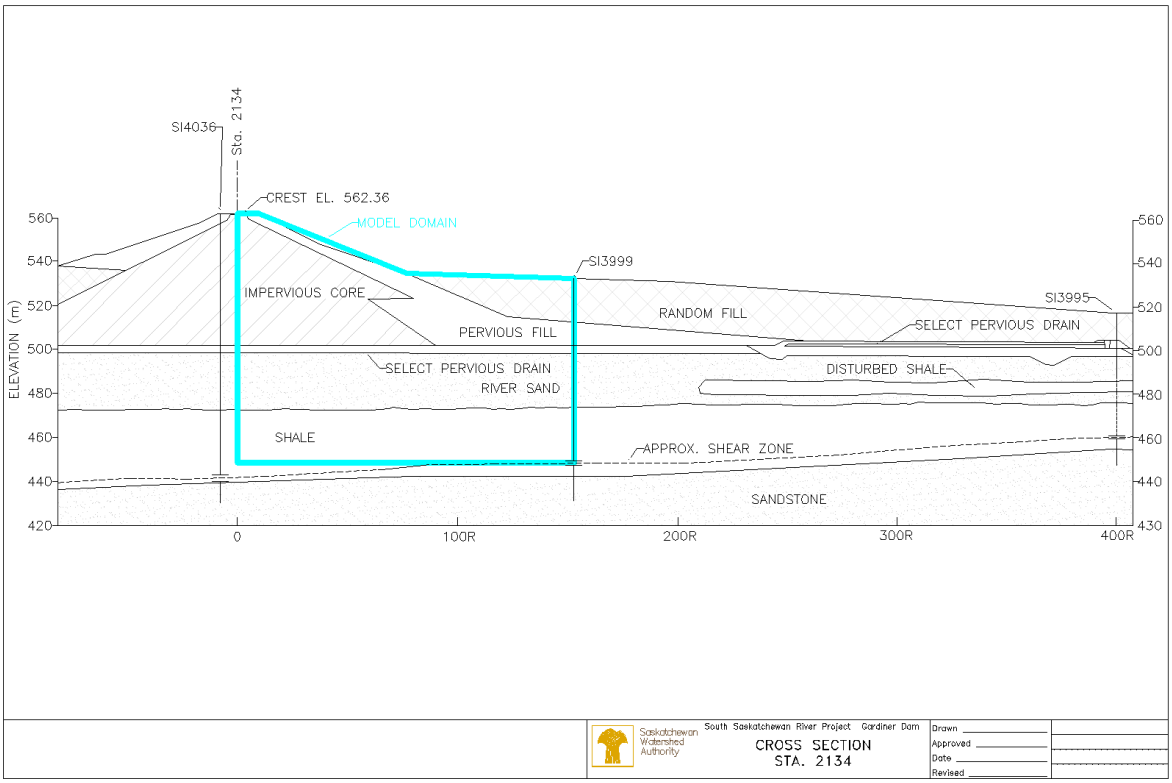

Figure 5.2 River embankment cross section, defining conceptual model domain

5.3 Conceptual Model Boundary Conditions

The model domain was considered as a free body; therefore, the loading conditions discussed in the section will be applied to the free body. To evaluate the conceptual model, several loads were considered to act on the domain, including; 1) reservoir hydraulic horizontal load, 2) shearing resistance at the base of the free body, 3) horizontal soil loading, 4) piezometric uplift pressure, and 5) model domain gravitational body loading.

The forces applied to the domain from the reservoir load, soil horizontal load and uplift at the base of the domain, were derived from the application of a stress distribution to the domain as illustrated in Figure 5.3. The stress distributions were then resolved into forces applied to the domain. Figure 5.4 illustrates the base forces resolved from the stress distributions and the additional forces applied to the domain, such as the body load and the shear zone resistance.

The ongoing displacement was observed to be primarily a function of the variation in the reservoir level and associated incremental horizontal load. Therefore, constant loads such as 2)-5) as described previously, were ignored and only loads influenced by the reservoir fluctuations were considered.

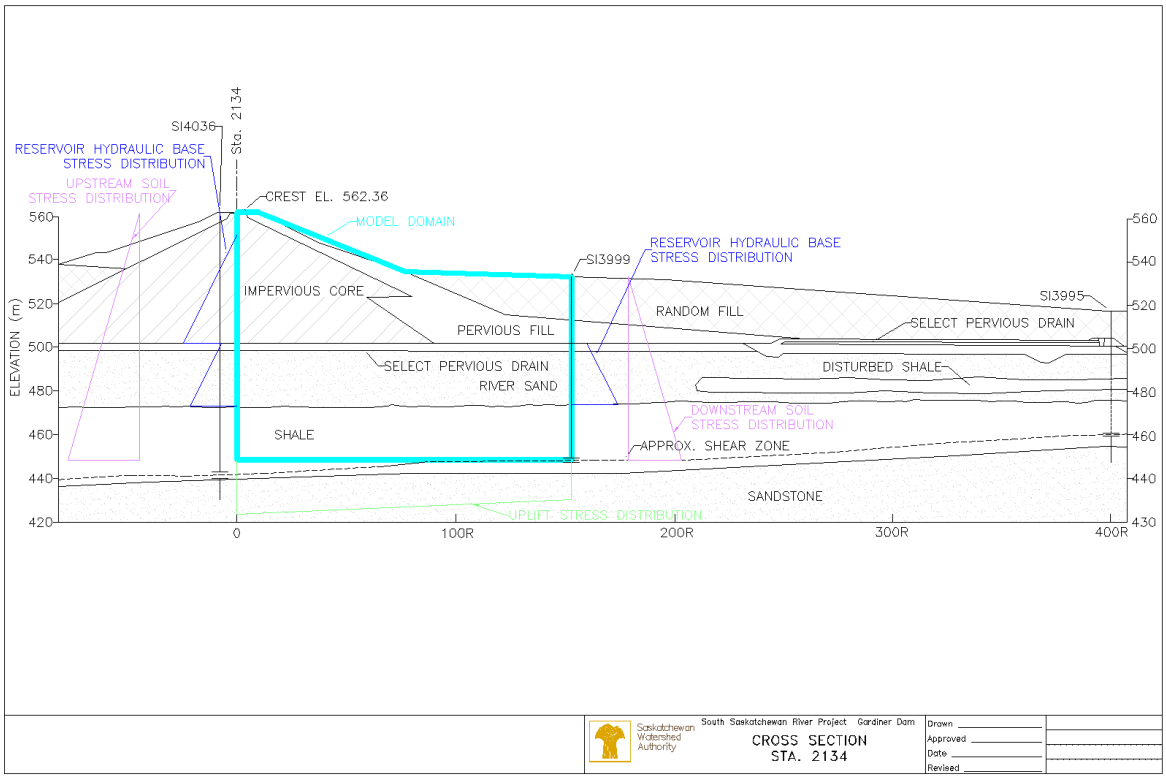

Figure 5.3 River Embankment cross section, defining domain boundary stress distributions

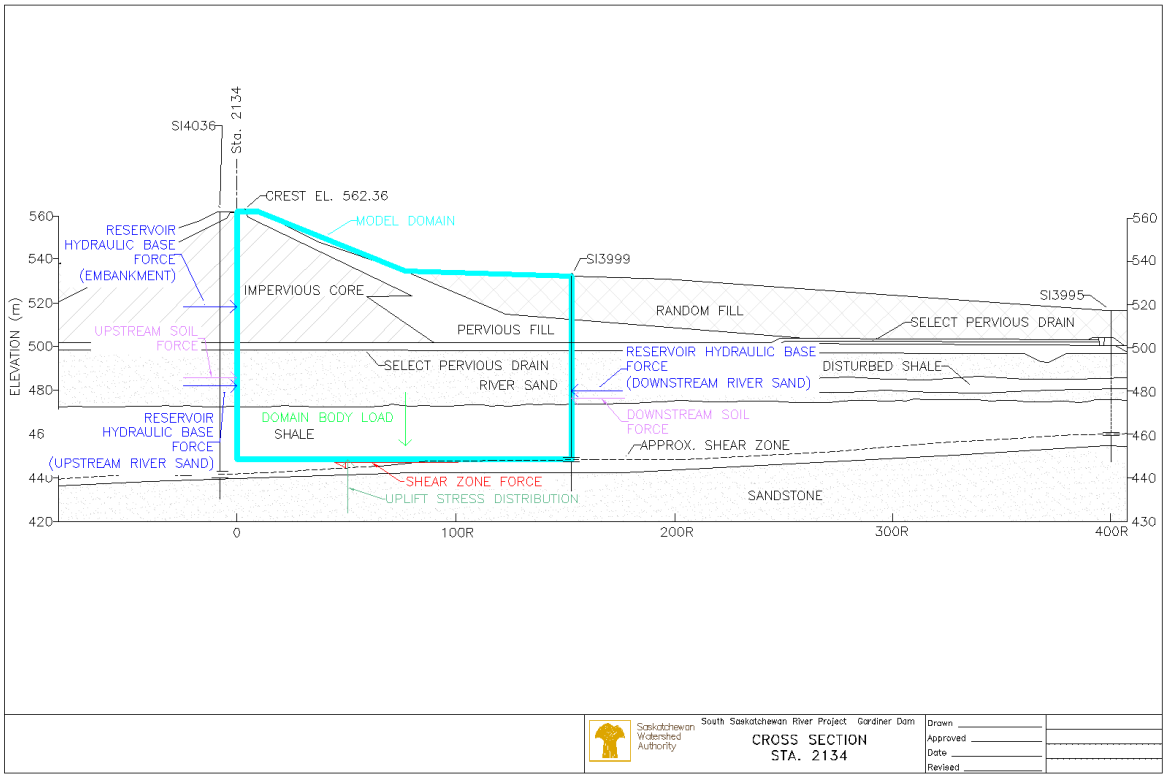

Figure 5.4 River Embankment cross section, defining domain boundary forces

The incremental forces resulting from changes in the reservoir were from the change in the hydraulic stress applied to the embankment, river sand and the resulting increase in the soil passive resistance. It was assumed that the horizontal reservoir pressure was transferred from the upstream face of the embankment to the upstream face of the domain with minimal loss. Due to the high hydraulic conductivity of the river sand, an incremental horizontal stress was applied to the domain as a result of the pore pressure change in the river sand. In addition to the hydraulic stress applied, an increase in the passive soil stress was also applied to set the domain to equilibrium. The incremental stress applied to the domain was on both the upstream and downstream boundaries. Figure 5.5 illustrates the applied stress distribution resulting from an increase in the reservoir. The incremental stress distributions were then resolved into horizontal forces acting on the model domain as illustrated in Figure 5.6.

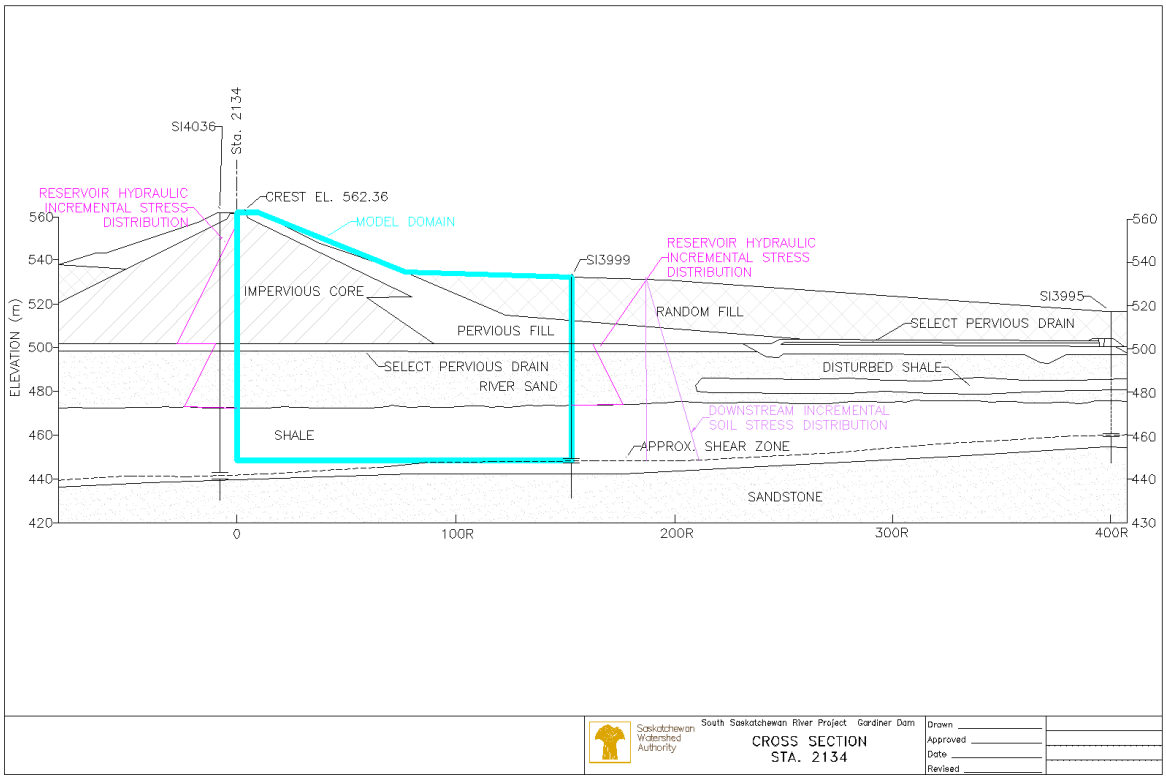

Figure 5.5 River Embankment cross section, defining domain boundary incremental stress distributions

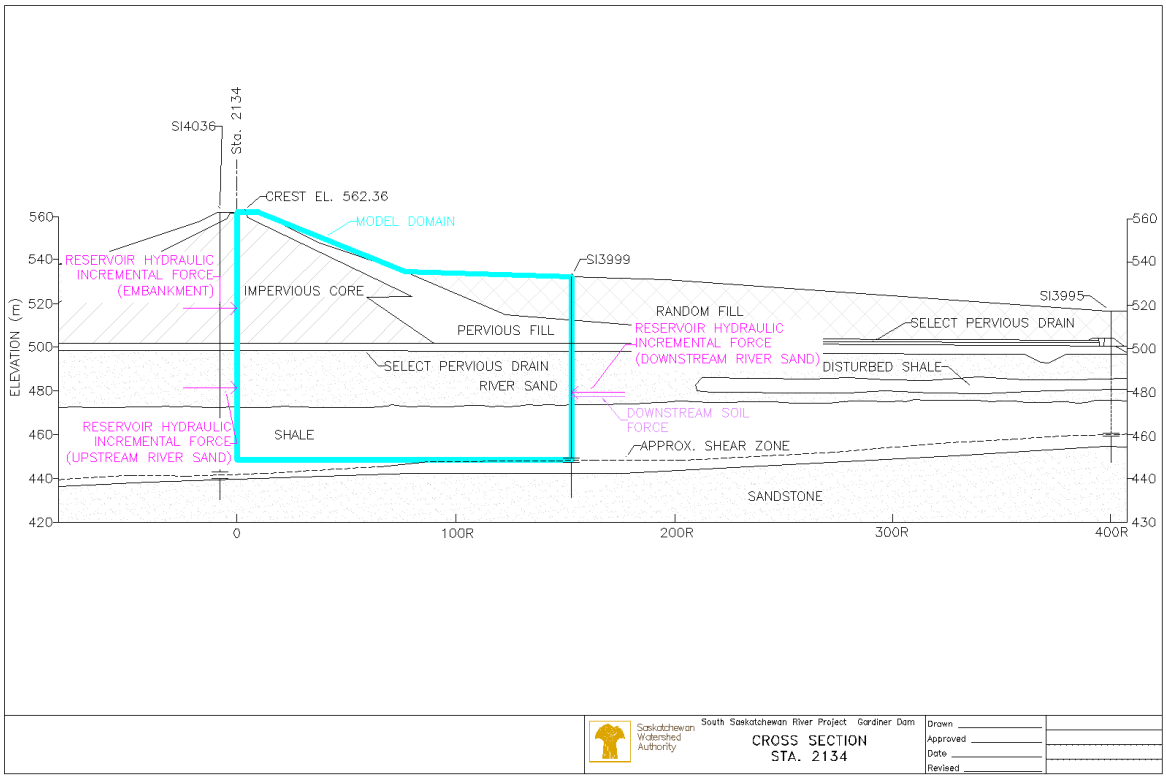

Figure 5.6 River Embankment cross section, defining domain boundary incremental forces

An incremental load was not applied through the shale; however, as discussed previously, it was assumed there is minimal transmission of the total head increase in the shale over the relativity short time frame of one reservoir cycle. This increase was proposed to be from the transfer of total stress of the reservoir. Therefore, it was assumed that any change in piezometric level was the result of the incremental reservoir load and does not add to the loading conditions.

In addition, as the reservoir increased, there was no change in the gravitational body load of the domain. However, with an increase in the reservoir level, the shale piezometric level would result in an increase in the uplift pressure acting on the domain. This would then result in a reduction in the effective vertical load of the domain. The reduction in the effective vertical load would reduce the shear resistance at the bottom of the domain. The reduction in shear stress was reviewed to assess its potential influence on the deformations. The reduction in shearing resistance along the base of the domain represented approximately 2 % of the incremental horizontal load caused by the reservoir. As a result, this reduction in the horizontal loading was considered minimal given the conceptual level of this work and was considered essentially constant.

To allow for the transfer of the incremental horizontal reservoir load to the shale, the shear strength of the embankment and the river sand were assumed to be greater than the shear zone. This was a reasonable assumption as the shear zone is near the residual strength of between ϕ_r'=2.5°-9° and c'=0 kPa. The river sand shear strength was found to be ϕ'=37° and 0 kPa, and the embankment shear strength was found to be ϕ'= 26° and c'=52 kPa (PFRA 1980, PFRA 1981, Stark and Eid 1994). Therefore, the combination of the shear resist at the base of the domain and the passive resistance at the downstream limit resist the horizontal reservoir load.

Assuming the upstream and downstream limits of the domain were rigid, the applied forces were then evenly distributed on the upstream and downstream limits of the model domain as shown in Figure 5.7. This allows for the transfer of the force applied to the domain through the embankment and river sand to the shale. Assuming the horizontal forces are balanced on the upstream and downstream limits of the domain, the upstream pressure distribution was used throughout this work to calculate the total stress applied to the shale.

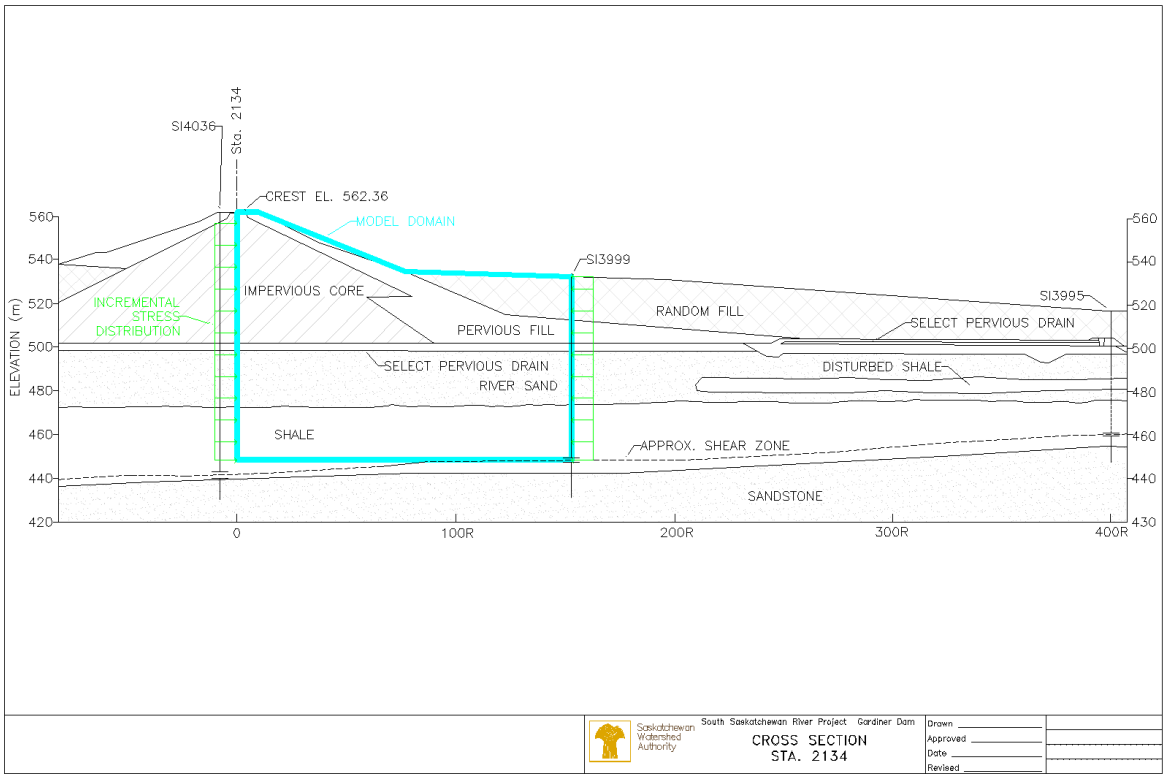

Figure 5.7 River Embankment cross section, defining domain boundary evenly distributed forces

5.4 Analytical Piezometric Response

Using the effective stress principal (Terzaghi et al. 1996), the horizontal load applied to the shale was assumed to be applied relatively quickly, effectively allowing zero drainage initially. Because the soil was initially acting undrained, an increase in stress on the soil caused a proportional increase in porewater pressure. However, as the soil stiffness became closer to that of water, such as for the heavily over consolidated shale (Skempton 1954, Bishop 1973, Bishop 1977), the pore-pressure response was controlled by the elastic pore-pressure coefficient B as described by Skempton (1954). The increase in porewater pressure was then due to the increase in all-around stress caused by the incremental reservoir load, as a function of B.

5.5 Analytical Deformation Response

The deformation of the shale was based on a combination of elastic deformation due to quick loading of the shale (Bishop 1973 and Bishop 1977) and one dimensional consolidation (Terzaghi et al. 1996). The deformation was assumed to occur in the shale above the shear zone and the material below the shear zone was assumed to be stable.

The elastic deformation during rapid loading was generally thought to be near zero as water was assumed to be incompressible relative to the soil. However, since the shale compressibility was closer to water as compared to many other soils and B <1, elastic deformation was considered to occur. The elastic deformation of the shale immediately following loading was assumed to be dependent on the compressibility of the porewater (Bishop 1977).

Consolidation occurred when an increase in total stress was applied to a soil (Terzaghi et al. 1996). When the increased stress was applied to the shale, the majority of the load was taken by the pore fluid as excess pressure, assuming undrained conditions immediately after loading. As time progressed, the excess pressure dissipated and the soil structure rearranged and replaced the discharged porewater, thus causing consolidation. As the increased loading from the reservoir was applied to the shale, excess pressures were developed proportional to the total stress. The reservoir typically remained high for a period of several months; therefore, there was sufficient time for the dissipation of a portion of the excess pressures and consolidation of the shale.

Of the two deformation mechanisms, consolidation will be the primary mechanism as the magnitude of the deformation caused by the consolidation is generally significantly greater than the elastic deformation due to the porewater compressibility.

Throughout the deformation, the shale was assumed to be the controlling compression member of the modelled domain as the shale had the lowest compressibility of the foundation and embankment materials. As a result, the other members such as the river sand and embankment materials were assumed to deform at the same rate and magnitude as the shale. This assumption was confirmed with the inclinometer casings at the limits of the model not indicating additional slip surfaces above the shear zone in the shale. It is recognized that the river sand may not deform in the same manner as the shale and embankment; however, given the lack of deformation in the river sand and the conceptual level of this model, this simplifying assumption was valid. The effects of the compressibility of the river sand should be investigated further at a later date. Due to the normally consolidated nature of the embankment material and the highly over consolidated nature of the shale, it is reasonable to assume that the compressibility of the embankment was greater than the shale.

5.6 Analytical Model Limitations

The model developed within this section is conceptual in natural and due to this, there are several associated limitations. This model was intended to provide confirmation of the general mechanism of movement by using basic principles of geotechnical engineering and review of the historical instrumentation data. Therefore, several simplification assumptions of the geometry and soil properties, such as homogeneity and isotropy were made.

To allow for a clearer preliminary understanding of the mechanisms, only a finite area and select instrumentation was considered. This resulted in some of the instrumentation data and the larger domain of the embankment and foundation being ignored. It will be necessary to test the proposed analytical model against other instrumentation and a larger section of the embankment at a later date.

5.7 Analytical Model Methodology Conclusions

The development of this analytical model has laid the groundwork for the introduction of an analytical model. The next section transfers the conceptual model into an analytical model and compares the analytical model results with the observed piezometric response and the deformations in the shale.

CHAPTER 6 ANALYTICAL MODEL MATERIALS, BOUNDARY CONDITIONS AND METHODOLOGY

6.1 Overview

In the previous section the analytical model was described in a general manner, this section will further define the analytical model. The analytical model will be described in terms of: the detailed model domain, material properties, analytical calculation methodology, model calibration methodology, model sensitivity evaluation and model verification methodology. The calculation methodology was a major aspect of this section; therefore, it was further broken into three steps; 1) calculation of the horizontal loading, 2) determination of the shale piezometric levels, 3) calculation of the displacement of the model. This analytical model was then developed and solved using a spread sheet program.

6.2 Analytical Model Geometry and Assumptions

As previously described, the model is based on a cross section at Station 2134 m perpendicular to the dam centerline. The model domain was defined as a block from the embankment surface, upstream vertical face at dam center line, downstream vertical face at SI3999 and VW179 (150 m and 146 m downstream respectively) and the shale shear zone. The shear zone is represented by a horizontal surface extending from the shear zone at SI3999 to the upstream domain limit. To add to this description for use in the analytical model, details for model domain will be described. Figure 6.1 illustrates the model geometry, providing reference to the specific measurements and applied loading areas described throughout this section.

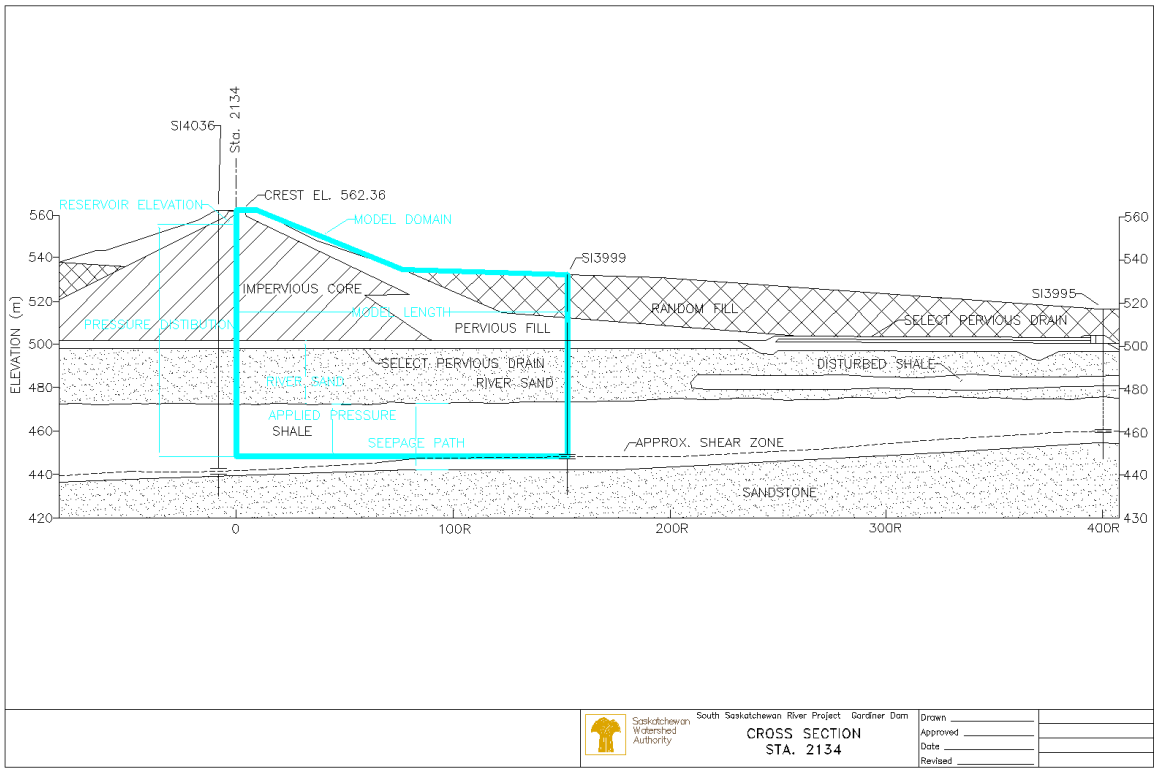

Figure 6.1 River Embankment Cross Section Defining Conceptual Model Geometry

The thickness of the river sand was defined as the difference between the surfaces of the river sand and the shale. The shale thickness was described in two sections; 1) the thickness for the applied pressure, and 2) the drainage path length for consolidation thickness. The applied pressure shale thickness was defined from the shale surface to the shear zone. The thickness for calculating the drainage path length was defined from the surface of the shale to the surface of the underlying sandstone. The length for distributing the incremental horizontal load was the distance between the reservoir surface and the shear zone. The overall length of the model was defined from the dam centerline line to the SI3999 (150 m downstream). Details of the geometry are shown in Table 6.1.

Table 6.1 Conceptual model geometry details

Parameter	Value	Comments
Centerline station (m)	2134	
River sand surface elevation (m)	498.52	Bore hole log SI3999
Shale surface elevation (m)	472.70	Bore hole log SI3999
Shear zone elevation (m)	447.75	Inclinometer SI3999
Surface of sand stone elevation (m)	442.70	Bore hole log SI3999
Thickness of shale (m)	30.00	
Embankment centerline to SI3999 (m)	150.00	SI3999 data Sheet
VW179 tip elevation (m)	450.50	Bore hole log VW179

6.3 Material Properties

The material properties assumed were from several sources of information. The majority of the materiel properties were from laboratory or field testing completed during or shortly after construction by PFRA. More recent laboratory testing was completed in 2009 on undisturbed shale samples. To supplement and verify the laboratory testing results, select published papers were also referenced. The material properties assumed throughout the evaluation are summarized in Table 6.2 and Table 6.3.

Table 6.2 Embankment and foundation material properties

Soil Property	Material Type			
	Embankment (Impervious Core)	River Sand	Intact Shale	SZ Shale
Shear Strength Average (except SZ)				
ϕ'	24.5 [3]	37 [3]	33 [3]	2.5 - 9.8 [4,5]
c' (kPa)	52 [3]	0 [5]	268 [3]	0 [4,8]
Hydraulic conductivity (Hard Shale)				
k_v = vertical (m/s)			1.3e-9 - 1.3e-13	
Compression properties (Hard Shale)				
Coefficient of volume compressibility m_v (1/kPa)			1.3e-4 - 2.7e-6 3.0e-5 average [6]	
Coefficient of consolidation C_v (cm^2/s)			1.77e-4 - 1.63e-5 [6] 1.16e-5 (used in model)	
Pore-pressure coefficient B			0.3-0.7 [1]	
Drained Young's modulus E' (MPa) Calculated			139	
Bulk unit weight γ (kN/m^3)	20.4 [2]	20.4 [2]	20.4 [3,6]	
Void ratio (Hard Shale) e			0.49 - 0.63 [6]	
Porosity Shale n (calculated from void ratio)			0.36	

[1]PFRA (1965a); [3]PFRA (1980); [5]Stark and Eid (1994);
[2]PFRA (1965b); [4]PFRA (1981); [6]Watershed Authority; (2009)

Table 6.3 Porewater properties

Parameter	Value	Comment
γ_{water} (kN/m^3)	9.81	
Coefficient of compressibility water β (1/kPa)	4.60E-07	Fine and Millero (1973)

6.3.1 Embankment Properties

The material properties assumed for the embankment material were from the impervious core which has the largest volume in the embankment. The impervious core was described as medium plastic glacial clay. The strength parameters were developed from laboratory measurements of compacted in place material (PFRA 1980).

6.3.2 River Sand Properties

The river sand was deposited by fluvial deposition and consists of uniformly graded material between fine and coarse sand sizes. Silt and gravely layers are frequent with no evidence of continuous layering of silts and gravels. The material properties were found by consolidated undrained triaxial testing (PFRA 1980).

6.3.3 Snakebite Shale Properties

The shale properties were developed from testing the "hard" shale as defined by PFRA (1980). The hard shale makes up the majority of the Snakebite member therefore will dominate the response observed within the shale.

Snakebite Shale Shear Strength

Jaspar and Peters (1979) observed horizontal movement occurring on a finite shear plane located in the heavily over consolidated shale of the foundation. Due to the finite shear plane and similar material properties, it was expected the shale was pre-sheared due to glacial loading similarly to the other Saskatchewan shale of the late Cretaceous period (Insley et al. 1977, Sauer 1978, Krahn et al. 1979, Sauer 1983, Sauer 1984, Christiansen and Sauer 1984, Clifton et al. 1986, Sauer and Christiansen 1987, Eckel et al. 1987, Wilson et al. 1989, Sauer et al. 1990, Misfeldt et al. 1991, Kelly et al. 1995). Hence, it was reasonable to assume that the shear strength in the defined shear zone was at residual shear strength (Sauer 1978 and Sauer et al. 1990). The shear strength was based on multiple reversal direct shear testing, ring shear testing, and slope back analysis (PFRA 1981 and Stark and Eid 1994).

Even with the possibility of the presence of other pre-sheared zones above the defined shear zone, the shale above the shear zone was assumed to be intact. The shear strength is based on consolidated drained triaxial testing (PFRA 1980).

Snakebite Shale Hydraulic Conductivity

The hydraulic conductivity of the hard shale was determined with insitu falling and constant head tests (PFRA 1960b). The test results obtained from this program were converted to hydraulic conductive using the USBR nomographs. The test results provided the horizontal hydraulic conductivity, k_h. The vertical hydraulic conductivity, k_v was then assumed to be four

times less than the horizontal conductivity due to the horizontal structure of the marine deposited shale (PFRA 1960b). The vertical hydraulic conductivity was assumed as controlling for the model as the vertical direction provides the shortest distance to the river sand and sandstone boundaries.

Snakebite Shale Compression Properties

Due to the relatively low compressibility as compared to the other model material, the shale characteristics were assumed to dominate the deformation process. The shale has been described previously as heavily over consolidated. Sauer and Misfeldt (1993) found the preconsolidation pressure with the Bearpaw Shale to be approximately 11000kPa at different locations within Saskatchewan. This value was confirmed by laboratory testing completed on two samples within the shale in 2009 (Watershed Authority 2009). The loading created by the embankment and reservoir is assumed to be significantly less than the over consolidation pressure as there is only 64 m of fill in place in comparison to the estimated 550m of material (Sauer and Misfeldt 1993) during the shale consolidation period. For this model, it was assumed that any consolidation within the shale was occurring on the recompression portion of the consolidation curves and no virgin compression was occurring.

The undrained elastic modulus, E_u of intact hard shale samples was found by using an unconfined compression test (PFRA 1966b).

The undrained porewater response coefficients in the hard shale, B were found through the unconsolidated undrained triaxial tests (PFRA 1965a) and inferred from observed response to embankment loading (Ringheim 1964, Jaspar and Peters 1979).

6.4 Model Time Step

The model was completed as a time step process where the calculations were completed for each time period between reservoir readings. The reservoir levels measured for use in geotechnical instrumentation interpretation were at a 15 day frequency. Therefore, the modelled results were calculated based on the same 15 day frequency.

6.5 Model Calculations

The calculations performed in this model were separated into three independent steps including; horizontal loading, pore-pressure change, and displacement and are described separately in this section. A detailed explanation of the calculation can be found in Appendix C.

6.5.1 Horizontal Loading

The calculations of the applied horizontal loads are provided in this section. For an intuitive understanding of the calculations and interpretation of the results a "base" loading was calculated. The base loading was calculated assuming the reservoir was at the minimum median level (Elevation 550.8 m). Any horizontal load calculated from a reservoir level above the minimum median level was considered the "total" load. The horizontal load for both the base load and the total load were calculated in a similar manner. The incremental load was then determined by the difference between the total load and the base load. The incremental horizontal loading was ultimately used to determine the incremental increase in the shale piezometric level.

6.5.2 Piezometric Pressure

To simplify the interpretation and to provide an intuitive understanding of the piezometric levels during the modelling, a "base" piezometric elevation in the shale was used to provide an initial reading for the calculated change in piezometric elevation. The piezometric values assumed for the shale were selected for each modelled time period as the lowest value for the drawdown period prior to the start of the model.

To account for the dissipation of excess porewater pressure from the vertical consolidation of the foundation due to placement of the embankment and the associated increase in total vertical stress, a general downward trend was also applied to the total head in the shale. The downward trend was observed to occur in combination with the annual fluctuation of the piezometric levels in the shale. It is understood that vertical consolidation is a nonlinear process. However, as a simplifying assumption, the vertical consolidation was linearized over the period of interest between 1990 and 2010.

The piezometric level selected for the river sand was the minimum value during the drawdown period prior to the start of the model located at BP107 (dam centerline). The river sand piezometric level fluctuated consistently with the reservoir; therefore, only one value was used as a reference between each of the modeled periods. To determine the horizontal load developed through the river sand, a correlation between the reservoir and the piezometric level in the river sand was evaluated. To estimate the magnitude of influence the reservoir level had on the piezometric level in the river sand, the increase in piezometric level was compared with the reservoir level increase. The piezometric level in river sand was found to increase proportionally by approximately 9% of the reservoir increase.

The piezometric level in the river sand and shale were then calculated based on the reservoir level and applied load at the start of each time step. The reservoir load was assumed to remain constant throughout the time step. This allowed for the dissipation of excess porewater pressure within the shale to occur throughout the time step. The piezometric level within the river sand on the other hand, remained constant throughout the time step. The details of the base piezometric elevation used are included in Table 6.4.

Table 6.4 Conceptual model assumed base piezometric elevation

Parameter	Value	Comments
Percent change in river sand piezometric level with change in reservoir elevation	14%	BP107; 1990-2010
Base piezometric elevation river sand (m)	510.20	BP107; 23- May-1995
Base piezometric elevation shale (m)	569.48	VW179; 16-December-1994
Base piezometric elevation shale (m)	568.53	VW179; 18-January-2005
Shale piezometric downward trend (m/day)	0.000248	VW179; 1990-2010

6.5.3 Displacement

The change in the pore-pressure within the shale was assumed to directly impact the displacement within the shale in two ways; 1) The initial elastic response due to the relatively quick loading, and 2) the consolidation of the shale due to dissipation of excess porewater pressure.

For each time step, the change in pore-pressure was assumed to occur immediately at the start of the time step. This model assumes that the shale was constrained with little to no lateral strain occurring, i.e. any change in volume was equal to a change in horizontal length. The change in

horizontal volume due to elastic response was determined from the compressibility of the porewater (Bishop 1973).

The elastic deformation provided a small amount of the total horizontal displacement compared to the horizontal displacement calculated through consolidation. Consolidation in this model was assumed to occur horizontally in a one dimensional manner after Terzaghi et al. (1996). The coefficient of consolidation was assumed to remain constant throughout the consolidation process, as all of the consolidation occurred as recompression of the shale. Along with the coefficient of consolidation, the hydraulic conductivity and the compressibility in the shale were also assumed to be constant. The shale was assumed to be drained vertically on the top and bottom; therefore, the drainage distance was half of the shale thickness. The deformation was calculated at the end of each time step and the deformation calculated was then totaled as time progressed. The totaled displacement was then compared to the observed horizontal deformation at SI3999.

The modelled horizontal displacement was considered to represent the deformation at SI3999 (150 m downstream). This was a simplification because the upstream inclinometer SI4036 indicated less downstream movement than the SI3999. Because of the difference between the displacements, it is speculated that deformation is occurring only through a portion of the model domain. However, due to the lack of additional inclinometers and knowledge of the deformation between these two points, this assumption was made. The extents of the zone of consolidation should be looked at in greater detail in further work.

6.6 Model Calibration

6.6.1 Calibration Methodology

The calibration methodology involved two steps; 1) matching the modelled piezometric response with the observed response, and 2) matching the modelled deformations to the observed deformations.

The controlling parameters were adjusted to provide the modelled data with a "best fit," first to the observed piezometric level in the shale and secondly to the observed deformation in the shale. Following the calibration, several sensitivity tests were undertaken to evaluate the

influence of select variables on the porewater and displacement response. The parameters from the calibrated modelled were then used to model a second time period to verify the calibration parameters. The verification time period increased the confidence in the calibration parameters.

Through the calibration process, the controlling parameters were selected to be shale pore-pressure coefficient B, the shale vertical hydraulic conductivity k_v, and the coefficient of volume compressibility of the shale m_v. It is recognized that there are other variables which will affect the calibration of the analytical model; however, these variables were considered to have the largest impact on the modelling outcome. The other variables were considered constant through the calibration process.

6.6.2 Best-fit Criteria

Select variables were adjusted to achieve a "best-fit" of the modelled data to the observed data. The determination of "best-fit" was at the option of the author based on visual examination of the modelled and observed data.

A statistical evaluation of the modelled data compared to the observed data was out of the scope of this work.

6.6.3 Calibration Time Period

Calibration of the model was completed by selecting a "typical" two year period. A typical period was defined as a period where conditions for the reservoir operation, excess pressures, and shale deformation characteristics could be expected to be similar to current conditions. The selection process was objective and involved reviewing the reservoir levels, piezometric levels within the shale at VW179 and the displacement at SI3999.

A typical reservoir period was considered to not experience an extended low or high period and was relatively recent to reflect the current operating conditions of the reservoir. Typical piezometric levels included a constant decline due to dissipation of construction excess porewater pressures combined with an annual fluctuation with reservoir year to year. Typical displacements included a constant displacement rate from year to year. The calibration time period was selected as January 1, 1995 to January 1, 1997 as it matched the above criteria.

6.7 Model Sensitivity

A model sensitivity analysis of the calibrated model was undertaken to provide insight into the effects of select parameters. The sensitivity analysis was completed on parameters where the variability of the parameter was difficult to define or was known to be affected by the heterogeneity and anisotropy of the soil. To provide consistency, the sensitivity analysis was completed using the median reservoir level for a one year time period.

Several variables could affect the fit between the modelled and observed piezometric response including; the geometry, the assumed general piezometric decrease, the initial piezometric level assumed, ratio between the change in reservoir and the change in river sand piezometric level and shale pore-pressure coefficient B. In addition to the variables discussed in the shale piezometric response, several variables could affect the fit between the modelled and observed deformation response, including the coefficient of compressibility of water, the coefficient of compressibility of the shale, and vertical hydraulic conductivity of the shale.

The model sensitivity evaluation was undertaken in several steps. First, the analytical model was calibrated by achieving a best fit of the observed data. Several parameters were then adjusted within their normal expected range referenced from the historical data, published literature or laboratory testing. As each parameter was adjusted within their normal range, the remaining parameters were held constant at their calibrated value. The next several subsections describe the parameters which were adjusted. A summary of the ranges which the variables were evaluated is included in Table 6.5

Table 6.5 Sensitivity evaluation parameter range

Soil Property	Minimum	Maximum
Hydraulic conductivity (Hard Shale)		
k_v vertical (m/s)	1.3e-13	1.3 e-9
Compression properties (Hard Shale)		
Coefficient of compressibility m_v (1/kPa)	1.3e-4	2.7e-6
Pore-pressure coefficient B	0.3	0.7
Time Stepping (days)	1	15
Model Geometry (number of blocks)	1	2
Reservoir Range (daily)	Minimum	Maximum

6.7.1 Sensitivity to Time Stepping

Provided that time was a variable in the hydraulic conductivity of the shale, the effects of the time step size were evaluated. The time step was varied between the assumed 15 day period to 1 day period.

6.7.2 Sensitivity to Model Geometry

The model geometry was assumed to be constant through the modelling process. However, the model domain was assumed to be a single block in the analysis. The effects on the calculated piezometric level and deformation of reducing the size and increasing the number of the evaluated blocks were evaluated. This was completed by splitting the single block into two sections and remodelling.

6.7.3 Sensitivity to Reservoir Range

The reservoir level provides one of the largest unknowns; however, the range of reservoir levels is relatively well known. Since all the calculations are a function of the reservoir level, the sensitivity to the known range of reservoir levels was tested. The sensitivity was determined by adjusting the entire reservoir range to the minimum and maximum reservoir levels for any given day between 1980 and 2011, similarly to the median reservoir level.

6.7.4 Sensitivity to Pore-Pressure Coefficient B

The B parameter was identified as a controlling parameter as it has a largest potential impact on the calculated porewater pressure in the shale. This parameter was determined using laboratory testing and field observations. B has been found to be difficult to obtain in laboratory testing due to deviation from a fully saturated condition (Bishop 1976). Because of this discrepancy and the potential variability, the effects of changes to this parameter were evaluated.

6.7.5 Sensitivity to Vertical Hydraulic Conductivity k_v

The k_v variable was identified as a controlling parameter of the deformation modelling and has a large impact on the deformation of the shale. The insitu hydraulic conductivity of shale is known to depend on the intact material properties along with the variability of the formation structure including stratification, laminations and fractures (Terzaghi et al. 1996). Numerous structural discontinues and significant stratification in the shale were found by PFRA (PFRA

1960b, PFRA 1980); therefore, greatly impacting the consistency of the insitu hydraulic conductivity. Because of the variability of the insitu hydraulic conductivity, the effects of changing this parameter was assessed.

6.7.6 Sensitivity to Coefficient of Volume of Compressibility m_v

The m_v parameter was defined as a controlling parameter for the deformation within the shale. The coefficient of compressibility is dependent on the stress history of the material as compared to the currently applied stress, i.e. recompression vs. virgin compression (Terzaghi et al. 1996). Due to the highly over consolidated nature of the shale and the applied stress range of the embankment, the shale remains well within the recompression range; therefore, the variability of the coefficient of consolidation parameter remains limited. However, the laboratory testing indicated a range of two orders of magnitude for this value. This variable is sensitive to disturbance during sampling and testing; therefore, the variability in the lab testing results was expected (Terzaghi et al. 1996). Due to the variability of the laboratory testing results, the effects of changing this parameter were evaluated.

6.8 Model Verification

Verification of the model was completed by using the same parameters found in the calibration period and applying them to different reservoir time periods. This provided confidence that the conceptual model proposed can represent the deformation response in the foundation shale in response to with varying reservoir loadings. The initial verification period was a typical two year period between January 1, 2005 and January 1, 2007.The calibrated model results were then further verified with a fifteen year period from January 1, 1995 to January 1, 2010.

6.9 Analytical Model Methodology Conclusion

This section described the methodology used for the development of the analytical model. The items discussed included the detailed definition of the model domain, material properties, model calculations, calibration process, variable sensitivity evaluation process, and model verification process. The next section takes the details and process and presents the results from the analytical model.

CHAPTER 7 ANALYTIAL MODEL RESULTS

7.1 Overview of Analytical Model

The analytical testing outcome of the proposed conceptual model for the ongoing annual displacement of the foundation at Gardiner Dam is presented in this section.

The previous two sections included a description of the analytical model for the horizontal deformation mechanism within the foundation shale. The conceptual model generally described the transfer of the reservoir load to the shale pore-pressure and the deformation of the shale due to the dissipation of the excess pore-pressure. To test the proposed conceptual model, a simple analytical model was developed to verify the conceptual model. The analytical model was calibrated by adjusting select parameters to match the modelled data to the observed data. Following calibration, the sensitivity of the select variables was tested. The calibrated model was also verified by comparison over different time periods. The results of the model, calibration, sensitivity and verification are present in this section.

7.2 Calibration Outcome

Model calibration was achieved by varying the identified controlling parameters until the modelled data achieved a best fit with the observed data. The calibration involved a two-step process; 1) fitting the piezometric values in the shale, and 2) fitting the displacements values in the shale.

Following the calibration of the model, the modelled piezometric levels indicated a match of the magnitude at the high and low points of the piezometric data as shown in Figure 7.1. In addition, the magnitude of the deformation in the model appeared to match well, within 0.5 mm of the observed deformation at the end of year two. However, there was a discrepancy between the observed and modelled data at the end of year one by approximately 2.3mm. This discrepancy was thought to be caused by the relatively slow decrease in the reservoir elevation following the peak. The analytical model considered a decrease in reservoir elevation as removal of loading and zero dissipation of excess pore-pressure which in turn equaled zero displacement. The calibration illustrated that the analytical model may not match the exact observed deformation; however, on an annual basis, a prediction of deformation within ±2mm would be acceptable for

this level of model. This also confirms the conceptual process of the increase in shale pore-pressure and the downstream displacement.

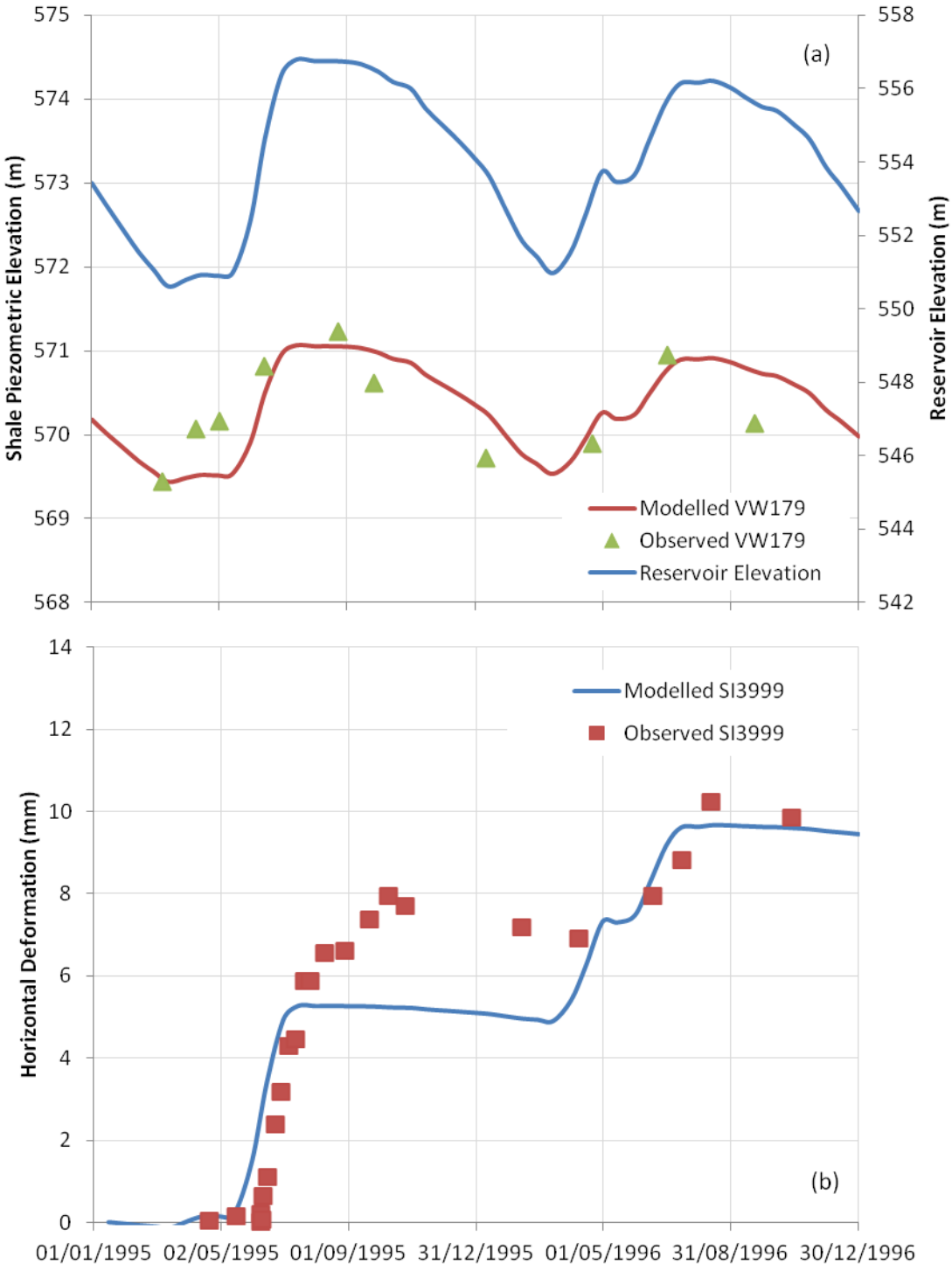

Figure 7.1 Analytical model calibration results, 1995-1997: (a) Reservoir elevation and shale piezometric response, and (b) Foundation horizontal deformation response

The values of the previously identified controlling parameters found to provide the best-fit in the calibration process ranged between the laboratory test and field observed values provided in Table 6.2, indicating the calibrated values were a reasonable representation of the laboratory and field values. The values for the controlling parameters determined from the analytical model are shown in Table 7.1.

Table 7.1 Calibrated controlling parameter values

Parameter	Value
Pore-pressure coefficient B Shale	0.5
Hydraulic Conductivity Shale k_v (m/s)	1.0e-10
Coefficient of volume compressibility shale m_v (1/kPa)	6.60E-05

7.2.1 Shale Stiffness Verification

To further verify the modelled stiffness of the shale, the stiffness properties of the shale were back calculated from the calibrated B value. The stiffness of the shale was back calculated with the following process.

The stiffness of materials generally reported from the literature uses a drained Young's modulus. Therefore, the following steps were taken to calculate the drained Young' modulus. The first step was to determine the coefficient of volume of compressibility from B. The coefficient of volume compressibility was calculated from B following (Skempton 1954):

$$m_v = n\beta(1 - B) \tag{7-1}$$

where n is the porosity of the soil, β is the coefficient of compressibility for water. The next step was to determine the constrained modulus by inverting the coefficient of volume compressibility as follows (Lamb and Whitman 1969):

$$D' = \frac{1}{m_v} \tag{7-2}$$

where D' is the constrained modulus.

The constrained modulus was then related to the Young's modulus by (Lamb and Whitman 1969):

$$E' = \frac{D'(1+\nu')(1-2\nu')}{(1-\nu')} \quad (7\text{-}3)$$

Mayne and Poulos (1999) found that the Poisson's ratio for most soil range was between 0.1 and 0.2. Therefore using B = 0.5, average shale n =0.36 and a ν' = 0.2, the calculated E' from the value of B was 10800 MPa. The literature indicated a range of drained Young's modulus for shale to be between E' = 139 MPa to 32000 MPa (PFRA 1966b, Jizba 1991, Gautam and Wong 2006, and Sarout et al. 2006). Since the back calculated E' is within the range presented in the literature, this provides confidence the model is providing appropriate results.

7.3 Sensitivity Outcome

7.3.1 Sensitivity to Time Stepping

Changing the time step of the model from 15days to daily resulted in a significant decrease in the observed displacement from the calibrated model. The results of the sensitivity can be found in Figure 7.2.

The piezometric analysis indicated that change to the daily time step reduced the calculated piezometric values by a small amount, <0.1m. This indicated a minimal effect from the change in the time stepping as expected since none of the parameters for modelling the piezometric pressure are time dependent.

The deformation analysis was particularly sensitive to the change in time stepping with a significant under estimate of the deformations. The daily time stepping estimated the deformation to be >3.5mm less than the 15 day time step. The discrepancy is likely the cause of the calculations for the coefficient of consolidation and one dimensional consolidation calculation, as the coefficient of consolidations is a time sensitive variable. This implies that time is a major consideration for this analysis in terms of reservoir change and rate of consolidation and should be considered in any further evaluations.

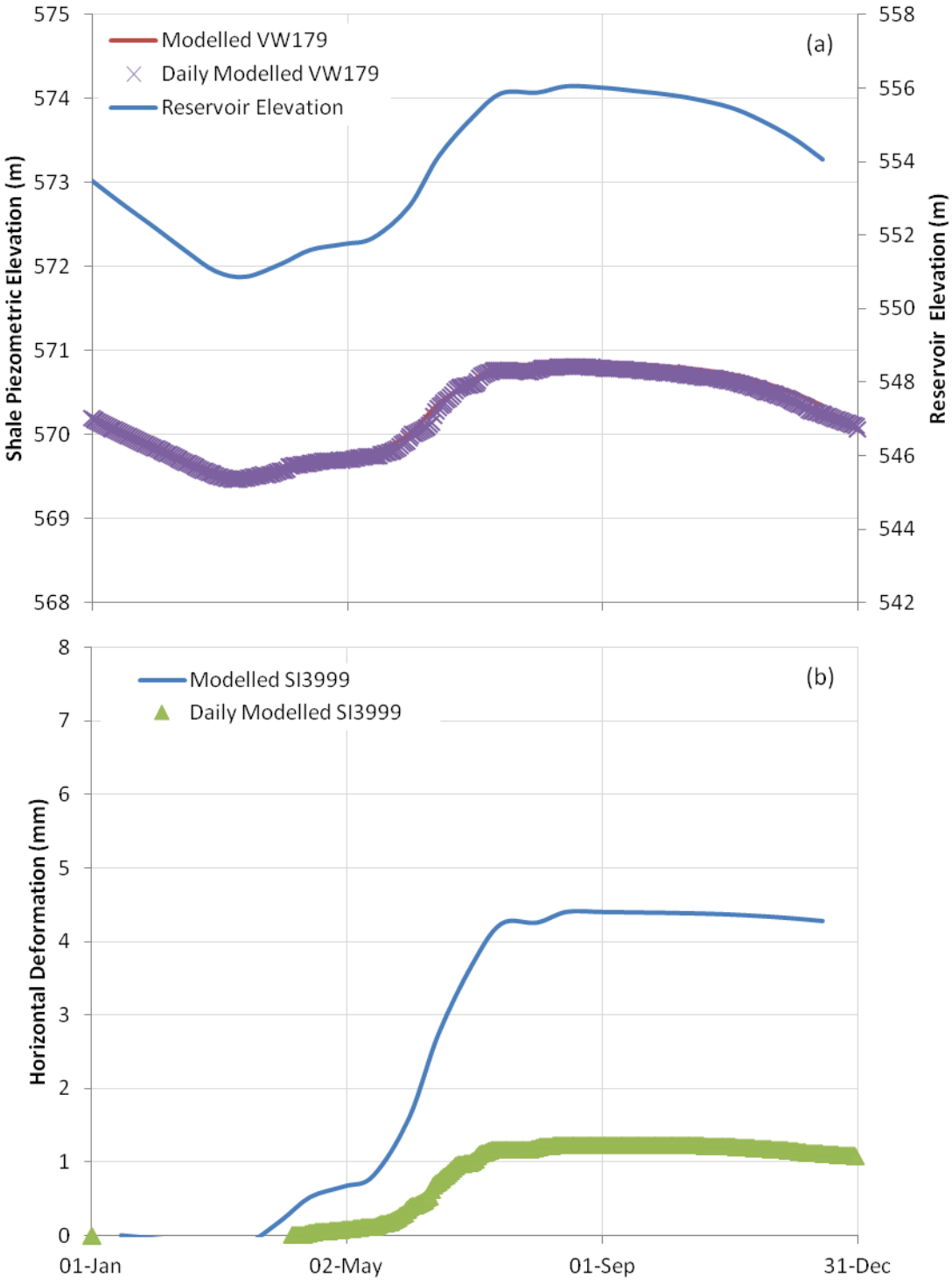

Figure 7.2 Sensitivity of the model to time step changes: (a) Reservoir elevation and shale piezometric response, and (b) Shear zone horizontal deformation response

7.3.2 Sensitivity to Section Model Geometry

Changing the size of the modelling blocks within the domain had noticeable effect on the piezometric response and minimal effect on the deformation response. The results of changing the analysis are shown in Figure 7.3.

The piezometric response appeared to be slightly sensitive to the size of the analysis blocks. This was expected as the pore-pressure is a function of the distance between the shear zone and the embankment surface at the upstream face of the block. Compared to a single block, the upstream block had a larger height; therefore, decreasing the piezometric response. The downstream block had a smaller height than a single block; therefore, increasing the pore-pressure response.

The combined deformation of the two blocks was relatively insensitive to the increase in number of blocks with a minimal deviation from the initially modelled deformation.

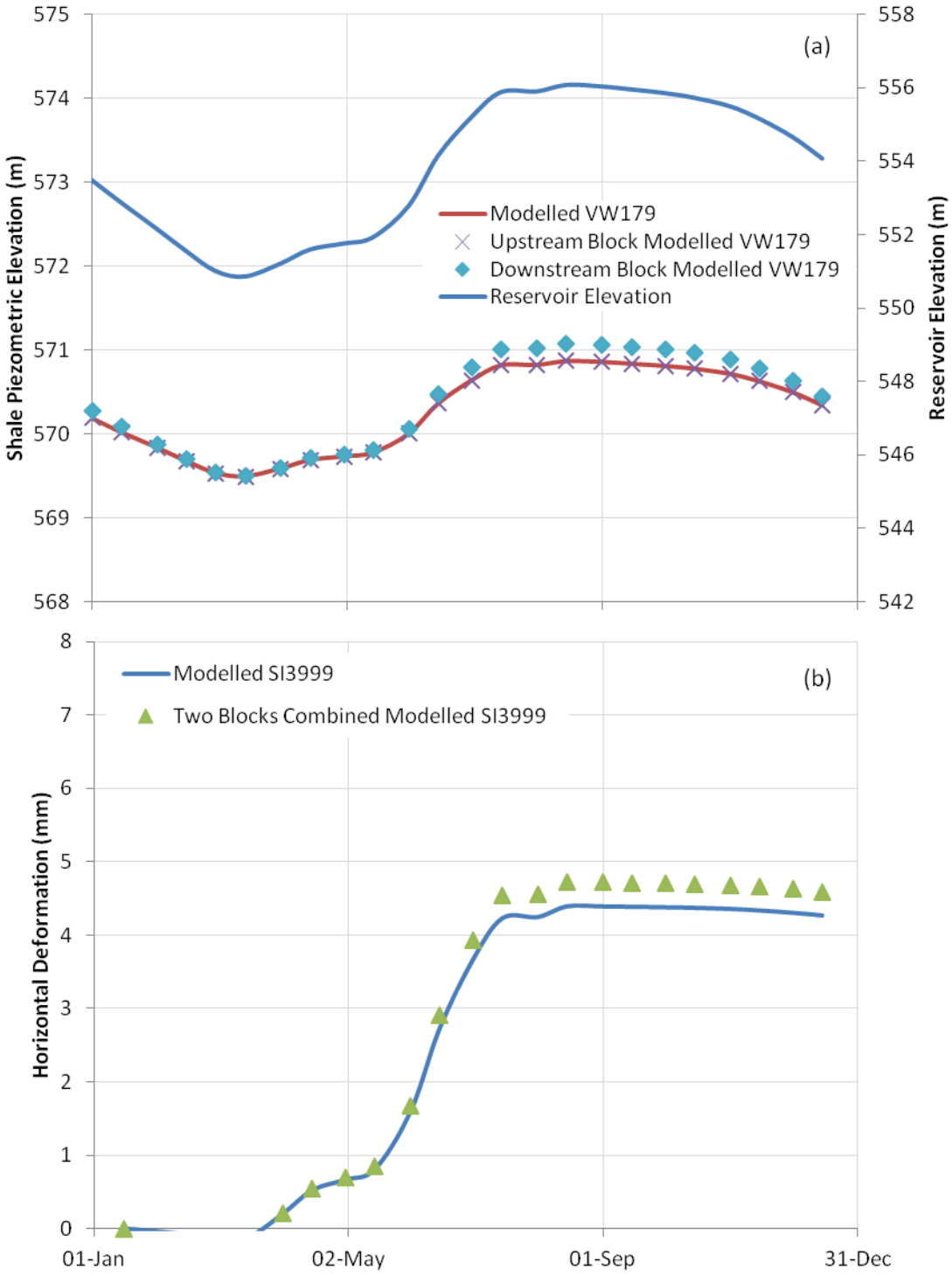

Figure 7.3 Sensitivity of the model to block size changes: (a) Reservoir elevation and shale piezometric response, and (b) Shear zone horizontal deformation response

7.3.3 Sensitivity to Reservoir Range

The reservoir range resulted in a large fluctuation in the porewater pressure calculation and the calculated deformation as expected. This evaluation showed that the effect the reservoir has on the piezometric response and the deformation response was more involved than simply comparing the maximum and minimum reservoir values to the median values. The effects of the change in the reservoir level are shown in Figure 7.4.

The piezometric response as expected was greatly influenced by the reservoir level. The maximum reservoir piezometric response was >1.1 m larger than the median reservoir level prior to the peak of the reservoir. The deviation between the maximum reservoir level and the median reservoir was less near the peak of the reservoir, since the reservoir normally operates near the maximum operating level on an annual frequency. The piezometric response to the minimum reservoir was >1.2m less than the median reservoir.

The deformation response, as expected, was sensitive to the range of reservoir levels. The response to the minimum reservoir level was >1mm below the median reservoir level. However, the direction of the deformation in response to the maximum reservoir level was unexpected. It was expected that the higher reservoir would produce larger deformations. The deformation was found to be approximately 1mm less than the median reservoir at the end of the modelled time period. However, during the increase in reservoir level the deformation response from the maximum reservoir level was greater than the median reservoir which was the expected response.

The discrepancy observed in the deformation response modelled was likely due to the way the median, maximum, and minimum reservoir values are achieved. The reservoir levels represent the median, maximum, and minimum value on a particular day, and as a result do not represent the true operation of the reservoir in any particular year. Furthermore, the maximum reservoir cycle has values that started high at the beginning of the year and remained high throughout the year. As a result, there was limited available room for the reservoir to increase; therefore, the magnitude of the incremental change in the reservoir was less than the median reservoir. As a result, the change in the piezometric response was less than the median reservoir period and the calculated deformation was less as there was less pore-pressure to dissipate. With less porewater

dissipation, there was less deformation, and at the end of the modelled time period there was less total deformation. The greatest difference between the median deformation and the maximum reservoir level occurred when the maximum reservoir increased at an earlier time than the median model.

With the above problems, the maximum and minimum reservoir levels do not necessarily represent the sensitivity of the model to reservoir level. Due to the uncertainty of the annual reservoir fluctuation, the sensitivity of the model to the reservoir level is difficult to ascertain as the reservoir level and time period both affect the sensitivity.

Even though the sensitivity of the reservoir level is difficult to ascertain, this evaluation provided insight into the effect of the magnitude of reservoir fluctuation on the calculated deformation. The minimum and maximum reservoir levels both have less overall change in magnitude than the median level per reservoir cycle. With the reduced magnitude of change in reservoir level, the deformation was reduced. This indicated that the sensitivity to the total magnitude of reservoir change is likely caused by the reduced development of excess pore-pressure with the minimum and maximum reservoir levels as compared to the median level.

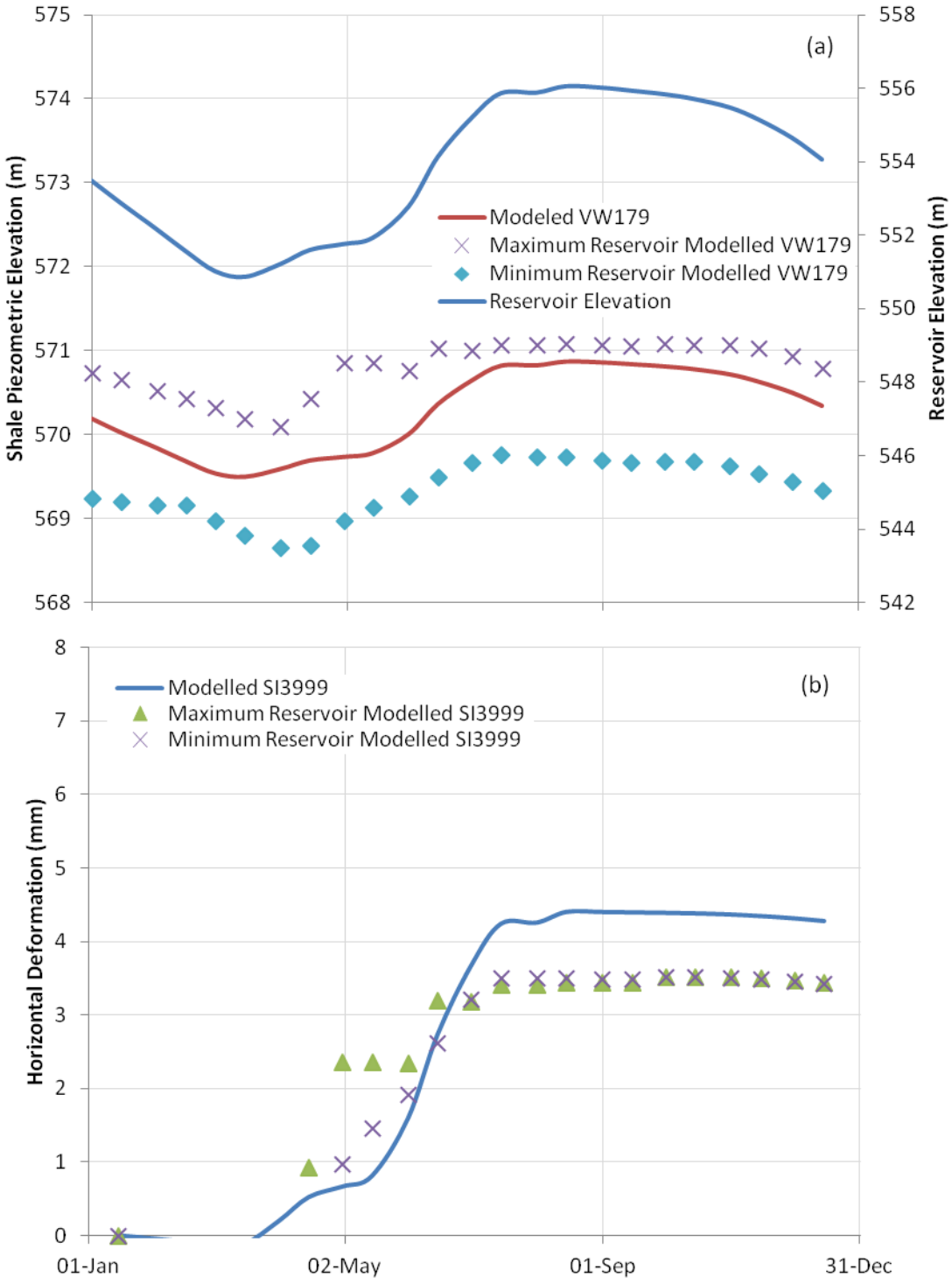

Figure 7.4 Sensitivity of the model to reservoir elevation changes: (a) Reservoir elevation and shale piezometric response, and (b) Shear zone horizontal deformation response

7.3.4 Sensitivity to Pore-Pressure Coefficient B

Changes in the pore-pressure coefficient B had a large effect on the piezometric response and as a result also had an effect on the deformation response. The sensitivity of the elastic pore-pressure pressure coefficient B in the analysis is shown in Figure 7.5.

The piezometric response was highly influenced by the changing of B. As the loading increased the deviation from the calibrated model also increased. This was seen with the increase in deviation between the calibrated model data and the maximum and minimum B values. The piezometric values deviated >±0.5 m from the median piezometric value.

As a result of the increased piezometric response, the deformation also responded to B. The range of B provided a deviation of approximately ±1.5 mm from the median deformation. The deviation occurred with a similar pattern as the deviation of the piezometric levels.

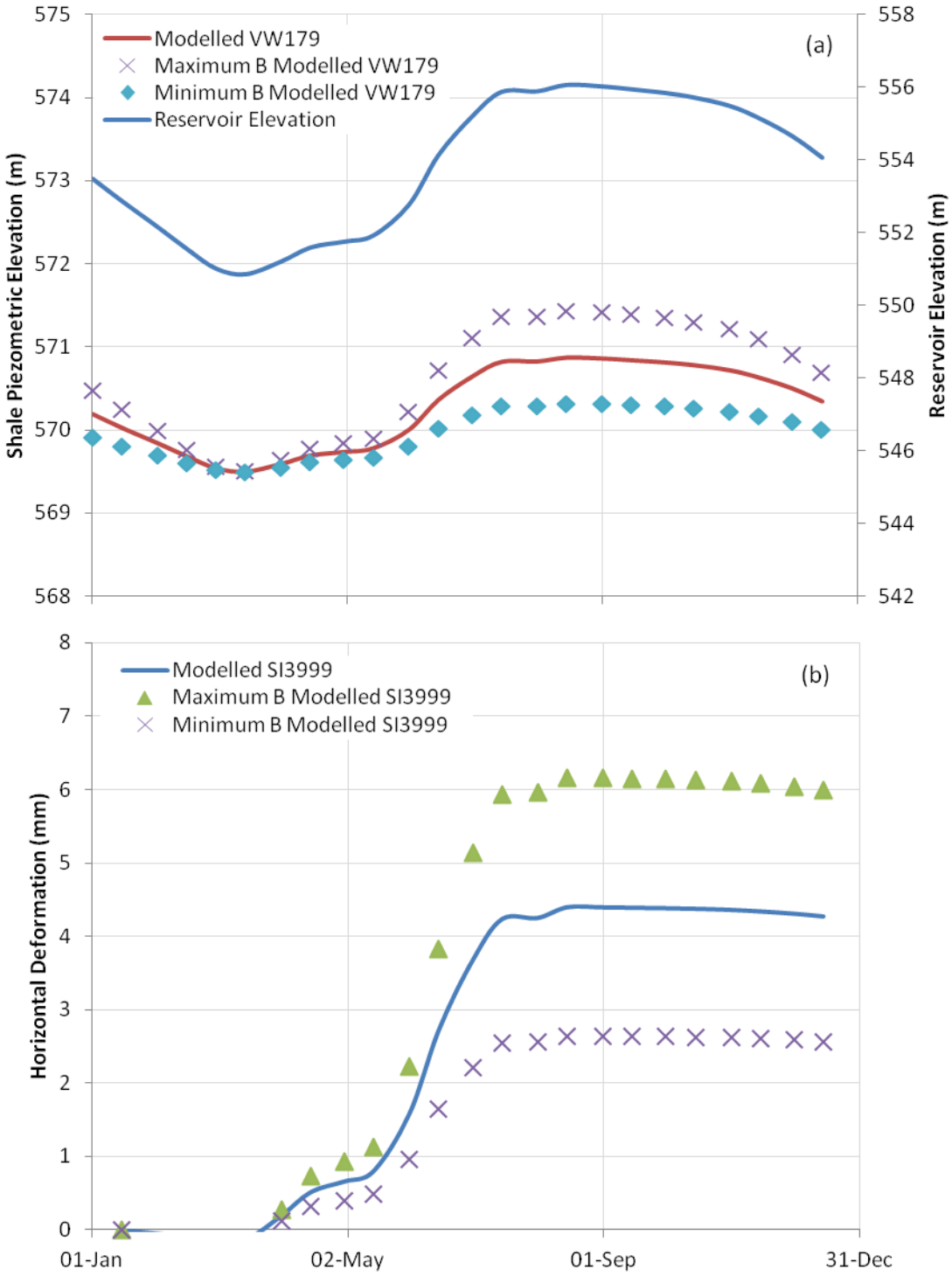

Figure 7.5 Sensitivity of the model to variations in pore-pressure coefficient B: (a) Reservoir elevation and shale piezometric response, and (b) Shear zone horizontal deformation response

7.3.5 Sensitivity to Vertical Hydraulic Conductivity k_v

Changes in the vertical hydraulic conductivity, k_v had a minimal impact on the piezometric response; however, it had a large impact on the deformation response. The effects of the range of k_v are shown in Figure 7.6.

The parameter k_v had minimal practical impact on the piezometric response. The difference in the response which was present was the result of the ability of the shale to dissipate the excess pressure through the time step. The dissipation of the excess pressure over a time step was in the order of centimeters of water; whereas, the change in the piezometric level due to the reservoir fluctuation was in the order of meters. As a result, the effect of the hydraulic conductivity on the piezometric pressures was over ridden by the influence of the addition of the reservoir load.

The deformation analysis was highly impacted by changes to k_v, as the hydraulic conductivity directly impacts the dissipation of excess porewater pressure and in turn influenced the deformation. Due to the high variability of k_v within the shale, there was an uncertainty of several orders of magnitude surrounding this value. The variability was reflected in the large difference between the modelled responses within the range of k_v values. With a higher hydraulic conductivity, the modelled magnitude was up to 10mm greater than the calibration parameters. With the lower hydraulic conductivity, the modelled magnitude was approximately 4mm less than the calibrated parameters. The maximum deviation from the calibrated parameters occurred when the maximum deformation occurred.

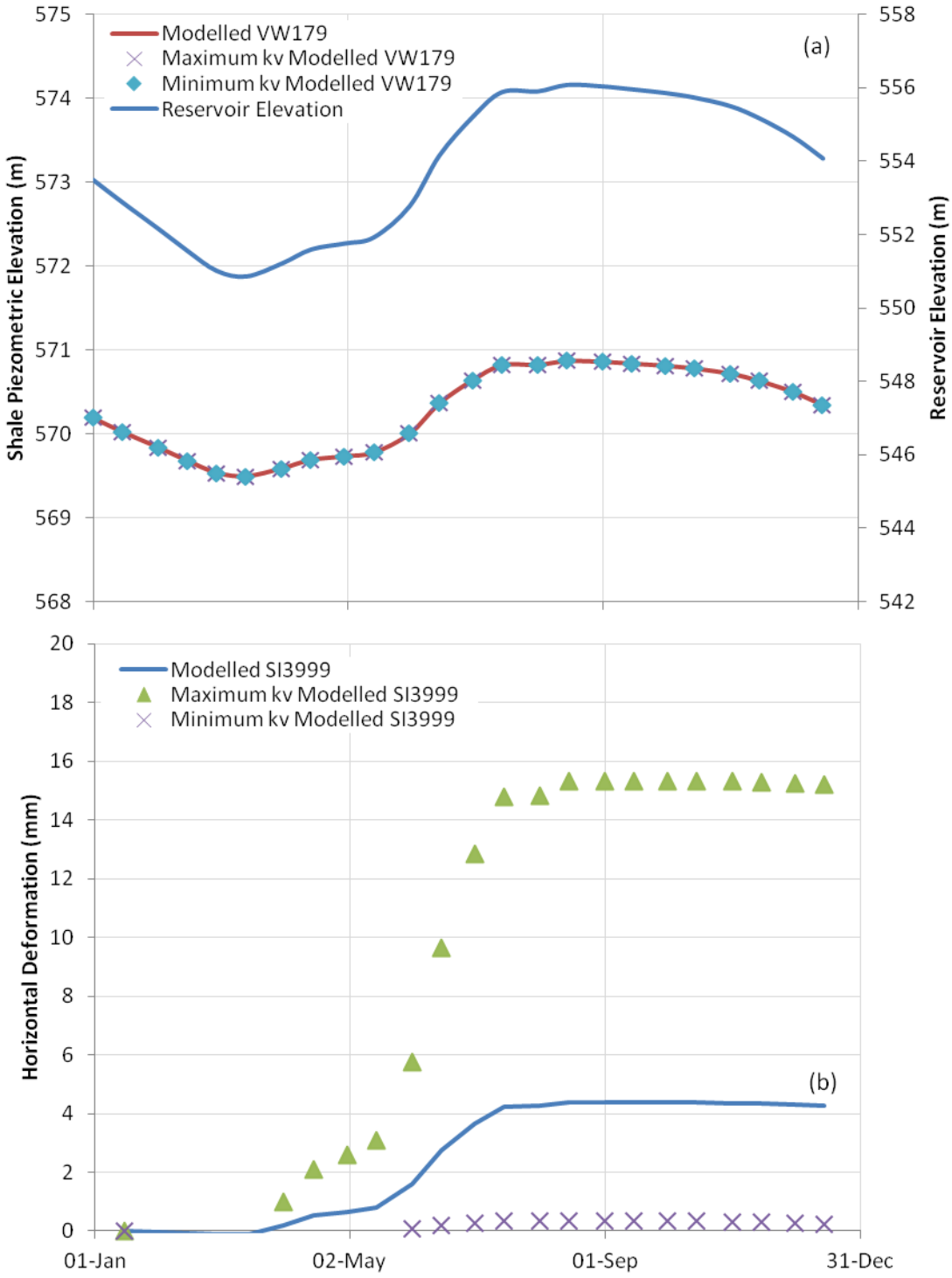

Figure 7.6 Sensitivity of the model to variability of the horizontal hydraulic conductivity k_v: (a) Reservoir elevation and shale piezometric response, and (b) Shear zone horizontal deformation response

7.3.6 Sensitivity to Coefficient of Volume of Compressibility m_v

Changes in the coefficient of volume compressibility resulted in no fluctuation of the piezometric level and a large influence for the deformation. The sensitivity of coefficient , m_v is shown in Figure 7.7.

The parameter m_v has no impact on the piezometric response as m_v is not related to the piezometric response.

The deformation analysis experienced a large influence due to changes in the value of m_v. The variability of m_v from the laboratory testing was much less than k_v; therefore, the range of deformation was significantly less. The highest coefficient of volume compressibility modelled was 2mm greater deformation than the calibrated parameters. The lowest coefficient of compressibility modelled the deformation approximately 3.3mm less than the calibrated parameters.

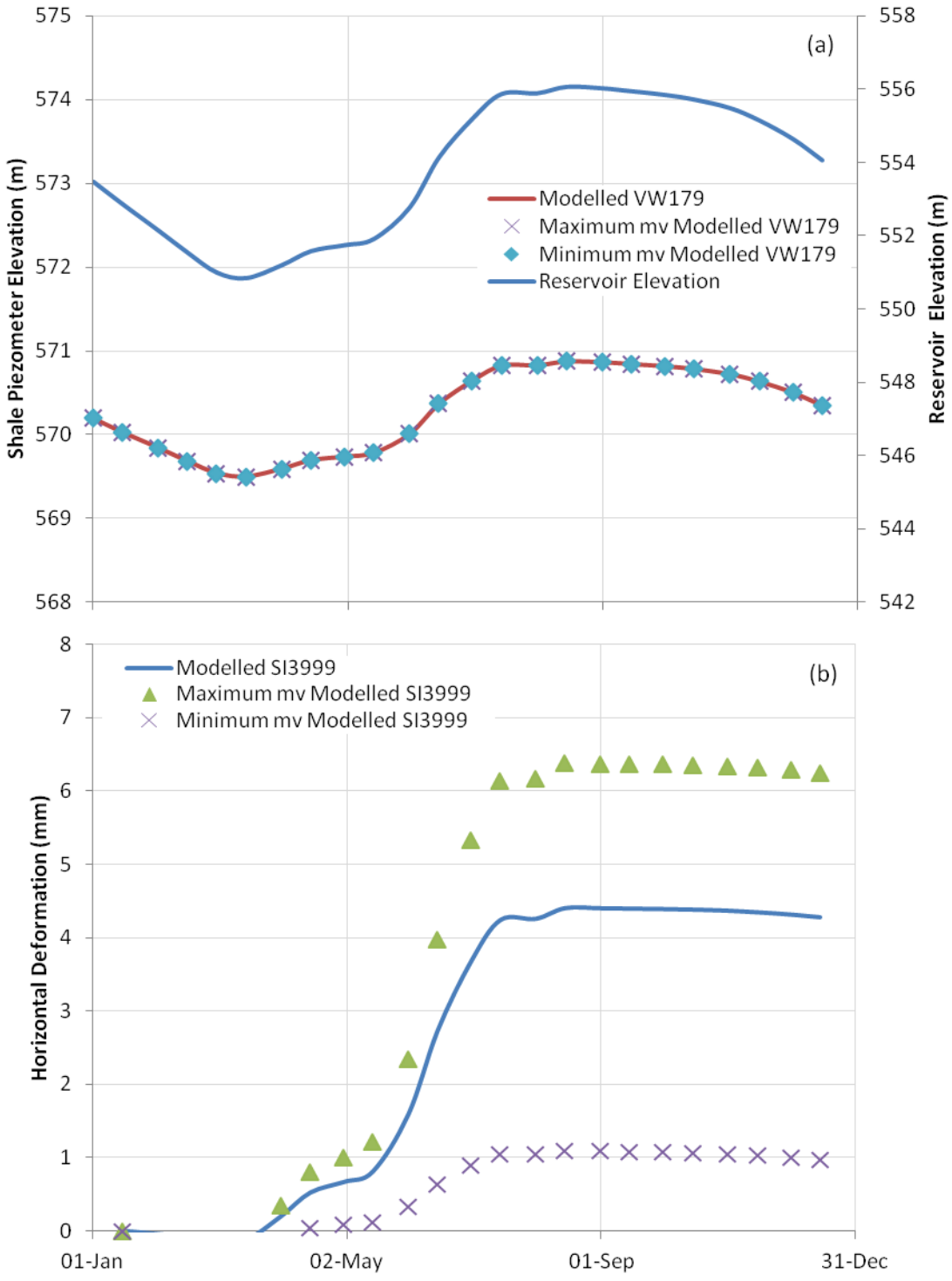

Figure 7.7 Sensitivity of the model to variability of coefficient of volume change m_v: (a) Reservoir elevation and shale piezometric response, and (b) Shear zone horizontal deformation response

7.3.7 Summary of Sensitivity

The sensitivity of each parameter within their measured range is difficult to interpret by looking at several figures individually. To allow for a comparison of the maximum and minimum deviations from the calibrated parameters, a tornado plot of this deviation is shown on Figure 7.8.

In this comparison, the largest variability in terms of piezometric response existed with reservoir level and B. The pore-pressure coefficient B indicated that the piezometric values could range by approximately ±0.6 m. The effect of the variability of the reservoir had on the piezometric response had been discussed previously; however, due to the difficulty in evaluating the sensitivity of the reservoir, further discussion will not be included here.

The variability of the piezometric response directly impacted the deformation model. The variability of the deformation provided by B was substantially less than the deformation variability due to k_v. Figure 7.8 clearly illustrates that k_v provided the largest deformation variability of the key parameters. The variability of k_v indicated that the deformation values could range between 10.9 mm greater or 4.1 mm less than the calibrated parameters.

The largest two controlling variables found in this analysis were found to be the pore-pressure coefficient B and vertical hydraulic conductivity k_v.

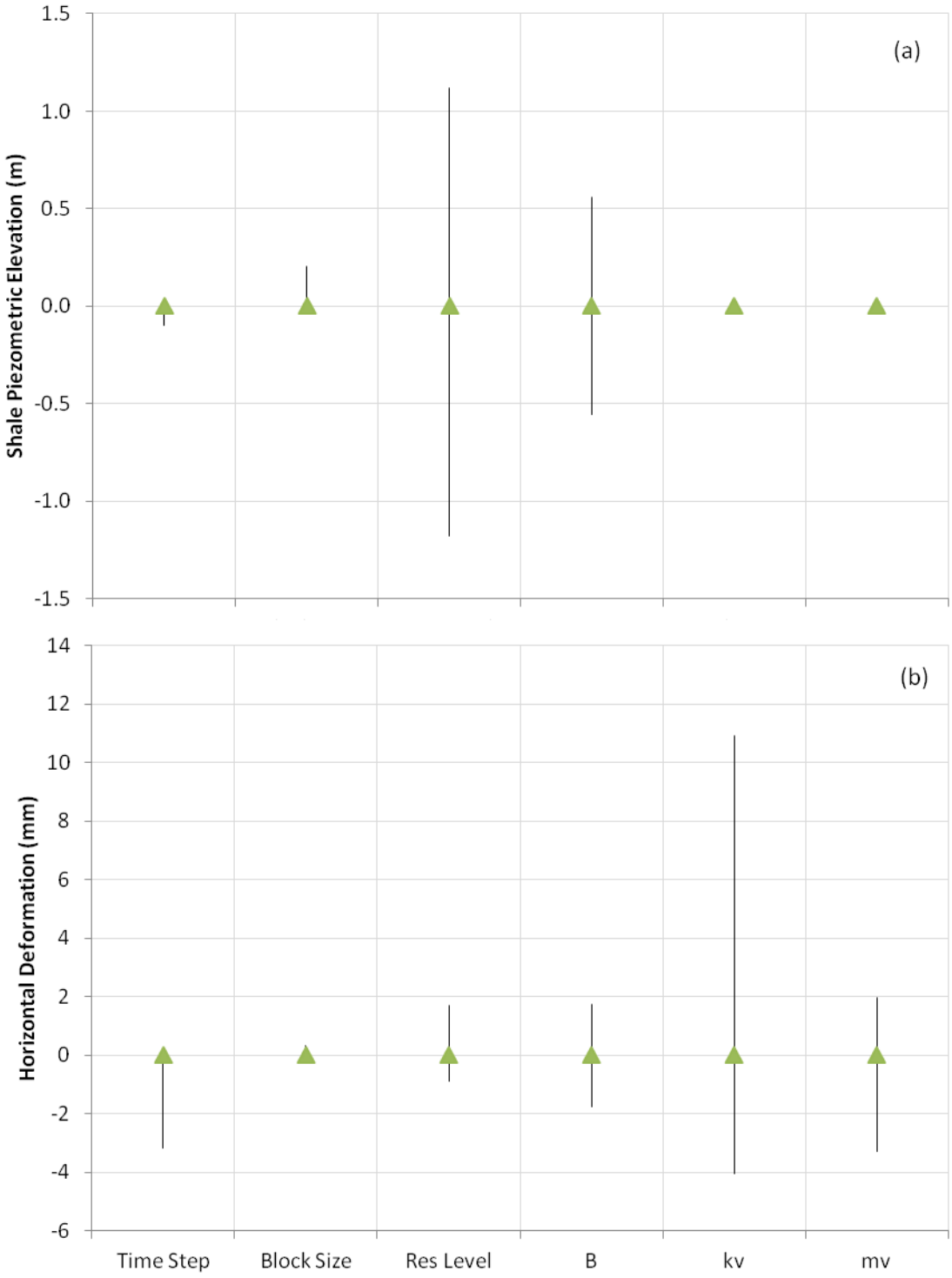

Figure 7.8 Key parameter sensitivity to variability as compared to the calibrated model: (a) Shale piezometric response, and (b) Shear zone horizontal deformation response

7.4 Model Verification

To verify and improve the confidence of the selected calibration parameters, two additional time periods were modelled and compared to the observed deformation. The verification time periods include the years 2005 and 2006 and the period between 1995 and 2010.

The modelled piezometric levels and deformations in the period between 2005 and 2006 indicated a relatively good fit to the observed data as shown in Figure 7.9. The modelled piezometric results were slightly less than the observed values but still acceptable. It appeared that there was an under predication of the deformation at the end of year one by <2.0 mm which was considered reasonable. The deformation model indicated a satisfactory match in the magnitude of deformation at the end of the two year period <1.0 mm.

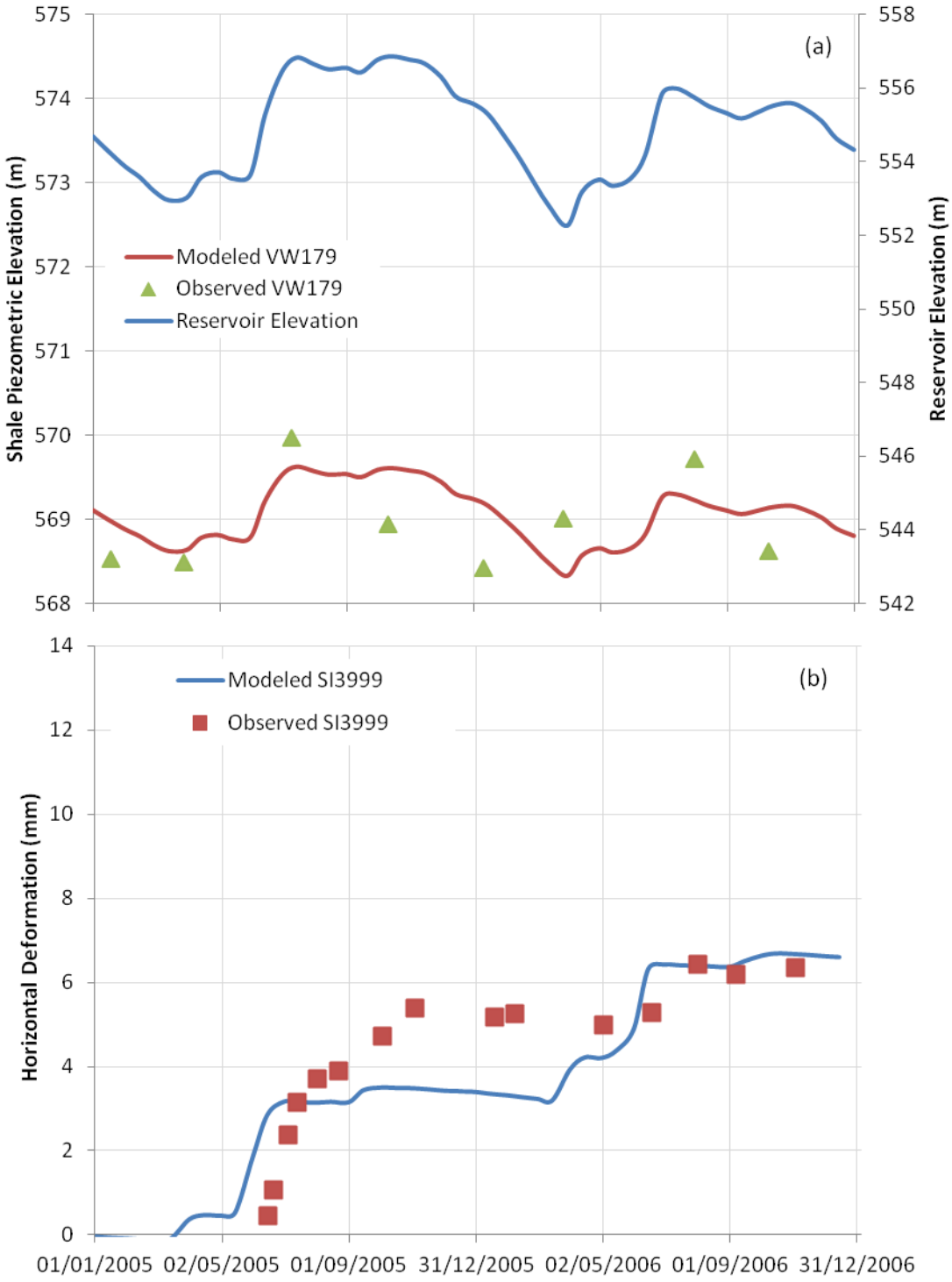

Figure 7.9 Analytical model calibration results, 2005-2007: (a) Reservoir elevation and shale piezometric response, and (b) Foundation horizontal deformation response

A longer modelling period of 15 years was used to further confirm the conceptual model's validity over a longer time period as illustrated in Figure 7.10.

The modelled piezometric results generally matched well with the observed piezometric response. However, during the period of several years of low reservoir levels, between 1999 and 2001, the piezometric levels were under predicted by approximately 0.5-1.0 m.

The deformation model behaved similarly to the piezometric response with a generally good agreement with the observed data prior to 2006. Following 2006, the model over predicted the deformation. This over prediction then cumulates in the followings years resulting in a larger over prediction. With the model carrying the over prediction forward to subsequent years, this indicated that this model may not be able to be used for long term prediction without an annual verification and correction. Finally, given the number of assumptions, the calibration and verification validates the conceptual model with having the ability to predict the deformation over several years within an acceptable range.

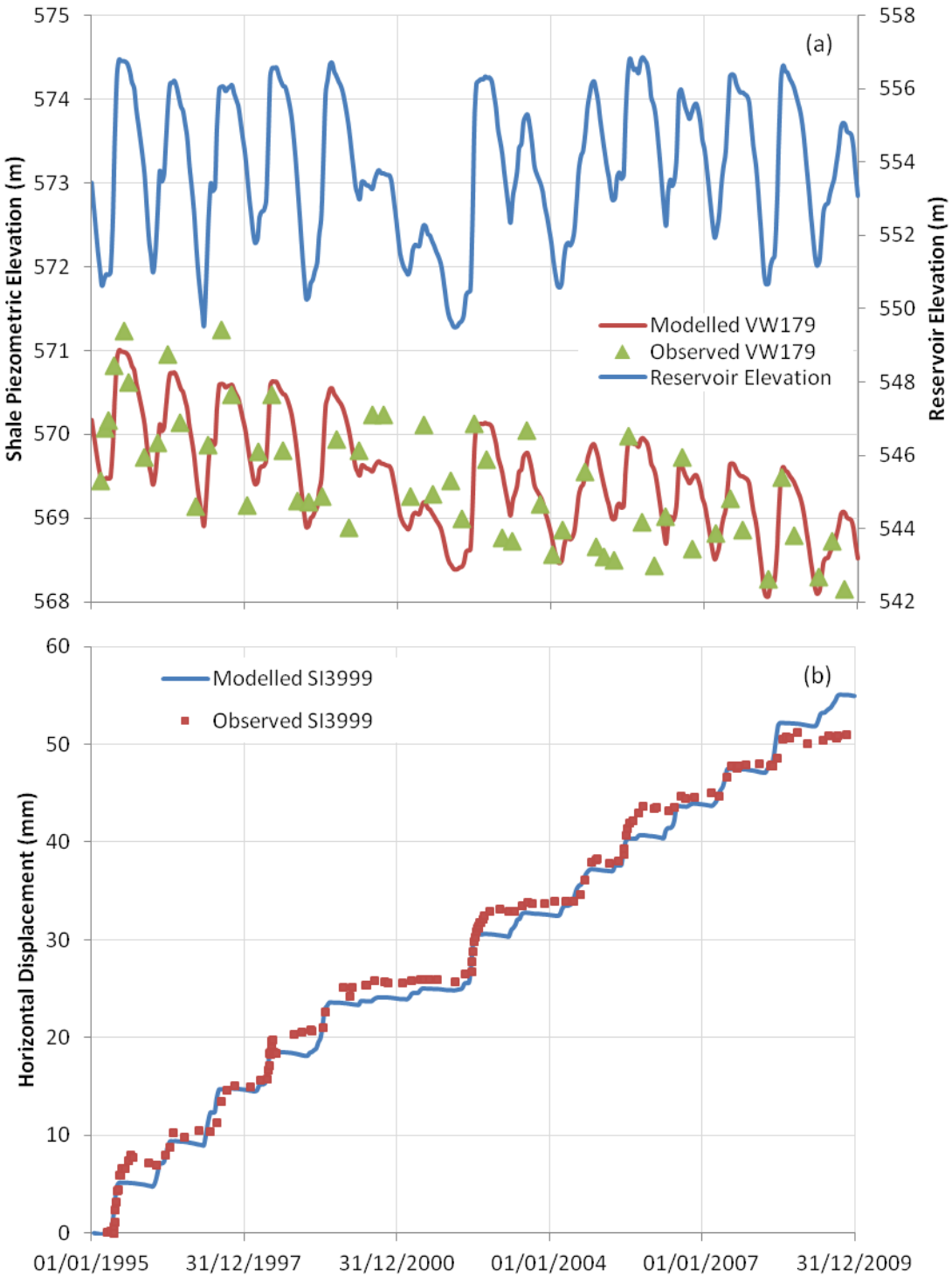

Figure 7.10 Analytical model calibration results, 1995-2010: (a) Reservoir elevation and shale piezometric response, and (b) Foundation horizontal deformation response

7.5 Discussion

The results from the comparison of the analytically modelled data representing the conceptual model and the observed data indicated a generally satisfactory agreement. The agreement verified the mechanism of movement proposed in the conceptual model. The analytical model was easily calibrated by varying select controlling parameters to achieve a best fit of the observed data in the selected calibration period. The calibration of the model was further verified by holding the calibration variables constant and applying them to different time periods. The modelled deformation through the verification time periods agreed reasonably well and provided more confidence in the proposed conceptual model.

The sensitivity analysis indicated the largest cause of variability to the deformation was a result of the vertical hydraulic conductivity in the shale not being well defined. The inconsistency of this variable was likely caused by the numerous structural discontinues and significant stratification in the shale (PFRA 1980). The deviation of the modelled deformation was generally within ±3.5mm for the evaluated parameters; however, k_v caused a significantly larger deviation up to 10.9 mm. Given the uncertainties in the reservoir level throughout a year, a modelled deformation range of ±3.5mm would be considered acceptable. In view of this, and the variability of k_v, this parameter should be further refined to a smaller range to reduce its effect on the sensitivity of the model.

The conceptual model assumed the reservoir has an impact on the deformation within the shale. As indicated in the previous sections, the modelled displacement did not appear to be significantly sensitive to the changes in reservoir level, particularly with the maximum reservoir level. However, it was found the sensitivity of the model to reservoir level is a particular difficult item to model as the reservoir level is a function of the operating plan for each year. For example, if a large runoff was expected, the reservoir level would be drawn down so the majority of the runoff would be stored in the reservoir. Given this scenario, it would be possible that this particular reservoir cycle could experience a minimum reservoir level and a maximum reservoir within the same year. Even though the sensitivity was shown to be minimal, this is likely not the case and to illustrate the true sensitivity would be extremely difficult with the use of any one particular reservoir cycle.

The modelled deformations in the 15 year verification period were generally in agreement with the observed deformations up to 2006. At that point, the model over predicted the observed data and as time progressed forward this error accumulates. Since this error occurs several years following the start of the model period, a deviation from the observed data is expected. The over prediction of deformation transferring forward could be resolved by reevaluating the deformation model with observed deformation on an annual basis.

Through this section the conceptual model was validated with its ability to predict the deformation in the shale, as a result of reservoir load, within an acceptable range. However, it can be seen that there are several improvements required to develop a robust model that may be better able to predict the deformations. The next section will discuss several of the recommendations that need to be considered in the future to build a more robust model.

CHAPTER 8 CONCLUSION AND RECOMMENDATIONS

8.1 Conclusion

A conceptual model was developed from a review of the historical instrumentation data. The historical data initially indicated a correlation with the piezometric fluctuations and the displacement within the shale as a result of the fluctuation in reservoir level. From further review, it was found that the shale piezometric elevation was greater than the reservoir elevation in select instruments. It was then proposed that the piezometric correlation with the reservoir was due to the horizontal load from the reservoir being applied to the shale foundation causing the development of excess porewater. As a result of the excess pressure dissipation, a horizontal consolidation of the shale occurred. This concept ultimately indicated that the deformation of the shale was the result of a stress response in the shale due to reservoir loading.

The conceptual model was validated with a simplistic analytical model. The analytical model was developed by relating the change in the shale piezometric level with the change in the reservoir level; followed by relating the change in the piezometric level and associated dissipation of excess pressure with the horizontal displacement in the shale. The analytical model was then verified by comparing the modelled piezometric and deformation responses to the observed data with general success. The successful comparison provided confidence the mechanism proposed for the ongoing movement within the shale was possible and should be researched further.

The deformation prediction of the conceptual model was limited by the ability to predict the reservoir level throughout the model period. Short term predictions, in the range of one reservoir cycle, may be possible if the prediction of the reservoir level is accurate. In the short term, if a relatively good reservoir prediction was possible and the shale hydraulic conductivity was further defined, the predicted deformation could be in the order of ±1.5mm. To perform long term predictions beyond the current reservoir period, the median reservoir cycle would likely be used; therefore, the predicted deformation could only provide a guideline to the expected deformation and not a precise value.

Several assumptions were made during the modelling process which requires further refinement. The next section discusses the recommended refinements and the recommended steps to further confirm the conceptual model and further build on this model.

8.2 Recommendations

To develop a conceptual level model, several assumptions were made resulting in model limitation and the requirement of further refinement. Further refinement would increase the understanding of the movement mechanisms and allow for the development of a more robust model allowing for increased accuracy in the deformation prediction.

Several key assumptions were made throughout this work and require further refinement as they are thought to have significant impact on the model. The key assumptions include the following: material homogeneity and isotropy, saturation of the river sand and shale, one dimensional consolidation, linear elastic stress-strain relationship, ridged boundaries of the free body, acceptance of previously performed material testing, compressibility of materials above the shale greater than the shale, limited model domain, time step calculations, size of time steps, directional consolidation characteristics, and the variability of the key parameters as consolidation occurs.

The material was assumed to be homogenous, isotropic, saturated, linear elastic, and have only one dimensional consolidation characteristics. These assumptions were made to simplify this analytical model. It is recognized that natural geomaterial generally does not act in this manner. These assumptions are recommended to be investigated to determine their effects on future models.

This investigation assumed the reservoir load was applied to an upstream rigid face of the model domain. Generally, geostructueres do not act rigidly and have a more ductile behavior. For example, the stress distribution was assumed to be evenly distributed throughout the model domain. The stress distribution likely varies throughout the domain due to compressibility characteristic of the materials. Therefore, it is recommended the effect of this assumption on the distribution of stresses imposed by the embankment and foundation be investigated further.

The majority of the material testing was completed throughout the 1960's and limited testing completed in 1970's. From the time of the initial investigations, significant improvements have been achieved in geotechnical materials testing and sampling. It is recommended that the procedures and results be reviewed to determine if they are acceptable to current standards. This review may find additional sampling and testing is required to confirm previous results. Regardless of the investigation into previous testing, the key variables,shale hydraulic conductivity and pore-pressure coefficient B require further refinement as they play the largest roles in the calculated deformation. Significant efforts should be directed to refining these variables through laboratory and insitu investigations.

It was assumed that the downstream deformation was governed by the compressibility characteristics of the shale as the materials above the shale were more compressible. This was a reasonable assumption for the embankment as this consists of mainly clay particles and is normally or lightly over consolidated. On the other hand, the river sand was described as silty sand; therefore, the compressibility may act differently than assumed. It is recommended to investigate the compressibility of the embankment and river sand further to confirm these assumptions and include in future models.

The conceptual model assumed consolidation of the shale one dimensionally in the horizontal direction; it was further assumed that the laboratory test results represented the horizontal compressibility of the shale. The compressibility characteristics of the shale found in laboratory testing was the result of vertically compressed samples. Due to the difference in the stress history of the shale in the vertical and horizontal directions, it is recommended that the compressibility characteristics of the shale in the horizontal direction be investigated further.

The model domain focused on an area of maximum displacement from the dam centerline to 150m downstream. The upstream inclinometer indicated less downstream movement than the inclinometer at the toe of the embankment. Because of the difference between the displacements, it is speculated that deformation is occurring only through a portion of the domain. The limits of this deformation were unknown. It is recommended that the limits of the deformation zone in the model domain be refined with the installation of additional inclinometers and potentially a finite element stress analysis.

The deformation was found to be sensitive to the time step size. To minimize this sensitivity, it is recommended in further investigations that the time step be reduced to a maximum of one day intervals.

The observed data within the dam provided sufficient information for the development of a model of this complexity. However, to complete a more detailed numerical modelling program, additional instrumentation and increase monitoring frequency of existing instrumentation will be required. Additional piezometers are required within the shale near the crest of the dam or as upstream as possible and at several locations downstream along the model cross section to further define the deformation pattern in the shale. The monitoring frequency of these instruments should be increased enough to indicate the true effects of the increase and decrease of the reservoir. Since all the slope inclinometer casings at Gardiner Dam are currently manually read, the implementation of automated monitoring of the casing should be investigated further.

Finally, the proposed conceptual model was verified by a simplistic analytical representation of the conceptual model; however, to provide more confidence for this conceptual model, it is recommended that a more computationally complex model be developed. This model would likely include a finite element package with the ability to model stress induced porewater changes and the effects this has on the deformation of the foundation and overriding embankment.

REFRENCES

Anochikwa, C.I., van der Kamp, G., and Barbour, S.L. 2012. Interpreting pore-water pressure changes induced by water table fluctuations and mechanical loading due to soil moisture changes, Canadian Geotechnical Journal, **49**: 357-366.

Biot, M.A. 1941. General theory of three-dimensional consolidation, Journal of Applied Physics, **12**: 155-164.

Bishop, A.W. 1977. The value of Poisson's ratio in saturated soils and rocks stressed under undrained conditions, Geotechnique, **27**(3): 369-384.

Bishop, A.W. 1976. The influence of system compressibility on the observed pore-pressure response to an undrained change in stress in saturated rock, Geotechnique, **26**(2): 371-375.

Bishop, A.W. 1973. The influence of an undrained change in stress on the observed pore pressure in porous median of low compressibility, Geotechnique, **23**(3): 435-442.

Bishop, A.W., Green, G.E., Garga, V.K., Andresen, A., and Brown, V.K. 1971. A new ring shears apparatus and its application to the measurement of residual strength, Geotechnique, **21**(4): 273-328.

Bjerrum, L. 1967. Engineering geology of Norwegian normally-consolidated marine clays as related to settlements of buildings, Geotechnique, **17**: 81-118.

Bromhead, E.N. 1986. The stability of slopes. Surry University Press, London.

Christiansen, E.A. 1979. The Wisconsinan deglaciation of southern Saskatchewan and adjacent areas, Canadian Journal of Earth Sciences, **16**: 913-938.

Christiansen, E.A. and Sauer, E.K. 1984. Landslide styles in the Saskatchewan Rivers Plain: A geological appraisal. *In* Canadian Case Histories - Landslides, Toronto, Ontario, pp. 35-48.

Cladwell, W.G.E. 1968. The late cretaceous Bearpaw formation in the South Saskatchewan River Valley. 8, Saskatchewan Research Council, Geology Division, Saskatchewan.

Clifton, A.W., Yoshida, R.T., and Chursinoff, R.W. 1986. Regina Beach - a town on a landslide, Canadian Geotechnical Journal, **23**: 60-68.

Craig, R.F. 1997. Soil mechanics 6th ed. E&FN Spon, New York.

Dewoolkar, M.M. and Huzjak, R.J. 2005. Drained residual shear strength of some claystones from front range, Colorado, Journal of Geotechnical and Geoenviromental Engineering, **131**(12): 1543.

Dunnicliff, J. 1988. Instrumentation for monitoring field performance. John Wiley & Sons Inc., Toronto.

Eckel, B.F., Sauer, E.K., and Christiansen, E.A. 1987. The Petrofka landslide, Saskatchewan, Canadian Geotechnical Journal, **24**: 81-99.

Eigenbrod, K.D., Burak, J.P., and Graham, J. 1987. Drained deformation and failure due to cyclic pore pressures in soft clay at low stress, Canadian Geotechnical Journal, **24**: 208-215.

Fine, R.A. and Millero, F.J. 1973. Compressibility of water as a function of temperature and pressure, Journal of Chemical Physics, **53**(10): 5529.

Gautam, R. and Wong, R.C.K. 2006. Transversely isotropic stiffness parameters and their measurement in Colorado shale, Canadian Geotechnical Journal, **43**: 1290-1305.

GEO-SLOPE INTERNATIONAL LTD. 2012. Geostudio 2012. Geo-slope International Ltd., Calgary, AB.

Grajczyk, M. 2012. Personal Communication. Lake Diefenbaker reservoir median, quartiles, min, max levels 1980 to 2011. Moose Jaw, SK.

Insley, A.E., Chattenai, P.K., and Smith, L.B. 1977. Use of residual strength for stability analyses of embankment foundations containing preexisting failure surfaces, Canadian Geotechnical Journal, **14**: 408.

James, P.M. 1971. The role of progressive failure in clay slopes. *In* 1st Australia-New Zealand Conference on Geomechanics, Melbourne, Vol. 1, pp. 344-348.

Jaspar, J.L. and Peters, N. 1979. Foundation performance of Gardiner Dam, Canadian Geotechnical Journal, **16**: 758-788.

Jizba, D.L. 1991. Mechanical and acoustical properties of sandstones and shales. Doctor of Philosophy, Stanford University, Stanford.

Kelly, A.J., Sauer, E.K., Christiansen, E.A., Barbour, S.L., and Widger, R.A. 1995. Deformation of the deer creek bridge by an active landslide in clay shale, Canadian Geotechnical Journal, (32): 701-724.

Krahn, J., Johnson, R.F., Fredlund, D.G., and Clifton, A.W. 1979. A highway cut failure in cretaceous sediments at Maymont, Saskatchewan, Canadian Geotechnical Journal, **16**: 703-715.

Lamb, T.W. and Whitman, R.V. 1969. Soil mechanics. John Wiley & Sons, Toronto, ON.

Matheson, D.S., Morgenstern, N.R., and Nussbaum, H. 1987. Design, construction and performance of Nipawin dams. *In* 40th Canadian Geotechnical Conference, Regina, Regina, SK, pp. 141-171.

Mayne, P.W. and Poulos, H.G. 1999. Approximate displacement influence factors for elastic shallow foundations, Journal of Geotechnical and Geoenviromental Engineering, **125**(6): 453-460.

Meehan, C.L., Brandon, T.L., and Duncan, J.M. 2007. Measuring drained residual strengths in the Bromhead ring shear, Geotechnical Testing Journal, **30**(6): 1-8.

Misfeldt, G.A., Sauer, E.K., and Christiansen, E.A. 1991. The Hepburn landslide: An interactive slope-stability and seepage analysis, Canadian Geotechnical Journal, **28**: 556-573.

Morgenstern, N.R. and Simmons, J.V. 1982. Analysis of the movements of Gardiner Dam. *In* Proceeding of Fourth International Conference on Numerical Methods in Geomechanics, Edmonton, Vol. 3, pp. 1033-1027.

Morgenstern, N.R. and Simmons, J.V. 1980. A deformation analysis of Gardiner Dam, South Saskatchewan River Project. Department of Civil Engineering University of Alberta., Edmonton, AB.

Munfakh, G., Arman, A., Samtani, N., and Castelli, R. 1997. Geotechnical and foundation engineering, module 1, subsurface investigations. FHWA HI-97-021, U.S. Department of Transportation, Federal Highway Administration, Springfield, VA.

Peters, N. and Ellis, J.H. 1972. Instrumentation for Gardiner Dam. *In* 25th Canadian Geotechnical Conference, Foundation Performance, Ottawa, Ontario, pp. 2-30.

Peterson, R. 1958. Rebound in the Bearpaw shale, Western Canada, Bulletin of the Geological Society of America, **69**: 1113-1124.

PFRA. 1992. South Saskatchewan River Project, modeling of embankment movements. Development Service, Saskatoon, SK.

PFRA. 1981. South Saskatchewan River Project, Gardiner Dam, laboratory strength tests on shale, period 1969-1978. Geotechnical Division, Saskatoon, SK.

PFRA. 1980. The design and construction of Gardiner Dam and associated works. Canadian Government Publishing Center, Hull, Quebec.

PFRA. 1966a. Shear strength parameters for Bearpaw shale as obtained from laboratory shear tests and their relationship to the strength of natural slopes. Soil Mechanics and Materials Division, Saskatoon, SK.

PFRA. 1966b. Gaps in knowledge in predicting stress-deformation characteristics of clay and clay-shale foundations. PFRA Engineering Services, Saskatoon, SK.

PFRA. 1965a. South Saskatchewan River Project, physical testing on shale, in term report. PFRA Engineering Division, Saskatoon, SK.

PFRA. 1965b. Report on, South Saskatchewan River Dam, embankment stability - river section, appendix I. PFRA Engineering Services, Saskatoon, SK.

PFRA. 1962. Summary of embankment stability, South Saskatchewan River Dam. PFRA Engineering Services, Saskatoon, SK.

PFRA. 1960a. Review of slope and embankment stability, South Saskatchewan River Dam. PFRA Engineering Services, Saskatoon, SK.

PFRA. 1960b. Report on constant and falling head permeability tests in the Bearpaw shale April to June, 1960. PFRA Engineering Services, Saskatoon, SK.

PFRA. 1955a. South Saskatchewan River Project Damsite no.10, strength studies of Bearpaw shale and application to the stability of proposed dam. PFRA Engineering Services, Saskatoon, SK.

PFRA. 1955b. Summary report on geology of the South Saskatchewan River Damsite. Air Photo Analysis and Engineering Geology Division, Engineering Services, Regina, SK.

Pollock, D.H. 1962. Geology of the South Saskatchewan River Project, The Engineering Journal, 37-46.

Rahman, M.G. and Kilgour, D.A. 2000. Gardiner Dam - three decades of performance monitoring. *In* Canadian Dam Association 3rd Annual Conference, Regina, SK, Vol. 1, pp. 212-224.

Ringheim, A.S. 1964. Experiences with the Bearpaw shale at the South Saskatchewan River Dam. *In* Large Earth Dams 8th, Edinburgh, pp. 529-550.

Sarout, J., Molez, L., Gueguen, Y., and Hoteit, N. 2006. Shale dynamic properties and anisotropy under triaxial loading: Experimental and theoretical investigations, J, Phys. Chem. Earth.

Sauer, E.K. 1984. Landslide in clay shale in the North Saskatchewan River valley, Canada, Engineering Geology, **20**(4): 279.

Sauer, E.K. 1983. The Denholm landslide, Saskatchewan. Part II: Analysis, Canadian Geotechnical Journal, **20**: 208-220.

Sauer, E.K. 1978. The engineering significance of glacial ice thrusting, Canadian Geotechnical Journal, **15**: 457-472.

Sauer, E.K. and Misfeldt, G.A. 1993. Preconsolidation of the Cretaceous clays of the western interior basin in Southern Saskatchewan. *In* 46th Annual Canadian Geotechnical Conference, Saskatoon, SK, Vol. 1, pp. 37-47.

Sauer, E.K. and Christiansen, E.A. 1987. Denholm landslide, Saskatchewan, Canada, an update, Canadian Geotechnical Journal, **24**(1): 163.

Sauer, E.K., Egeland, A.K., and Christiansen, E.A. 1993. Compression characteristics and index properties of tills and intertill clays in southern Saskatchewan, Canada, Canadian Geotechnical Journal, **30**: 257-275.

Sauer, E.K., Gareau, L.F., and Christiansen, E.A. 1990. Softening of overconsolidated Cretaceous clays by glacial erosion, Quarterly Journal of Engineering Geology, **23**: 307-324.

Skempton, A.W. 1985. Residual strength of clays in landslides, folded strata and the laboratory, Geotechnique, **35**(1): 3-18.

Skempton, A.W. 1964. Long-term stability of clay slopes, Geotechnique, **14**(2): 75-102.

Skempton, A.W. 1954. The pore pressure coefficients A and B, Geotechnique, **4**: 143-147.

Stark, T.D. and Eid, H.T. 1994. Drained residual strength of cohesive soils, ASCE. Journal of Geotechnical Engineering, **120**(5): 856-871.

Stark, T.D. and Eid, H.T. 1993. Modified Bromhead ring shear apparatus, Geotechnical Testing Journal, **16**(1): 100-107.

Terzaghi, K., Peck, R.B., and Gholamreza, M. 1996. Soil mechanics in engineering practice third edition. John Wiley and Sons, Inc., Toronto, ON.

Watershed Authority. 2009. 2009 Gardiner Dam soil laboratory testing. Saskatchewan Watershed Authority, Moose Jaw, SK.

Williams, P.J. 1966. Downslope soil movement at a sub-artic location with regard to variations with depth, Canadian Geotechnical Journal, **3**(4): 191-203.

Wilson, G.W., Clifton, A.W., Charleson, D., and Widger, R.A. 1989. Stability and performance of two adjacent bridges constructed on a landslide. *In* Materials: From Theory to Practice, Winnipeg, MB, pp. 325-335.

Wood, D.M. 1990. Soil behavior and critical state soil mechanics. Cambridge University Press, Cambridge.

APPENDIX A HISTORICAL INSTRUMENTATION DATA

A1. Introduction

Historical (1970 to 2010) and recent (1995 to 2010) geotechnical monitoring data and reservoir elevation are included in the Appendix. The figures included in this appendix provide additional data to illustrate the response in the foundation piezometric levels and deformation to time and reservoir fluctuation.

A2. Foundation Vertical Deformation

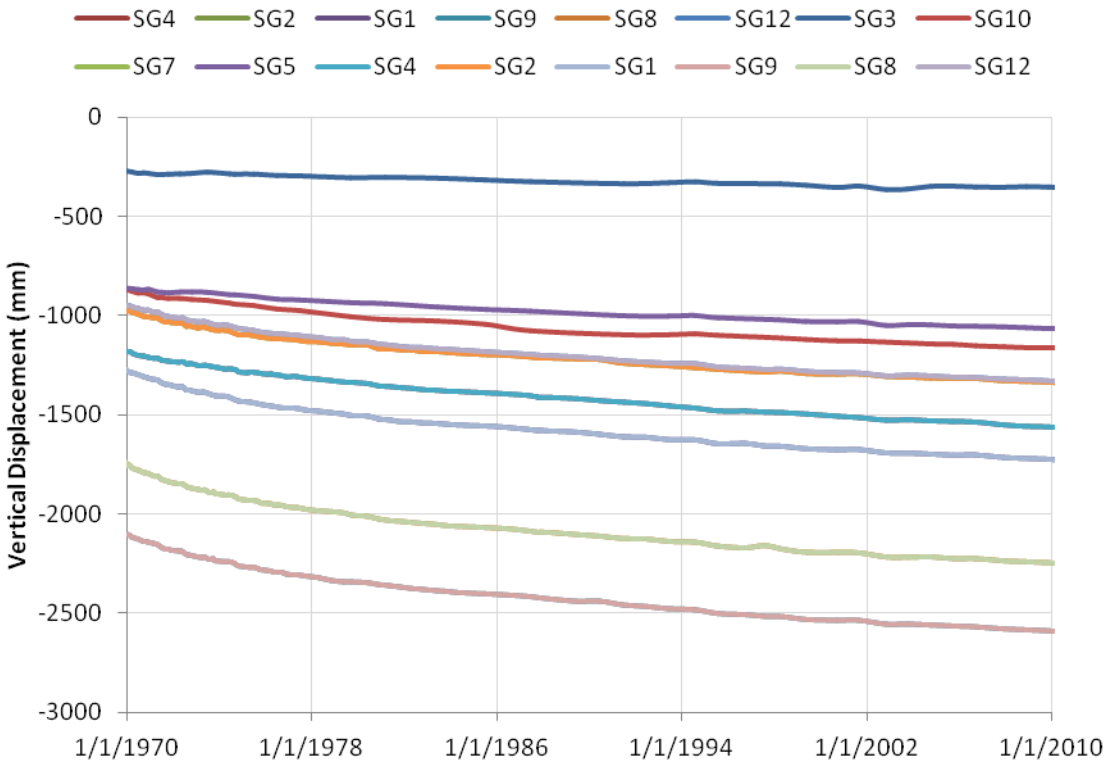

Figure A 1 Historic vertical foundation displacement: select settlement gauges

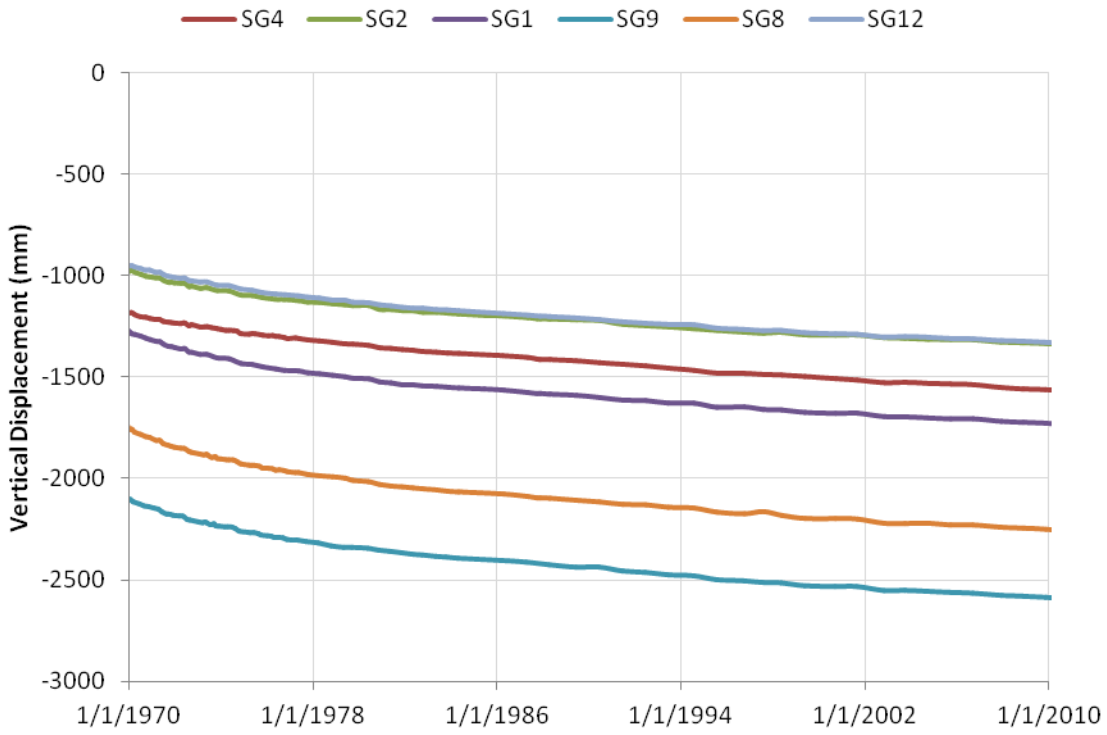

Figure A 2 Historic vertical foundation displacement: dam centerline

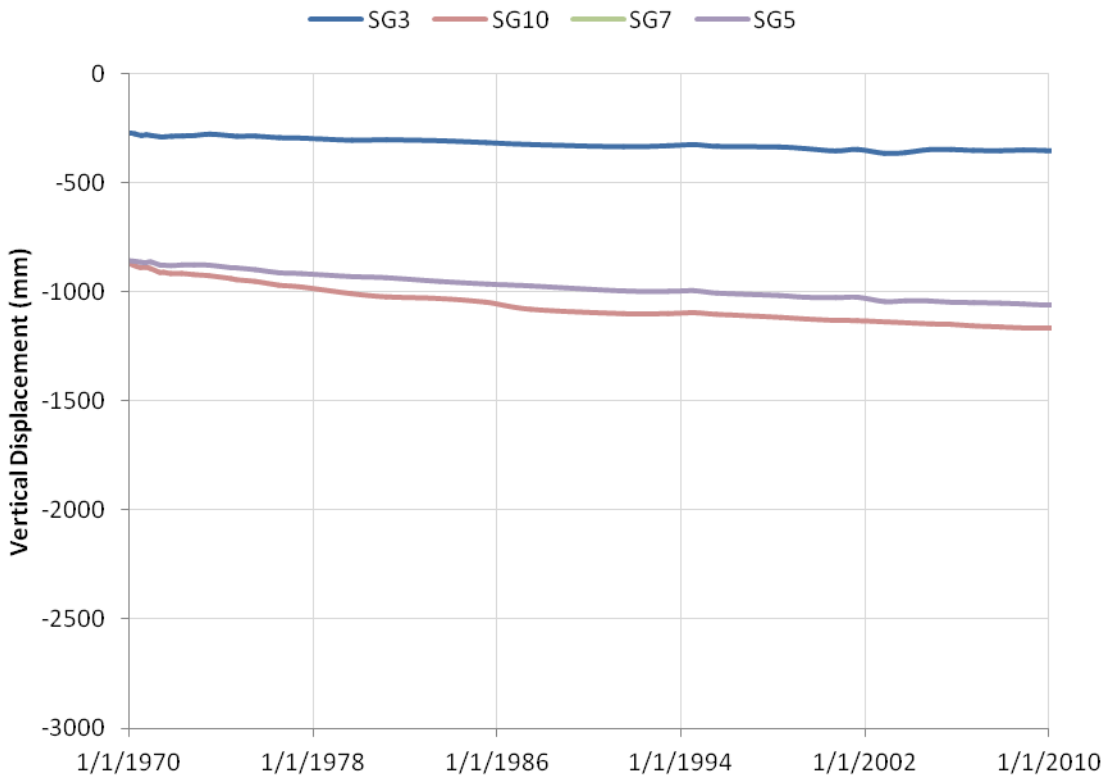

Figure A 3 Historic vertical foundation displacement: 150m downstream of centerline

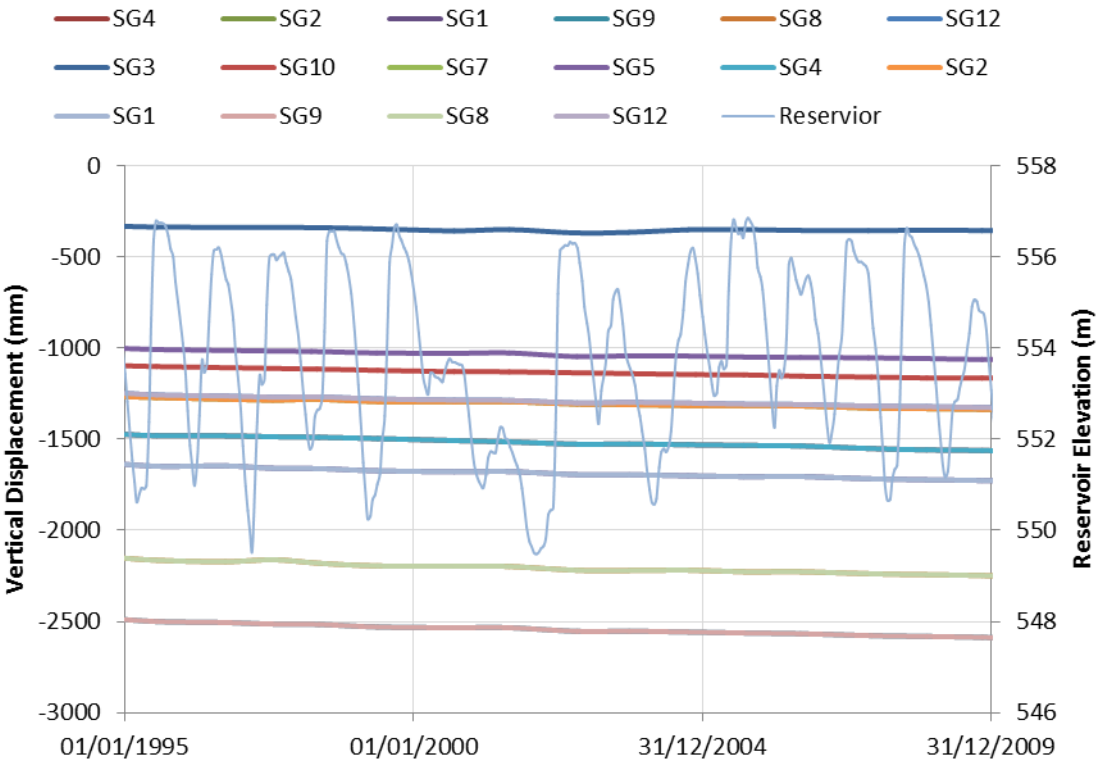

Figure A 4 Recent vertical foundation displacement and reservoir elevation: all settlement gauges

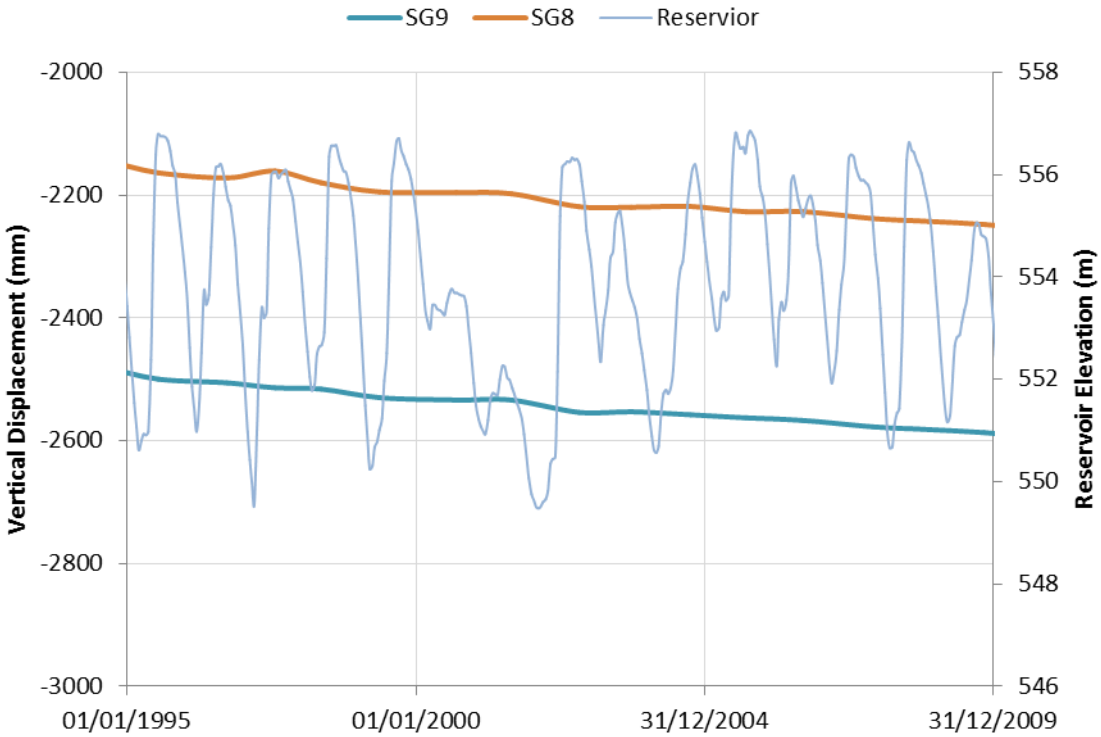

Figure A 5 Recent vertical foundation displacement and reservoir elevation: SG9 and SG8

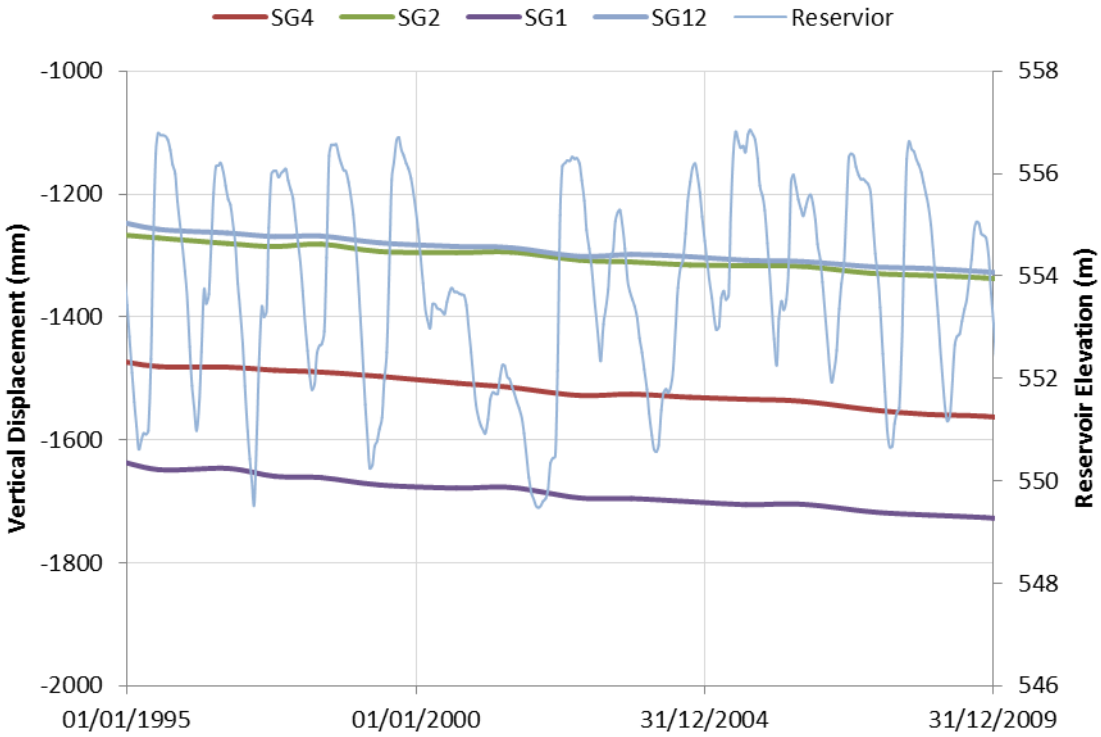

Figure A 6 Recent vertical foundation displacement and reservoir elevation: SG4, SG2, SG1, SG12

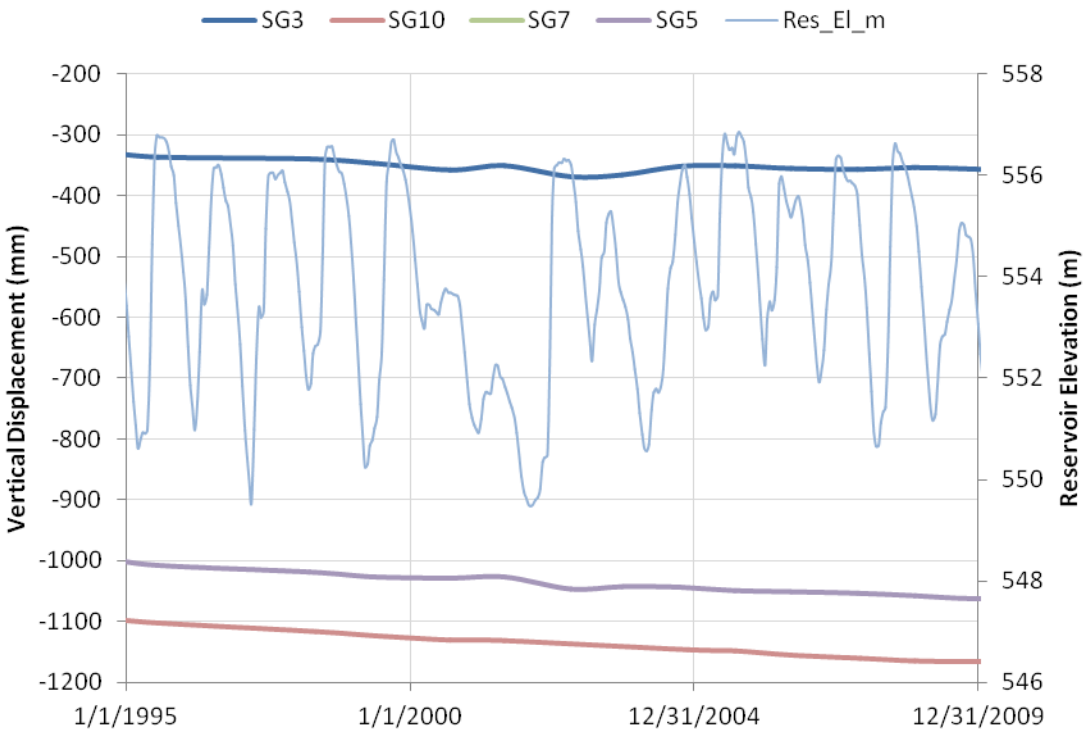

Figure A 7 Recent vertical foundation displacement and reservoir elevation: SG3, SG10, SG7, and SG5

A3. Foundation Piezometric Response; River Sand

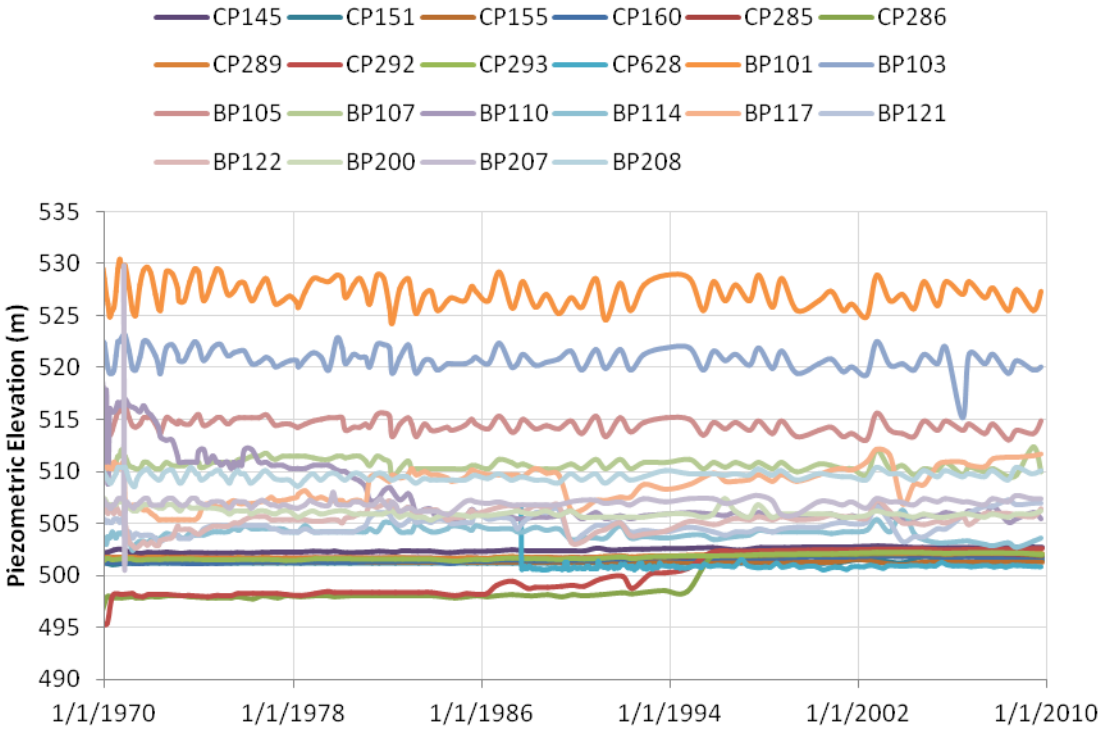

Figure A 8 Historic river sand piezometric response: select piezometers beneath River Embankment

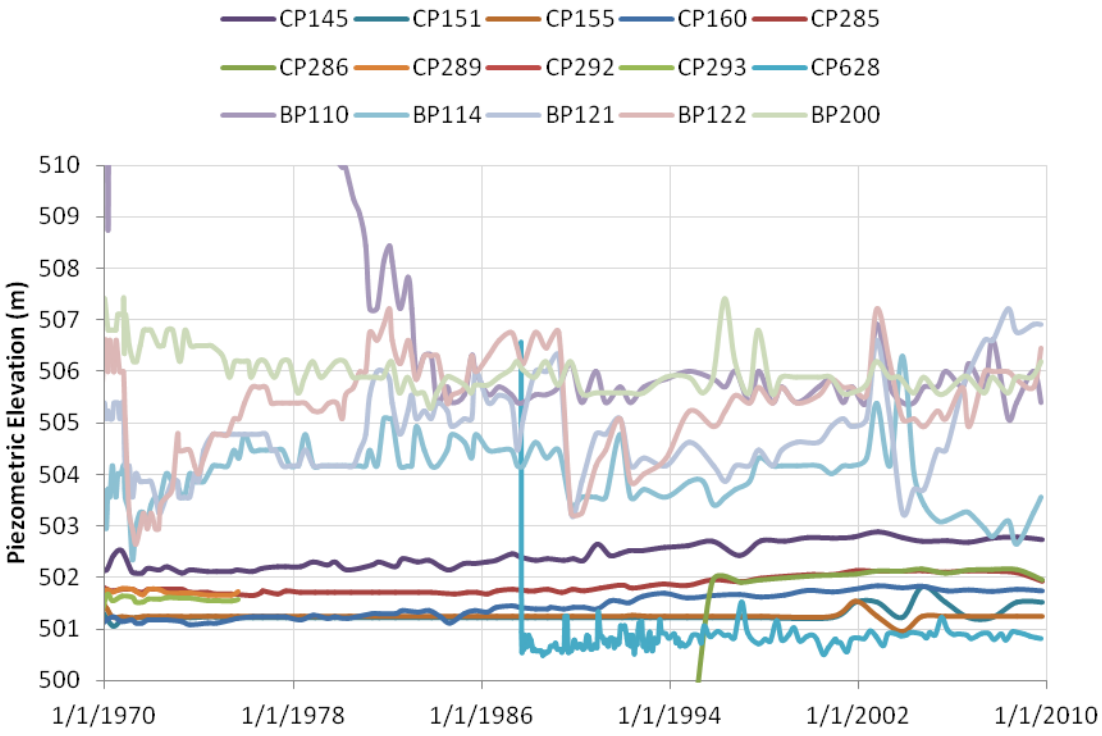

Figure A 9 Historic river sand piezometric response: >250 m downstream of centerline

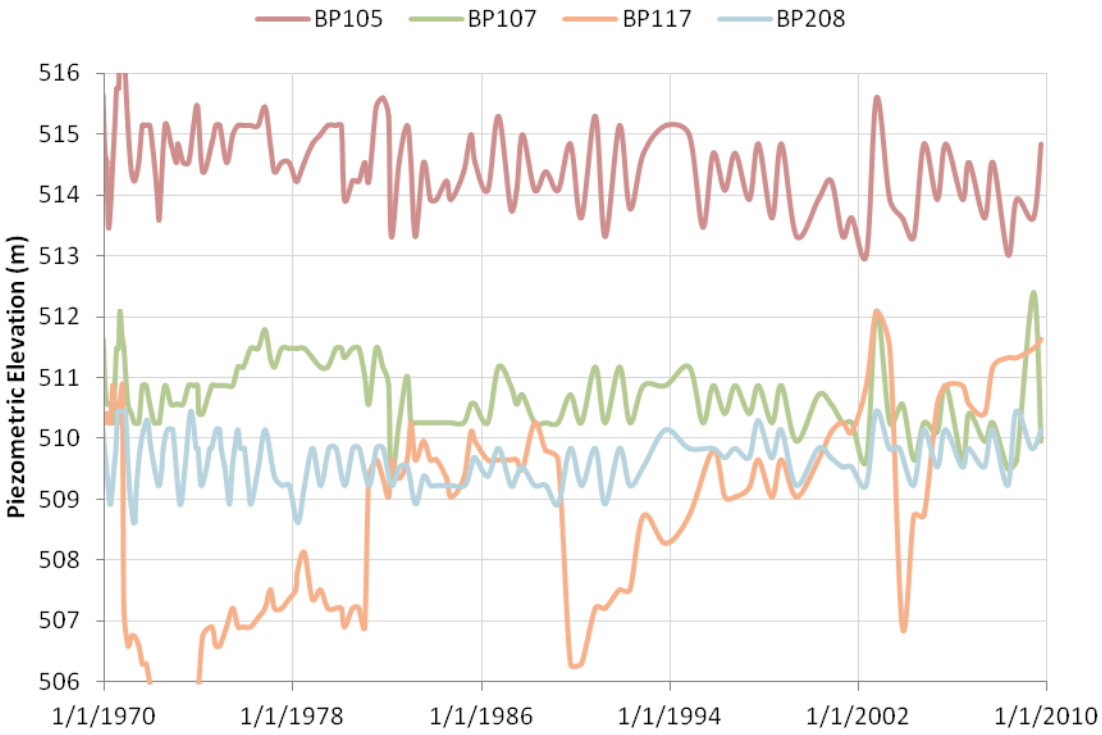

Figure A 10 Historic river sand piezometric response: 250 m<x<0 m downstream of centerline

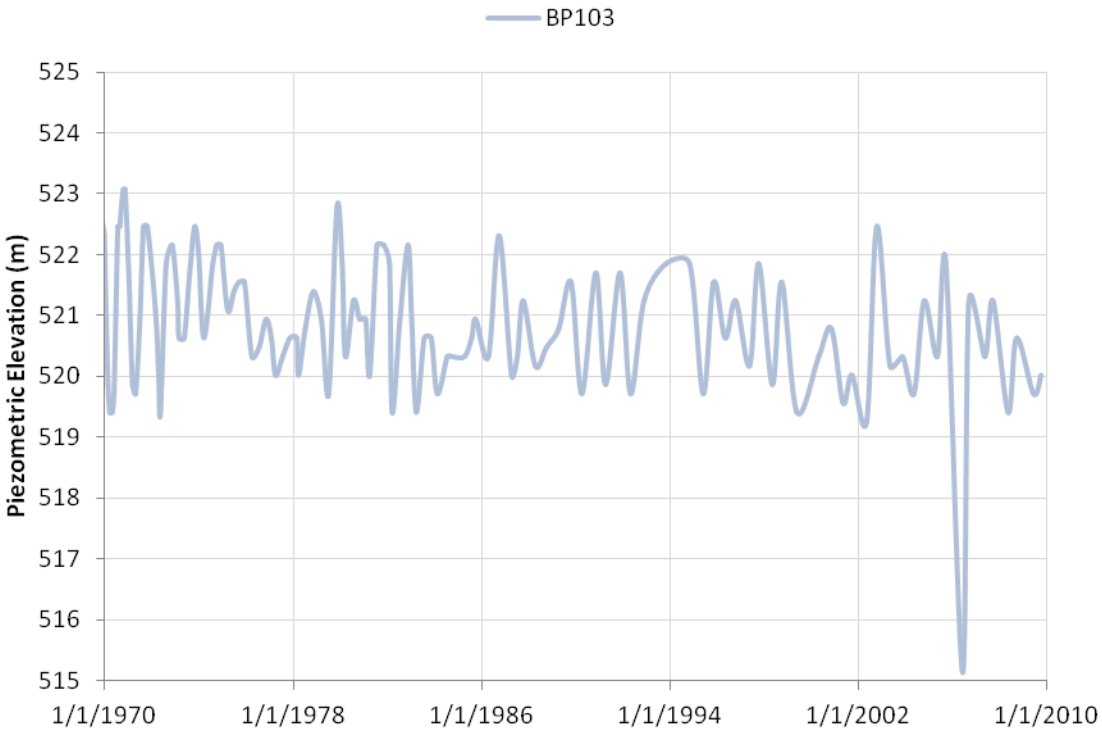

Figure A 11 Historic river sand piezometric response: 300 m upstream of centerline

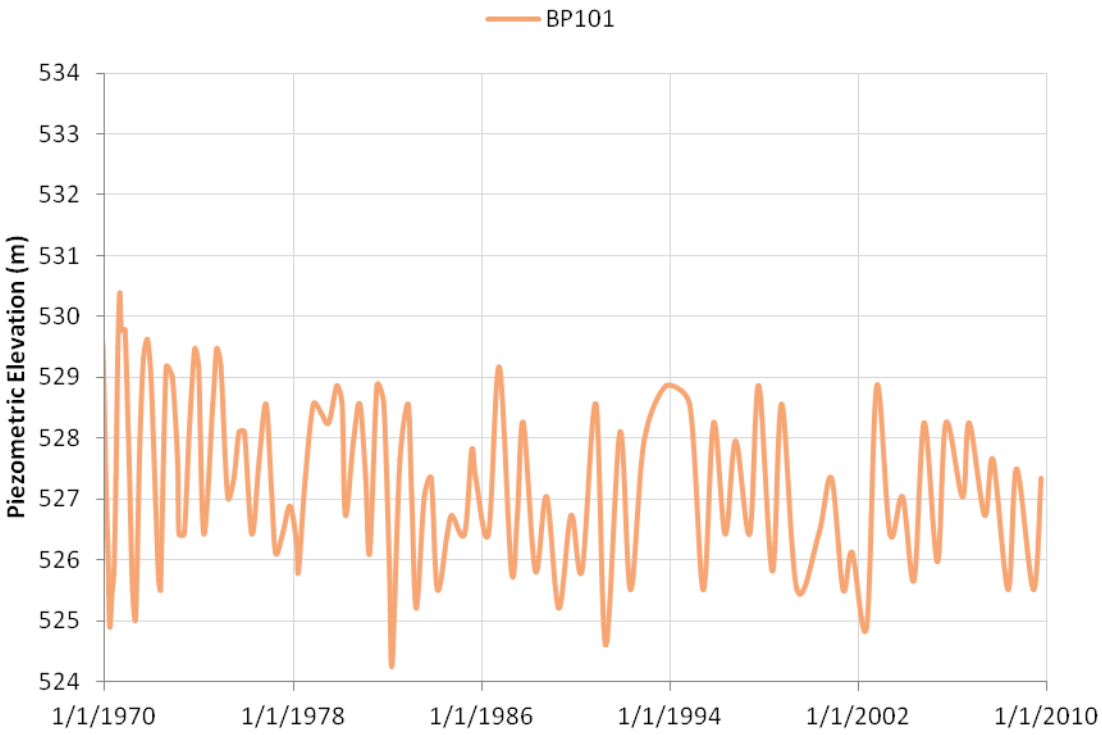

Figure A 12 Historic river sand piezometric response: 450 m upstream of centerline

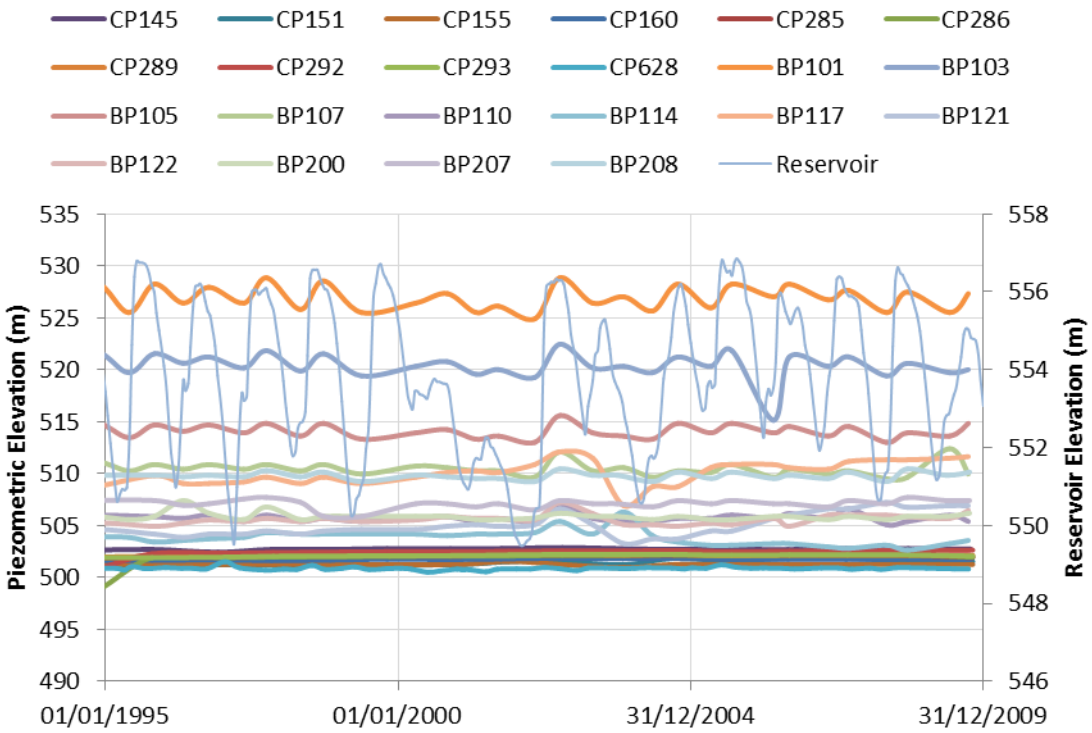

Figure A 13 Recent river sand piezometric response and reservoir elevation: select piezometers beneath River Embankment

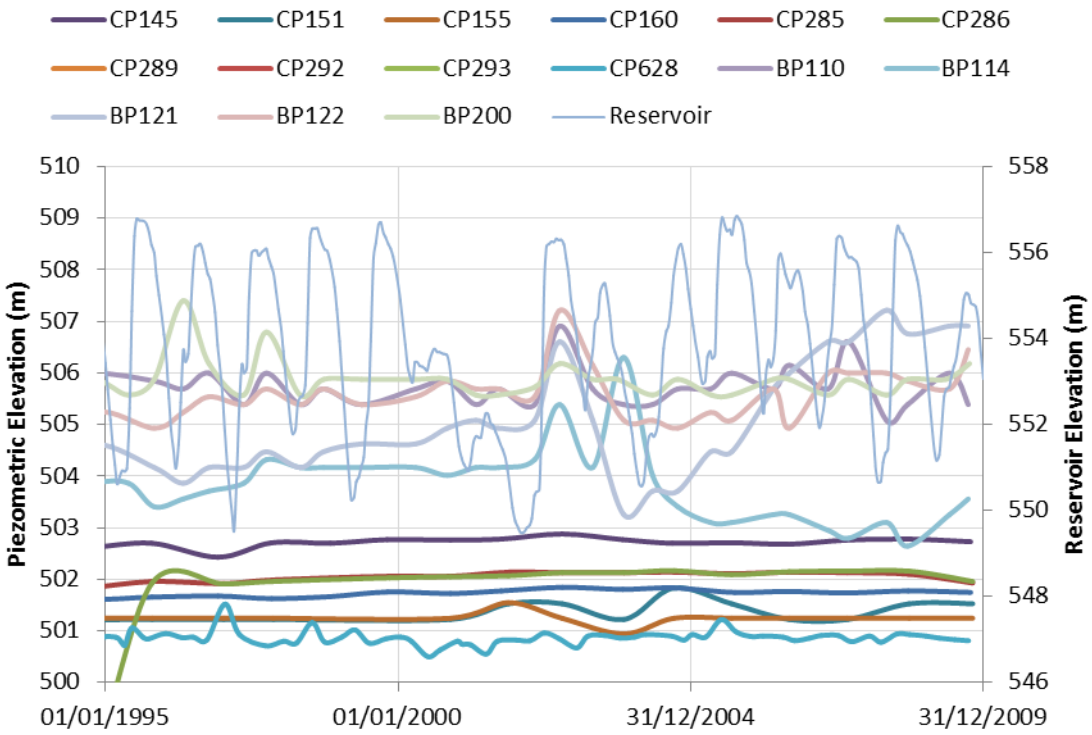

Figure A 14 River sand piezometric response to reservoir change and reservoir elevation: >250 m downstream of centerline

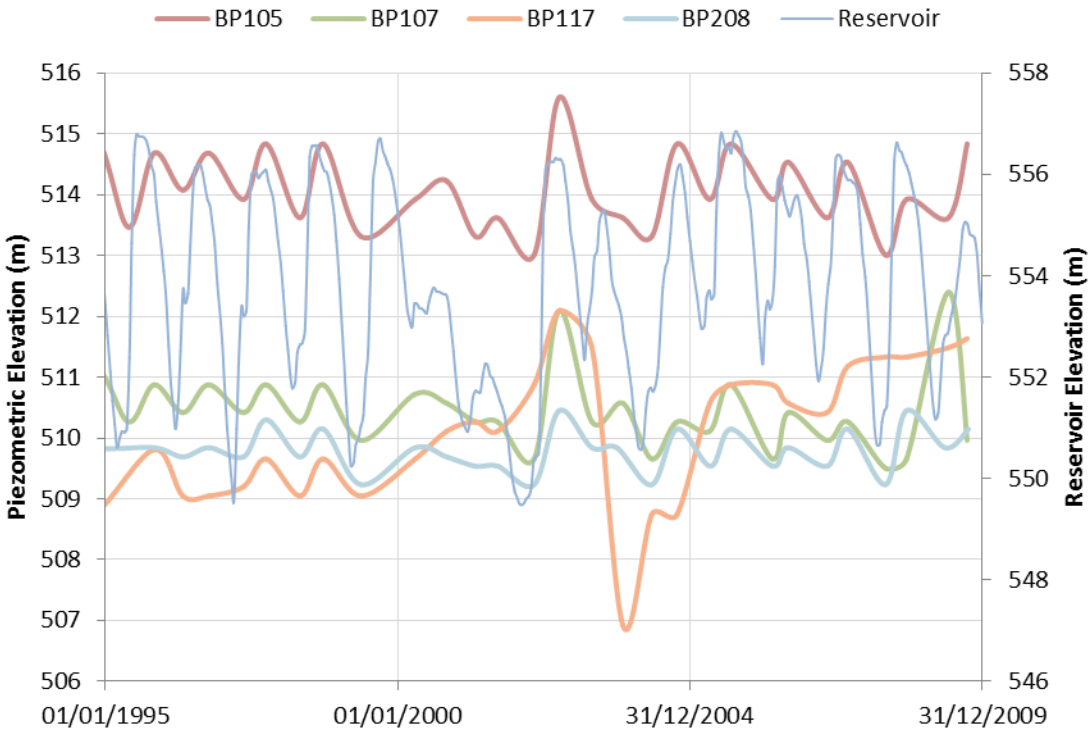

Figure A 15 Recent river sand piezometric response and reservoir elevation: 250 m<x<0 m downstream of centerline

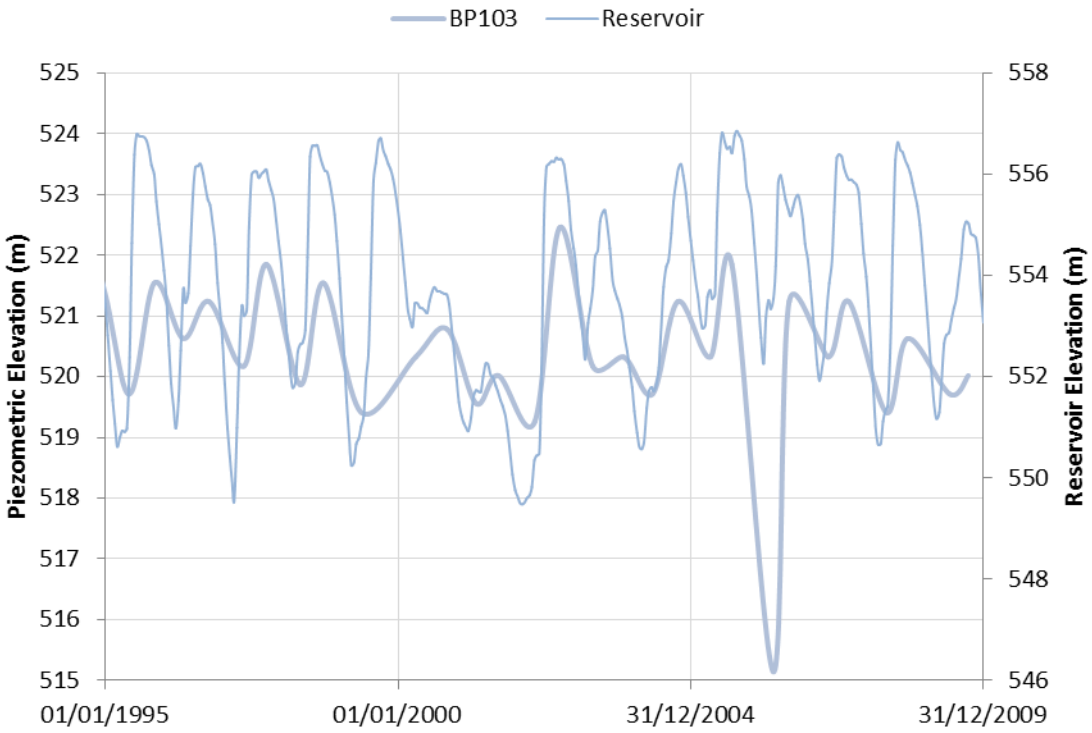

Figure A 16 Recent river sand piezometric response and reservoir elevation: 300 m upstream of centerline

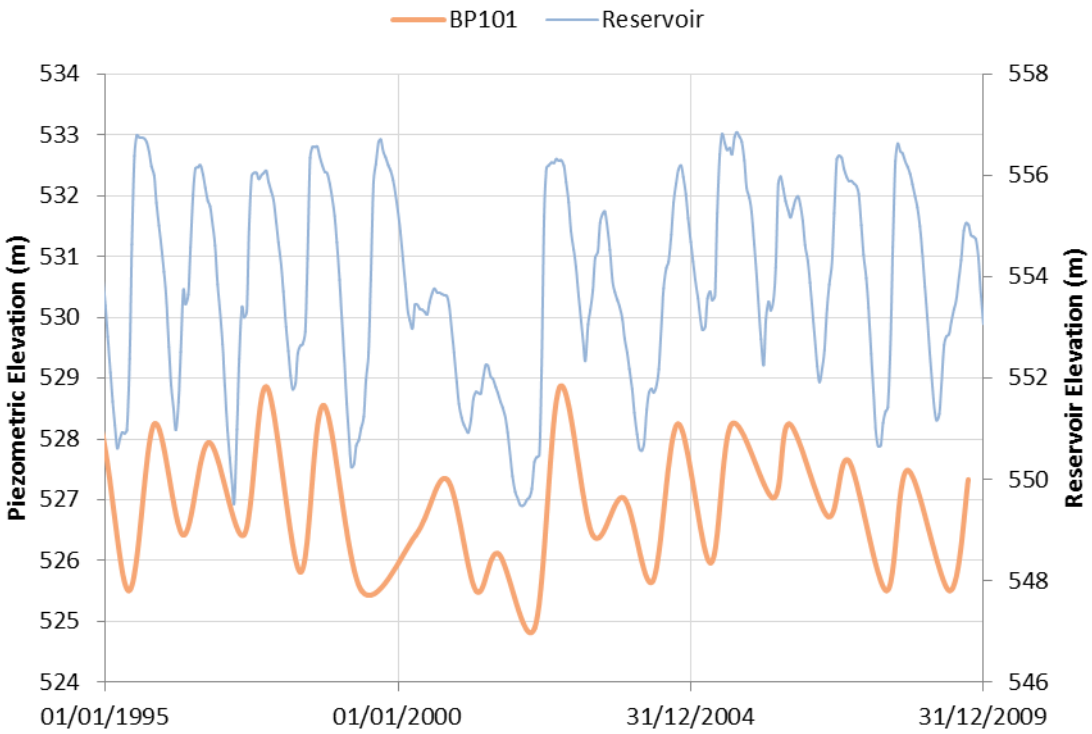

Figure A 17 Recent river sand piezometric response and reservoir elevation: 450 m upstream of centerline

A4. Foundation Piezometric Response; Shale

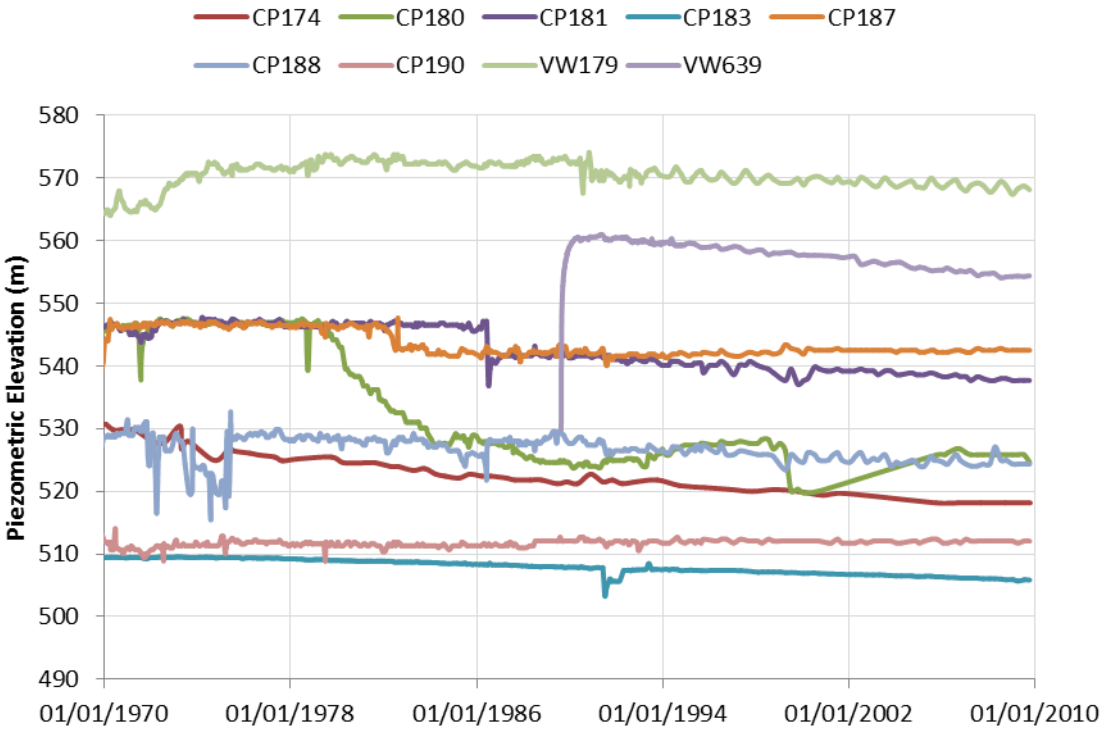

Figure A 18 Historic shale piezometric response: select piezometers beneath River Embankment

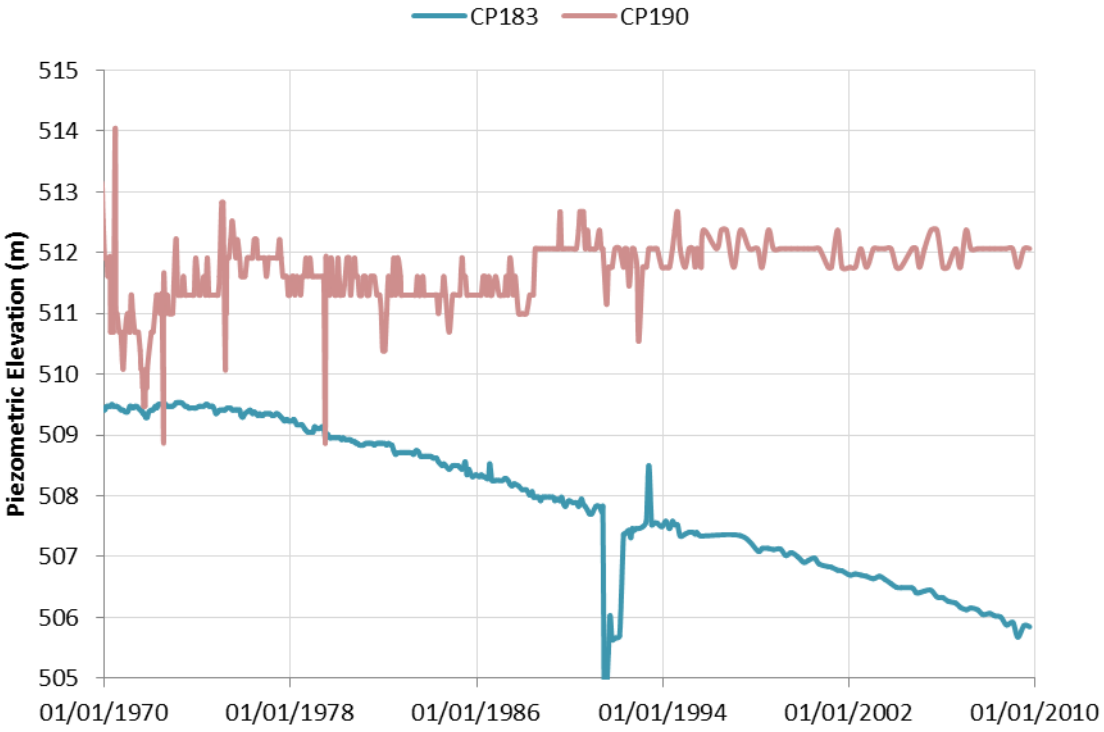

Figure A 19 Historic shale piezometric response: >1450 m downstream of centerline

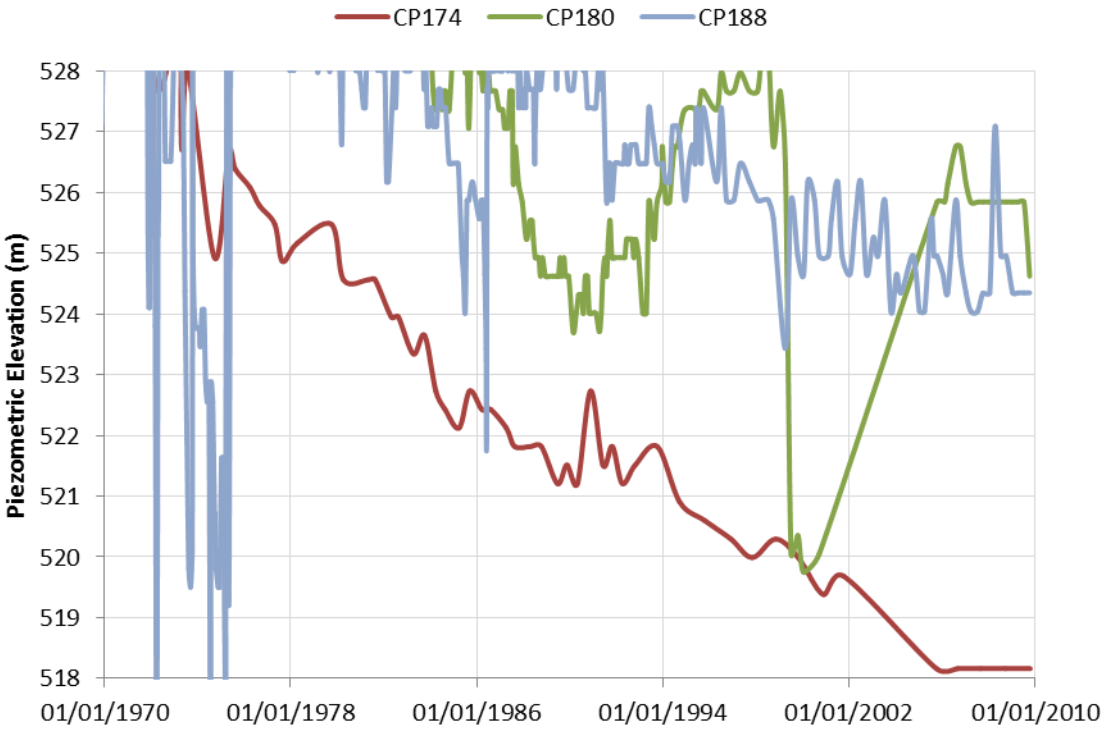

Figure A 20 Historic shale piezometric response: 1450 m >x>400 m downstream of centerline, CP174

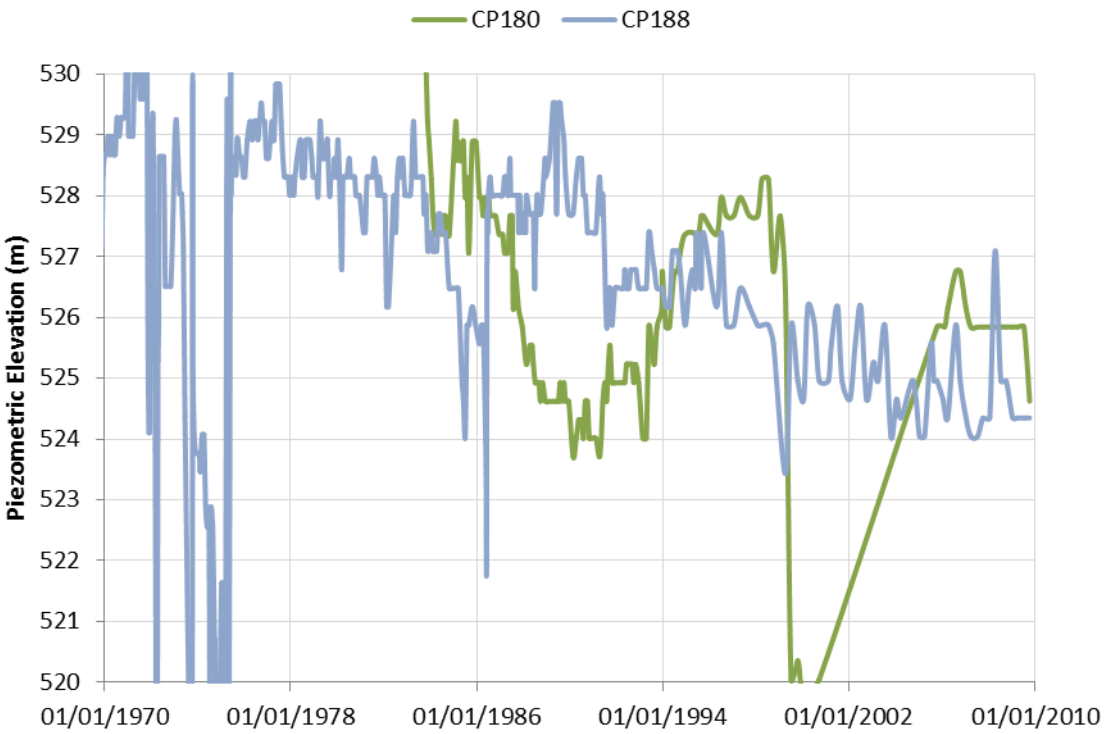

Figure A 21 Historic shale piezometric response: 1450 m >x>400 m downstream of centerline, CP180 and CP188

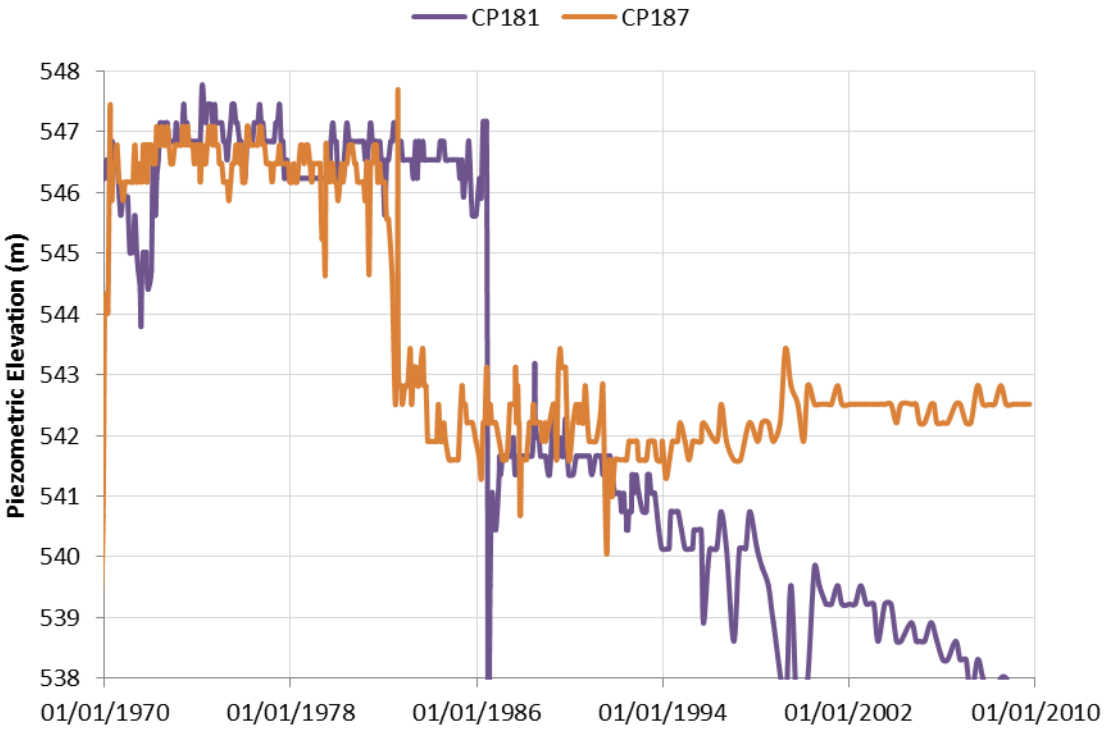

Figure A 22 Historic shale piezometric response: 1450 m >x>400 m downstream of centerline, CP181 and CP187

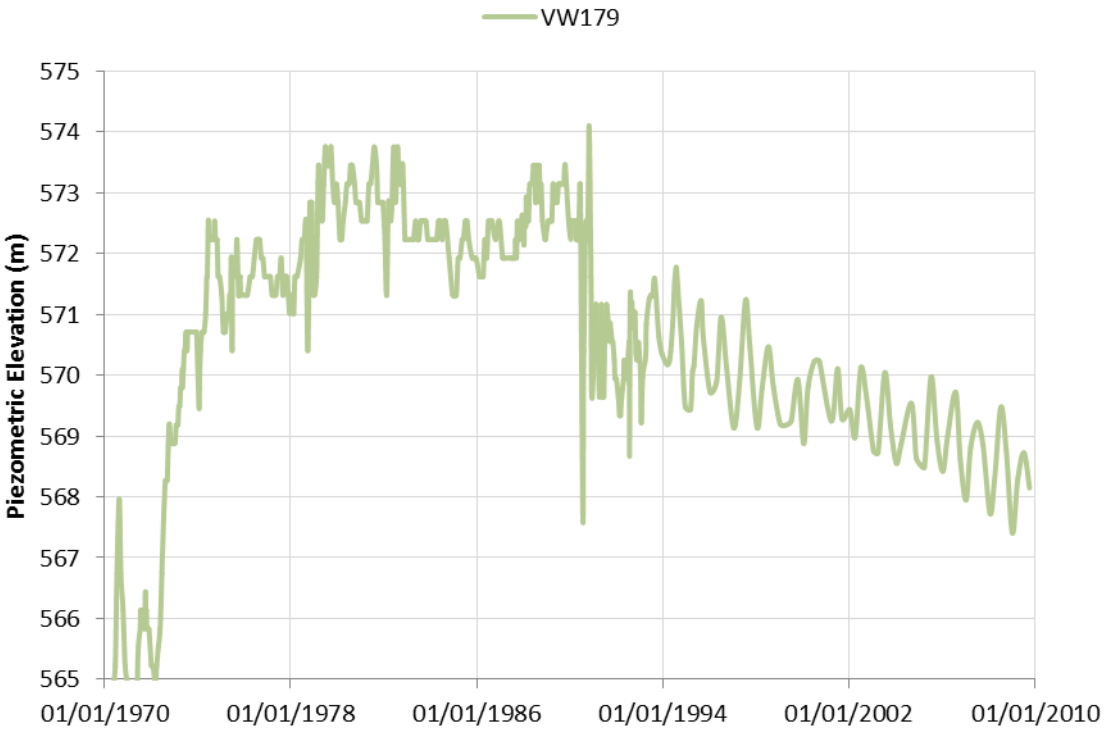

Figure A 23 Historic shale piezometric response: 146 m downstream of centerline

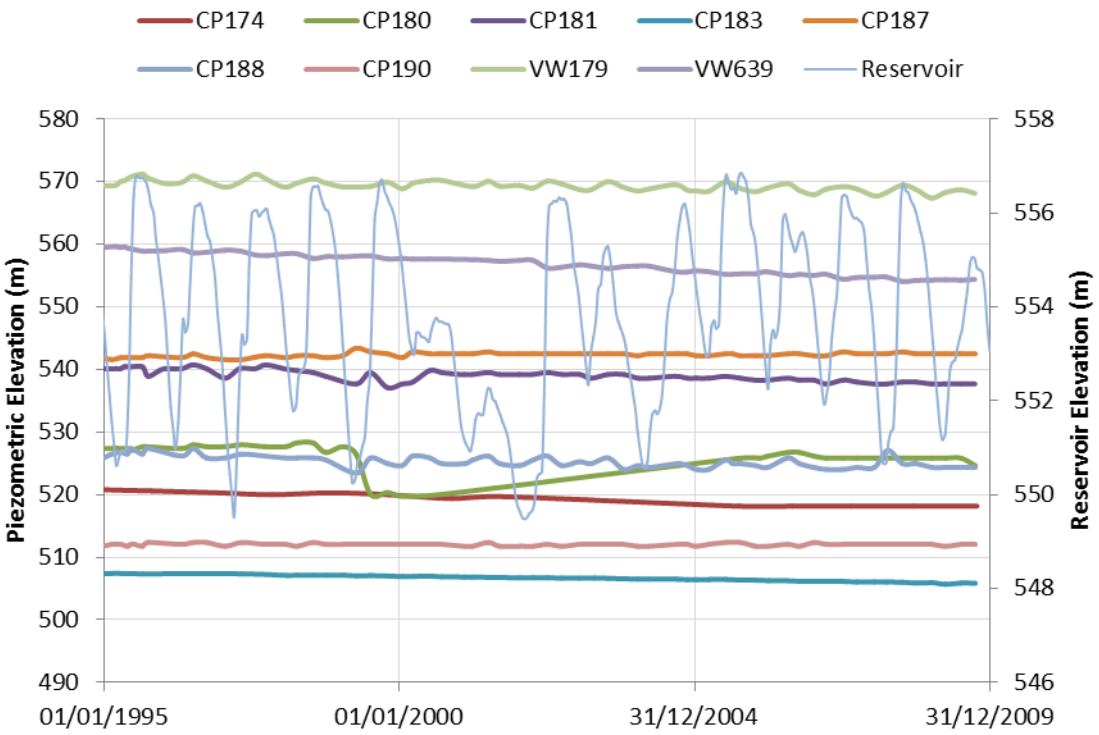

Figure A 24 Recent shale piezometric response and reservoir elevation: select piezometers beneath River Embankment

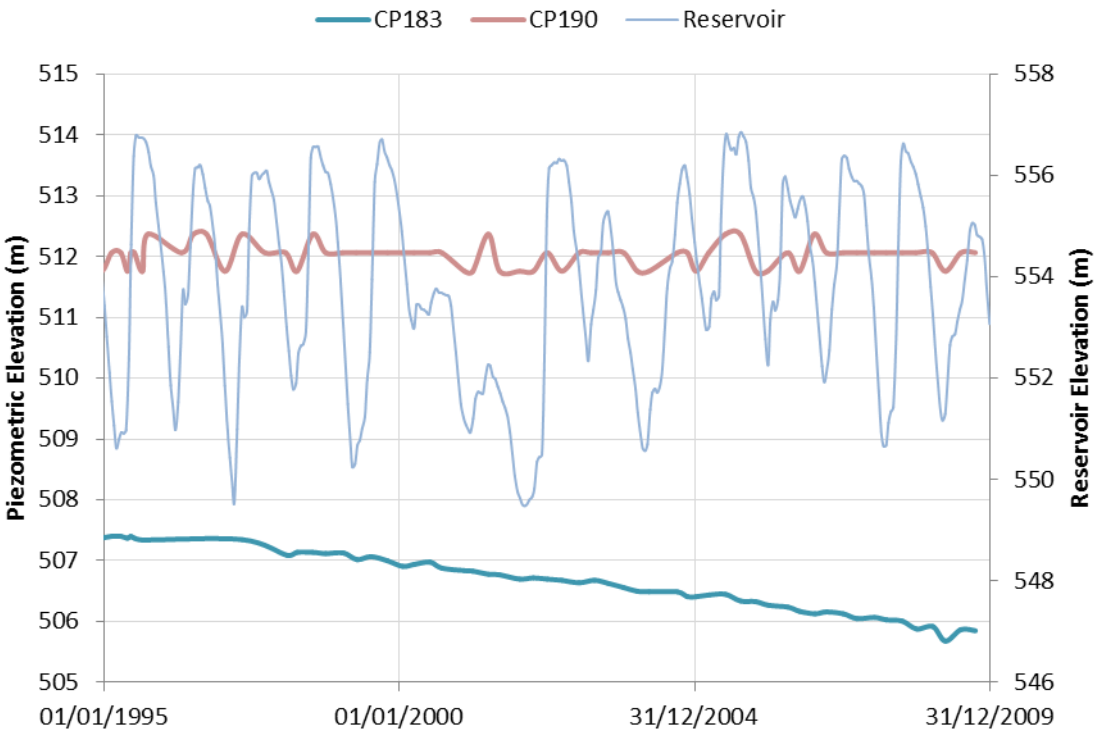

Figure A 25 Recent shale piezometric response and reservoir elevation: >1450 m downstream of centerline

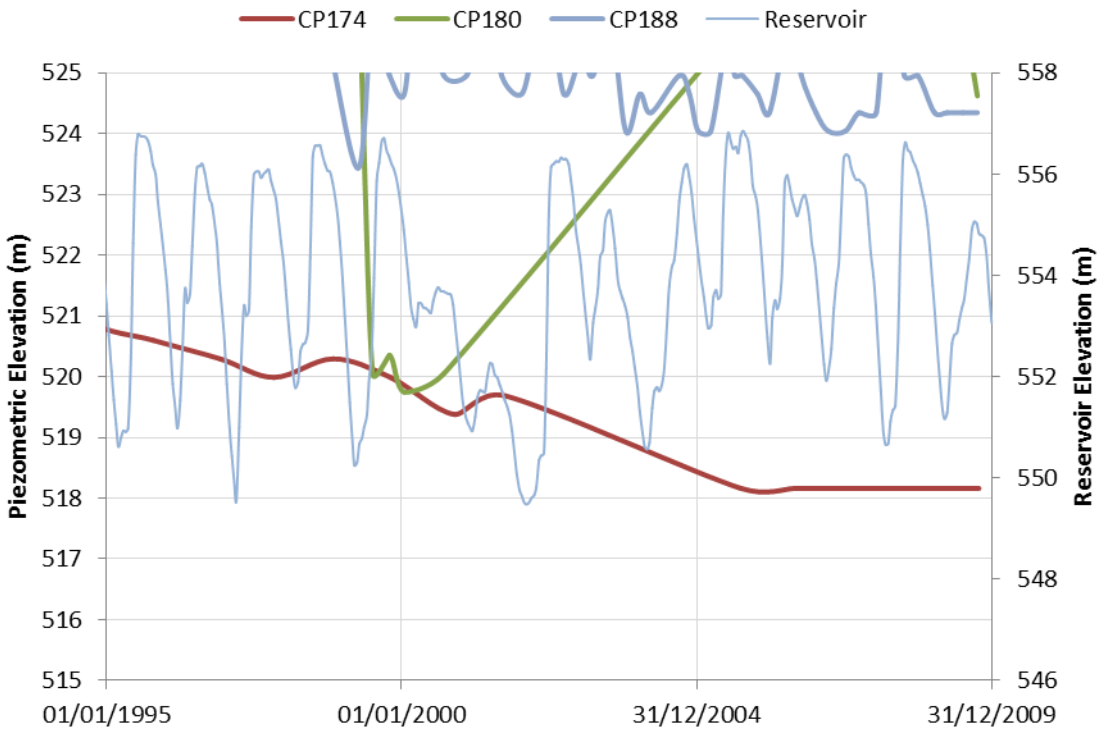

Figure A 26 Recent shale piezometric response and reservoir elevation: 1450 m >x>400 m downstream of centerline, CP174

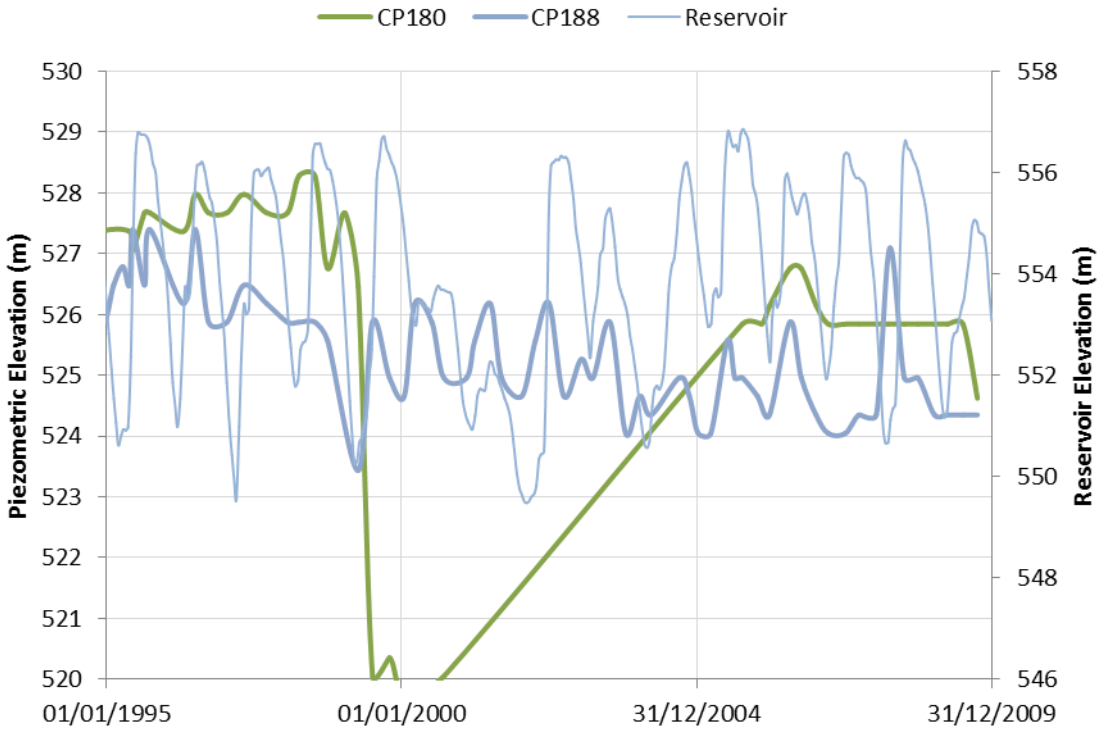

Figure A 27 Recent shale piezometric response and reservoir elevation: 1450 m >x>400 m downstream of centerline, CP180 and CP188

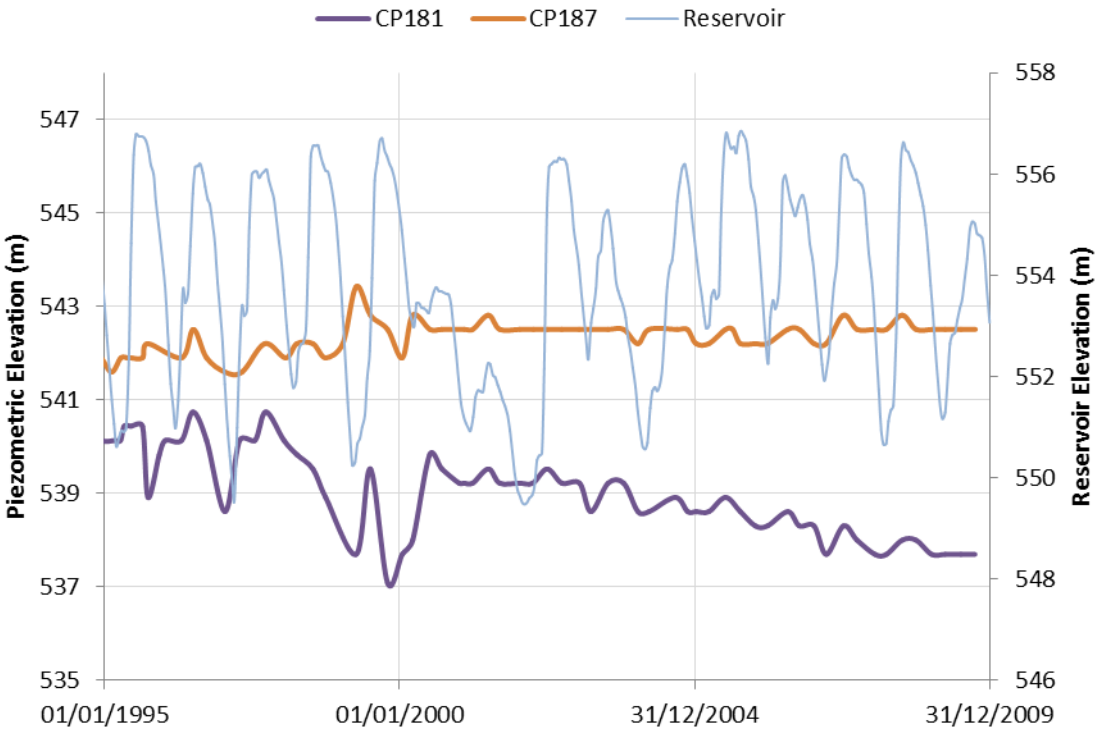

Figure A 28 Recent shale piezometric response and reservoir elevation: 1450 m >x>400 m downstream of centerline, CP181 and CP187

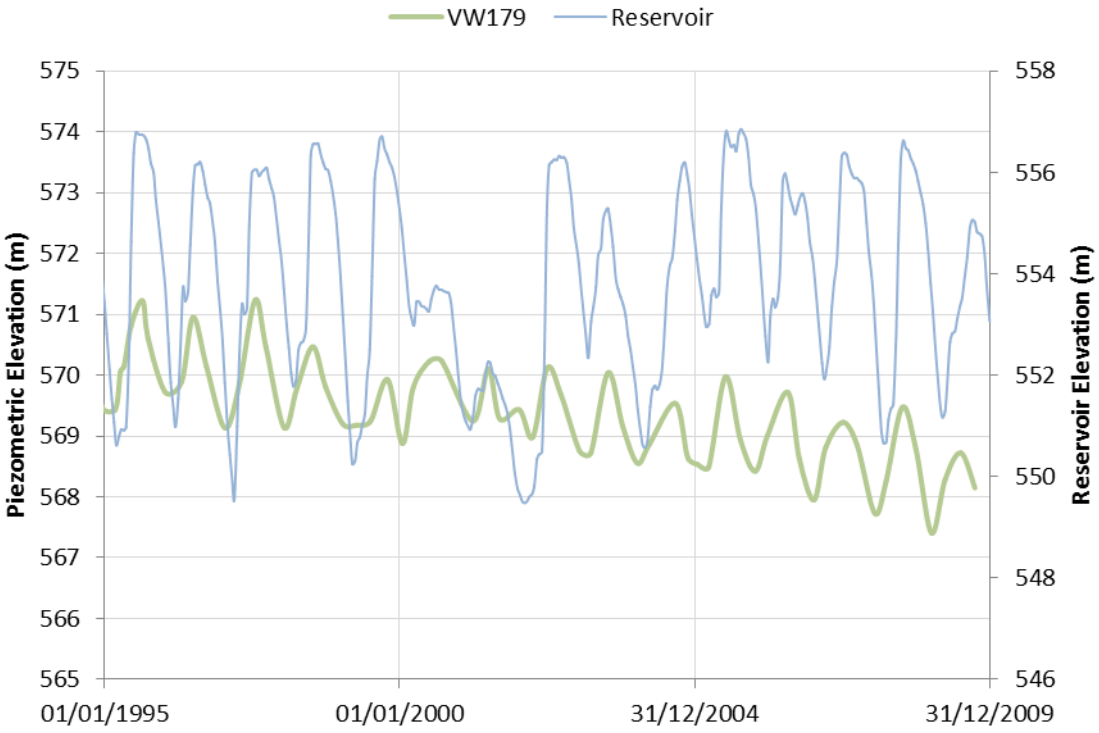

Figure A 29 Recent shale piezometric response and reservoir elevation: 146 m downstream of centerline

A5. Foundation Piezometric Response; Sandstone

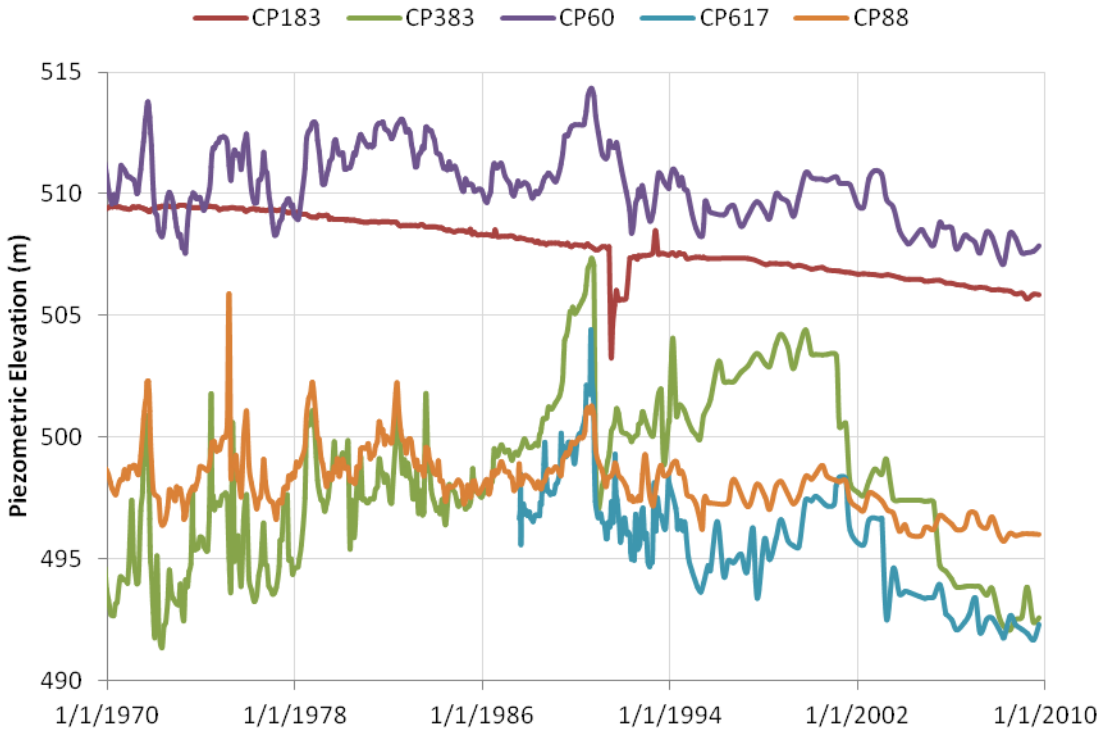

Figure A 30 Historic sandstone piezometric response: select piezometers beneath river embankment

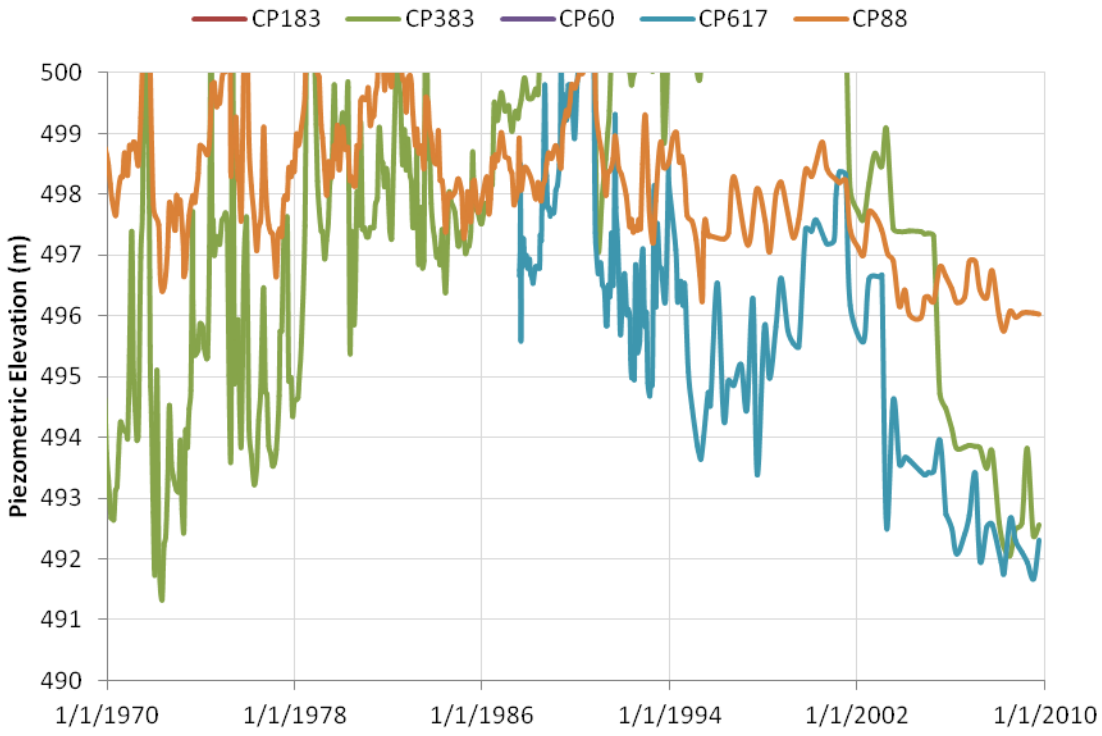

Figure A 31 Historic sandstone piezometric response: >650 m downstream of centerline

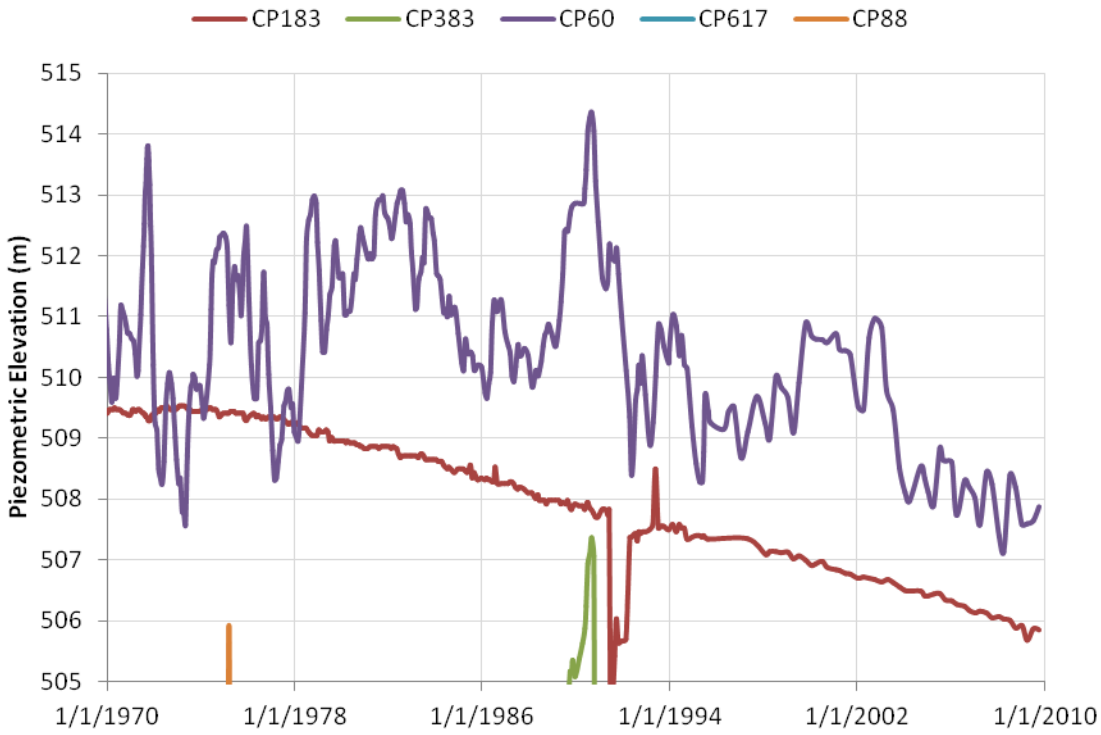

Figure A 32 Historic sandstone piezometric response: 650 m>x>0 m downstream of centerline

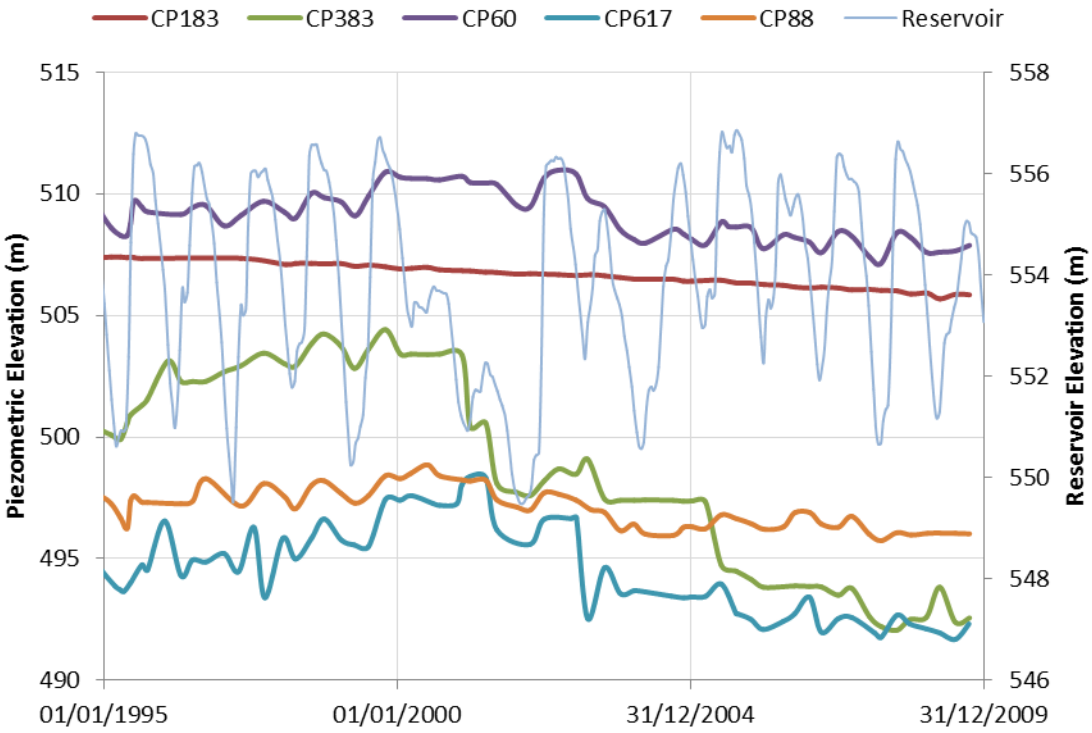

Figure A 33 Recent sandstone piezometric response and reservoir elevation: select piezometers beneath river embankment

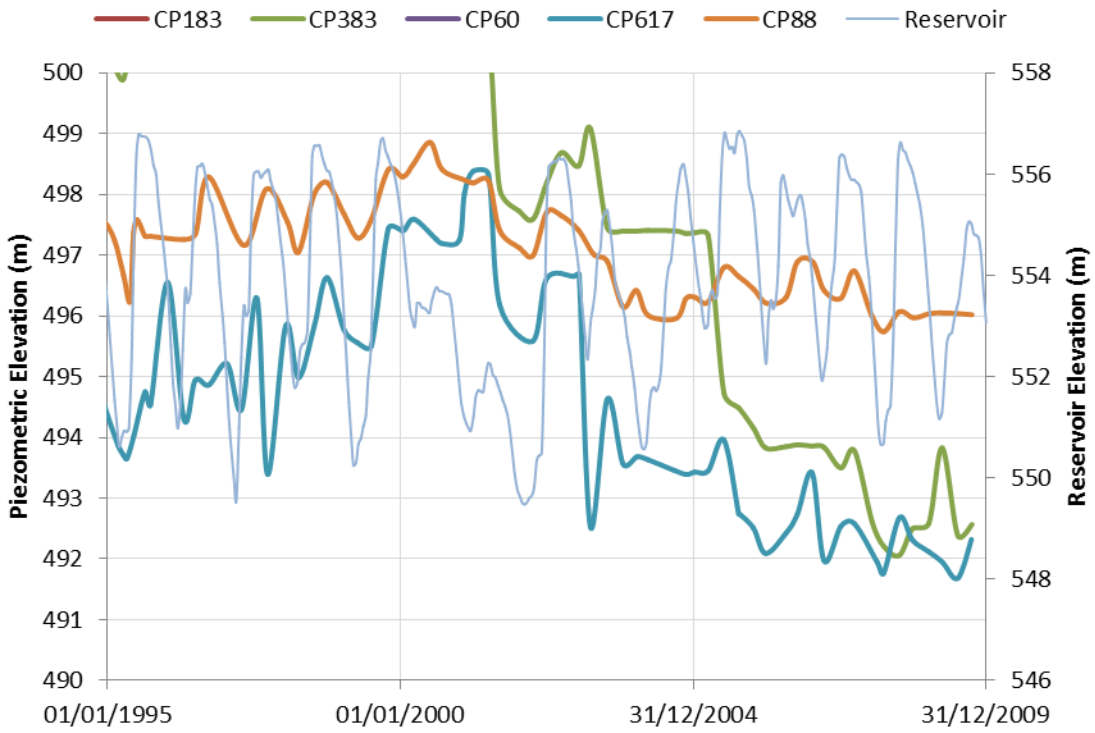

Figure A 34 Recent sandstone piezometric response and reservoir elevation: >650 m downstream of centerline

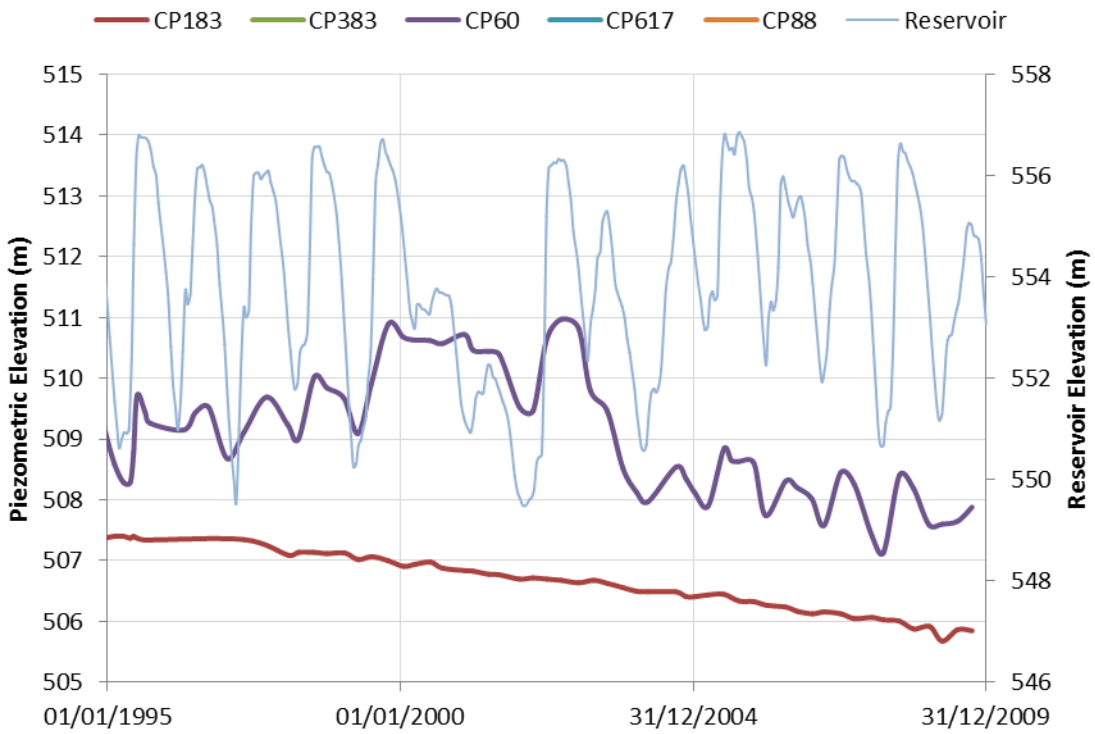

Figure A 35 Recent sandstone piezometric response and reservoir elevation: 650 m>x>0 m downstream of centerline

A6. Foundation Horizontal Deformation

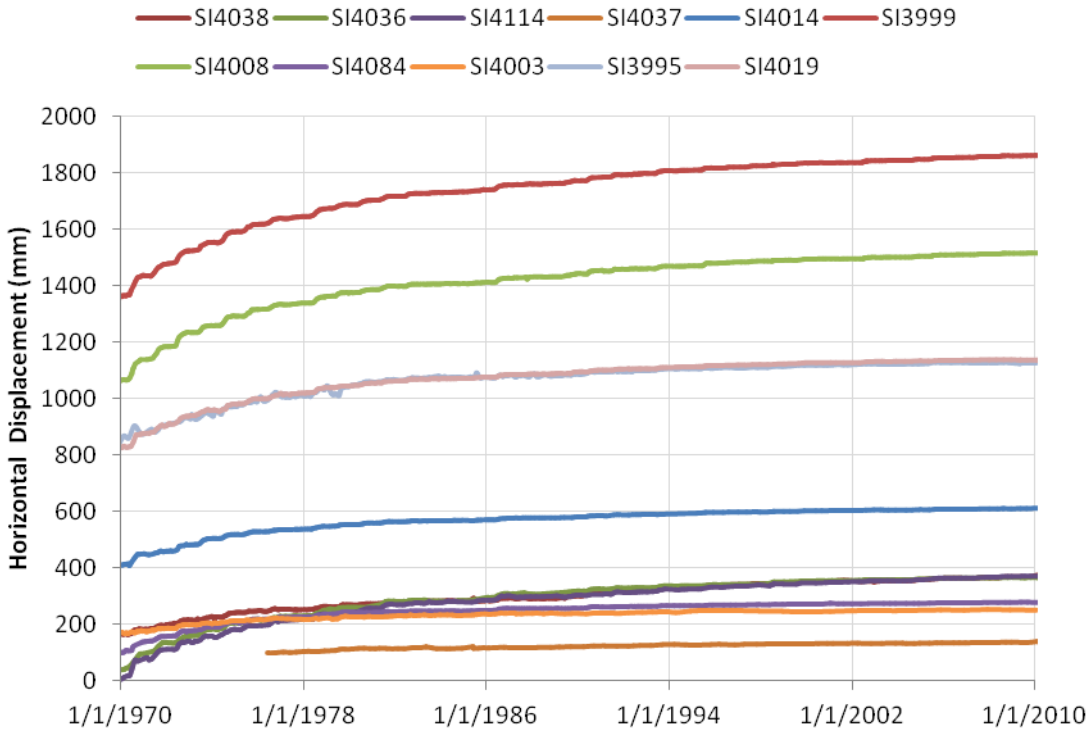

Figure A 36 Historical foundation horizontal displacement: select inclinometer casings

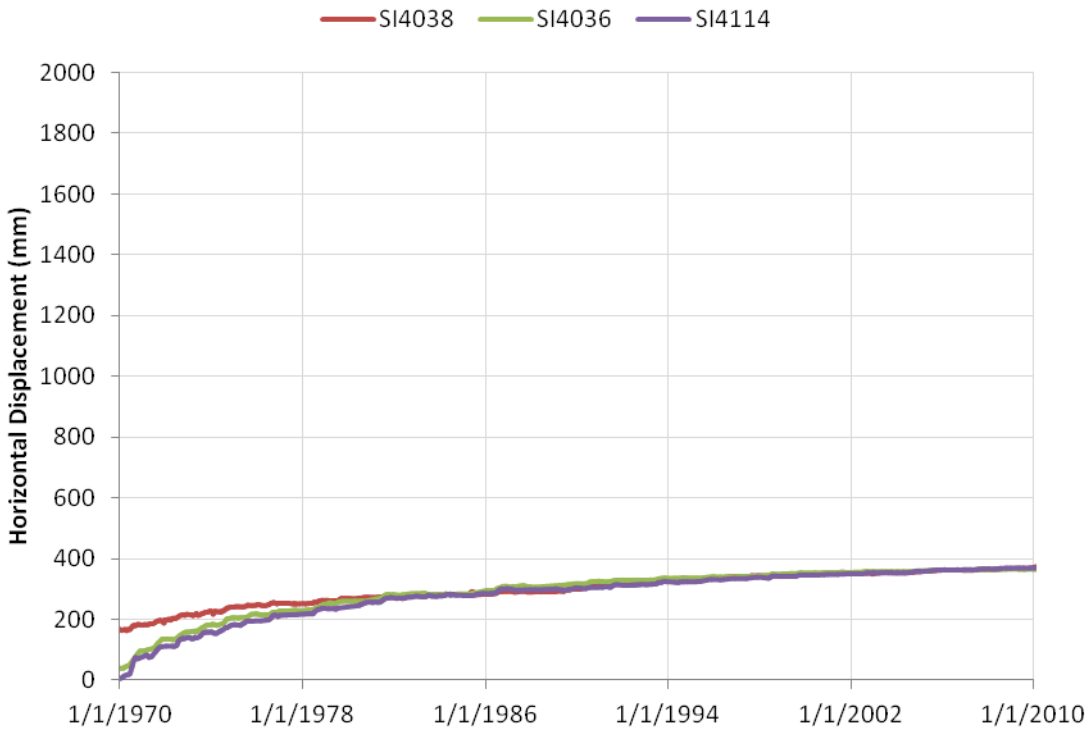

Figure A 37 Historical foundation horizontal displacement: centerline

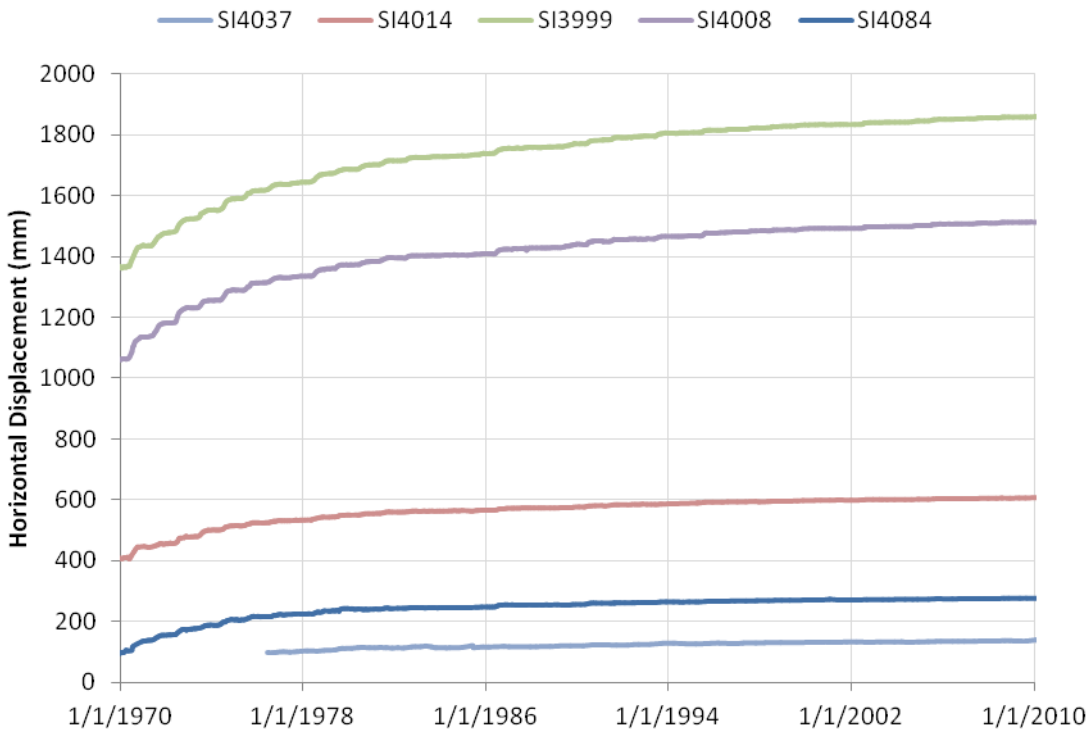

Figure A 38 Historical foundation horizontal displacement: 150 m downstream of centerline

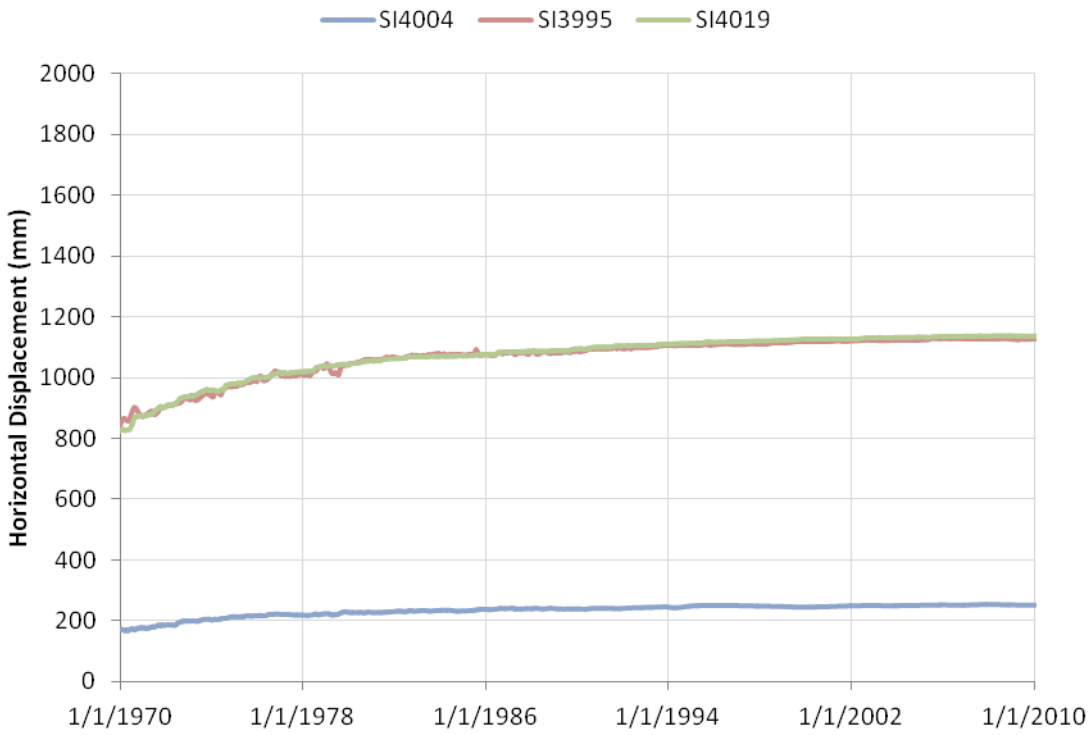

Figure A 39 Historical foundation horizontal displacement: 400 m downstream of centerline

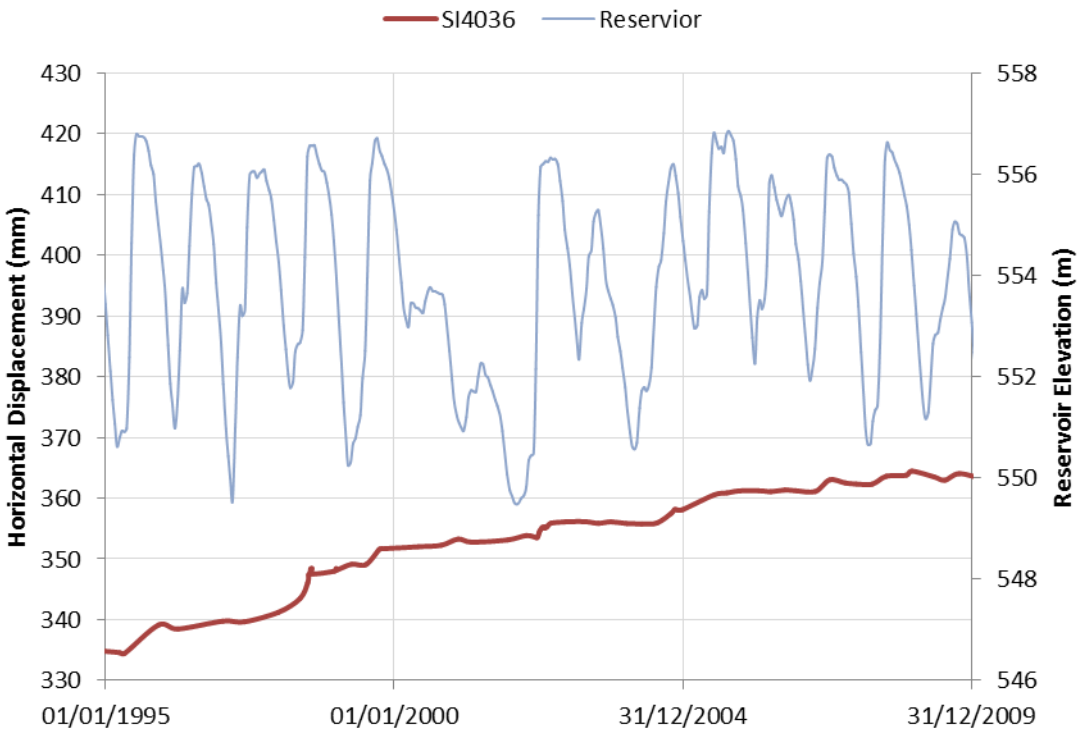

Figure A 40 Recent foundation horizontal displacement and reservoir elevation: SI4036

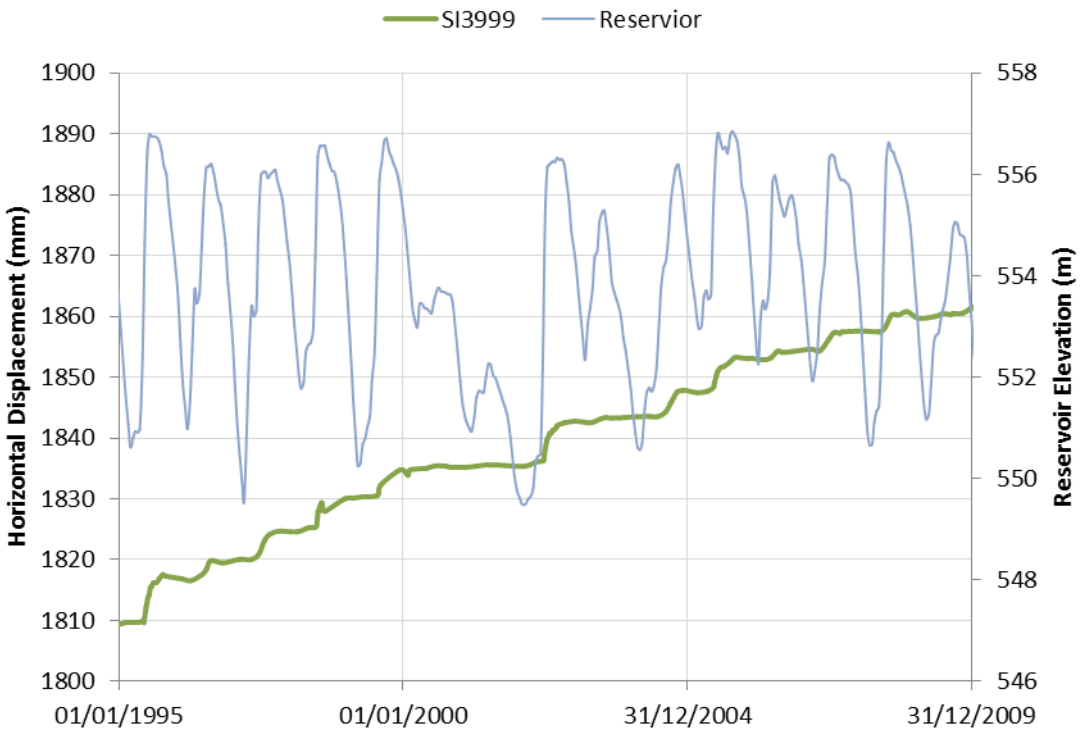

Figure A 41 Recent foundation horizontal displacement and reservoir elevation: SI3999 (150 m downstream of centerline)

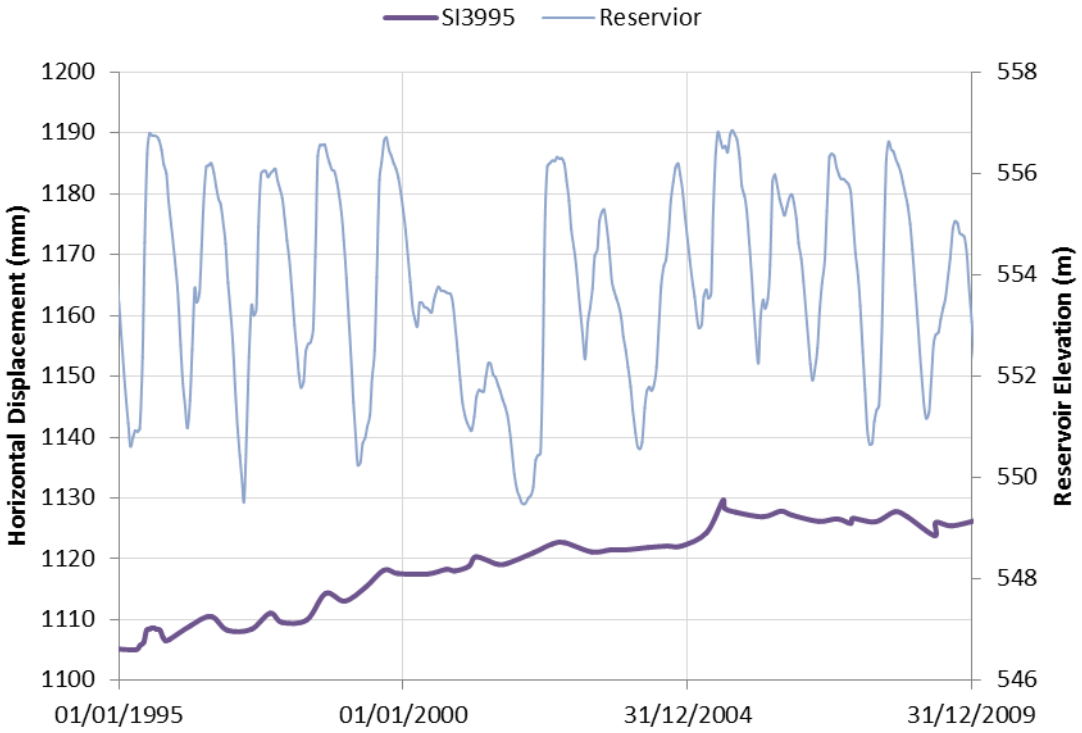

Figure A 42 Recent foundation horizontal displacement and reservoir elevation: SI3995 (400 m downstream of centerline)

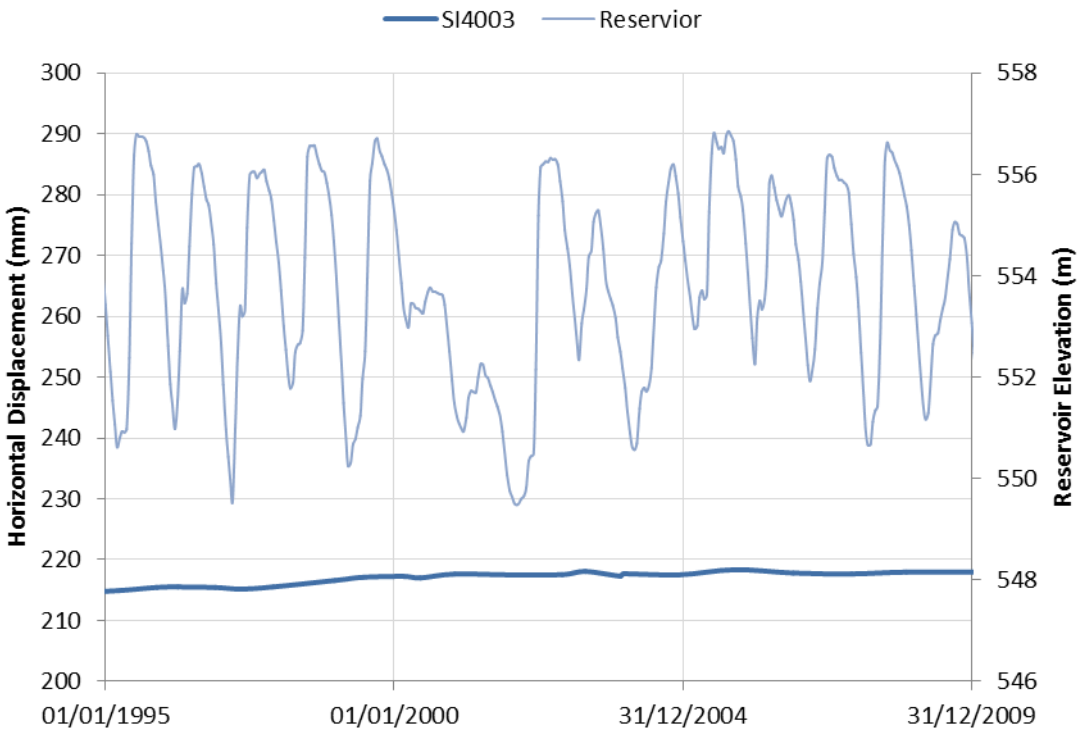

Figure A 43 Recent foundation horizontal displacement and reservoir elevation: SI4003 (700 m downstream of centerline)

APPENDIX B FINITE ELEMENT STRESS AND POREWATER RESPONSE MODEL

B1. Introduction

This appendix provides the modelled contours for the porewater, load deformation and coupled porewater/stress response models due to incremental changes in reservoir level. The results were produced using a simple finite element stress-strain and seepage model. The models were created using Sigma/W and Seep/W from the Geostudio software package (GEO-SLOPE INTERNATIONAL LTD. 2012). The purpose of this model was to provide general insight into the effects on the stress and porewater response to changes in the reservoir, stiffness properties of the shale and hydraulic conductivity of the shale. Therefore, the results determined from this model are used only for comparison purposes and the values present are not to be relied upon as true values.

B2. Analysis Types and Constitutive Model

Three types of analysis were completed for this evaluation including a porewater response model, load/deformation model and a coupled porewater/stress response model.

The porewater response model evaluated the changes in the total head within the model domain as a result of incremental changes in the reservoir level. With this model, the effects on the total head within the shale were evaluated due to changes in the hydraulic conductivity of the shale. The model was completed using a transient seepage model, assuming unsaturated/saturated properties for all the materials. The unsaturated material properties were estimated from the saturated hydraulic conductivity and the material general description. The hydraulic conductivity function was estimated using the Van Genuchten method and the volumetric water content function was estimated based on the sample function. Both estimations were developed using internal algorithms with SEEP/W.

The load/deformation model evaluated the changes in the stress within the model domain as a result of incremental changes in the reservoir level. The stress response in the shale was evaluated by varying the stiffness of the shale with the remaining materials being held constant. This model was completed by using a linear elastic constitutive model for all the materials.

The coupled porewater/stress model evaluated the combined changes in the total head and the stress within the model domain due to incremental changes in the reservoir level. This model was used to evaluate the porewater pressure and the stress response due to changes in the stiffness of the shale and the hydraulic conductivity of the shale. This model represented the material strength parameters using a linear elastic constitutive model with porewater change taken into consideration. The hydraulic material properties were represented using unsaturated/saturated material properties. The unsaturated material properties were estimated with this evaluation from the saturated hydraulic conductivity and the material general description. The hydraulic conductivity function was estimated using the Van Genuchten method and the Volumetric Water Content function was estimated based on the sample function both from within SEEP/W.

B3. Model Domain, Boundary Conditions & Mesh Definition

The geometry of the River Embankment and foundation was represented by a simplified geometry; therefore, the details of the insitu geometry have been removed from the numerical model.

There are several boundary conditions assumed thorough the various analyses. The hydraulic and stress-strain boundary conditions were similar when applied.

Hydraulic boundary conditions were applied as total head, pressure head and no flow boundary conditions. Total head boundary conditions were applied to the upstream face of the dam, the upstream and downstream limits of the river sand and sandstone. Pressure head boundary conditions were applied to the downstream face of the dam with a potential seepage review conducted. No flow boundary conditions were applied to the invert of the sandstone and the upstream and downstream limits of the shale.

Stress-strain boundary conditions were applied as fixed deformation and hydraulic pressure. The vertical upstream and downstream limits of the domain were fixed in the X direction and the horizontal invert of the domain was fixed both in the X and Y directions. Hydrostatic pressure of reservoir water was added to the upstream face of the embankment.

The reservoir total head and hydrostatic stress were the only boundary conditions changed throughout the three analyses. The boundary conditions are summarized in Table B 1. The geometry and boundary conditions are illustrated in Figure B 1through Figure B 3.

Table B 1 Assumed boundary conditions for finite element model

Soil	Position	Hydraulic Boundary Conditions		Stress Boundary Condition	
		Type	Value	Type	Value
Embankment	Upstream Face	Total Head	550 m -556 m	Hydraulic Pressure	550 m -556 m
Embankment	Downstream Face	Pressure Head	0 m Seepage Face Review	-	-
River Sand	Upstream Face	Total Head	550 m – 556 m	Deformation	Fixed X Direction
River Sand	Downstream Face	Total Head	499 m	Deformation	Fixed X Direction
Shale	Upstream and Downstream Face	No Flow	-	Deformation	Fixed X Direction
Sandstone	Upstream and Downstream Face	Total Head	509 m	Deformation	Fixed X Direction
Sandstone	Horizontal Invert	No Flow	-	Deformation	Fixed X and Y Direction

During the modelling process the properties used for the embankment, river sand, and sandstone were held constant with only the properties of the shale varied. The hydraulic material properties used for the embankment, river sand, and sandstone were found from PFRA (1980) and GEO-SLOPE INTERNATIONAL LTD. (2012). The stiffness properties for these materials were approximated from Munfakh et al. (1997). The hydraulic properties of the shale were referenced from PFRA (1980) and the stiffness properties of the shale were referenced from PFRA (1966b) and Gautam and Wong (2006). The values used in the models are illustrated in Table B 2.

Table B 2 Assumed material properties for finite element model

Soil	Material Description	Young's Modulus E' (MPa)	Poisson's Ratio ν	Hydraulic Conductivity k (m/s)
Embankment	Medium to Stiff Clay	15	0.49	1e-8
River Sand	Medium Dense Sand	25	0.35	1e-5
Sandstone	Medium Dense Sand	25	0.35	1e-5
Shale	N/A	139 - 1250	0.49	1e-9 - 1e-13

The finite element mesh was generated using the algorithm within Geostudio. The finite element mesh spacing was set to 5m. The finite element mesh generated is illustrated in Figure B 1 through Figure B 3

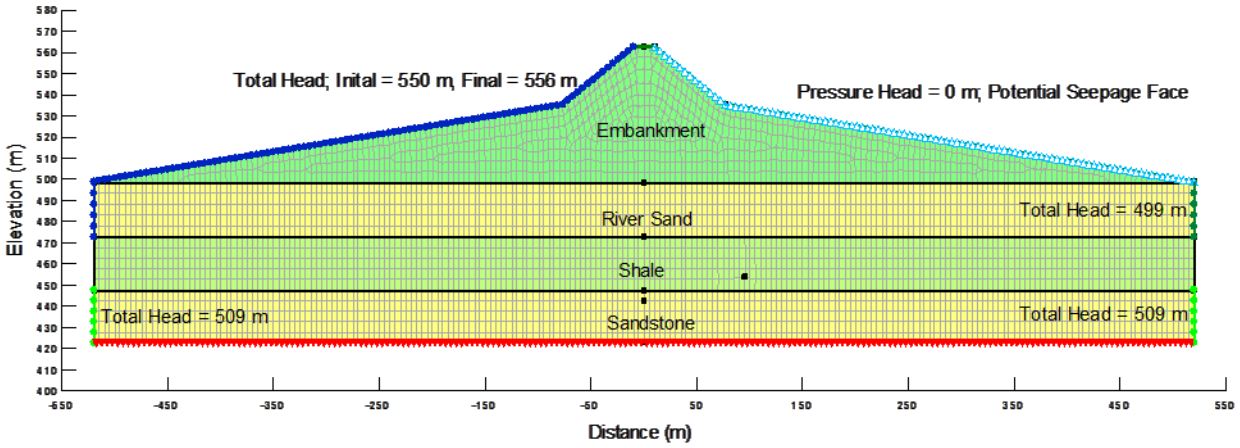

Figure B 1 Porewater model: domain with 5m mesh spacing

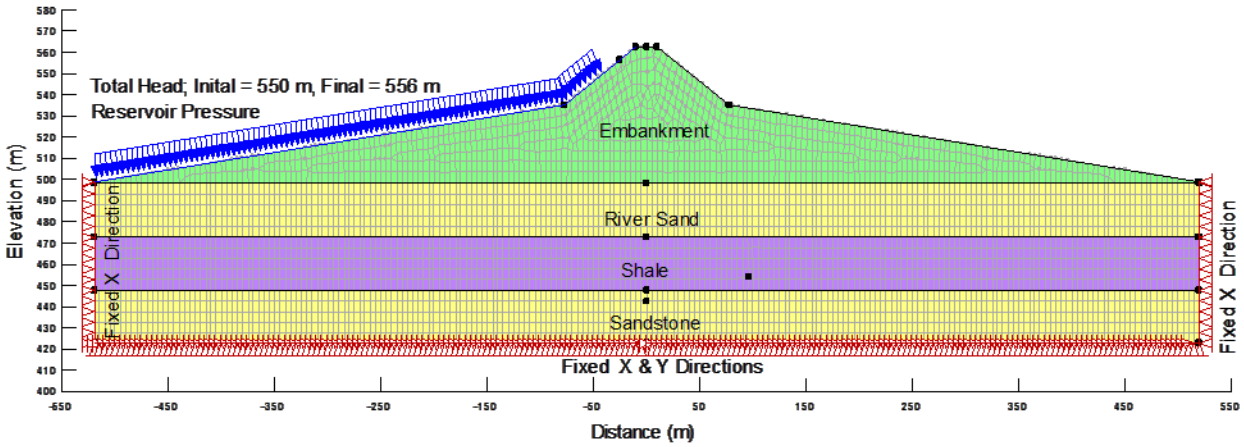

Figure B 2 Load/deformation model: domain with 5m mesh spacing

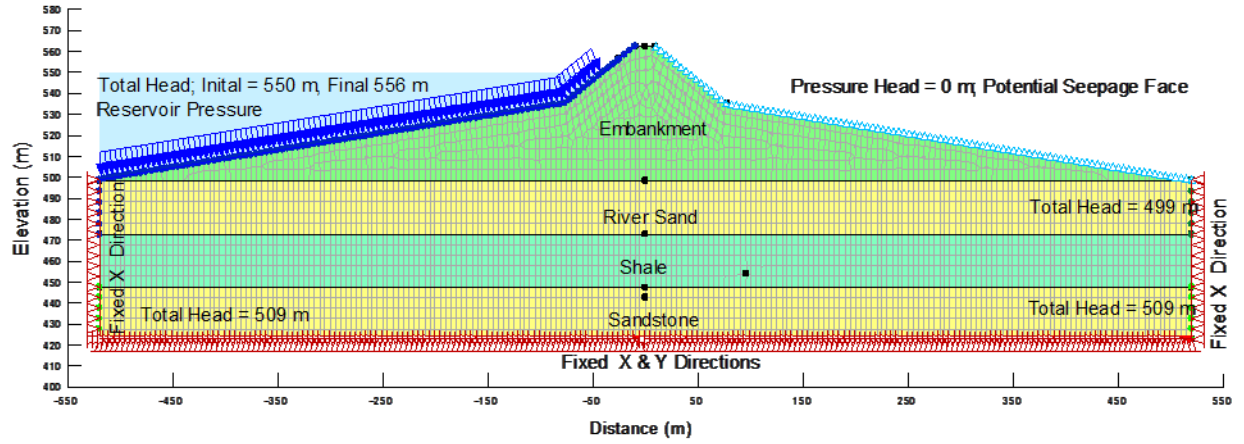

Figure B 3 Coupled porewater/stress model: domain with 5m mesh spacing

B4. Model Results

The following figures illustrate the results from the above described evaluations. There are several ways the results from a finite element model can be presented. Because the purpose of this set of evaluations was to gain insight into the effects of changes in stiffness and the hydraulic conductivity of the shale on porewater and stress response as a result of reservoir fluctuations, contours of the stress response and the total head for the model scenarios were illustrated. The total head response represents the porewater pressure total head in meters. The stress response represents the X stress in terms of kPa. The X stress was selected as the basis for the hypothesis for the increase in porewater as a result of the change in the reservoir level.

B5. Porewater Response

The evaluating of the porewater response alone indicated minimal change in the total head with the change in the reservoir from 550 m to 556 m. This was evident of both hydraulic conductivities evaluated. The porewater response is illustrated in Figure B 4 through Figure B 7. The stress change was not modelled during this evaluation.

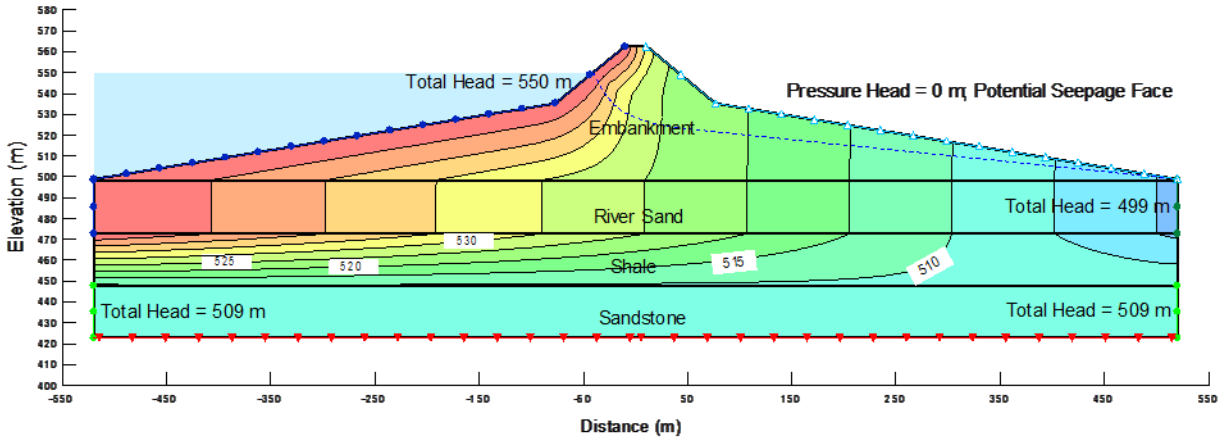

Figure B 4 Transient seepage, total head: reservoir 550 m, 1 day, k=1e-9 m/s

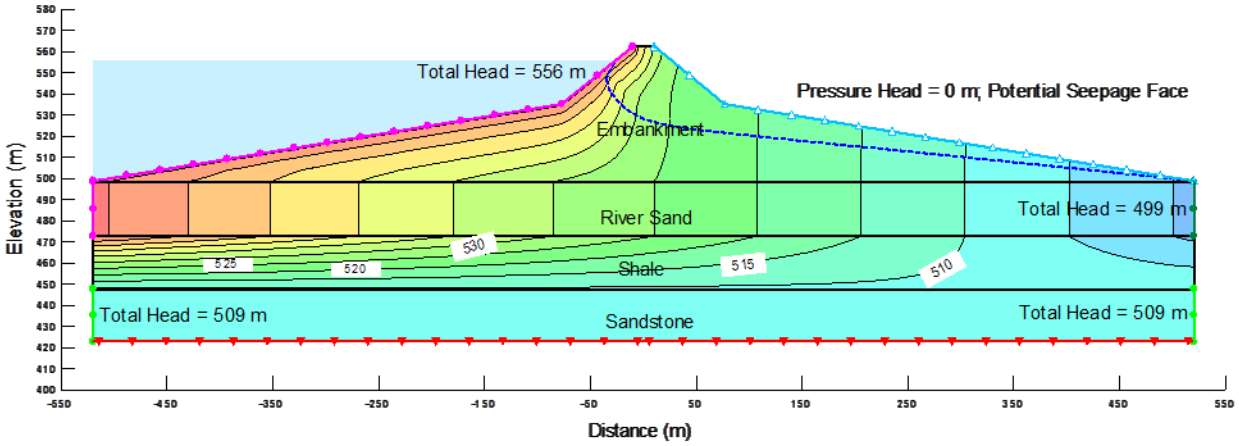

Figure B 5 Transient seepage, total head: reservoir 556 m, 23 days, k=1e-9 m/s

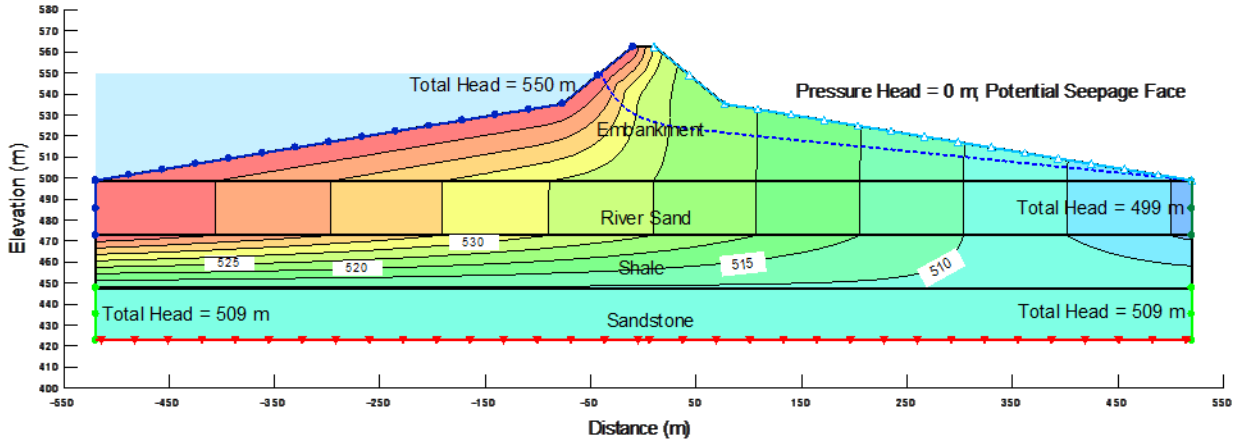

Figure B 6 Transient seepage, total head: reservoir 550 m, 1 day, k=1e-13 m/s

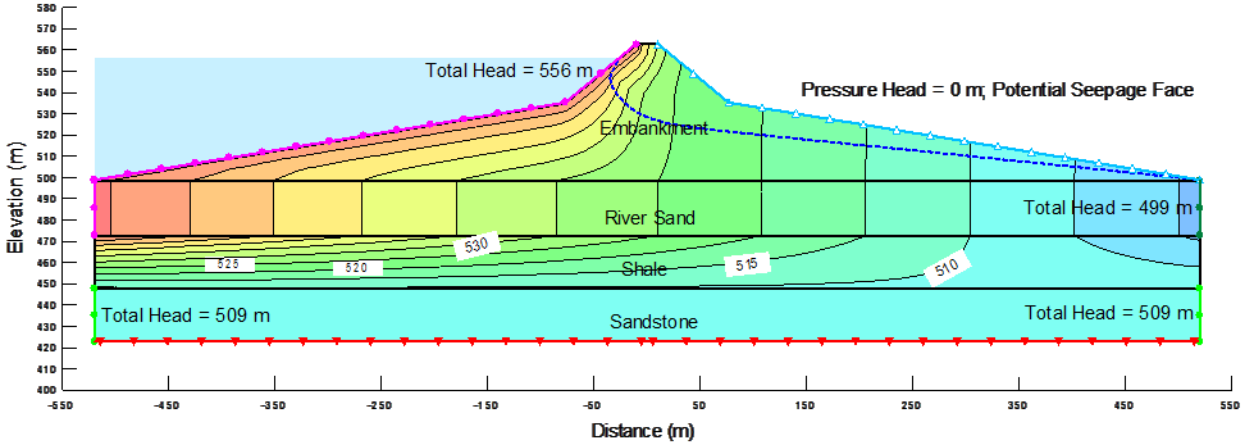

Figure B 7 Transient seepage, total head: reservoir 556 m, 23 days, k=1e-13 m/s

B6. Load/Deformation Response

The load/deformation results showed that with an increase in the hydraulic pressure applied by the reservoir, there is a distinct increase in the X total stress within the shale for both shale stiffness conditions. It was also evident that as the stiffness increased, there was a larger relative increase in the X total stress within the shale. This evaluation also indicated that as the reservoir hydraulic pressure was applied, the increase in the X total stress was generally limited to the shale zone verifying the assumption that a change in reservoir could cause an increase in stress within the shale beneath the dam. This evaluation indicated that the reservoir influence decreased in the downstream direction similarly to the magnitude of horizontal displacement along the shear zone observed by the inclinometers. The stress redistribution response is illustrated in Figure B 8 through Figure B 11.

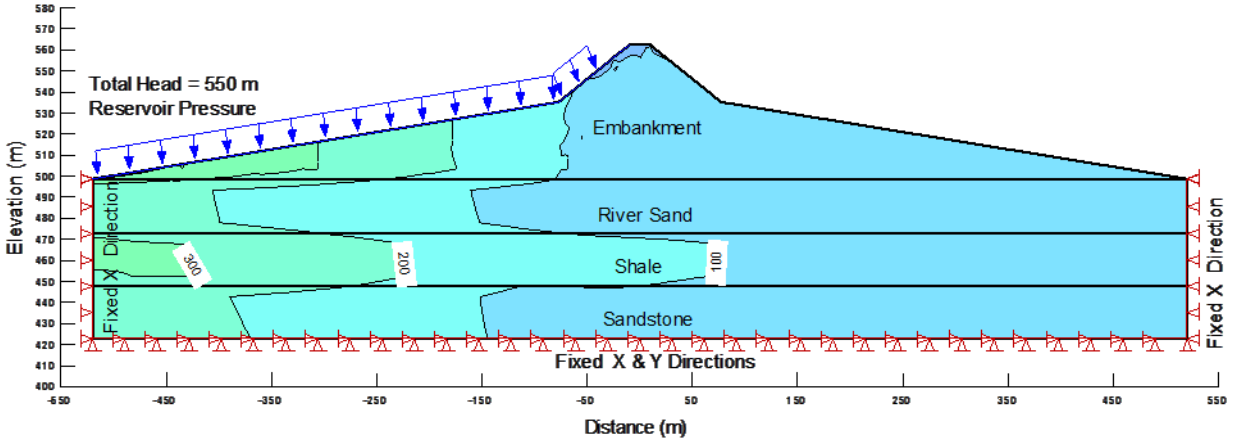

Figure B 8 Load/deformation, X total stress: reservoir 550 m, E'=139 MPa

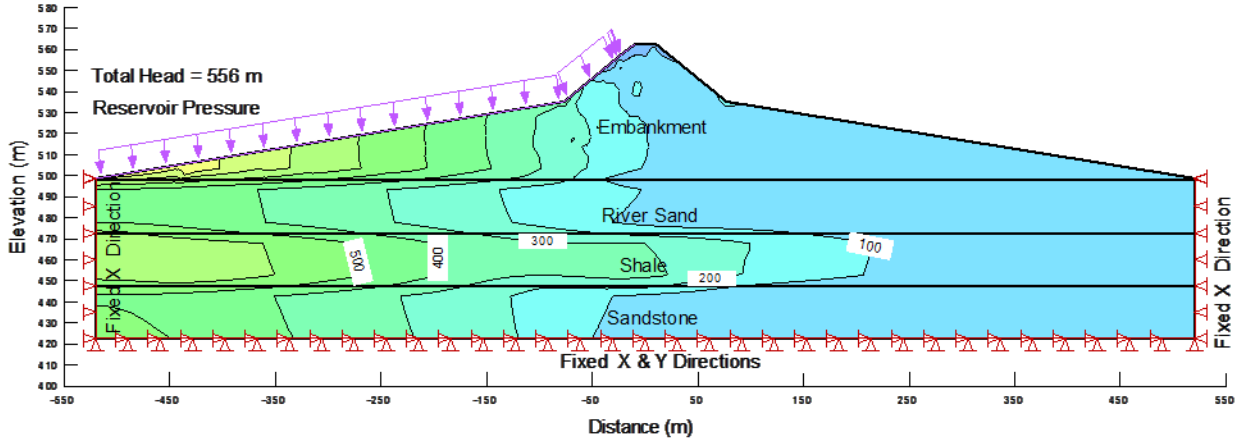

Figure B 9 Load/deformation, X total stress: reservoir 556 m, E'=139 MPa

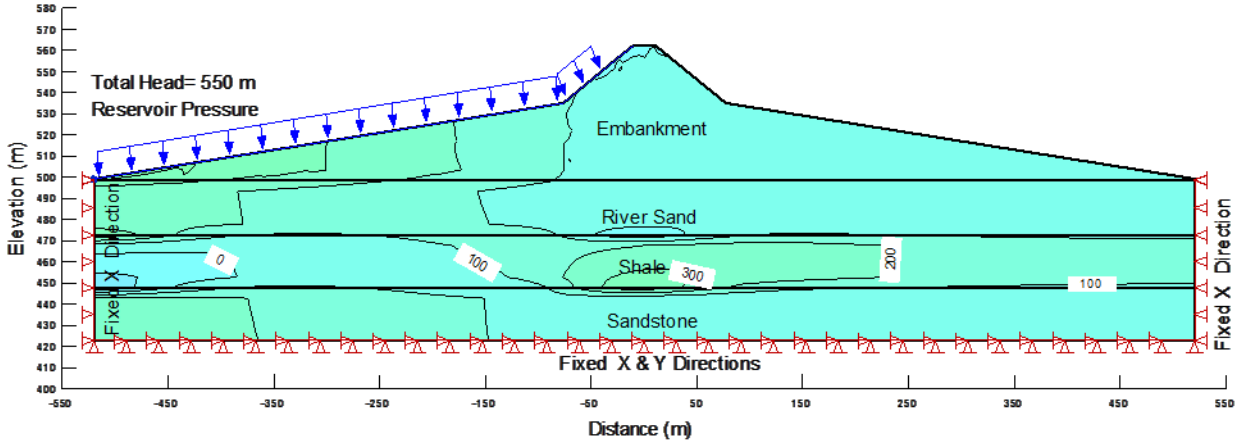

Figure B 10 Load/deformation, X total stress: reservoir 550 m, E'=1250 MPa

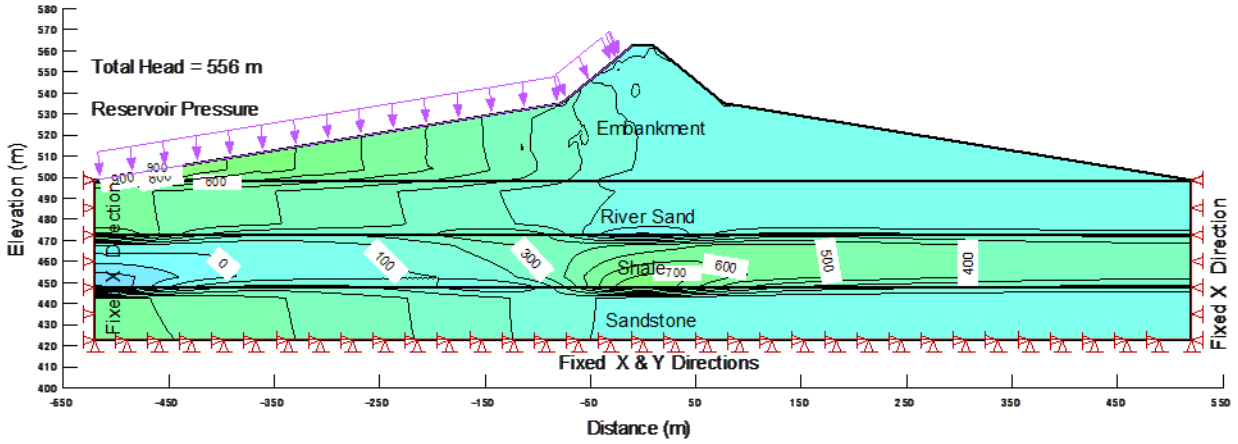

Figure B 11 Load/deformation, X total stress: reservoir 556 m, E'=1250 MPa

B7. Porewater/Stress Response

Similarly to the load deformation model, with the increase in reservoir level an increase in X total stress resulted in the shale. And as the stiffness of the shale increased, so did the relative increase in the X total stress response. The X total stress response was also limited to the shale and the X total stress contours in the embankment and river sand remained relatively vertical, verifying the conceptual model assumptions as discussed previously.

The X total stress response was also impacted by the varying of the hydraulic conductivity of the shale. As the hydraulic conductivity decreased so did the X total stress response. This was illustrated by comparing the contours with the same shale stiffness with varying hydraulic conductivities. The X total stress response is illustrated in Figure B 12 to Figure B 19.

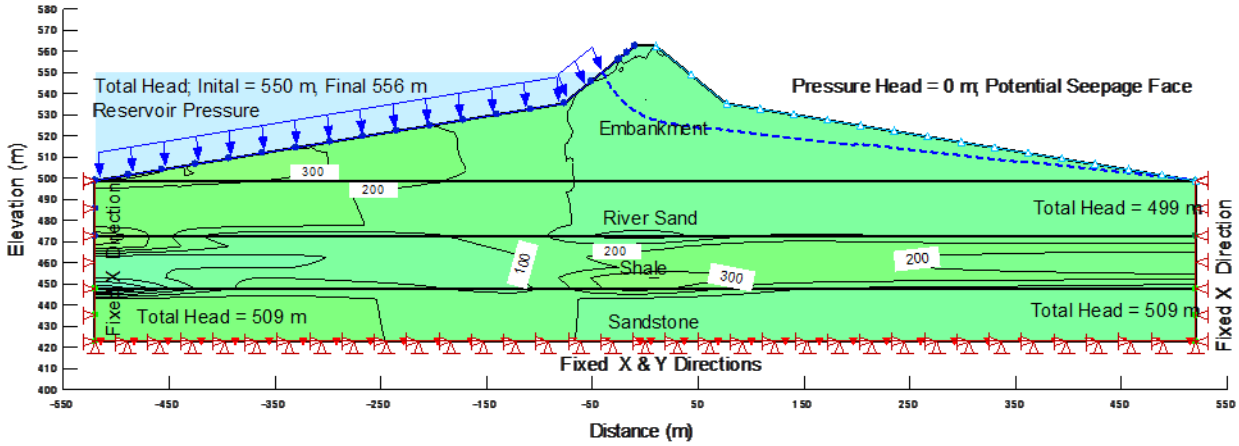

Figure B 12 Coupled X total stress: reservoir 550 m, 11 days, E'=1250 MPa, k=1e-13 m/s

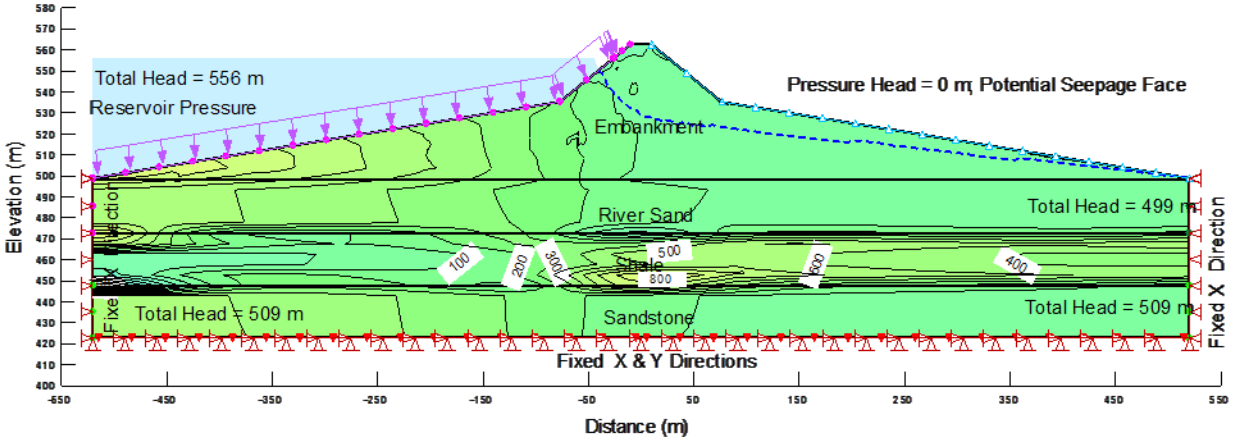

Figure B 13 Coupled X total stress: reservoir 556 m, 23 days, E'=1250 MPa, k=1e-13 m/s

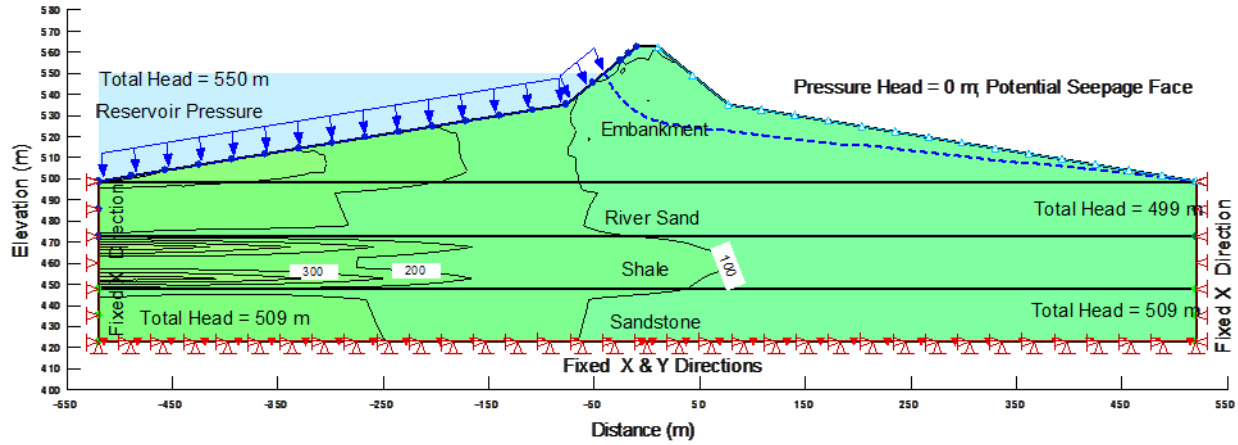

Figure B 14 Coupled X total stress: reservoir 550 m, 11 days, E'=139 MPa, k=1e-13 m/s

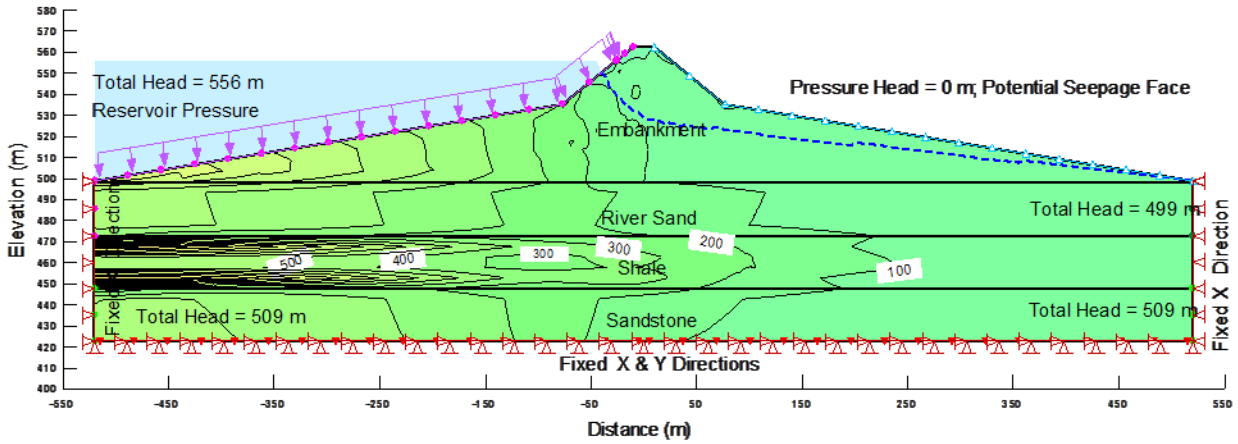

Figure B 15 Coupled X total stress: reservoir 556 m, 23 days, E'=139 MPa, k=1e-13 m/s

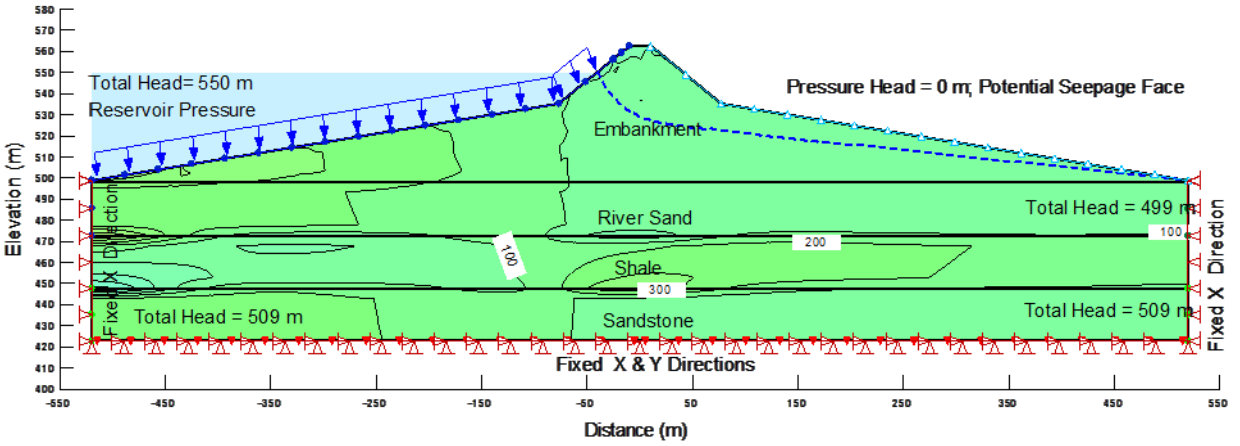

Figure B 16 Coupled X total stress: reservoir 550 m, 11 days, E'=1250 MPa, k=1e-9 m/s

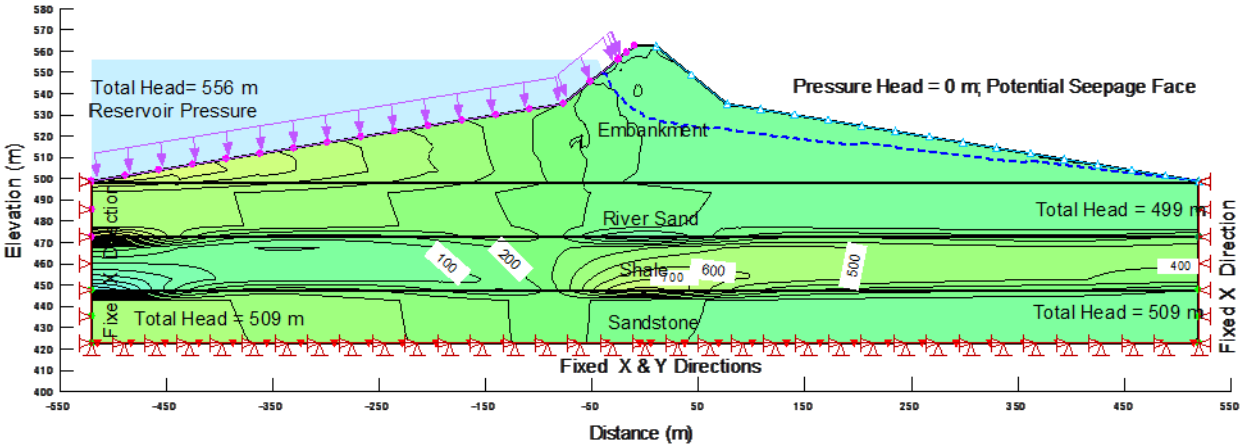

Figure B 17 Coupled X total stress at reservoir 556 m; 23 days; E'=1250 MPa; k=1e-9 m/s

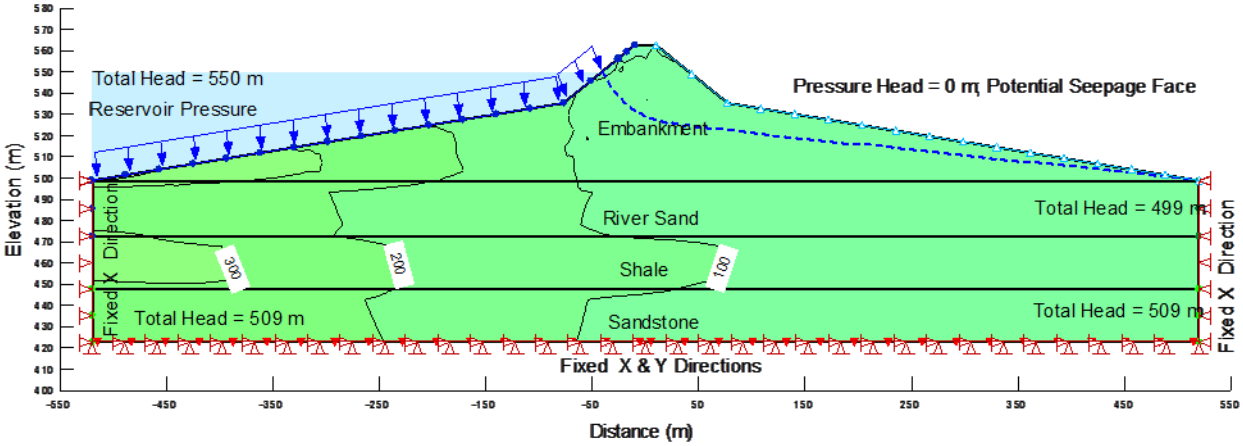

Figure B 18 Coupled X total stress: at reservoir 550 m, 11 days, E'=139 MPa, k=1e-9 m/s

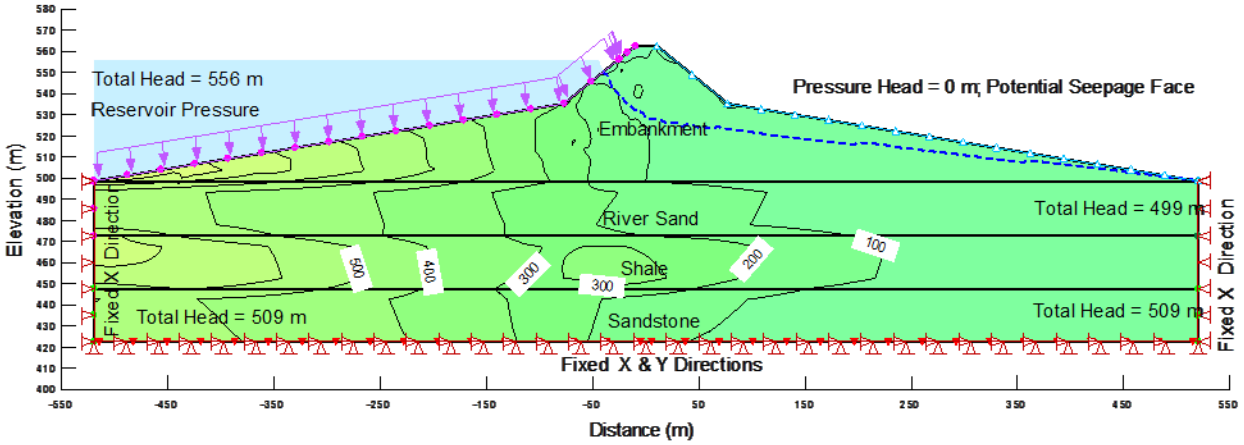

Figure B 19 Coupled X total stress: reservoir 556 m, 23 days, E'=139 MPa, k=1e-9 m/s

Unlike the porewater evaluation alone, the pore pressure was greatly influenced by changes in the reservoir throughout this evaluation as illustrated by Figure B 20 through Figure B 27. The porewater response was illustrated by the change in the total head within the shale as the reservoir hydraulic pressure increased. Similarly to the X total stress increase as the stiffness of the shale increases so did the increase in the total head response. The hydraulic conductivity of the shale also impacted the porewater response due to the increase in reservoir pressure. With the higher shale stiffness, it was evident that as the hydraulic conductivity of the shale was reduced, so did the total head response. However, with lower shale stiffness, the hydraulic conductivity had less influence over the total head response in the shale.

The total head response illustrated within this evaluation confirms the conceptual model that the change in the pore-pressure within the shale was a result of a change in stress caused by an increase in the reservoir hydraulic pressure.

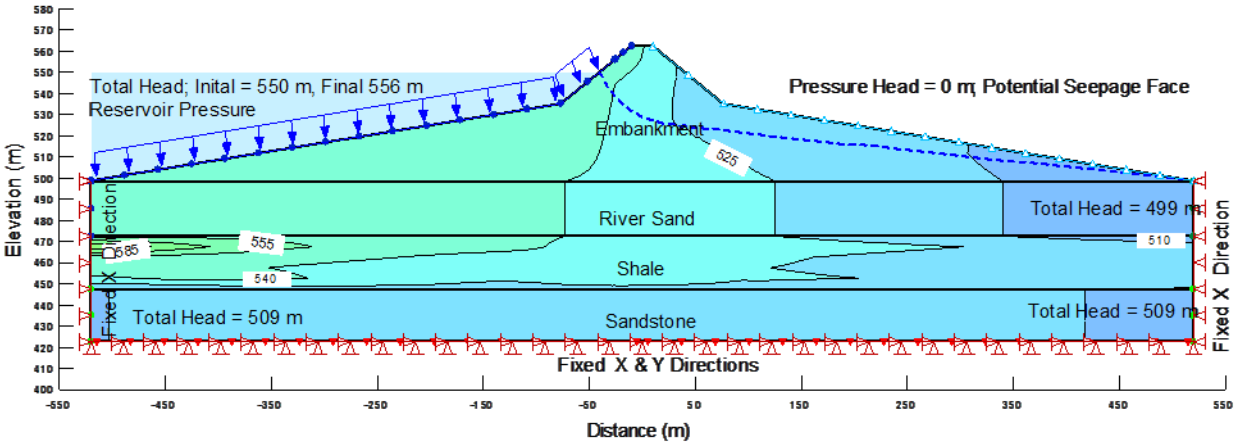

Figure B 20 Coupled total head: reservoir 550 m, 11 day, E'=1250 MPa, k=1e-13 m/s

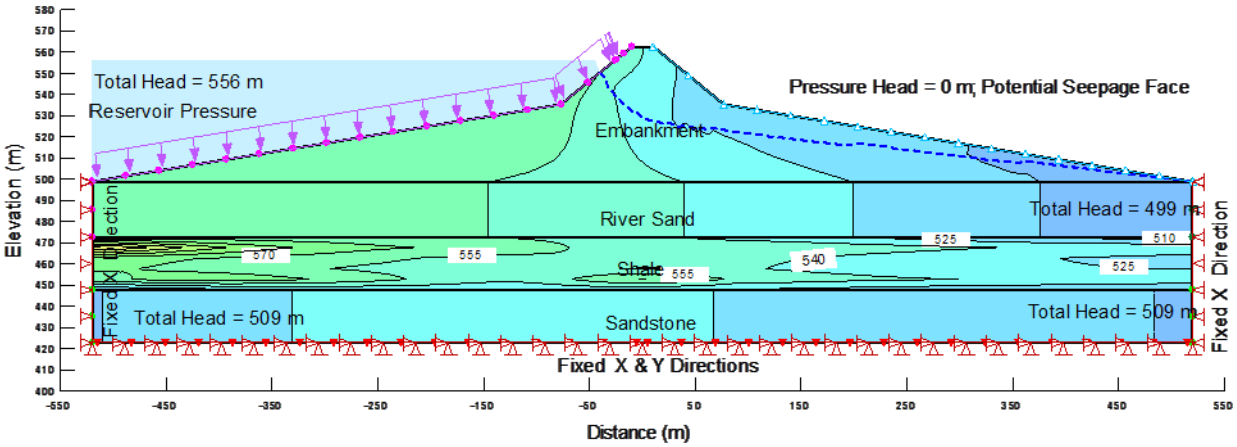

Figure B 21 Coupled total head: reservoir 556 m, 23 days, E'=1250 MPa, k=1e-13 m/s

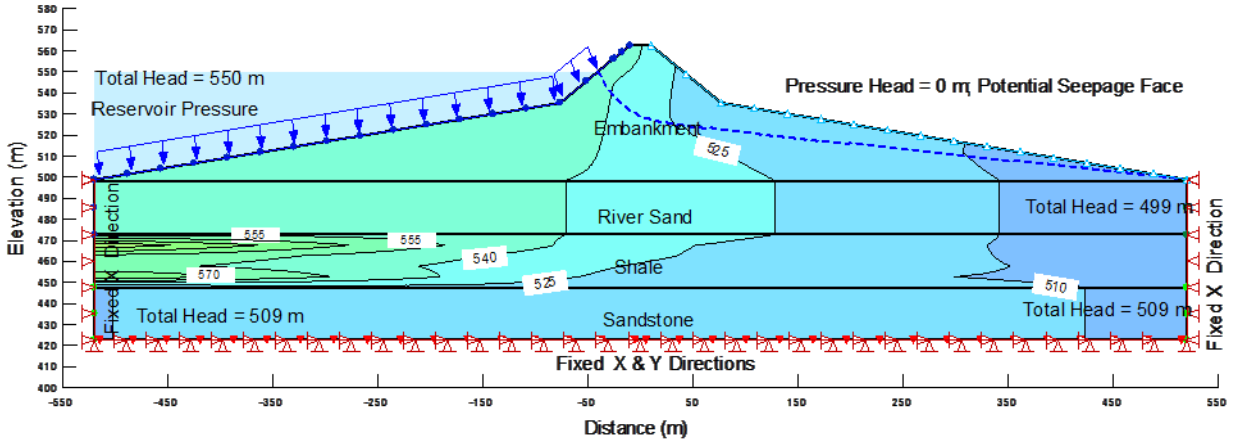

Figure B 22 Coupled total head: reservoir 550 m, 11 day, E'=139 MPa, k=1e-13 m/s

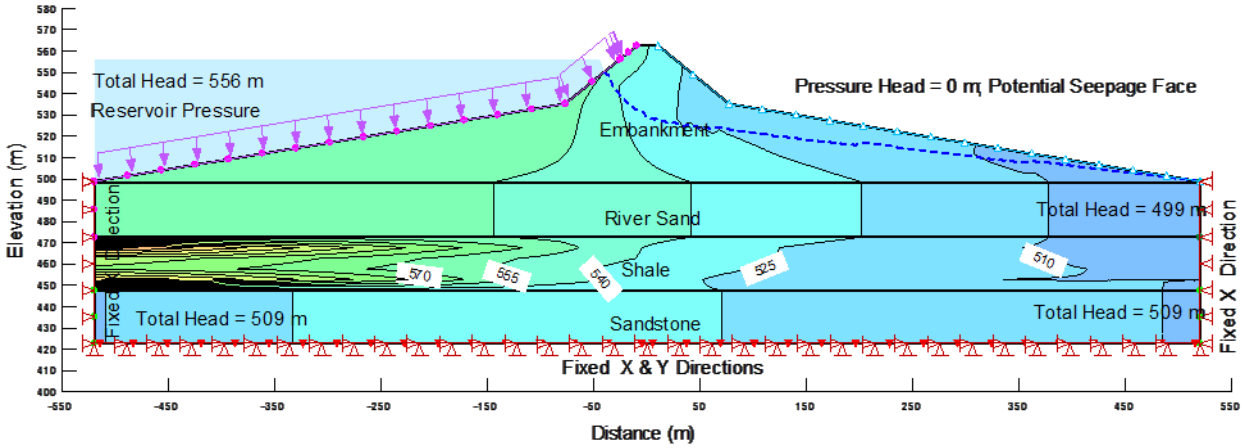

Figure B 23 Coupled total head: reservoir 556 m, 23 days, E'=139 MPa, k=1e-13 m/s

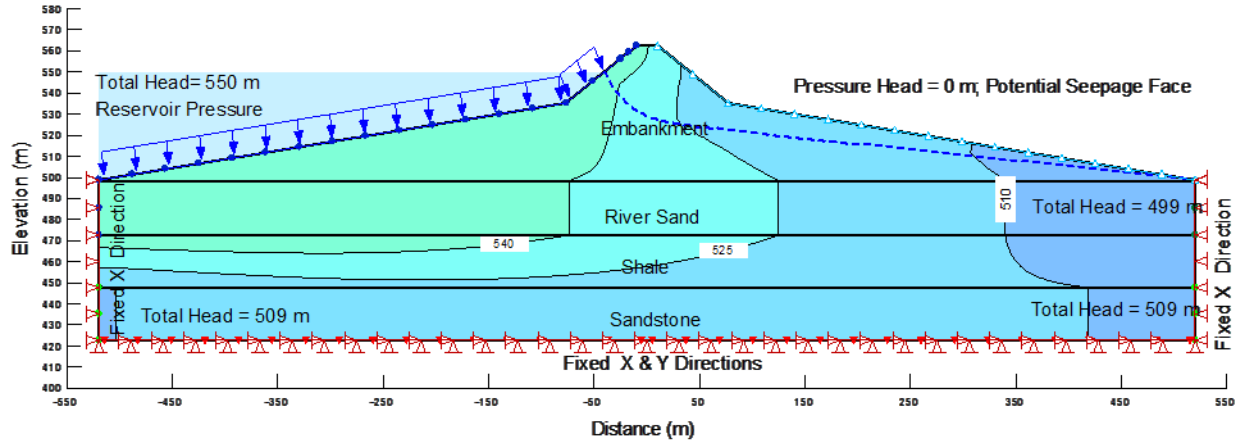

Figure B 24 Coupled total head: reservoir 550 m, 11 day, E'=1250 MPa, k=1e-9 m/s

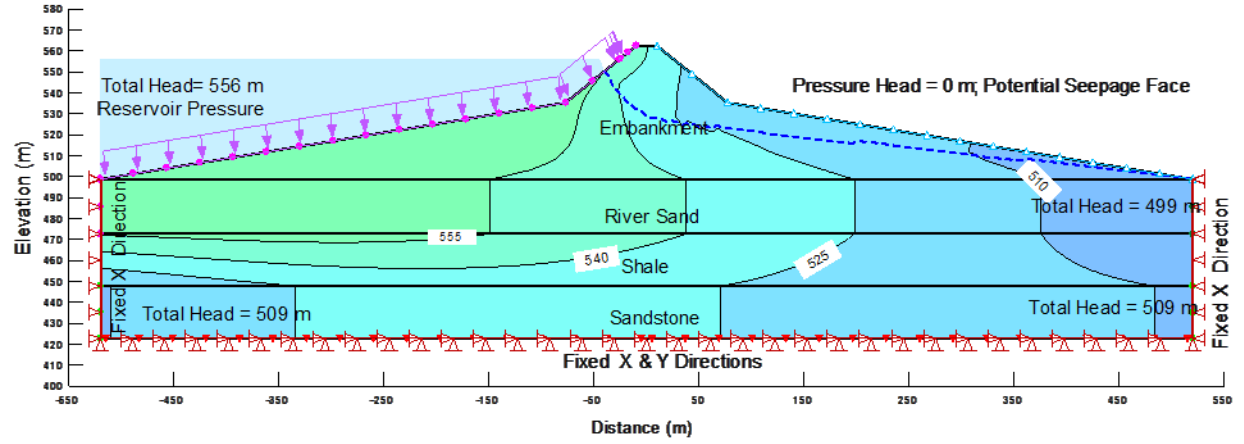

Figure B 25 Coupled total head: reservoir 556 m, 23 days, E'=1250 MPa, k=1e-9 m/s

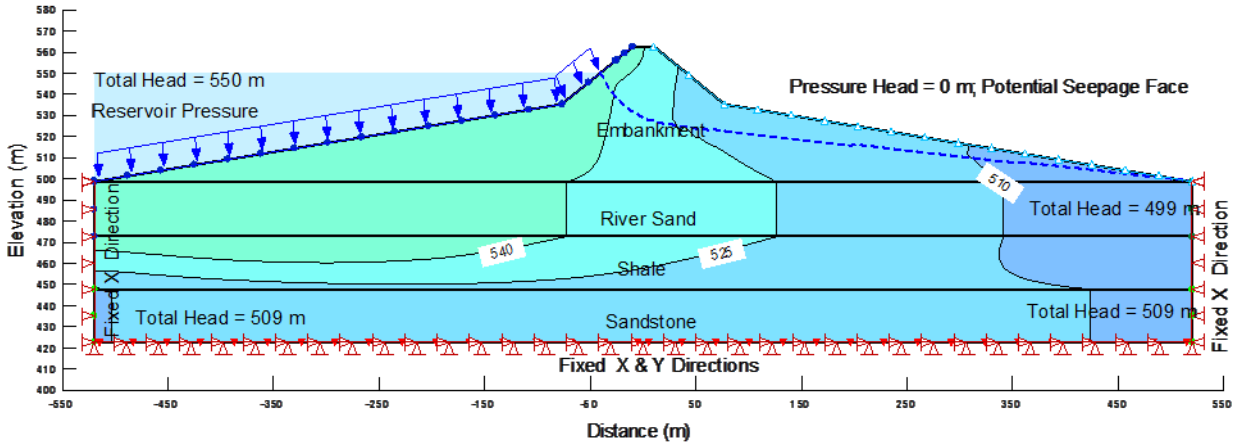

Figure B 26 Coupled total head: reservoir 550 m, 11 day, E'=139 MPa, k=1e-9 m/s

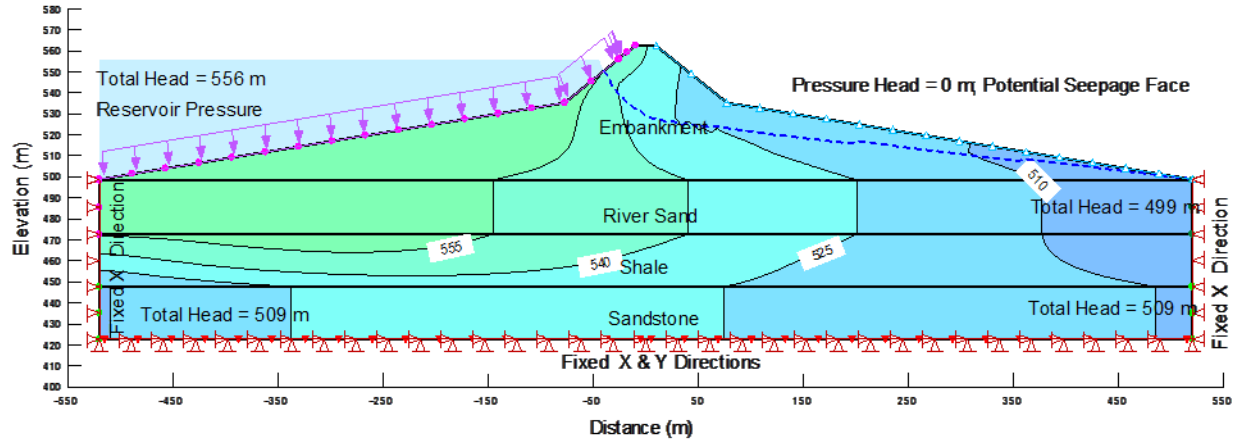

Figure B 27 Coupled total head: at reservoir 556 m, 23 days, E'=139 MPa, k=1e-9m/s

B8. Conclusion

The evaluation of the porewater response, load deformation response and a coupled porewater/stress response was completed. These three evaluations confirmed several assumptions made during the development of the conceptual model. The first being the pore-pressure change within the shale was likely the result of a stress change in the shale due to a change in reservoir hydraulic pressure on the embankment. The second being the X total stress is applied relatively evenly in the embankment and the river sand.

APPENDIX C ANALYTICAL MODEL CALCULATIONS

C1. Introduction

The calculations performed as part of the analytical model have been presented in this Appendix. The calculations have been separated into three independent steps including; horizontal loading, pore-pressure increase, and displacement. These three calculation steps will be described separately with their interaction described within each section. Figure C 1 illustrates the position of the forces and pressures described in the next sections, on the model domain.

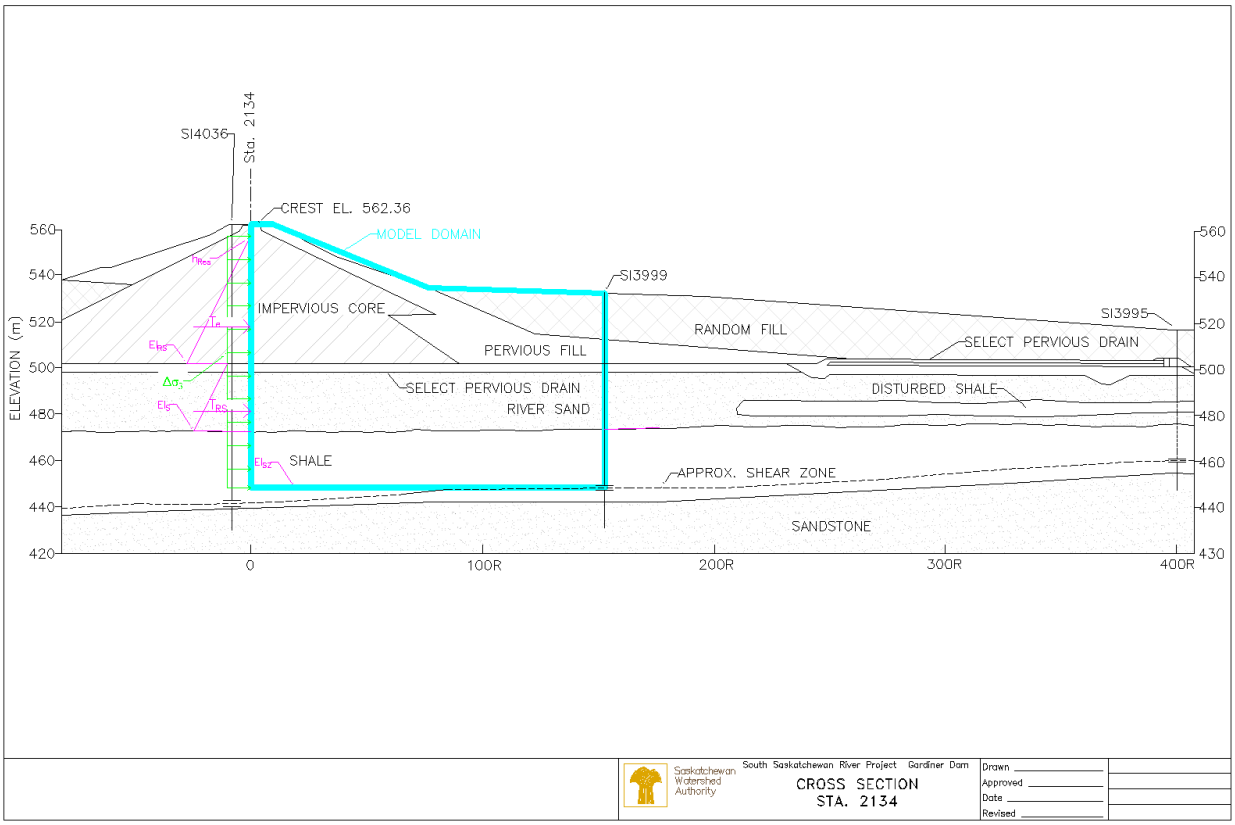

Figure C 1 River Embankment cross section, defining calculated forces and pressures

C2. Horizontal Loading

The horizontal downstream forces were calculated from the reservoir elevation above the base level. The incremental force was determined by calculating the force at each time step for the incremental force and subtracting it from the base force. The calculations of the stress throughout this section assumes that the model extends one unit laterally into the page.

The following indicates the calculation for the horizontal hydraulic reservoir force applied to the model domain:

$$T_e = \frac{1}{2}(h_{Res} - El_{RS})^2 \gamma_w \quad \text{(C-1)}$$

where T_e represents the horizontal hydraulic reservoir force developed applied to the embankment, h_{Res} represents the total head due to the reservoir at the start of the time step, El_{RS} represents the elevation of the surface of the river sand, and γ_w represents the unit weight of water.

The piezometric level within the river sand must be known to calculate the hydraulic horizontal loading from the porewater in the river sand. The piezometric level within the river sand was found to fluctuate as a ratio of the increase in reservoir level. The following calculation estimates the head in the river sand as a function of the reservoir level referred to a base elevation

$$h_{RS} = h_{BRS} + (h_{Res} - h_{BRes}) r_{RS} \quad \text{(C-2)}$$

where h_{RS} is the total head in the river sand, h_{BRS} is the base total head in the river sand, h_{BRes} represents the base total head in the reservoir and r_{RS} represents the ratio between the change in river sand total head and change in reservoir total head above the base level i.e. $r_{RS} = \frac{\Delta h_{RS}}{\Delta h_{Res}}$.

The horizontal hydraulic loading in the river sand at the upstream face was calculated from the total head in the river sand at the upstream face. The hydraulic force can be derived from a hydrostatic, triangular distribution based on water at the top of the river sand and a rectangular portion based on the estimated piezometric level in the river sand. The downstream horizontal force in the river sand was calculated as follows:

$$T_{RS} = \left[\frac{1}{2}(El_{RS} - El_S)^2 + (h_{RS} - El_{RS})(El_{RS} - El_S)\right] \gamma_w \quad \text{(C-3)}$$

where T_{RS} represents the downstream force developed in the river sand, and El_s represents the shale surface elevation.

The hydraulic horizontal forces applied to the upstream face of the model domain were then totaled and subtracted from the base force:

$$\Delta T_i = (T_{ei} + T_{RSi}) - (T_{Be} + T_{BRS}) \quad \text{(C-4)}$$

where ΔT_i represents the incremental hydraulic reservoir force above the base, T_{Be} represent the base hydraulic reservoir force applied to the embankment, and T_{BRS} represents the base hydraulic force applied to the river sand from the porewater.

Assuming that the incremental force is applied evenly from the reservoir surface to the shear zone, the mean total stress is equal to the change in the horizontal hydraulic stress as follows:

$$\Delta\sigma_3 = \frac{\Delta T_i}{(El_{Res} - El_{SZ})} \quad \text{(C-5)}$$

where $\Delta\sigma_3$ represents the increase in all around stress due to the horizontal loading, El_{Res}represents the elevation of the reservoir surface, and El_{SZ} represents the elevation of the shear zone.

C3. Shale Piezometric Pressure

The shale piezometric pressure was related to the increased principal stress applied to the shale. The principal stress is assumed to be applied evenly in both the vertical and horizontal directions throughout the shale in the model domain. This again is a simplification which relates to the use of the average embankment elevation. This simplification allows the objective of the model to be achieved.

The piezometric response within the shale due to the increase in principal stress was determined after Skempton (1954) as follows:

$$\Delta u_s = B\Delta\sigma_3 \quad \text{(C-6)}$$

where B represents the elastic pore-pressure coefficient, and Δu_s represents the change in the pore-pressure in the shale. A general downward trend was also applied to the total head in the shale. The downward trend was a result of dissipation due to excess porewater pressure developed during construction. The porewater dissipation for each time step has been assumed to be the observed general dissipation rate for the modelled time period as follows:

$$\Delta u_g = m_{us}(t_{si} - t_{s0}) \quad \text{(C-7)}$$

where Δu_g represents the decrease in the shale pore-pressure due to ongoing dissipation of excess pressures developed during construction from the start of the model time period, m_{us} represents the overall rate of dissipation of pore-pressure in the shale, t_{si} is the time of any time step, t_{s0} is the time at the start of the model period. The change in pore-pressure was then converted to the change in head and added to the base total head of the shale.

$$h_s = (\Delta u_s - \Delta u_g)\gamma_w + h_{Bs} \quad \text{(C-8)}$$

where h_s represents the total head in the shale and h_{Bs} represents the base total head in the shale.

C4. Displacement

The change in the pore-pressure within the shale impacted the horizontal displacement two ways. Initially, the deformations were due to an elastic compression of the porewater due to relatively quick loading. Secondly, the deformations were due to consolidation of the shale from dissipation of excess porewater pressure from the initial undrained response due to the relatively quick loading.

Bishop (1973) indicated that the elastic volume change in a soil element is due to equal changes in volume caused by the compressibility of the porewater and the compressibility of the soil particles. Therefore, the volume change due to elastic response was determined using the compressibility of the porewater. At each time step the change in pressure was assumed to occur immediately at the start of the time step. The model assumed that the shale was constrained with little to no lateral strain, i.e. any change in volume is equal to a change in horizontal length of the domain. The change in length due to the compressibility of the porewater was determined as follows:

$$\Delta l_{ei} = n\beta l(\Delta u_{si} - \Delta u_{si-1}) \quad \text{(C-9)}$$

where Δl_{ei} represents the change in the horizontal length for any time increment, n represents the shale porosity, β represents the coefficient of compressibility for water, l represents the model domain horizontal length, Δu_{si} represents the change in porewater pressure above the base for the time increment, and Δu_{si-1} represents the change in porewater pressure above the base for the previous time increment.

The elastic displacement provided a small portion of the total displacement compared to consolidation. Consolidation was described as the result of a restructuring of soil elements when excess porewater pressures dissipate and effective stress increases. Consolidation was assumed to occur in a 1D manner, i.e. no lateral displacement following Terzaghi et al. (1996). The calculation of the displacement caused by consolidation involved several steps. With the time step process, consolidation was determined for each time step. The consolidation for each time step was determined by assuming an immediate increase of pore-pressure at the start of each step and allowing the excess pressure to dissipate over the length of the time step.

The first step in the consolidation calculation was to determine the total horizontal consolidation that would be possible due to a total dissipation of excess pore-pressure for each time step. The total horizontal consolidation was calculated as follows:

$$\Delta l_{ct} = m_v(\Delta u_{si} - \Delta u_{si-1})l \tag{C-10}$$

where Δl_{ct} represents the total horizontal change in length due to consolidation, m_v represents the coefficient of volume compressibility for shale. The coefficient of volume compressibility was assumed to remain constant throughout the consolidation process. All of the consolidation was assumed to occur as recompression of the shale and no virgin consolidation was occurring, i.e. stresses induced by the embankment and reservoir were below the preconsolidation pressure of the shale.

The next step was to calculate the coefficient of consolidation which was dependent on the coefficient of compressibility and the hydraulic conductivity of the shale as follows:

$$c_v = \frac{m_v}{k_v \gamma_w} \tag{C-11}$$

where c_v represents the coefficient of consolidation, and k_v represents the vertical hydraulic conductivity. The unit less time factor for drainage to occur was then calculated. The time factor was dependent on the distance to the free draining surface and coefficient of consolidation then in turn, the hydraulic conductivity of the soil. The time factor was calculated as follows:

$$T_v = \frac{c_v(t_{si} - t_{si-1})}{[0.5(El_S - El_{AS})]^2} \tag{C-12}$$

where, t_{si-1} represents the time of the pervious time step, El_S represents the elevation of the shale surface, and El_{AS} represents the elevation of the Ardkenneth Sandstone surface. It was assumed that the shale is drained on the top and bottom; therefore, the drainage distance is half of the shale thickness. Next, the degree of consolidation was found. The degree of consolidation defines the percentage of the total consolidation which has occurred. The following determines the degree of consolidation Craig (1997):

$$U = \left(\frac{4T_v}{\pi}\right) \tag{C-13}$$

where U represents the degree of consolidation. The final step for calculating the horizontal deformation due to consolidation of each time step was to determine the displacement, which was equal to the product of the total displacement and the degree of consolidation as follows:

$$\Delta l_{ci} = \Delta l_{ct} U \tag{C-14}$$

where Δl_{ci} represents the change in horizontal length from consolidation at any time step. The elastic and consolidation horizontal displacement were then summed for each time step with an initial displacement value as follows:

$$\Delta l_t = \Delta l_0 + \sum_{i=1}^{n} [\![(\Delta l_{ei} +]\!] \Delta l_{ci}) \tag{C-15}$$

where Δl_{ci} is (Δl_{ci} where >0 and Δl_{ci}=0 where ≤ 0), Δl_t represents the total horizontal displacement, and Δl_0 represents the initial horizontal displacement at the start of the model period. During this summation, the value of the horizontal incremental consolidation was summed when it is positive and assumed to be zero when negative, since consolidation is assumed to be non-reversible. This constraint was not applied to the incremental elastic displacement as elastic deformation was assumed reversible.

The model assumes the horizontal deformation is caused by a combination elastic compression of the porewater and consolidation of the model domain. The observed displacement at the downstream end of the domain is considered to represent the deformation from the dam centerline to the first downstream slope inclinometer casing (SI3999).

APPENDIX D ANALYTICAL MODEL RESULTS

D1. Introduction

The analytical model results were included in this Appendix. The analytical model results include observed and modelled piezometric and deformation responses in the shale for the calibration and verification time periods. The analytical results also include the sensitivity analysis by defining the sensitivity of the variability of each parameter.

To receive a copy of the results please contact the author at jody_scammell@yahoo.ca